Doctoral Dissertation
Doctoral Program in Civil and Environmental Engineering (36th Cycle)

Habitat modeling in perennial and non-perennial rivers: developments and applications

Giovanni Negro
* * * * * *

Supervisor
Prof. Paolo Vezza

Politecnico di Torino
June, 2024

This thesis is licensed under a Creative Commons License, Attribution - Noncommercial - NoDerivative Works 4.0 International: see www.creativecommons.org. The text may be reproduced for non-commercial purposes, provided that credit is given to the original author.

I hereby declare that, the contents and organisation of this dissertation constitute my own original work and does not compromise in any way the rights of third parties, including those relating to the security of personal data.

Giovanni Negro
Turin, June, 2024

Acknowledgments

First of all, I would like to extend my gratitude to my supervisor, Prof. Paolo Vezza, whose guidance, unwavering support, and mentorship were invaluable throughout all my academic journey. Much of scientific and personal growth I have experienced during my PhD is attributable to him.

I also want to extend heartfelt gratitude to Prof. Guido Zolezzi, Prof. Stefano Fenoglio, Dr. Alex Laini, Dr. Alessandro Candiotto, Eng. Luca Astegiano and Dr. Paolo Lo Conte, whom I had the opportunity of encountering during my PhD. Their passion and expertise significantly contributed to expanding my interest and understanding of rivers and their ecosystems.

A thanks is extended to the Compagnia Valdostana delle Acque (CVA spa) and the Autorità di Bacino delle Alpi Orientali (DAO) for their financial support throughout this research endeavour.

I profoundly thank my family of origin Cristina, Corrado and Virginia for their steadfast support and encouragement through every phase of my personal and educational pursuits.

Last, but not least, I wish to express my deepest gratitude to my newfound family, Dida, Artemide, and Rijeka. Dida, your endless patience, encouragement, and unwavering belief in me during all these years have been my greatest strength.

Summary

Rivers provide essential ecosystem services for human well-being and supply habitat for a vast multitude of animal species. However, river ecosystems are facing degradation and biodiversity loss due to significant pressures from hydrological and morphological alterations caused by water abstractions and hydropower generation. To preserve freshwater ecosystems and enhance water resource management, meso-scale Habitat Suitability Models (HSMs) are increasingly recognized as valuable tools. In particular, the MesoHABitat SImulation Model (MesoHABSIM) has proven effective for assessing the impact of water abstraction and designing ecological flows (e-flows) in regulated rivers, promoting more sustainable water use while preserving river ecosystems and the services they provide. MesoHABSIM uses geomorphic and hydraulic units (GUs or mesohabitats) and their local hydro- (e.g., water depth and flow velocity) morphological (e.g., substrate, channel geometry) attributes to quantify the physical habitat availability for freshwater species. Habitat assessments rely on habitat suitability criteria (HSC, or species distribution models), which link hydro-morphological features to species' habitat preferences. However, broader implementation of MesoHABSIM is hindered by gaps in knowledge regarding habitat preferences of freshwater species and, consequently, in the availability of validated HSC. Additionally, river habitat modeling have traditionally focused on perennial rivers, neglecting non-perennial rivers (NPRs), which constitute over half of the global stream network. Main constraints include limited knowledge on the spatio-temporal distribution of flow intermittency within river networks and the lack of theoretical approaches and analytical tools to properly model habitat evolution when discharge is close or equal to zero (i.e., during non-flowing periods).

This thesis focuses on advancing meso-scale habitat modeling for both perennial and non-perennial rivers, enhancing the applicability of the MesoHABSIM approach, particularly in Italy.

Part I focuses on developing new HSC for Italian endemic and threatened freshwater species in perennial rivers. A systematic literature review compiled physical habitat preferences for 31 freshwater fish species and 3 freshwater lampreys, representing 75% of Italy's endemic freshwater fish community. This review highlighted significant information deficits for over 30% of these species, particularly during critical spawning periods. To address these gaps, meso-scale HSC were developed and tested for the Italian vairone (*Telestes muticellus*) and applied to a regulated river reach, demonstrating practical application of collected literature information. According to the findings from the literature review, further studies were conducted to develop new empirical meso-scale HSC for two Italian threatened freshwater species, for which little quantitative data existed. Specifically, data on habitat preferences for the Po brook lamprey (*Lampetra zanandreai*), an autochthonous freshwater lamprey, were gathered, identifying significant mesohabitat attributes and sediment requirements for species distribution. The analysis was performed by training a Random Forest (RF) model which allowed the definition of the first meso-scale HSC in literature for considered lamprey. The results indicated that lamprey ammocoetes can play a crucial role as indicators of river ecosystem quality within the Po river basin, offering insights for more targeted investigations. Meso-scale HSC were also developed for the spawning period of the anadromous Twaite shad (*Alosa fallax*). The study was conducted in the Tagliamento river (Northeastern Italy), using Uncrewed Aerial Systems (UAS) and a two-dimensional (2D) hydrodynamic model to characterize local hydro-morphological features. Key spawning mesohabitat requirements were again identified using a RF model, which allowed the definition of the first meso-scale HSC in literature for an anadromous species during the spawning period. To observe and record the mating behaviour of the monitored *Alosa fallax* population, infrared cameras were deployed over two consecutive nights. Analysis of the video revealed mating behaviour consistent with previously reported findings in the literature, thereby enhancing the understanding of the reproductive ecology of Mediterranean populations of shads. These findings can contribute to developing effective conservation strategies and fisheries management practices for this species. Finally, meso-scale HSC for five fish species, previously developed and made available for applications of the MesoHABSIM approach in Italy, were tested in terms of transferability across different rivers. HSC predictions were compared

with field data on fish distribution within GUs from nine rivers distributed in Northern Italy. The study demonstrated high predictive performance for considered HSC, suggesting effective transferability among streams.

Part II of this thesis concentrated on NPRs. An innovative approach to assess the spatio-temporal distribution of flow intermittency within river networks is presented. It is based on the use of multispectral Sentinel-2 images to monitor changes in water surface presence along NPRs. By identifying the main hydrological conditions (flowing, ponding and dry conditions) which mark NPRs using a supervised classification of satellite images, and developing RF models to predict these conditions on a daily scale, the study demonstrated a high-accuracy method with significant potential for the identification and hydrological characterization of NPRs. In the last study, the new module of the MesoHABSIM approach dedicated to NPRs (i.e., NPRs-module) is introduced using a practical application. Specifically, by integrating the new NPRs-module with remote sensing information and locally recorded hydrological data it was effectively possible to assess the aquatic habitat availability during both flowing and non-flowing conditions in a regulated and non-perennial reach of the Sangone river (Northwestern Italy). This new NPRs-module represents a significant advancement in river habitat modeling tools for preserving aquatic ecosystems and biodiversity in non-perennial streams.

Contents

1. INTRODUCTION 1

1.1 River habitat modeling: a brief overview 3
1.2 The MesoHABSIM approach 6
1.3 Non-perennial rivers (NPRs) 12
1.4 The MesoHABSIM module for non-perennial rivers (NPRs-module) 14
1.5 Thesis contents 17
1.6 Novel contributions 18

PART I: MESO-SCALE HABITAT SUITABILITY CRITERIA IN PERENNIAL RIVERS 19
2. HABITAT PREFERENCES OF ITALIAN FRESHWATER FISH 21

2.1 Introduction 21
2.2 Materials and methods 22
2.2.1 Literature review 22
2.2.2 Data Analysis 23
2.2.3 Application of the MesoHABSIM model 26

2.3 Results 28
2.4 Discussion 29

3. ECOLOGICAL NOTES ON AN ENDEMIC FRESHWATER LAMPREY, *LAMPETRA ZANANDREAI* (VLADYKOV, 1955) 33

3.1 Introduction 33
3.2 Materials and methods 35
3.2.1 Study area 35
3.2.2 Mesohabitat description and lamprey distribution 36
3.2.3 Data analysis 38

3.2.4 Granulometry 39

3.3 Results 40
3.3.1 Mesohabitat description 40
3.3.2 Habitat preference analysis 41
3.3.3 Granulometry 42

3.4 Discussion 43

4. MESOHABITAT SPAWNING PREFERENCE OF THE ANADROMOUS TWAITE SHAD (*ALOSA FALLAX*, LACÉPÈDE 1803) IN THE TAGLIAMENTO RIVER 47

4.1 Introduction 47
4.2 Materials and methods 50
4.2.1 Study area 50
4.2.2 Field surveys and data collection 51
4.2.3 Data analysis and habitat description 54
4.2.4 Mesohabitat suitability criteria 57

4.3 Results 59
4.4 Discussion 62

5. TRANSFERABILITY OF MESOHABITAT SUITABILITY CRITERIA IN NORTHERN ITALY 69

5.1 Introduction 69
5.2 Materials and methods 71
5.2.1 Case study 71
5.2.2 MesoHABSIM approach 71
5.2.3 Field data collection 72
5.2.4 Mesohabitat suitability criteria 73

5.3 Results 74
5.4 Discussion 76

PART II: NON-PERENNIAL RIVERS 79
6. EXPLOITING SENTINEL-2 DATASET TO ASSESS FLOW INTERMITTENCY IN NON-PERENNIAL RIVERS 81

6.1 Introduction 81
6.2 Materials and methods 84
6.2.1 Case study 84
6.2.2 Remote sensing datasets and filed surveys 86

6.2.3 Meteo-hydrological data 88
6.2.4 Method for the identification of the hydrological condition 88
6.2.5 Random Forest Classification 89

6.3 Results 91
6.3.1 Spectral signature analysis and false color images 91
6.3.2 Comparison of false color images with ground truth 93
6.3.3 Relation between hydrological condition extracted by FCIs and hydrological data 97
6.3.4 Random Forest results of oversampled models 98
6.3.5 Duration of hydrological condition 100

6.4 Discussion 101

7. MESO-SCALE HABITAT MODELING IN NON-PERENNIAL RIVERS 105

7.1 Introduction 105
7.2 Materials and methods 106
7.2.1 Study area 106
7.2.2 The MesoHABSIM module for NPRs 108
7.2.3 Hydro-morphological data collection and analysis 110
7.2.4 Hydrological characterization 112

7.3 Results 114
7.4 Discussion 116

8. CONCLUSIONS 123
9. LIMITATIONS AND PERSPECTIVES 129
REFERENCES 133
APPENDIX A. GENERAL APPENDIX 149

A.1 Physical habitat attributes of the MesoHABSIM model 149
A.2 Workflow for the development of Habitat suitability Criteria with the Random Forest classification algorithm: 150
A.3 Metrics for assessing Habitat Suitability Criteria performances: 152
A.4 The Random Forest models considered in Chapter 5 and 7. 153

APPENDIX B. APPENDIX FOR CHAPTER 2 159

B.1 Number of bibliography sources per species 159

APPENDIX C. FURTHER PERSONAL CONTRIBUTIONS IN PUBLISHED ARTICLES ON APPLICATIONS OF THE MESOHABSIM APPROACH 161

C.1 Comparing Multi-Criteria Decision-Making Methods for the Assessment of Flow Release Scenarios From Small Hydropower Plants in the Alpine Area 161

C.2 The combined impact of hydropower plants and climate change on river runoff and fish habitats in lowland watersheds 162

List of Tables

Table 2-1. Search strings used for the database screening. All possible combinations of species' scientific/common names both in English and Italian language and the following habitat-related statements were used. 24

Table 3-1. Name, location, characteristics and morphological classification of surveyed reaches. River morphology codes (according to [56]): C = confined; P = partly confined; U = unconfined; SS = straight-sinuous; M = meandering; S = sinuous; PM = pseudo-meandering. Reach width represents the mean value of the active river channel width in each surveyed reach. 37

Table 3-2. Correlations between volume and mass of the different granulometric size classes. 42

Table 5-1. Name, location, morphological classification, and characteristics of surveyed reaches. River morphology codes (according to [56]: C = confined; P = partly confined; U = unconfined; SS = straight-sinuous; M = meandering; PM = pseudo-meandering; B = braided. Reach width represents the mean value of the active river channel width in each surveyed reach. 73

Table 5-2. Random Forests models of freshwater fish species and life stages considered in the study. For each model the reaches name in which it was applied with the corresponding total amount of sampled GUs are reported. 74

Table 5-3. Predictive performances obtained for the considered RF models. 76

Table 6-1. Characteristics of the studied reaches. Reach morphology codes: C = confined; PC = partially confined; U = unconfined; W = wandering; S = sinuous. 86

Table 6-2. Characteristics of Sentinel-2 Multispectral Instrument (MSI). 88

Table 6-3. Pairs of Sentinel-2 and ground truth images. 93

Table 6-4. Predictive variables and performances obtained for the oversampled RF models. Models variables are listed in terms of descending importance for

classification result (from left to right). Binary models code: F/NF = non-flowing/flowing, P/D = dry/ponding. Predictive variables code: R90 = cumulative 90-days rainfall, R30 = cumulative 30-days rainfall, R10 = cumulative 10-days rainfall, T90_MAX = average of previous 90-days maximum air temperature, T30_MAX = average of previous 30-days maximum air temperature, T90_MEAN = average of previous 90-days mean air temperature. 99

Table A-1. The physical habitat attributes of the MesoHABSIM model used for the geomorphic units (GUs) description in Chapter 2, 3, 4, 5, and 7. In cyan are highlighted the 44 predictors taken into account in Chapter 3 and 4 for the development of Habitat Suitability Criteria (HSC) using the classification Random Forest (RF) algorithm. The same habitat attributes are considered to establish the rank of suitability (not suitable/suitable/optimal) of each GUs for quantifying the available habitat for target species in Chapter 2, 5, and 7. 149

Table B-1. Number of bibliography sources (Num.) reporting the preferred categories (Cat.) of habitat attributes derived from the review analysis for each species, life stage (A=adult, J=juvenile) and bioperiod (S=spawning). Species are sorted with respect to the total amount of corresponding number of bibliography sources found (Pub.). The color-gradient is picturing high (21, blue) to low (0, red) number of bibliography sources reporting the preferred habitat categories . Water depth (D) and current velocity (V) are represented by 9 categories of 15 cm (from 0 up to > 120 cm) and 15 cm/s (from 0 up to > 120 cm/s) respectively. The codes used for substrate and cover/shelter categories are reported in Table A-1. The Table shows, in numerical terms, the results depicted in Figure 2.1. 159

List of Figures

Figure 1.1. An anabranching reach of the Yukon river (Alaska, USA), one of the longest free-flowing rivers in the world, with the well-preserved ecosystem and minimal hydro-morphological impacts [8]. Picture from [24]. 2

Figure 1.2. Conceptual framework of a habitat suitability model. To the hydro-morphological characterization of the river system, habitat suitability criteria for target species are applied to assess the habitat suitability (CASiMiR, [38]). 4

Figure 1.3. Main submerged geomorphic units of mountain alluvial bed streams considered within the MesoHABSIM approach (modified form [60]). 7

Figure 1.4. Conceptual framework of the MesoHABSIM approach with the three macro-components. 8

Figure 1.5. Hierarchical morphological classification structure from the catchment scale to the river element. The mesohabitats correspond to the geomorphic and hydraulic units (modified from [60]). The reference spatial scales of the MesoHABSIM approach are highlighted in green. 9

Figure 1.6. a) An example of habitat-flow rating curves obtained using the SimStream-Web service (https://mesohabsim.isprambiente.it/app/home/) by applying the MesoHABSIM approach to a regulated river reach. b) One-year natural flow time series for the considered river reach. c) Corresponding habitat time series for the adult Marble trout (*Salmo marmoratus*) selected as target species. 10

Figure 1.7. Habitat integrity classes for the IH index considered within the MesoHABSIM approach. 12

Figure 1.8. Overview of the three different hydrologic conditions that may occur in NPRs: a) flowing, b) ponding, and c) dry. The pictures represent a reach of the Sciarapotamo river, located in the province of Salerno (Southern Italy). ...12

Figure 1.9. Conceptual framework for the identification of the hydrological conditions in NPRs using Sentinel-2 satellite images [29]. The pictures

corresponding to different hydrological conditions represent a reach of the Sciarapotamo river, located in the province of Salerno (Southern Italy). 14

Figure 1.10. An example of the habitat-flow-time rating curves of the new module of the MesoHABSIM approach dedicated to NPRs. Evolution of total wetted area (% or m^2) and available habitat (% or m^2) for a target species (juvenile European eel, *Anguilla anguilla*) per discharge and time. In pink is highlighted the dry, in yellow the ponding, in blue the flowing conditions. 16

Figure 2.1 List of autochthonous Italian freshwater species included in the study. The orientation of the arrows suggests the preferred category (Cat.) of habitat attributes for each species, life stage (A = adult, J = juvenile) and bioperiod (S = spawning), and the size expresses the corresponding number of sources (Num.) reporting the same information. For a clearer depiction of the result, species are sorted according to the corresponding number of bibliography sources found (Pub.). Background colors are used to highlight the three groups of species: species with quite copious information (yellow), species with limited available data (orange), and species with very poor information (red). Water depth (D) and current velocity (V) are represented by nine categories of 15 cm (from 0 up to >120 cm) and 15 cm/s (from 0 up to >120 cm/s) respectively. Substrate categories codes: GI, *gigalithal*; ME, *megalithal*; MA, *macrolithal*; MS, *mesolithal*; MI, *microlithal*; AK, *akal*; PS, *psammal*; PE, *pelal*; DE, *detritus*; XY, *xylal*; SA, *sapropel*; PH, *phytal*. Covers/shelters categories codes: BD, boulder; CS, canopy shading; OV, overhanging vegetation; RO, roots; SV, submerged vegetation; FV, floating vegetation; EV, emerging vegetation; UB, undercut bank; WD, woody debris; RI, riprap; SM, shallow margins. For a better understanding, sample diagrams are given at the bottom of the Figure. The numerical values depicted as oriented arrows are reported in Table B-1. 25

Figure 2.2. Presence/absence HSC for (A) adult and (J) juvenile life stages of *Telestes muticellus*, depicted by using a decision tree representation. Habitat suitability maps expressing the available habitat (H) assessed for adults *T. muticellus* at (B) 0.25 m^3/s and (C) 2.2 m^3/s, and for juveniles *T. muticellus* at (E) 0.25 m^3/s and (F) 2.2 m^3/s, in the Argentina Creek. 27

Figure 3.1. Location of the surveyed reaches considered in the study. Surveyed stream reaches: 1 = Belbo river; 2-3 = Ghiandone river; 4 = Orco river; 5 = Pellice river. 36

Figure 3.2. a) Sampling station, Ghiandone river (NW Italy); b) sediment cores; c) Bertel mechanical sieve; d) sample with the five granulometric classes considered. 40

Figure 3.3. *Lampetra zanandreai* ammocoetes RF model. Selected physical attributes (in order of importance) for the oversampled parsimonious model. The relationship between variables and probability of presence is reported using partial dependence plots (PDPs). 42

Figure 3.4. Principal Component Analysis ordination plot. Labels indicate granulometric classes, dots represent sample cores. 43

Figure 4.1. The study area: a) the Tagliamento watershed, and b) the surveyed sub-reach, as depicted in the RGB orthomosaic obtained on July 1st 2022. The yellow triangle represent the approximate position of the water level sensor installed in the study site. The primary flow direction is indicated by the blue arrow. 50

Figure 4.2. The simulation results for a) depth and b) velocity under the flow condition of 11.90 m^3/s, using the bathymetrically corrected DEM as background. Depth and velocity are color-coded according to the corresponding categories of the MesoHABSIM approach (Table A-1), ranging from the smallest (in blue) to the highest (in red). c) The geomorphic units (GUs) mosaic at flow rate of 11.90 m^3/s. d) The GUs where the spawning activities of *A. fallax* were observed are highlighted in purple. The primary flow direction is indicated by the blue arrow. 53

Figure 4.3. a) Daily mean air (in grey) and water temperature (in blue) time series from May 11th 2022 to August 11th 2023 registered by the HOBO U20L in the study site. The minimum threshold corresponding to 12°C, above which spawning activities were assumed to start, is represented by a dotted red line. b) Water level (in black) time series expressed as daily mean values. The date in which the discharge measurements were performed during the field campaigns are displayed using red dots. c) The flow duration curve of the spawning period. The simulated discharges for training the Random Forest model are highlighted in blue. For all images the variable corresponding to the spawning period is represented by a continuous orange line. 56

Figure 4.4. The Random Forest model for the spawning period of *A. fallax*. The selected physical attributes (Table A-1) for the SMOTE parsimonious model are presented (in order of importance) through Partial dependence plots, which express the relationship between attributes and the probability of presence. 59

Figure 4.5. Video frames and pictures recorded during the field campaign in May 2023 with infrared and optical cameras. a) Example of successful mating event recorded by the infrared camera. The primary flow direction is indicated by the blue arrow. b) A pre-mating activity (tail splashing). c) A daily vision of the analyzed spawning sites. d) A specimen of *A. fallax* captured by Dr. Davide Lesa within a deep pool closed to the spawning site. 62

Figure 4.6. Occurrence (orange dot) and duration (dot size) of mating events recorded by the infrared camera during the first night of observation of the field campaign of May 2023. The broken line in grey represents the cumulative frequency of total mating events (44) recorded during the observation period. In blue is highlighted the assessed peak spawning time. 67

Figure 5.1. Location of the surveyed reaches considered in the study. Regions of interest: ER = Emilia-Romagna; L = Liguria; P = Piemonte; TAD = Trentino-Alto-Adige; VDA = Valle d'Aosta. Surveyed river reaches: 1 = Argentina; 2 = Belbo; 3 = Ghiandone; 4 = Malacqua; 5 = Orco; 6 = Pellice; 7 = Rabbies; 8 = Savara; 9 = Trebbia. 72

Figure 5.2. GUs, observed distribution, and habitat suitability map for reach 8. a) GUs mosaic and b) observed distribution for adult brown trout (Salmo trutta) assessed during the field campaign at 0.3 m3/s of discharge. c) predicted distribution for adult brown trout by the application of corresponding RF model. 75

Figure 6.1. Geographical framework of the study area. 85

Figure 6.2. a) Spectral signature of late spring season, Google Earth of June 2019, b) spectral signature of winter, field pictures of February 2021, c) spectral signature of late autumn season, ortophoto of December 2021. 92

Figure 6.3. Test case n°1, M1 reach, (a) Maps Data: Google, © June 14th 2019, (b) RGB extracted by Sentinel-2 acquisition of June 12th 2019 and (c) FCI extracted by Sentinel-2 acquisition of June 12th 2019. 94

Figure 6.4. Test case n°4, M3 reach, (c) FCI extracted by Sentinel-2 image of September 19th 2020 with the geolocation points of the photos, (c1),(c2) and (c3) geo-located photos take on September 19th 2019. 95

Figure 6.5. Test cases n°2,4,5, S1 reach, (a) FCI of June 26th 2020, (b) FCI of September 19th 2020, (c) FCI of February 6th 2021, (red point) photo shooting location, (d) photo taken on June 26th 2020, (e) photo taken on September 19th 2020, and (f) photo taken on February 6th 2021. 96

Figure 6.6. Test cases n°2,3,5, S1 reach, (a) FCI of June 26th 2020, (b) FCI of July 26th 2020, (c) FCI of February 6th 2021, (a1,a2 and a4) photos taken on June 26th 2020, (b3,b2 and b4) photos taken on September 19th 2020, and (c3,c5 and c6) photos taken on February 6th 2021. Photo-taking orientation are reported in brackets in the labels of a, b and c panels. Note: White boxes are used to cover people incidentally taken from the photos. 97

Figure 6.7. Distribution of water levels for considered hydrological conditions: Flowing, Ponding and Dry. (a) M3 reach, (b) L1 reach. 98

Figure 6.8. Daily occurrences of flowing (blue), ponding (yellow) and dry (red) conditions predicted by the individual RF models for each reach during the study period from 2015 to 2020. 101

Figure 7.1. The study area. The Sangone river and its catchment near the metropolitan city of Torino. The study site (in blue) located below the Trana gauging station (represented by a green dot) and the main agricultural weirs (represented by a red dot), which hindered the lower part of the watercourse. The location of the rain gauge belonging to the upper part of Sangone catchment is represented by a yellow dot. The main flow direction is indicated by the blue arrow. 107

Figure 7.2. Simulation results for a) water depth and b) velocity under the flow condition present during the UAS flight (Q = 0.15 m^3/s), utilizing the bathymetrically-corrected DEM as background. Depth and velocity are color-coded according to the corresponding categories of the MesoHABSIM approach (Table A-1), ranging from the smallest (in blue) to the highest (in red). c) Corresponding GUs mosaic overlaid on the RGB orthomosaic. The main flow direction is indicated by the blue arrow. 109

Figure 7.3. Sentinel-2 false-color images (bands 11-8-4) corresponding to a) flowing (August 22nd 2022), b) ponding (August 24th 2022), and c) dry (August 27th 2022) conditions during the most drought event of summer 2022. The RGB orthomosaic representing the surveyed reach (in red) is depicted on the top of the image. The main flow direction is indicated by the blue arrow. The recession in the extent of the wetted area, transitioning from a flowing phase to completely dry within five days, is clearly evident. 113

Figure 7.4. Time series of discharge (in black) and rainfall (in gray) during the most severe drought period affecting the study site, which corresponded to summer 2022 (June-September). The hydrological conditions classified from the Sentinel-2 images analysis during the same period are presented by dotted segments in blue (flowing condition), yellow (ponding condition), and red (dry condition). The threshold flow value (Q*) below which in the surveyed sub-reach are observed discharge interruptions is represented in magenta. The shortest ponding condition durations corresponding to 5 days assessed in two events in late August and early September are highlighted. 116

Figure 7.5. a) The habitat-flow-time rating curves for the surveyed sub-reach computed using SimStream-Web. The evolution of total wetted area (%) and available habitat (%) for adult (black filled square dot) and juvenile (black empty square dot) *T. muticellus*, and adult *P. bonelli* (black empty ex dot) per discharge and time. The flowing condition is highlighted in blue, the ponding condition,

estimated to stand for 5 days, in yellow, and the dry condition in red. b) The altered flow time series estimated in the surveyed sub-reach during summer 2022. The corresponding habitat time series for c) adult *T. muticellus* and d) adult *P. bonelli* obtained via SimStream-Web. The sequence of periods corresponding to each assessed hydrological condition is highlighted. For discharges higher than 3 m^3/s, conversion into habitat terms was not possible, and these values were replaced with not-a-number (NaN) values. 121

Figure A.1. The workflow followed in Chapter 3 and 4 for the development of Habitat Suitability Criteria (HSC) using the classification Random Forest (RF) algorithm. a) Hydro-morphological characterization of the riverine habitat. Each Geomorphic Unit (GU) serves as a sample for training the trees of the forest. The habitat attributes (see Table A-1 for details) collected for each GU, organized into 44 categories, are used as predictors to define the models. b) Species distribution is assessed for each GU and represent the observations (Y). c) RF model predictions yield a probability of presence based on majority voting among the decision trees in the forest; if this probability exceeds 50%, the GU is classified as suitable (1) for the species. If not, the GU is classified as not suitable (0). Model performances are than evaluated using the statistical metrics reported in A.3. d) A representation of the input table, characterized by 44 predictors and 1 response variable (fish: absent, 0/present, 1), used for the RF models definition. The codes used for the habitat attributes are listed in Table A-1..... 150

Figure A.2. The absence/presence Random Forest model of adult Brown trout (*Salmo trutta*) available in SimStream-Web (https://mesohabsim.isprambiente.it/app/home/)..... 153

Figure A.3. The absence/presence Random Forest model of adult Marble trout (*Salmo marmoratus*) available in SimStream-Web (https://mesohabsim.isprambiente.it/app/home/)..... 154

Figure A.4. The absence/presence Random Forest model of juvenile trout (*Salmo trutta/marmoratus*) available in SimStream-Web (https://mesohabsim.isprambiente.it/app/home/)..... 154

Figure A.5. The absence/presence Random Forest model of adult Bullhead (*Cottus gobio*) available in SimStream-Web (https://mesohabsim.isprambiente.it/app/home/)..... 155

Figure A.6. The absence/presence Random Forest model of adult Italian barbel (*Barbus plebejus*) available in SimStream-Web (https://mesohabsim.isprambiente.it/app/home/)..... 155

Figure A.7. The absence/presence Random Forest model of adult Italian vairone (*Telestes muticellus*) available in SimStream-Web (https://mesohabsim.isprambiente.it/app/home/). 156
Figure A.8. The presence/abundance Random Forest model of adult Italian vairone (*Telestes muticellus*) available in SimStream-Web (https://mesohabsim.isprambiente.it/app/home/). 156
Figure A.9. The absence/presence Random Forest model of juvenile Italian vairone (*Telestes muticellus*) available in SimStream-Web (https://mesohabsim.isprambiente.it/app/home/). 157
Figure A.10. The presence/abundance Random Forest model of juvenile Italian vairone (*Telestes muticellus*) available in SimStream-Web (https://mesohabsim.isprambiente.it/app/home/). 157
Figure A.11. The absence/presence Random Forest model of adult Padanian goby (*Padogobius bonelli*) available in SimStream-Web (https://mesohabsim.isprambiente.it/app/home/). 158
Figure A.12. The presence/abundance Random Forest model of adult Padanian goby (*Padogobius bonelli*) available in SimStream-Web (https://mesohabsim.isprambiente.it/app/home/). 158

Chapter 1

1. Introduction

Rivers and streams provide essential services for human well-being, including food, drinking water, flood regulation, and energy resources [1]. These services, known as ecosystem services, rely on the effective functioning of fluvial systems, which necessitate the maintenance of appropriate flow and sediment regime, and organic material supply, as well as the quality of channel morphology (**Figure 1.1**) [2]–[4]. Despite their crucial importance, fluvial ecosystems are currently among the most threatened environments on the planet [5]. Hydro-morphological alterations resulting from water abstractions, flow regulation and hydropower generation are recognized as significant pressures with profound impacts, leading to the degradation of river ecosystems and loss of biodiversity [6]–[8].

Looking forward, the already complex challenges facing river ecosystems are expected to intensify. Population growth, particularly in developing countries, is projected to drive increased water demand [9]. Additionally, efforts to expand hydropower production are underway as part of initiatives for reducing energy production from fossil fuel [10], [11]. Furthermore, climate change is expected to alter rivers flow regime, fundamentally modifying the current availability of water resource [12].

Addressing these pressing challenges has fostered the emergence of an innovative interdisciplinary field known as eco-hydraulics [13]. Eco-hydraulics focuses on understanding the intricate interactions between ecological processes and hydro-morphological dynamics to effectively characterize river ecosystems [14]. Its practical applications include assessing ecological flows (e-flows, [2], [15]), restoring river continuity with natural fish passes, and designing river restoration measures [16].

Within the eco-hydraulics framework, Habitat Suitability Models (HSMs) have emerged as valuable tools for mitigating the impacts of hydro-morphological alterations, thereby preserving river ecosystem functioning and biodiversity [17]. In particular, the more recent meso-scale HSMs, such as the Meso-scale HABitat SImulation Model (MesoHABSIM, [18]), have proven effective in assessing

physical habitat availability for riverine species (e.g., [19]–[22]). Aquatic habitat availability commonly is evaluated using habitat suitability criteria (HSC, or species distribution model), which aim to relate freshwater species ecological requirements with the hydro-morphological features constituting physical riverine habitat [23].



Figure 1.1. An anabranching reach of the Yukon river (Alaska, USA), one of the longest free-flowing rivers in the world, with the well-preserved ecosystem and minimal hydro-morphological impacts [8]. Picture from [24].

However, widespread implementation of the meso-scale HSMs is hindered by limitations in their applicability and adaptability to diverse river contexts. A major challenge is the general scarcity of validated HSC for freshwater species, which are essential for accurately quantifying aquatic habitat availability based on flow and local morphology in regulated reaches [25]. This gap is rooted in a general lack of knowledge about the habitat preferences of freshwater species [26] and their specific ecological requirements [27]. Indeed, developing robust HSC generally requires significant efforts to gather and analyze empirical data on species distribution from multiple rivers, with the aim of ensuring a comprehensive coverage of diverse habitat conditions and species utilization patterns [28]. In addition to the challenge of limited HSC availability, there is still a lack of comprehensive understanding of the ecological functioning of entire river networks, particularly those branches constituted by non-perennial rivers. Major constraints include a general lack of information about the spatial distribution of flow intermittency within river networks and insufficient data on the frequency and duration of non-flowing periods [29]. Furthermore, accurately describing aquatic

habitat availability in NPRs requires the development of appropriate theoretical frameworks and analytical tools, which are still in the early stages of development. Indeed, traditional HSMs that rely on hydrodynamic modeling to define water depth and velocity parameters are inadequate for assessing habitats when surface flow approaches zero and fail to capture habitat dynamics during non-flowing periods [30].

This thesis addresses these limitations by providing new ecological data and meso-scale HSC for endemic and threatened Italian freshwater species. Furthermore, an innovative approach to identify NPRs assessing their degree of temporariness is presented [29], as well as the new module of the MesoHABSIM approach to facilitate river habitat modeling for non-perennial streams (i.e., NPRs-module).

1.1 River habitat modeling: a brief overview

River habitat modeling falls within the field of eco-hydraulics and involves simulating and analyzing the physical habitat of river ecosystems [13]. Habitat availability assessment is achieved through HSMs, which quantify the amount of suitable environment for target species or ecological communities by analyzing hydro-morphological descriptors that mainly influence species spatial distribution [31]. The conceptualization, development, and initial applications of HSMs trace back to North America in the 1970s [23]. The Physical HABitat SIMulation (PHABSIM) system, introduced by [32], is recognized as the pioneering instream HSM and continues to be widely utilized today. Since the definition of PHABSIM, numerous developments and alternative models have emerged, seeking to enhance the comprehension of the complex interplay among hydrological, geomorphological, and ecological processes within river systems. The shared assumption among all these HSMs is that the variability of the hydrological regime is influenced by the morphological characteristics of the watercourse, which provide the physical habitat for the species inhabiting the river corridor [33]. HSMs are currently acknowledged as one of the most scientifically robust and legally reliable approaches for addressing the impact of hydro-morphological alterations on river ecosystems [17]. They were specifically developed for (i) the design of e-flows to mitigate the effects of river damming and water abstraction, and (ii) the assessment of the efficacy of river restoration projects (e.g., [34], [35]). Furthermore, they can provide effective insights for driving freshwater species and ecosystems conservation programs (e.g., [17], [36]).

Despite numerous habitat suitability models exist today, HSMs share common characteristics, as they typically require (i) a hydro-morphological characterization of the river system and (ii) a habitat suitability criteria for the local freshwater fauna to assess the amount of available habitat (**Figure 1.2**). The hydro-morphological characterization of the aquatic habitat is commonly achieved by evaluating local attributes such as water depth, flow velocity, and substrate (e.g., [37], [38]).

However, more recent and sophisticated HSMs integrated additional habitat features such as the channel geometry or the presence of covers and shelters for local species (e.g., [18], [39]). These attributes are taken into account within the HSC for predicting the presence or abundance of target species, thereby assessing habitat availability. Historically, HSMs focused on fish as the target freshwater community due to their consistent and negative ecological response to hydro-morphological alterations [40]. However, certain application involved other communities, such as the macroinvertebrates (e.g., [20], [22], [41]).

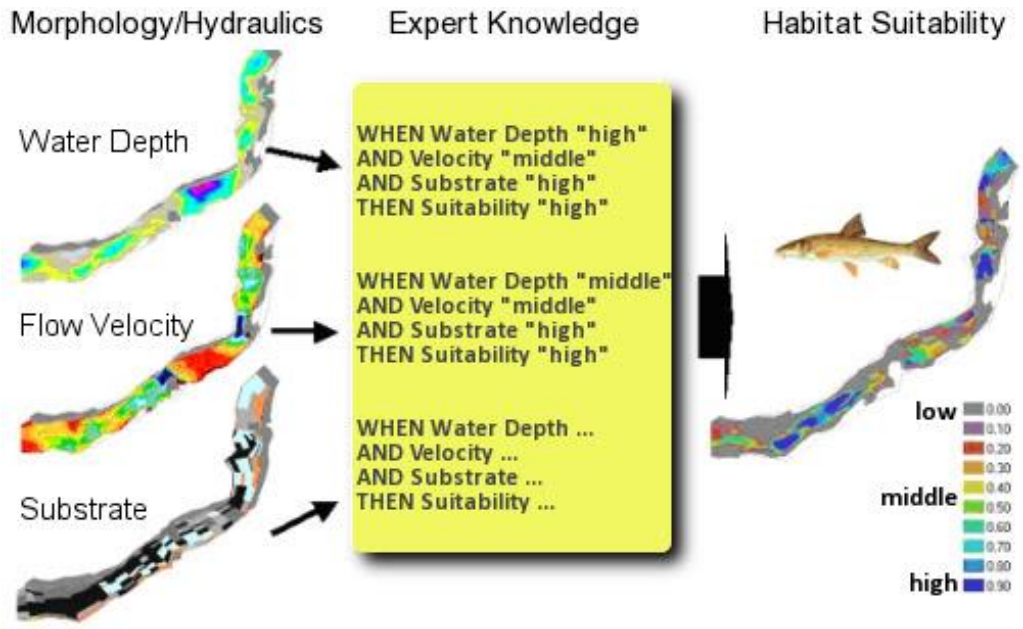


Figure 1.2. Conceptual framework of a habitat suitability model. To the hydro-morphological characterization of the river system, habitat suitability criteria for target species are applied to assess the habitat suitability (CASiMiR, [38]).

The hydro-morphological description is typically obtained through field surveys, by collecting habitat attributes under various flow conditions. To reduce field efforts or in case of not wadable conditions, many HSMs allow the definition of the hydraulic variables (such as depth and velocity) using hydrodynamic models [42]. It is possible to observe that the evolution in habitat modeling closely mirrors the advancements in hydraulic modeling software solutions and computational power. Initially, early HSMs, like PHABSIM [32], relied on cross-sectional data from simple one-dimensional hydrodynamic models. However, with the development of two- and three-dimensional hydrodynamic modeling in recent decades, HSMs have progressed to consider a more detailed spatial description of hydraulic variables, facilitating a more exhaustive assessments of the physical habitat (e.g., [43], [44]).

In recent decades, significant advancements have been also made in the statistical techniques used to define the HSC [23]. Earlier HSM, like PHABSIM [32], predominantly relied on simple univariate habitat suitability curves to establish the preferences of target species with respect to specific habitat attributes,

such as water depth or flow velocity. However, these approaches have been questioned for their limited applicability and theoretical validity (e.g., [45]). Nowadays, to better account for interaction effects between habitat attributes, more complex statistical techniques are preferred. These include logistic regression (e.g., [18]), machine learning like Random Forest (e.g., [46]) or Bayesian networks (e.g., [47]). The collection of information concerning the distribution of target species is a fundamental step in defining HSC. Such empirical HSC generally require remarkable field efforts to gather species distribution information from multiple rivers, to better captures the species-specific response to environmental variability [28]. When collecting information on species distribution in the field poses difficulties, alternative frequently used methods include decision trees (e.g., [48]) and fuzzy techniques (e.g., [49]). These approaches enable the establishment of HSC through expert knowledge or considering the information available in the literature. Although they expedite the definition of suitability criteria, they may oversimplify the relationship between species distribution and environmental features leading to inaccurate quantifications of actual habitat availability. Before their application, a local validation is therefore advisable. In this thesis, a decision tree approach was employed to delineate the HSC of the indigenous Italian vairone (*Telestes muticellus*) using a combination of literature data on species' habitat preferences and locally gathered information on fish distribution (see Chapter **2**, [26]). Nevertheless, the availability of HSC, despite its critical relevance, remains fragmented and generally focuses on the most common species or those of particular economic value (e.g., [50]). Consequently, there is a limited capacity to widely implement HSMs in regulated rivers, ensuring adequate habitat for the entire fish community, especially during the most critical life stages (i.e., juvenile and spawning periods).

Two primary approaches regarding the spatial scale of analysis in river habitat modeling have emerged: micro- and meso-scale HSMs. The earliest HSMs concentrated on the micro-scale, examining individual river elements characterized by localized attributes such as depth, velocity, and substrate. Examples include the PHABSIM [32], RHYHABSIM [51], CASiMiR [38], and River2D [52] models. These traditional microhabitat approaches have faced criticism due to their (i) extensive field data requirements, resulting from a reduced transferability of HSC, (ii) limitation in the habitat characterization, and (iii) a general lack of robust morphological assessment [53], [54]. Indeed, these HSMs often consider only a narrow range of variables (i.e., water depth, velocity) neglect factors beyond microhabitat characteristics, such as channel geometry features or the presence of nearby covers (or shelters), which can significantly influence the presence of mobile species like fish [18], [55]. Additionally, doubts persist regarding the scalability of micro-scale studies to larger spatial scales (i.e., reach-, segment- or catchment-scale, [56], as they typically lack a robust hierarchical morphological characterization.

In an attempt to overcome the main drawbacks of micro-scale models, in the last decades innovative HSMs shifted focusing to the broader meso-scale. The

meso-scale corresponds to mesohabitats which are recognized as a significative spatial components of river systems, closely tied to the life cycle of different communities [33], [57]. Prominent models at the meso-scale include the MEM [39], MesoCASiMiR [58], Norvegian Mesohabitat Method [59], and MesoHABSIM [18], [54]. These HSMs commonly utilize as the reference scale of analysis geomorphic and hydraulic units (**Figure 1.3**, [60]) which are matched to mesohabitats, enabling a more comprehensive river habitat description at an ecologically relevant spatial scale. This morphological approach for representing the aquatic habitat facilitates easier upscaling to the river segment- or catchment-scale [59]. Moreover, at the meso-scale, a broader range of habitat attributes can be incorporated into the habitat characterization. In addition to common hydrodynamic variables such as water depth and velocity, other hydraulic parameters, like the Froude number, and ecological features, like the presence of shelters from predators or stress, can also be considered [28]. Furthermore, meso-scale HSMs reduce the effort required for field data collection compared to micro-habitat models, enabling longer reaches to be surveyed [18]. Additionally, HSC developed at the meso-scale have shown potential for transferability across rivers [59].

1.2 The MesoHABSIM approach

Among the more consolidated methodologies for assessing hydro-morphological impacts on river ecosystems there is the MesoHABSIM [18] approach, which currently serves as the primary river HSM for Italy. The procedural guide for applying this methodology within the Italian context is outlined in the " Manuale tecnico-operativo per la modellazione e la valutazione dell'integrità dell'habitat fluviale" [54], published by the Italian National Institute for Environmental Protection and Research (ISPRA) This type of habitat model is endorsed at the European level by the Common Implementation Strategy Guideline No. 31 (CIS Guideline No. 31, [15]), cited as a suitable tool for defining e-flows (Case Studies No. 6 and No. 8). Additionally, it is globally acknowledged as a highly reliable HSM, as indicated in the Guidance on Environmental Flows published by the World Meteorological Organization [2]. Currently, MesoHABSIM stands as the unique HSM available in literature offering dedicated modules and tools for analyzing aquatic habitat availability in both perennial and non-perennial rivers [30], [54].

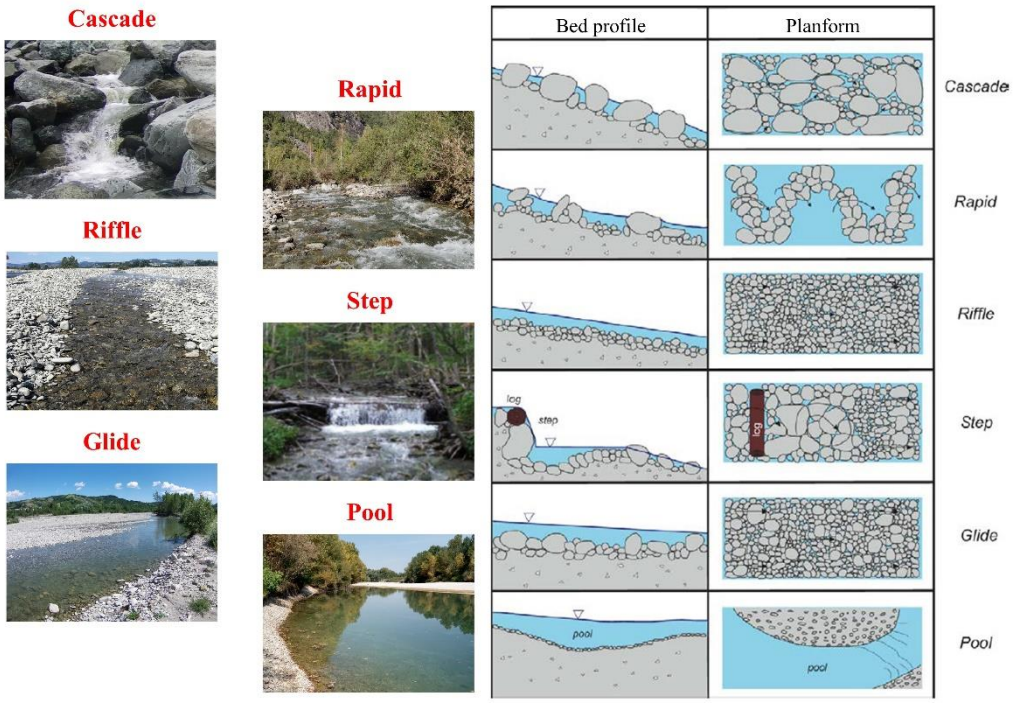


Figure 1.3. Main submerged geomorphic units of mountain alluvial bed streams considered within the MesoHABSIM approach (modified form [60]).

The MesoHABSIM approach is as a physical river HSM designed to assess the spatio-temporal variation of a designated ecological parameter (e.g., presence/absence/abundance of a species or community) with respect to the flow and local river morphology. Commonly, it operates by conducting multi-temporal stage-dependent mapping of the geomorphic and hydraulic units (GUs or mesohabitats, **Figure 1.3**, [60]) for evaluating the availability of aquatic habitat for target species. The methodology typically employs freshwater fish habitat as a practical and effective metric for quantifying the impact of hydro-morphological alterations on watercourses biocenosis. The utilization of such a physical metric, namely available habitat, serves as a proxy able to connect the local hydro-morphological conditions to the biotic components of the river ecosystem. This approach enables to evaluate, through modeling, the effects of potential hydro-morphological pressures on river ecosystems, even before they are exerted [54].

The MesoHABSIM methodology can be understood by examining its breakdown into three primary macro-components (**Figure 1.4**):

a) The characterization of physical habitat through a hierarchical hydro-morphological assessment.
b) The use of habitat suitability criteria to quantify the habitat availability at surveyed flow conditions.
c) The analysis of the spatio-temporal variations in the available habitat for a target species or community.

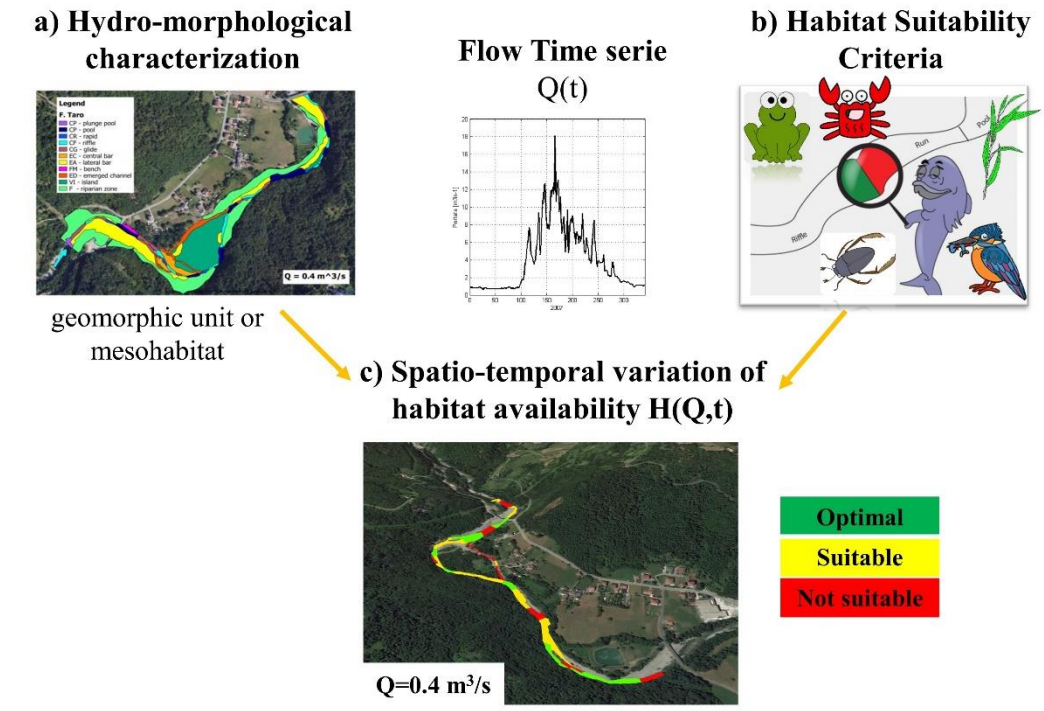


Figure 1.4. Conceptual framework of the MesoHABSIM approach with the three macro-components.

The characterization of rivers physical habitat relies on a robust hierarchical hydro-morphological classification structure [56], [60]. This hierarchical framework allows the segmentation of the river network by analyzing key morphological variables and metrics across different scales, from the catchment- to the micro-scale (**Figure 1.5**). The MesoHABSIM approach primarily considers scales from the reach (10^2-10^4 m) to the geomorphic and hydraulic units (10^{-1}-10^2 m), the latter represents the meso-scale. According to [56] and [61], a hydro-morphologically homogeneous river reach is defined based on several factors (i) its riverbed morphology (including channel pattern and level of confinement), (ii) notable discontinuities in controlling variables (such as flow rates and slopes), and (iii) the sediment type which characterized the riverbed. This morphological description generally implies a broad characterization of the geomorphic and hydraulic units present (presence/absence of GUs characterizing a given morphology) within the river reach. Indeed, each morphological type (e.g., single-channel sinuous, braided, meandering), within certain limits, displays a particular GUs mosaic, whose assemblage is the result of the processes that have generated that particular local morphology. These processes are influenced by different guiding variables and boundary conditions operating at broader spatial and temporal scales [61].

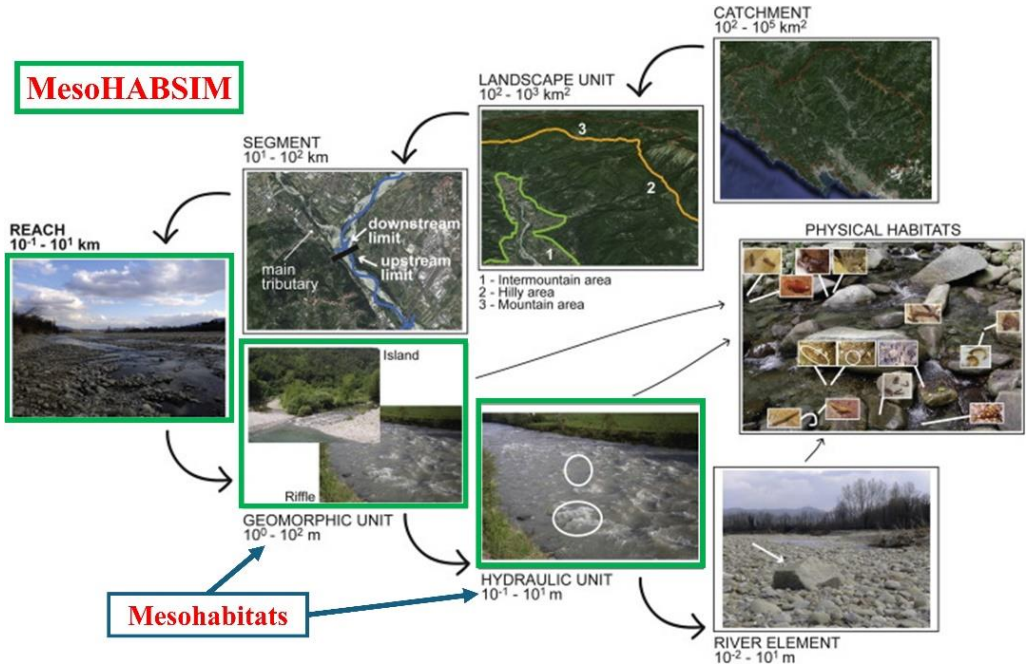


Figure 1.5. Hierarchical morphological classification structure from the catchment scale to the river element. The mesohabitats correspond to the geomorphic and hydraulic units (modified from [60]). The reference spatial scales of the MesoHABSIM approach are highlighted in green.

According to the MesoHABSIM approach, a wide array of habitat attributes (wetted area extension, frequency distributions of depth and velocity, substrate typology and size, water surface mean gradient, presence of cover and shelters from physical stresses or predators, **Table A-1**) is employed to characterize the GUs, representing the physical habitat at local flow conditions. Such habitat attributes can be obtained through field surveys, which constitute the more consolidated method [54], or derived from spatial information acquired through proximal sensing and obtained with hydrodynamic modeling. The latter approach is particularly effective for large rivers or non-wadable river reaches (e.g., [62]). In this thesis, it is utilized in Chapter **4** and **7** to depict the physical habitat of the Tagliamento and Sangone rivers (Northern Italy).

Habitat assessment is achieved through the use of particular HSC. These HSC, defined by a specific combination of environmental descriptors at the meso-habitat scale (**Table A-1**), enable the assessment of the available habitat based on the prediction in terms of presence or abundance of target species within the GUs. Currently, the MesoHABSIM methodology encompasses HSC for the most common Italian autochthonous fish species [21], [63]. These HSC, within this thesis, were tested in terms of transferability, in order to evaluate their validity within the domain of Northern Italy (see Chapter **5**, [25]). Furthermore, thanks to this thesis, novel HSC were developed for the freshwater Po brook lamprey (*Lampetra zanandreai*, see Chapter **3**, [19]) and the spawning period of the anadromous Twaite shad (*Alosa fallax*, see Chapter **4**). Such HSC were defined using the Random Forest (RF, [64]) classifier algorithm, a machine learning technique widely employed in ecology [65]. This technique already proved its

effectiveness in modeling freshwater species distribution (e.g., [46]) demonstrating higher performances compared to other statistical approaches in predicting the presence and abundance of fish within GUs (e.g., [66]).

By identifying GUs through field surveys that are deemed suitable or optimal by the application of the HSC, it becomes possible to calculate the available habitat for the target species. In the presence of multiple river surveys at different flow conditions, the relationship between the habitat and the discharge can be represented through the habitat-flow rating curve, which encompass the amount of suitable wetted area for freshwater fauna at the river reach scale. By integrating the habitat-flow rating curve with a flow time series, it becomes feasible to examine both the spatial and temporal fluctuations of the aquatic habitat availability. Such variation is represented by the habitat time series (**Figure 1.6**, [67]), which represent habitat variation over time and can be statistically analyzed to comprehend most stressful events for freshwater species [48].

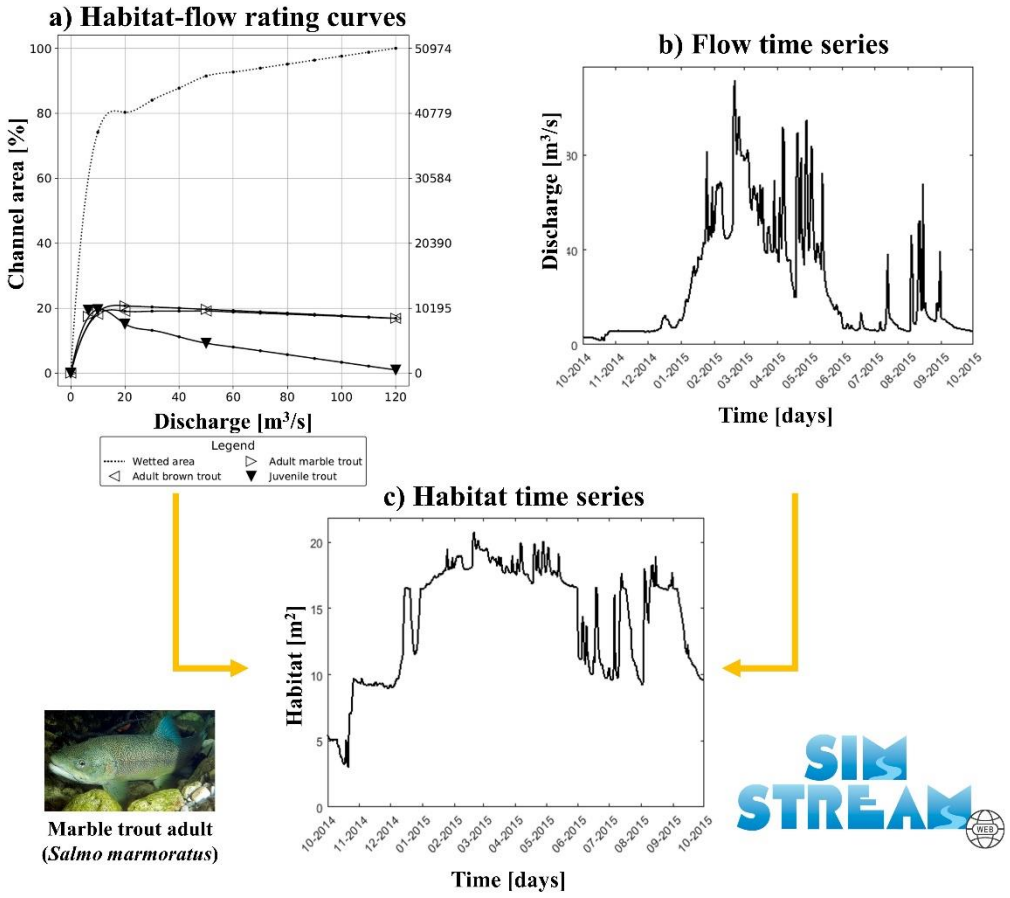


Figure 1.6. a) An example of habitat-flow rating curves obtained using the SimStream-Web service (https://mesohabsim.isprambiente.it/app/home/) by applying the MesoHABSIM approach to a regulated river reach. b) One-year natural flow time series for the considered river reach. c) Corresponding habitat time series for the adult Marble trout (*Salmo marmoratus*) selected as target species.

In practical applications of the MesoHABSIM methodology within the Italian context, the statistical analysis of the habitat time series is performed using the Habitat Integrity index (IH index, [54]). The IH index, comprising two sub-indices: the Index of Spatial River Habitat Availability (ISH index) and the Index of Temporal River Habitat Availability (ITH index), is finalized to assess the hydro-morphological impacts of water abstractions on river ecosystems. The IH index is derived by comparing two hydrological conditions: the reference state, representing the natural condition of the system (pre-impact), and the altered state, reflecting the modified condition of the system (post-impact). Both hydro-morphological conditions are evaluated based on habitat time series averaged on a daily basis. This comparison, by evaluating different hydrological release scenario, can enable the definition of e-flows according to CIS Guideline No. 31 [15]. In particular, the ISH index assesses the average habitat loss for a target species in response to a particular impact (e.g., the presence of a dam), while the ITH index measures the duration of limited habitat availability, leading to stressful conditions for the target species or community [68]. The final value of the IH index is derived from the scores assigned to the two sub-indices, ISH and ITH. It is calculated as the minimum value between ISH and ITH, ranging from 0 to 1. In this scale, 0 indicates a very high degree of alteration in river habitat quality, while 1 signifies no alteration, indicating habitat quality aligning with the reference condition (absence of hydro-morphological alteration). The IH index has been categorized into 5 distinct habitat integrity classes (POOR, LOW, MODERATE, GOOD, HIGH) in accordance with the Water Framework Directive (WFD) standards (**Figure 1.7**).

The IH index was recently utilized as an environmental index in a multi-criteria decision-making process for water abstraction licensing for hydropower purposes in the Valle d'Aosta Region (Northwestern Italy). This application demonstrated the potential for integrating the Italian habitat suitability reference method into holistic approaches [69] for defining optimal e-flow scenarios to be released by hydropower plant, aiming at balancing the requirements of energy production, economic viability, and environmental conservation (see **Appendix C**, [70]). Another effective application of the MesoHABSIM approach and the IH index concerned the evaluation of how the combined effect of climate change and flow regulation related to hydropower generation affect fish habitat availability in Lithuanian rivers (see **Appendix C**, [71]).

To enhance the application of the MesoHABSIM approach, the recently developed SimStream-Web (https://mesohabsim.isprambiente.it/app/home/) service has been made available. This free of charge service enables the quantification of habitat availability for target species, communities, or life stages in both perennial and non-perennial rivers. It automatically generates various outputs, including geo-referenced habitat maps in shapefile format, habitat-flow rating curves, and habitat time series. Additionally, for projects focusing on e-flow design, the service computes the Habitat Integrity index (IH) associated with one or more hydrological or morphological management scenarios at the reach, segment, or catchment scale.

IH	Classes
IH ≥ 0.8	HIGH
0.6 ≤ IH < 0.8	GOOD
0.4 ≤ IH < 0.6	MODERATE
0.2 ≤ IH < 0.4	LOW
IH < 0.2	POOR

Figure 1.7. Habitat integrity classes for the IH index considered within the MesoHABSIM approach.

1.3 Non-perennial rivers (NPRs)

According to the WFD, non-perennial rivers (NPRs) are defined as watercourses that may dry up for some period of time within the year, encompassing various degrees of intermittency, ranging from rivers with episodic water presence to quasi-perennial streams [72]. [73] identified three primary hydrological conditions which essentially characterized NPRs: flowing, ponding, and dry conditions (**Figure 1.8**). The flowing condition indicates a continuous surface flow within the river channel. In contrast, the ponding condition describes the presence of water within the river channel organized into disconnected pools (i.e., isolated ponds), when surface flow is zero. A dry condition implies the absence of the water.

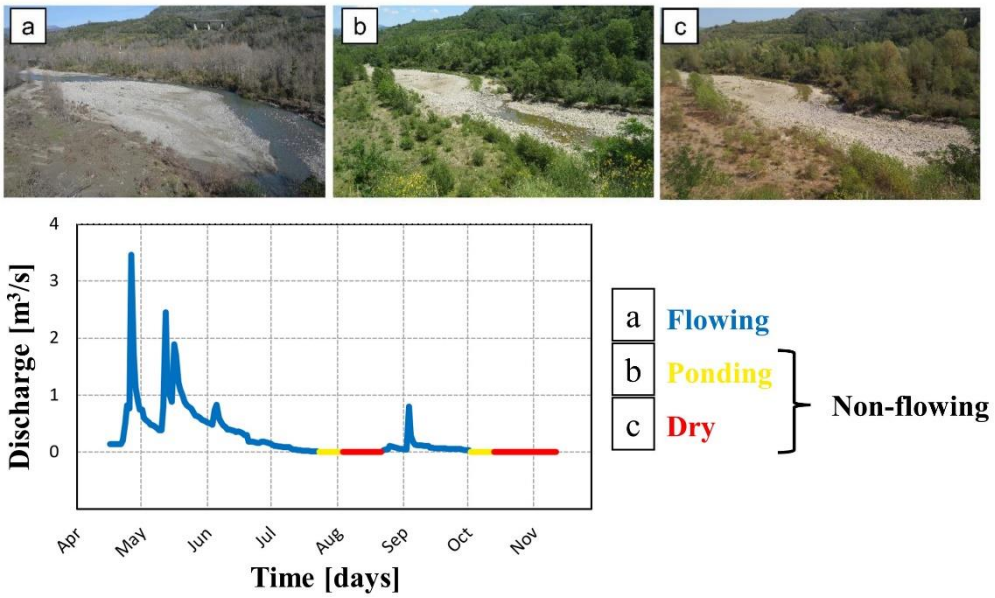


Figure 1.8. Overview of the three different hydrologic conditions that may occur in NPRs: a) flowing, b) ponding, and c) dry. The pictures represent a reach of the Sciarapotamo river, located in the province of Salerno (Southern Italy).

NPRs are considered ubiquitous watercourses, constituting over 50% of the global stream network [74]. However, flow intermittency is projected to increase in future scenarios due to various anthropogenic pressures, including climate change and increased water withdrawals (e.g., [75], [76]). Over the past five decades, major rivers such as the Nile, Yellow, Indus, and Colorado, previously known for being perennial, have experienced non-flowing conditions in some reaches [77]. This phenomenon has recently also affected the Po river, Italy's principal river, where totally dry conditions were observed in some reaches of its upper course at the foot of the Alps [78].

NPRs are recognized to play essential roles in groundwater regulation, support unique aquatic and riparian species, and maintain biogeochemical integrity. They provide a multitude of ecosystem services essential for environmental health and human well-being [72], [79].

Despite their importance and wide spatial distribution, NPRs often suffer from a lack of public awareness regarding their role within river networks (e.g., [80]). Consequently, legislation, such as the WFD which aims to protect all water bodies, often overlooks a several number of NPRs as they belong to small catchments (< 10 km^2). This exclusion highlights a gap in regulatory frameworks, which hindered effective management practices crucial for preserving the ecosystems and services provided by NPRs [81].

Similarly to the legislative gaps, NPRs typically lack an adequate monitoring network, resulting in a scarcity of natural flow data from conventional gauging stations and limited information on the spatio-temporal distribution of flow intermittency within the river network [74]. Furthermore, hydrological modeling currently struggle to accurately predict flow discharge variability in NPRs [73]. They tend to overestimate zero-flow events as modeling surface-groundwater interaction in these environments is challenging. Consequently, these constraints commonly hinder the establishment of appropriate e-flows necessary for preserving such ecosystems, even with the more simplistic hydrological methods [30]. Recently, advancements in sensor technology have enabled pioneering studies to estimate the flow intermittency in river networks using satellite data (e.g., [29], [82]). These approaches seems promise for characterizing NPRs regimes as they can efficiently monitor large areas with high temporal resolutions in a cost-effective manner. In this thesis, an approach utilizing a supervised classification of freely available Sentinel-2 multispectral images is presented to identify NPRs and to assess their degree of temporariness according to the duration of local hydrological conditions (**Figure 1.9**, see Chapter **6**, [29]).

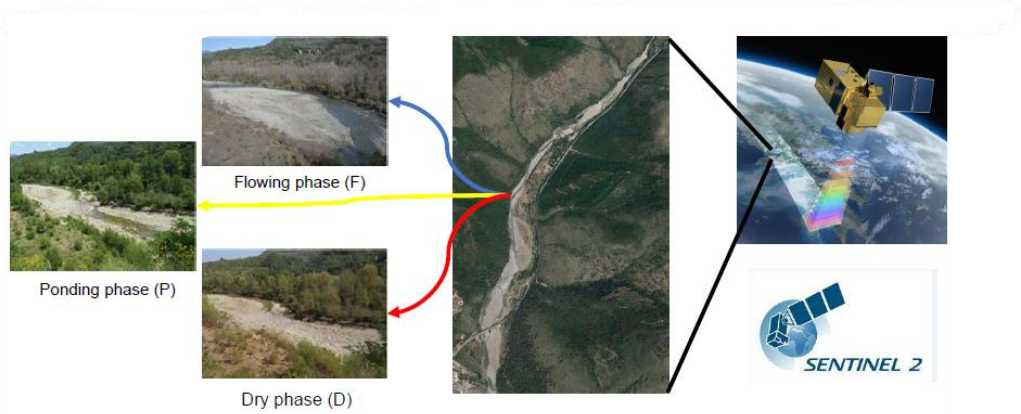


Figure 1.9. Conceptual framework for the identification of the hydrological conditions in NPRs using Sentinel-2 satellite images [29]. The pictures corresponding to different hydrological conditions represent a reach of the Sciarapotamo river, located in the province of Salerno (Southern Italy).

NPRs have been largely disregarded in river habitat modeling due to the challenges in assessing and characterizing their aquatic habitat dynamics. Traditional HSMs, which depend on hydrodynamic modeling for defining water depth and velocity variables, pose limitations, especially when flow approaches zero or when aquatic habitat fragments into isolated pools (ponding condition, [30]. After flow cessation, indeed, water surfaces moves into isolated wetted areas that still offer a potentially suitable habitat for freshwater species [83].

To address these shortcomings, the MesoHABSIM approach has been enhanced with a new module designed specifically to model habitat dynamics in NPRs (NPRs-module), encompassing both flowing and non-flowing periods [30]. This innovative NPRs-module is presented within this thesis in Chapter **7**, demonstrating its applicability to an intermittent regulated reach of the Sangone river (Northwestern Italy).

1.4 The MesoHABSIM module for non-perennial rivers (NPRs-module)

To assess aquatic habitat availability during both flowing and non-flowing conditions, within the framework of the MesoHABSIM approach (paragraph **1.2**), a new NPRs-module was recently developed to specifically model and evaluate fish habitat evolution depending on flow and time passed after discharge interruption.

Similar to the approach used for perennial rivers, this NPRs-module enables the definition of e-flows for regulated NPR reaches, using the Habitat Integrity index (IH index, [54]). Integrated into the SimStream-Web service to facilitate its implementation, it is substantially based on the same three macro-components of the module for perennial rivers, presented in the previous paragraph **1.2**.

For the NPRs case, additional field efforts may be necessary for characterizing their physical habitat. Specifically, surveys conducted during non-flowing periods are important to describe aquatic habitat evolution after flow ceased. Moreover, it

is critical to determine if and when the considered river reach moves to a completely dry condition. For reaches where local hydro-geo-morphological factors prevent the river reach from drying completely between subsequent flowing conditions, the NPRs-module allows for consideration of a permanent ponding condition where remaining pools and ponds are considered to never disappear between subsequent flowing conditions.

The interplay between flow, time and habitat availability is elaborated by means of the construction of a particular rating curve able to consider simultaneously the intermittent behavior of aquatic habitat availability. In particular, the computed habitat values achieved after applying a HSC to the hydro-morphological information collected in the field are interpolated by using a mathematical spline function to represent the evolution of aquatic habitat during both flowing and and-flowing conditions. This curve directly derives from the habitat-flow rating curve of common HSMs, to which, on the second quadrant of the graph, is added the recession of wetted area and habitat availability with respect to the amount of time after flow interruption. The resulting curve is named habitat-flow-time rating curve (**Figure 1.10**). The definition of this curve lead to the generation of the habitat time-series (**Figure 1.6**) for NPRs that enables analyzing the spatio-temporal variation of aquatic habitat availability in this ecosystems. Similarly to the perennial river case, this series are considered for the computation of the IH index corresponding to a particular hydrological release scenario.

Figure 1.10 illustrates an example of a habitat-flow-time rating curve for a morphologically homogeneous [56] NPRs reach. In the first quadrant (in blue), both aquatic habitat and wetted area consistently increment as the flow increases. Conversely, in the second quadrant representing the non-flowing condition, the river reach achieves a completely dry condition after 6.2 days since the flow ceased. During this period, corresponding to the ponding condition, both wetted area and available habitat monotonically decrease.

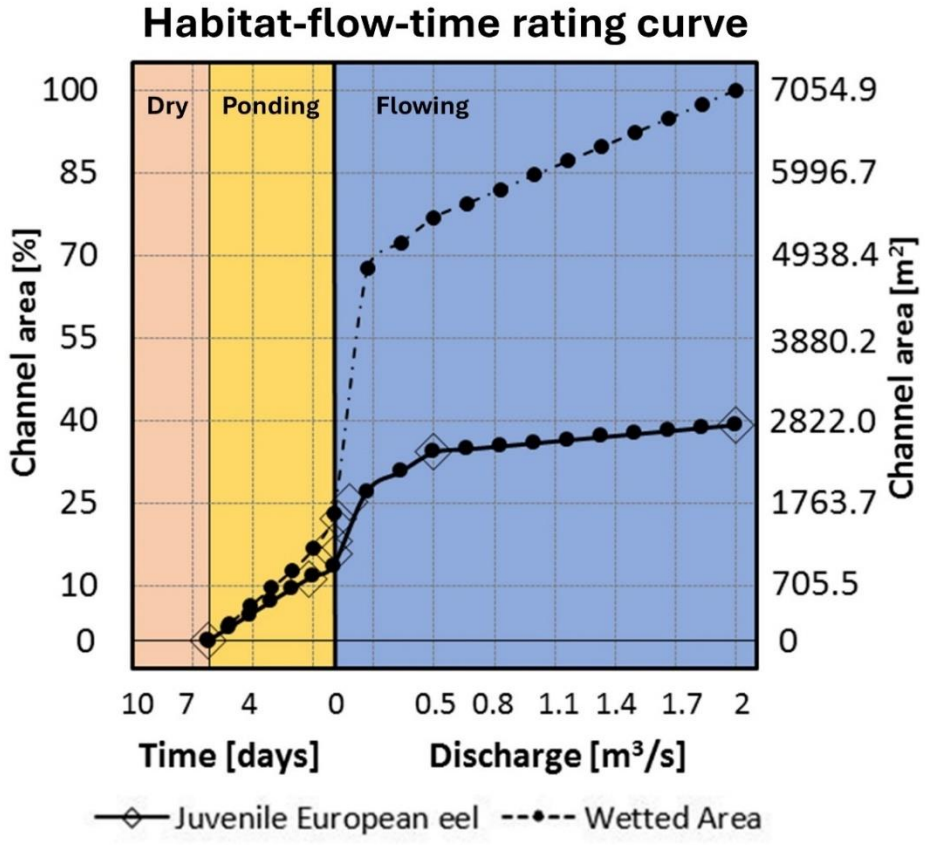


Figure 1.10. An example of the habitat-flow-time rating curves of the new module of the MesoHABSIM approach dedicated to NPRs. Evolution of total wetted area (% or m^2) and available habitat (% or m^2) for a target species (juvenile European eel, *Anguilla anguilla*) per discharge and time. In pink is highlighted the dry, in yellow the ponding, in blue the flowing conditions.

1.5 Thesis contents

The following thesis is divided into two parts:

1. **Part I**, composed of Chapter **2**, **3**, **4** and **5**, mainly regards the developments I contributed to concerning the development and validation of meso-scale HSC for Italian endemic freshwater species in perennial rivers.
   In Chapter **2**, the current knowledge on habitat preferences of autochthonous Italian freshwater fish is investigated through a literature review. The species for which more researches are required are clearly highlighted [26].
   In Chapter **3**, following what emerged from previous Chapter **2**, a meso-scale HSC for the endemic Po brook lamprey (*Lampetra zanandreai*) was defined. This represents the first application of the MesoHABSIM approach for riverine lampreys [19].
   In Chapter **4**, following what emerged from previous Chapter **2**, a meso-scale HSC for the spawning period of Twaite shad (*Alosa fallax*) was developed. This represents the first application of the MesoHABSIM approach for an anadromous species during the spawning period.
   In Chapter **5**, five HSC for Italian freshwater fish, previously developed and made available in the SimStream-Web service for applications of the MesoHABSIM approach, were tested in terms of transferability among different rivers across Northern Italy [25].

2. **Part II**, composed of Chapter **6** and **7**, specifically regards my personal contributions concerning non-perennial rivers.
   In Chapter **6**, a novel approach for estimating the spatio-temporal distribution of flow intermittency and NPRs hydrological regimes by exploiting satellite data is presented [29].
   In Chapter **7**, from the findings of Chapter **6**, the developments performed for adapting the MesoHABSIM approach to non-perennial rivers are presented by the application of the innovative NPRs-module to a regulated reach of the Sangone river (Northwestern Italy).

At the conclusion of the document, two appendix offer supplementary details for some Chapters of the thesis. The last appendix provides additional studies in which I contributed during my PhD (i.e., [70], [71]). For brevity, only the abstracts of these published papers are reported in this document.

1.6 Novel contributions

- G. Negro, S. Fenoglio, E. Quaranta, C. Comoglio, I. Garzia, and P. Vezza, "Habitat Preferences of Italian Freshwater Fish: A Systematic Review of Data Availability for Applications of the MesoHABSIM Model," *Frontiers in Environmental Science*, vol. 9. Frontiers, p. 305, Jul. 27, 2021, doi: 10.3389/fenvs.2021.634737.
- G. Negro *et al.*, "Ecological notes on an endemic freshwater lamprey, Lampetra zanandreai (Vladykov, 1955)," *Eur. Zool. J.*, vol. 90, no. 2, pp. 556–567, 2023, doi: 10.1080/24750263.2023.2226680.
- G. Negro *et al.*, "Transferability of Mesohabitat Suitability Criteria in Northern Italy," in *Proceedings of the IAHR World Congress*, 2022, pp. 1416–1423, doi: 10.3850/IAHR-39WC2521716X20221044.
- C. Cavallo, M. N. Papa, G. Negro, M. Gargiulo, G. Ruello, and P. Vezza, "Exploiting Sentinel-2 dataset to assess flow intermittency in non-perennial rivers," *Sci. Rep.*, vol. 12, no. 1, pp. 1–16, Dec. 2022, doi: 10.1038/s41598-022-26034-z.
- E. Vassoney, A. Mammoliti Mochet, E. Desiderio, G. Negro, M. G. Pilloni, and C. Comoglio, "Comparing Multi-Criteria Decision-Making Methods for the Assessment of Flow Release Scenarios From Small Hydropower Plants in the Alpine Area," *Front. Environ. Sci.*, vol. 9, p. 635100, Apr. 2021, doi: 10.3389/fenvs.2021.635100.
- V. Akstinas *et al.*, "The combined impact of hydropower plants and climate change on river runoff and fish habitats in lowland watersheds," *Water (Switzerland)*, vol. 13, no. 24, p. 3508, Dec. 2021, doi: 10.3390/w13243508.

Chapter **4** an **7** will form the basis for other journal publications.

PART I: meso-scale habitat suitability criteria in perennial rivers

Chapter 2

2. Habitat Preferences of Italian Freshwater Fish

The work presented in this chapter has been partially derived from [26].

2.1 Introduction

Preserving freshwater ecosystems is one of the most difficult challenges humans face globally. Although these ecosystems provide crucial services to society, they are one of the world's most threatened environments [5]. Hydrological and morphological alterations related to water abstractions and hydropower generation are identified as high impact pressures causing degradation of river ecosystems and biodiversity loss [6]. Since the 1980s, Habitat Suitability Models (HSMs), such as PHABSIM [32], have been promoted and applied to enhance water resources management and preserve aquatic ecosystems. Among these models, the recent MesoHABitat SImulation Model (MesoHABSIM, [84]), has proven to be adequate for assessing habitat availability for riverine fish [17]. The MesoHABSIM model, commonly, uses habitat suitability criteria (HSC, or species distribution models) to predict the amount of available habitat for a certain species or life stage in regulated rivers [28]. The HSC can be built using empirical data collected in environmental reference sites with natural conditions of river morphology, flow regime, fish community composition [63], [85]. Alternatively, these criteria can be derived by collecting available information from the literature or using expert knowledge [28], [48]. Despite its critical relevance, the availability of such information is still scattered and limited to the most common species or those of particular economic value (e.g., [50]). This results in a reduced capacity to widely implementing HSMs in regulated rivers, to ensure adequate habitat for the entire fish community, especially for the most critical life stages.

Starting from 2017, HSMs have been increasingly used in Italy. The Decrees n. 29/STA-13.02.2017 and n. 30/STA-13.02.2017 of the Ministry for Environment, Land and Sea Protection established the MesoHABSIM as a reference method for ecological flows design and impact assessment of water abstractions [54]. MesoHABSIM is a methodological approach that uses geomorphic and hydraulics units (GUs or mesohabitats, [60]) as the spatial unit of analysis. After segmenting the river into homogeneous hydro-morphological reaches, a multiple, stage-dependent description of GUs provides basic maps, which are used to calculate the spatio-temporal variation in aquatic habitat availability. Standardized data collection is required to describe GUs in terms of wetted area, frequency distribution of water depth, flow velocity and substrate, presence of covers/shelters, water surface gradient, Froude number and velocity standard deviation.

With the aim of improving the applicability of the MesoHABSIM approach in the Italian territory, we carried out a systematic review focused on physical habitat preferences for 31 freshwater fish species and three freshwater lampreys of Italian rivers. Collected information was organized into a nationwide database and summarized using the MesoHABSIM protocol and standards. As an example of application, two literature-based HSC for adult and juvenile life stages of Italian vairone (*Telestes muticellus*) were built and used to assess fish habitat availability in a regulated reach of the Argentina Creek (Province of Imperia, NW Italy). This analysis demonstrates the potential for applying information from the current review to other fish species.

2.2 Materials and methods

2.2.1 Literature review

In an effort to develop quantitative relationships between physical habitat conditions and the distribution of autochthonous Italian fish species, we reviewed 250 bibliography sources published over the last 8 decades, describing habitat preferences of 34 autochthonous freshwater species (31 Osteichthyes and 3 Petromyzontiformes). These species (**Figure 2.1**) represent the 75% of the total indigenous freshwater fish community of Italy [86]. Due to the scope of the study, we focused exclusively on riverine species. As habitat use by freshwater fish shifts during their life cycle [87], we explored information on habitat requirements for two main life stages (adult and juvenile) and two bioperiods (rearing/growth and spawning). For catadromous and anadromous species (e.g., *Anguilla anguilla* and *Alosa fallax*), we considered only the freshwater phase of corresponding life cycles. Furthermore, to simplify the data analysis, the juvenile stage of freshwater lampreys was associated to the ammocoetes phase.

We exclusively considered researches performed in European rivers within the distribution area of the species as defined in [88]. For Salmo trutta, we tried to purely focus to the Mediterranean/Adriatic lineage (Adriatic lin., [89]) by exploring only researches performed within the circum-Mediterranean basins of Europe. To

collect all available information, publications concerning 1) fish habitat preferences/use, 2) species HSC, and 3) autecological studies at different spatial scales (micro-, meso-, and macro-scale) were considered as suitable for the present study and reliable sources of information. Four habitat attributes, largely recognized as mainly influencing the patterns of habitat use by freshwater fish in rivers [18], were considered as target physical habitat attributes: 1) water depth, 2) current velocity, 3) biotic/abiotic substrates, 4) covers/shelters. For water depth and velocity values, a source was included in the database only if quantitative information was present and, for every species, the entire range of reported values was considered. Concerning substrates and covers/shelters, the review revealed a significant difference in the classification and taxonomy adopted in each source. Therefore, prior to the database compilation, a standardizing process was implemented to ensure data consistency. It is important to highlight that a source could provide information for more than one species, life stages, bioperiods or attributes at once. The sources search was mainly carried out by leveraging the database of Web of Knowledge, Scopus and Google Scholar, as well as exploring the grey literature. Literature screening was achieved by using as search strings a combination of species' scientific/common names, both in English and Italian language, and several habitat-related statements (**Table 2-1**).

2.2.2 Data Analysis

The collected information were stored in a nationwide, easily accessible database, keeping track of the corresponding bibliography source, year of publication, river or study area, species, life stage, bioperiod. These data were then summarized into species-specific boards and organized according to life stages and bioperiods. During this step, habitat attributes were systematically stored and noted according to the MesoHABSIM protocol and standards (see **Table A-1** for details). Specifically, water depth and velocity values were processed according to their frequency distribution and split in nine categories, respectively in 15 and 15 cm/s increments (range 0–120 cm, or cm/s, and above). Data on biotic/abiotic substrates were regrouped into 12 categories, following the classification proposed by [90], as reported in the MesoHABSIM standards. Finally, information concerning covers/shelters were summarized into 11 categories [54].

For each species, life stages, bioperiods, and for every single category of the habitat attributes, it was therefore possible to calculate the number of sources reporting the same information. In this way, we could quantify the current available knowledge on habitat preferences of Italian freshwater fish and to estimate the preferred categories of habitat attributes for each species. Species or life stages for which information on habitat preferences were rare or not available were clearly derived and highlighted (**Figure 2.1**).

Table 2-1. Search strings used for the database screening. All possible combinations of species' scientific/common names both in English and Italian language and the following habitat-related statements were used.

Species' scientific/common names		**Habitat-related statements**
species scientific name (e.g., *Anguilla anguilla*)	+	habitat preferences
species common name in English (e.g., eel)	+	habitat use
species common name in Italian (e.g., anguilla)	+	habitat selection
	+	habitat requirements
	+	habitat
	+	microhabitat
	+	mesohabitat
	+	macrohabitat
	+	habitat suitability curves
	+	biological model
	+	species distribution model
	+	habitat model
	+	biology
	+	life cycle
	+	reproduction
	+	spawning
	+	adult habitat
	+	juvenile habitat
	+	spawning habitat
	+	depth preferences
	+	flow velocity preferences
	+	substrate preferences
	+	cover preferences

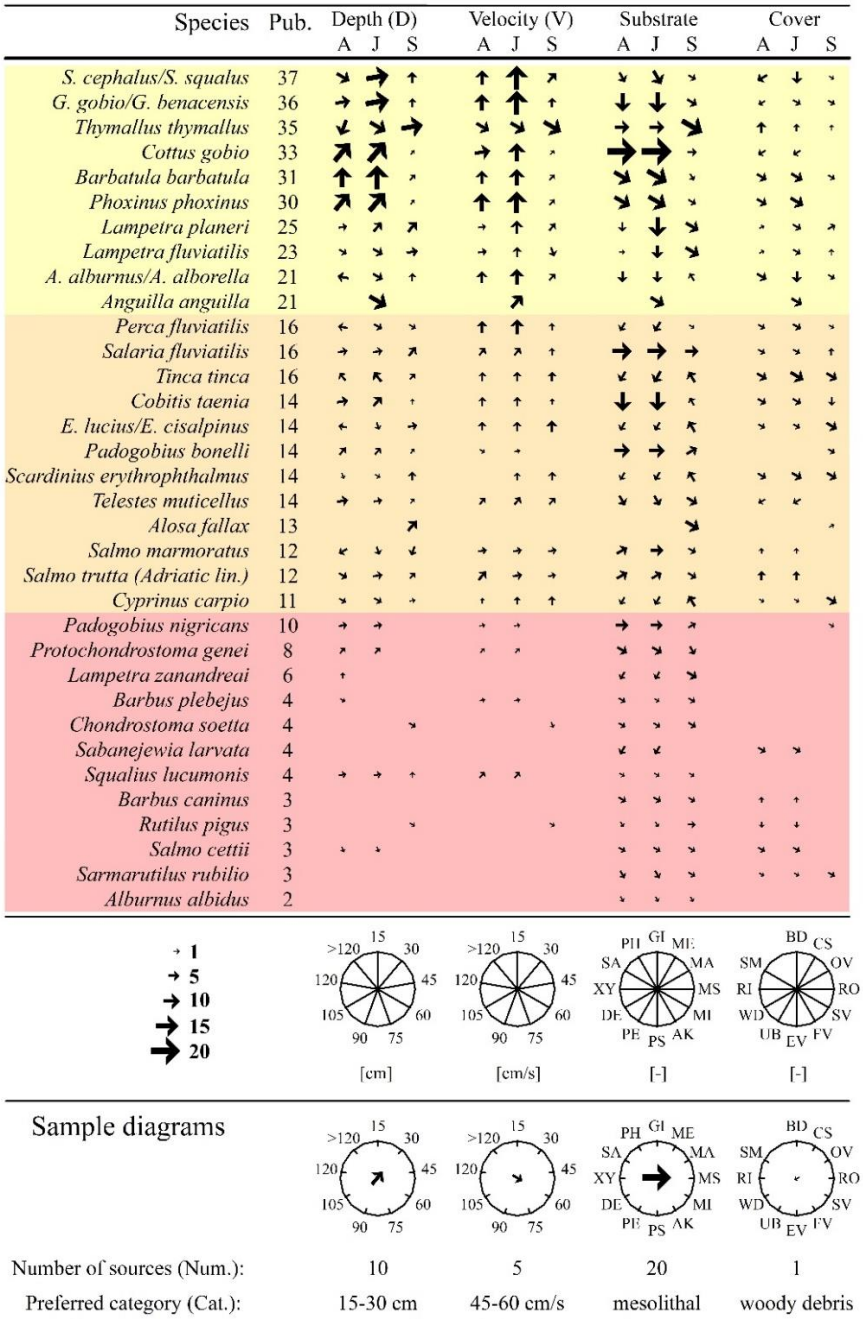


Figure 2.1 List of autochthonous Italian freshwater species included in the study. The orientation of the arrows suggests the preferred category (Cat.) of habitat attributes for each species, life stage (A = adult, J = juvenile) and bioperiod (S = spawning), and the size expresses the corresponding number of sources (Num.) reporting the same information. For a clearer depiction of the result, species are sorted according to the corresponding number of bibliography sources found (Pub.). Background colors are used to highlight the three groups of species: species with quite copious information (yellow), species with limited available data (orange), and species with very poor information (red). Water depth (D) and current velocity (V) are represented by nine categories of 15 cm (from 0 up to >120 cm) and 15 cm/s (from 0 up to >120 cm/s) respectively. Substrate categories codes: GI, *gigalithal*; ME, *megalithal*; MA, *macrolithal*; MS, *mesolithal*; MI, *microlithal*; AK, *akal*; PS, *psammal*; PE, *pelal*; DE, *detritus*; XY, *xylal*; SA, *sapropel*; PH, *phytal*. Covers/shelters categories codes: BD, boulder; CS, canopy shading; OV, overhanging vegetation; RO, roots; SV, submerged vegetation; FV, floating vegetation; EV, emerging vegetation; UB, undercut bank; WD, woody debris; RI, riprap; SM, shallow margins. For a better understanding, sample diagrams are given at the bottom of the Figure. The numerical values depicted as oriented arrows are reported in **Table B-1**.

2.2.3 Application of the MesoHABSIM model

With the aim of highlighting the capabilities of the current review, two HSC were developed for adult and juvenile life stages of *T. muticellus* for their application in the MesoHABSIM modeling approach (**Figure 2.2**A,D). The information collected from literature was used to define conditional HSC, according to the indications reported in [28]. Two binary presence/absence models were designed to distinguish between suitable and not suitable mesohabitats and depicted, for clarity, using decision trees (see e.g., [48]). The conditional models were built using the highest frequencies of habitat attributes reported in the literature. In addition, the mesohabitat was considered as suitable by imposing that at least 25% of the mesohabitat area should be characterized by a certain range of water depth, velocity, substrates, and a certain category of covers/shelters. The developed models were applied to a regulated reach of the Argentina Creek (Province of Imperia, NW of Italy), where geo-spatial information on GUs composition and empirical data on fish community were available.

In 2015 a complete application of the MesoHABSIM methodology [54], [91] was carried out in the Argentina Creek (UTM 32N E: 406391.00 m; UTM 32N N:4865963.25 m, NW Italy) to assess the environmental impact of a hydropower plant. From this data collection campaign, we extracted two hydro-morphological surveys carried out at 0.25 m^3/s and 2.2 m^3/s, which correspond to typically low (90-percentile of flow duration curve) and medium (25-percentile of flow duration curve) discharge conditions of the Argentina Creek. Together with the river survey at the lowest flow condition (0.25 m^3/s), a quantitative fish data collection was performed at the mesohabitat scale to describe fish species distribution (presence/absence). GUs and fish data collection was carried out following the MesoHABSIM protocols and standards [63]a;[54]. In particular, by using the multi-scale characterization procedure proposed by [56] and [60], it was possible to identify a morphologically homogeneous reach downstream the hydropower plant. A study site (sub-reach) was then selected and the GUs description was based on a mobile mapping technique defined in [54], [91]. This technique is based on the use of a rangefinder (TruPulse 360B, Laser Technology, Inc.), a rugged PC (Nomad TDS, Field Environmental Instruments, Inc.) and a Geographic Information System (GIS) software to properly record the GUs with all their habitat attributes (see **Table A-1**). In particular, by walking downstream, the GU areas were delineated and stored in a GIS environment, and the mesohabitat-scale features (GU type, GU longitudinal connectivity, GU gradient, presence of covers/shelters, shores characteristics) were recorded. Coming back upstream, depth and velocity values were measured using a flow meter (Marsh McBirney Flo-Mate 2000) and substrate composition were assessed from each of the mapped mesohabitats [91]. Finally, flow measurements were performed at the beginning and the end of each survey. The two river surveys permitted to outlined 56 GUs, 37 GUs at 0.25 m^3/s and 19 GUs at 2.2 m^3/s. Fish data were collected by sampling 20 GUs within the study site with backpack electrofishing (i.e., two-pass removal method, [92]) at the lowest flow condition (0.25 m^3/s). To ensure the direct association between sampled GUs

and the captured fish species, each mesohabitat was kept separated by using nets [63]. Collected fish were recognized at species level, measured in terms of total length (TL) and successively released within the same sampled mesohabitat. In total, 424 fish were captured, most of which were Italian vairone (*Telestes muticellus*, 317), classified as adult or juvenile according to the length/age relationships reported in [21].

This information was then used to validate the prediction performances of the developed HSC for adult and juvenile *T. muticellus*. The validation was evaluated using four performance metrics, i.e., accuracy, sensitivity, specificity, and true skill statistic (TSS), which are commonly used for HSC [46] (see **A.3** for further details). The validated presence/absence models were finally applied and the habitat availability for adult and juvenile *T. muticellus* was calculated at the two considered discharges (**Figure 2.2**B,C,E,F).

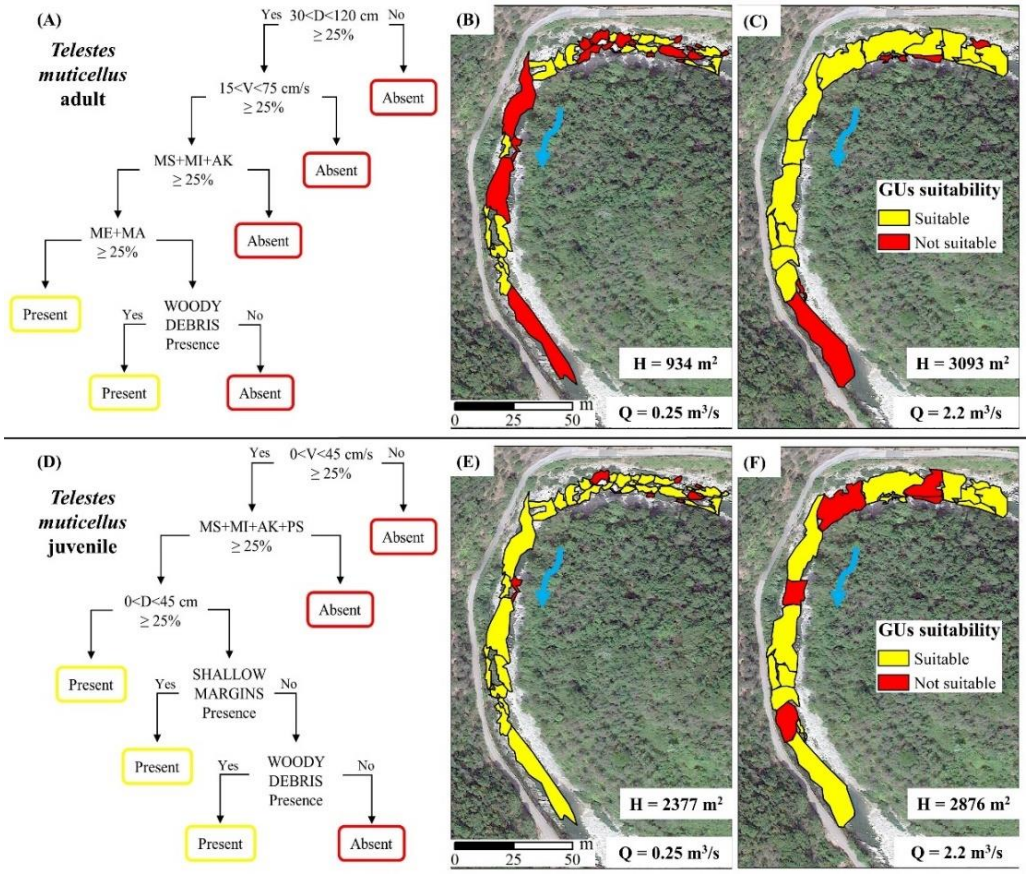


Figure 2.2. Presence/absence HSC for (A) adult and (J) juvenile life stages of *Telestes muticellus*, depicted by using a decision tree representation. Habitat suitability maps expressing the available habitat (H) assessed for adults *T. muticellus* at (B) 0.25 m^3/s and (C) 2.2 m^3/s, and for juveniles *T. muticellus* at (E) 0.25 m^3/s and (F) 2.2 m^3/s, in the Argentina Creek.

2.3 Results

Overall, we considered 250 bibliography sources, most of which (206) were peer-reviewed researches and the remaining were represented by books or book sections (20), PhD thesis (7) and grey literature sources (i.e., governmental or NGOs reports; 17). For brevity, the bibliographic sources are not reported in this thesis; however, the complete list is available in [26].

Most of the bibliography sources focused on fish habitat preferences/use (112) and species HSC studies (101), while fewer references (37) were related to autecological aspects. To determine the habitat features preferred by specific species, the vast majority of studies (178) relied on sampling abundance (e.g., [93]) or local fish density (e.g., [94]). Whereas, the remaining studies (72) considered exclusively species presence (e.g., [21]).

Available information on habitat preferences highly varied depending on the species (**Figure 2.1**). The highest number of publications was found for *Squalius cephalus* (37 Pub.), followed by *Gobio gobio* (36) and *Thymallus thymallus* (35). Conversely, very little information was found for several endemic Italian species (e.g., *Sarmarutilus rubilio*, *Salmo cettii*, *Rutilus pigus*, *Barbus caninus*: 3; *Alburnus albidus*: 2). From our analysis, Italian freshwater fish species can be classified into three groups, depending on the available knowledge and amount of publications. The first group can be composed by 10 species (from *S. cephalus* to *A. anguilla*, yellow group in **Figure 2.1**) with quite copious available information on habitat preferences (>20 Pub.) for almost all considered attributes, life stages and bioperiods. The second group (from *Perca fluviatilis* to *Cyprinus carpio*, orange group in **Figure 2.1**) comprises 12 species for which available data were found to be limited (10<Pub.≤20), and not covering all considered life stages and bioperiods. The third group (from *Padogobius nigricans* to *Alburnus albidus*, red group in **Figure 2.1**) is composed by the remaining 12 species for which information resulted very poor (≤10 Pub.) and several life stages or bioperiods exhibit absence of information. It is interesting to note that the third group is exclusively composed by purely Italian endemic species.

Considering life stages and bioperiods, the collected information on the rearing/growth bioperiod for juveniles (176 Pub.) and adults (135) was higher compared to those referring to spawning habitat preferences (98). Furthermore, focusing on the considered habitat attributes, we observed a greater amount of information regarding substrate preferences (208 Pub.), rather than depth (169), velocity (142) or cover (107). Preferred categories of water depth (D), varied significantly according to life stages and bioperiods (**Figure 2.1**). Moderate to high depth (from 30 to 120 cm) resulted suitable for the majority of adult species (24 species, 70% of the total). Conversely, for juvenile fish and spawning bioperiod, 26 species (77% of total) preferred shallow to medium water depth (from 0 to 75 cm). For velocity (V) no species exhibited a preference for a flow rate higher than 75 cm/s. Concerning abiotic substrates, for 22 species (65% of the total), the most preferred categories ranged from *akal* (AK) to *macrolithal* (MA), whereas for Cobitidae, Petromyzontidae and few species of Cyprinidae the preferred substrates

were *psammal* (PS) and *pelal* (PE). For spawning, 26 species (76% of the total) preferred coarser grain sizes, mainly *akal* (AK), *microlithal* (MI) and *mesolithal* (MS). *Phytal* (PH) as spawning substrate was recorded for six species (18% of the total) of Cyprinidae, Cobitidae, and Esocidae. Finally, submerged vegetation (SV), boulder (BD), and woody debris (WD) were found to be the preferred covers/shelters for 20, four and two species, respectively.

Moderate to high water depth values (from 30 to 120 cm) and moderate velocities (from 15 to 75 cm/s) were found to be appropriate habitat attributes for the adult stage of *T. muticellus*. Whereas, its juvenile stage prefers shallow areas (water depth <45 cm) and low velocities (<45 cm/s). Considering substrate, coarser material (mainly AK, MI, and MS) resulted mostly preferred by both life stages, whereas WD was found to be the preferred cover/shelters (**Figure 2.2**A,D). The validation performance of conditional models for *T. muticellus* was quite good and considered acceptable: accuracy 67% and 81%, sensitivity 53% and 78%, specificity 100% and 100%, and TSS 53% and 78%, respectively for adult and juvenile life stages. Habitat availability (H) varied significantly with respect to the analyzed flow conditions, increasing from 934 m^2 at 0.25 m^3/s to 3,093 m^2 at 2.2 m^3/s (**Figure 2.2**B,C). Available habitat for juvenile *T. muticellus* was almost similar between the two surveyed discharges, showing a slight increase from 2,377 m^2 at 0.25 m^3/s to 2,876 m^2 at 2.2 m^3/s (**Figure 2.2**E,F). At 2.2 m^3/s the GUs classified as not suitable (**Figure 2.2**F, red areas) for juvenile *T. muticellus* were mostly related to rapids, characterized by velocities much higher than 45 cm/s.

2.4 Discussion

The systematic review of habitat preferences for Italian freshwater fish revealed substantial deficits in knowledge and data availability for the considered species. In particular, for more than 30% of the Italian fish, such information resulted remarkably scarce (≤10 Pub.). Generally, a higher number of publications was found for species with a higher economic value or a larger distribution area. Indeed, the first group (from *S. cephalus* to *A. anguilla* in **Figure 2.1**) is composed by largely studied species that are distributed in more than 80% of European countries. Conversely, the third group (from *P. nigricans* to *A. albidus* in **Figure 2.1**) resulted exclusively consisting of the most threatened endemic species of the Italian territory, whose distribution ranges are restricted to certain Italian watercourses [88]. These results are consistent with previous researches which pointed out that species with a higher socio-economic importance are generally better investigated [27]. In our opinion, future research and investments should be directed to study the habitat of endemic Italian species, to plan and better design habitat restoration actions.

A critical issue is increasing the knowledge related to spawning habitat requirements. Although reproduction is a crucial phase for freshwater fish life cycle, surprisingly we observed a general lack of information for this bioperiod. In

particular, the information we found mainly derived from historical data and publications (e.g., [95]) or ecological reviews (e.g., [96], [97]) carried out in the Northern part of Europe. This indicates that spawning habitat requirements for Italian freshwater fish are not sufficiently investigated. Actually, we found only 11 studies (4% of the total) carried out in Italian rivers, which means, on average, less than one study per species. With the aim of preserving freshwater fish biodiversity as reported in the EU Biodiversity Strategy for 2030 [98], accurate information on physical habitat requirements for spawning are crucially required. In this regard, this review can provide important insights to direct future researches on this significant topic.

Although we encountered several data regarding substrate preferences for almost all considered species and life stages, available information on the remaining habitat attributes was found to be more scattered. The data collection strategies, adopted in the considered publications for characterizing physical river habitat, seems to influence the amount of available information. For instance, for substrate classification, semi-quantitative procedures which use simple visual estimation were found to be extensively used (e.g., [93], [99]). This resulted in a larger amount of data regarding fish substrate preferences. Nevertheless, substrate classification was found to largely differ among the considered studies, making the comparison and aggregation of information difficult. For water depth and velocity, several publications reported only bulk estimation of mean values over an entire river reach, which can be considered a poor and low quality source of information in terms of physical habitat preferences (e.g., [100]). Finally, with respect to covers/shelters, the lower amount of data can be mainly related to the scale and spatial resolution used by the considered studies to analyze fish habitat requirements. This was specifically due to the wider application of micro-habitat suitability models (e.g., PHABSIM, [32]), in which covers/shelters are not usually taken into account (e.g., [94]).

Meso-scale HSMs derived from literature demonstrated high effectiveness in predicting fish distribution in the Argentina Creek. This result was in line with previous studies [48], [66] that used literature information to infer habitat suitability for fish. However, it is important to state that HSC derived from literature may be currently built in Italy only for the first and second group of species (from *S. cephalus* to *C. carpio* in **Figure 2.1**). Due to the very limited amount of information we would exclude to build HSC for species of group three (from *P. nigricans* to *A. albidus* in **Figure 2.1**).

The MesoHABSIM approach has already proved high potential in assessing habitat availability for freshwater species in various hydro-morphological contexts of European rivers [30], [91]. In particular, in Italy such model is currently used for impact assessment of hydropower and ecological flows (e-flows) design in regulated rivers [54], [68]. Nevertheless, one of the most important limitation for implementing MesoHABSIM to the entire Italian territory consists in a limited amount of available HSC, for which extensive field data collection and analysis are currently required. In this regard, the present systematic literature review represents a notable step forward. The analysis carried out for *T. muticellus*, can be repeated

for other species and further literature based models could be defined based on the collected information. However, we suggest that HSC derived from literature should be always locally validated before using them in impact assessment and e-flows design procedures.

Chapter 3

3. Ecological notes on an endemic freshwater lamprey, *Lampetra zanandreai* (Vladykov, 1955)

The work presented in this chapter has been partially derived from [19].

3.1 Introduction

In 1955, Vladim Vladykov received lamprey samples from the Po valley and realized that they belonged to a species new to science, distinctly separable from the well-known European river lamprey *Lampetra fluviatilis* (Linnaeus, 1758) on the basis of precise morphological characters, such as disposition and number of teeth on oral disc, number of trunk myomeres, coloration and body proportions. In honor of the colleague who sent them to him, the ichthyologist named the species *Lampetra zanandreai* (Vladykov, 1955). Subsequent studies discovered that this species is present in a larger area, more or less corresponding to the ancient river Po basin during the Würm glaciation, i.e., the current Po basin, some areas in central Italy (Bianco, 1992) and probably some Adriatic basins of Slovenia and Croatia [101]–[103].

The Po Brook Lamprey is a non-parasitic lamprey with ammocoetes that reach greater dimensions than adults, in both length and weight. Ammocoetes probably live four or five years, then metamorphose to spend six to eight months in the adult stage. Larval stages are bottom filter feeders, with a digestive system that degenerates soon after metamorphosis [104]. During the adult stage these lampreys do not feed, and energy for metamorphosis, gonadogenesis and spawning comes from body reserves: for these reasons, reproductive stages are distinctly smaller than their last larval stages. Metamorphosis takes place from August to October,

reproduction occurs from January to June and adults expire after spawning (Bianco, 1986).

Lampetra zanandreai is considered an endangered species, listed in Annexes II and V of the EEC (European Economic Community) Habitats Directive 92/43, in the Appendix II and III of the EEC Bern Convention and in the IUCN (International Union for Conservation of Nature) Red List of Threatened Species [105]. The distribution of this species is considered discontinuous and declining, with a strong diminution over the past decades [106]. Very little is known about the ecology of this species, which has been the subject of few mostly dated studies.

The Po Brook Lamprey has an enormous potential of interest as it is a very ancient species, with a basal position in the development line of vertebrates, a very interesting biogeographical distribution and a state of conservation that deserves attention and insights. As reported before, scientific studies on this lamprey have always been sporadic and mainly dedicated to specific biological aspects. In the first few decades after its discovery, studies focused on the description of biological characteristics of the species, considering for example biometry and morphology [107], systematic position [108], geographic distribution [109]–[111], endocrinology [112], [113], and cytology [114]. More recently, other authors have focused mainly on genetic aspects [106], [115], [116].

Interestingly almost nothing is known about the ecology of this species. For example, information about habitat preferences is quite generic and descriptive, with hardly any quantitative data available in the current literature, as pointed out by [26]. Since most of the life cycle is spent in the larval stage, which is also extremely important because it is the only phase in which the organisms feed, any strategy to improve the conservation of the species must be based on a better knowledge of the habitat of the ammocoetes. Regarding the ecology of the species, one of the earliest indications can be found in [113], which reports that *L. zanandreai* occurs from the sea level to 600 m in elevation, inhabiting muddy or sandy riverbeds. Basically, all the other more or less recent studies have not added anything to this summary description, using more or less the same words. For example, [117] reported that larval stages live in lowland rivers, with moderate water current, muddy or sandy bottom, and the same can be found in [104], [101] and others. Even, in a FAO (Food and Agriculture Organization) book [118] dedicated to lampreys the ecological requirements of *L. zanandreai* are limited to a single word (i.e., Habitat: freshwaters).

To quantitatively describe and predict the distribution patterns of freshwater species, Habitat Suitability Models (HSMs) have been increasingly used in river ecology [17]. Such models are based on the use of habitat suitability criteria (HSC, or species distribution models), which allows researchers to estimate suitable riverine patches for a target species (or group of species) according to local habitat attributes (e.g., water depth, current velocity, substrate composition, presence of covers [119]. The definition of HSC (i.e., habitat preferences of target species) can be achieved by statistically analyzing empirical data collected in the field, to identify the habitat requirements of target species (e.g., [21], [94], [120]). Among the different statistical techniques proposed in the literature for defining species

habitat preferences [119], the Random Forest (RF) classification algorithm [64] is gaining prominence in ecology [121]. The RF algorithm is a machine learning ensemble arising from the classification and regression trees (CART, [122]) and the bagging [123] techniques. By combining the prediction of a large set of randomized trees fitted on the dataset, it produces results with high accuracy requiring little computational time and reduced tuning, and provides readily available outputs [65], [121].

RF has already been successfully applied to define habitat preferences of fish [63] and macroinvertebrates [22] in Italian rivers, by analyzing species distribution with respect to the mesohabitat attributes, as described in the MesoHABSIM approach [18]. The MesoHABSIM is a meso-scale HSM increasingly used at the European level for hydro-morphological impact assessment and definition of ecological flows (e.g., [48], [54], [124]). It enables river habitat description using an ecologically relevant spatial scale (i.e., the mesohabitat or geomorphic unit scale; [60]), it is based on a robust and adequate hydro-morphological characterization of the river stretch, and it allows researchers to consider in the analysis a large range of biotic and abiotic environmental descriptors, not only at the point where the organism is observed.

The aim of this study is to provide the first quantitative description of Po brook lamprey ammocoetes habitat preferences, by developing the first meso-scale HSC for this species and by analyzing its favored substrate composition.

3.2 Materials and methods

3.2.1 Study area

The study domain consisted of five hydro-morphologically homogeneous [60] stream reaches distributed within four rivers of the Alpine catchments of the Po river basin (NW Italy, **Figure 3.1**).

Reach 1 refers to the Belbo river, located in hilly areas of the southern Piemonte Region. The reach is characterized by a single-thread channel, a high gradient, and a cobble-gravel substrate composition with some sand and silt. Reaches 2 and 3 were approximately 2 km apart from each other and were both located in the Ghiandone river. The two reaches are pooled by gentle slopes, and are characterized by a similar sediment composition, which mostly consisted of fine gravel, sand and cobbles. Reach 4 was located in an unconfined reach of the Orco river, characterized by a pseudo-meandering morphology [56] with few secondary channels. In this reach river bed material comprised mainly cobbles and gravels with some sandy and silty patches located in the shallower marginal areas. Lastly, reach 5 was located in the Pellice river, also characterized by a pseudo-meandering morphology with a gravel-sand sediment composition and a sequence of pools,

riffles and bank-attached river bars. The main characteristics of the surveyed stream reaches are summarized in **Table 3-1**.

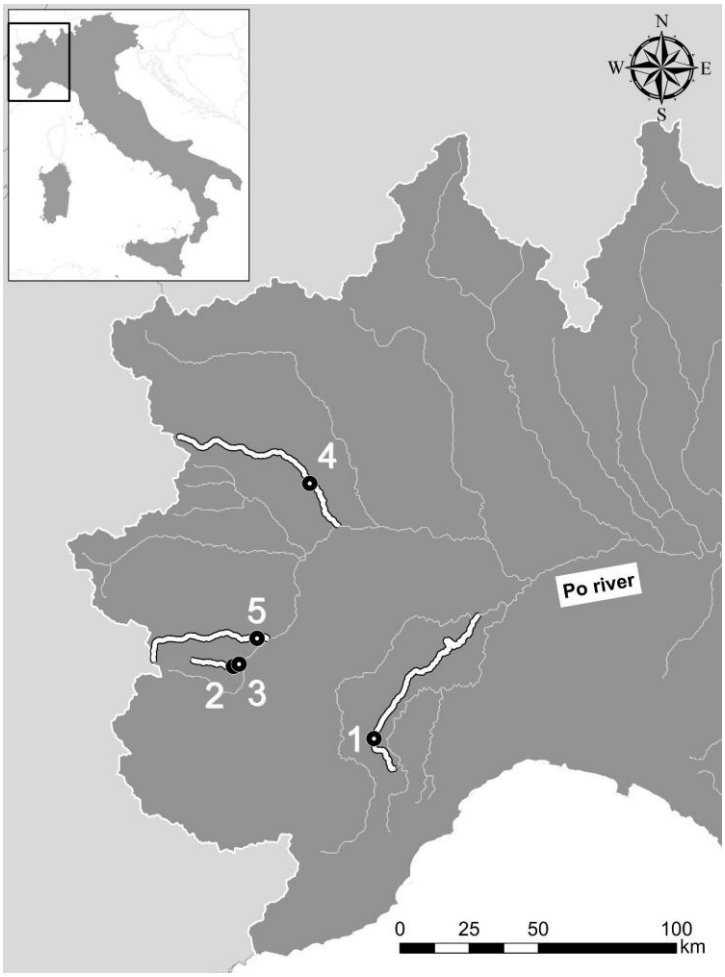


Figure 3.1. Location of the surveyed reaches considered in the study. Surveyed stream reaches: 1 = Belbo river; 2-3 = Ghiandone river; 4 = Orco river; 5 = Pellice river.

3.2.2 Mesohabitat description and lamprey distribution

Between the autumn of 2019 and the summer of 2021, five field campaigns were performed in different seasons, in order to investigate the distribution of lamprey ammocoetes with respect to the physical habitat characteristics of the considered river reaches (for further details please see **Figure A.1**). In particular, within the five representative stream reaches (**Figure 3.1**), 42 geomorphic units (GUs) were identified and described following the MesoHABSIM approach [18], [63]. Surveys were carried out using the MapStream software [54], by mapping each GU in the QGIS environment by means of a rangefinder (Trupulse 360R, Laser Technology, Inc., Centennial, CO, USA), a photographic tripod, a rugged field computer (Panasonic Toughbook FZ-M1, Panasonic Corporation, Kadoma, Japan) and multi-band RTK GNSS receiver (Emlid Reach RS2, Emlid, Budapest, Hungary). GU types included pool, glide, riffle and backwater, following the

geomorphic unit classification reported in [60]. To cover the spatial variability of flow conditions and sediment composition in each GU, between 7 and 30 point measurements of water depth, mean water column velocity and substrate type were collected [63]. Seven measurements were empirically chosen as the smallest statistically relevant quantity [18]. Substrates consisted of 12 categories - *gigalithal* (rocks), *megalithal* (>40 cm), *macrolithal* (20-40 cm), *mesolithal* (6-20 cm), *microlithal* (2-6 cm), *akal* (gravel > 0.2 cm), *psammal* (sand), *pelal* (silt and clay), *detritus* (organic matter), *xylal* (woody debris, roots), *sapropel* (dark anoxic mud), and *phytal* (submerged plants) - whereas covers consisted of 11 categories - boulders, canopy shading, overhanging vegetation, exposed roots, submerged vegetation, floating vegetation, emerging vegetation, undercut banks, woody debris, riprap, shallow margins. GU, cover types and longitudinal river connectivity were broken down into multiple variables in binary (No/Yes) format, and measurements of depth and velocity were divided into frequency categories of 15 cm and 15 cm/s increments respectively. The dominant substrate category was visually identified in each point measurement. Finally, the water surface mean gradient was recorded for each GU. The total list of the collected habitat attributes is reported in **Table A-1**.

Table 3-1. Name, location, characteristics and morphological classification of surveyed reaches. River morphology codes (according to [56]): C = confined; P = partly confined; U = unconfined; SS = straight-sinuous; M = meandering; S = sinuous; PM = pseudo-meandering. Reach width represents the mean value of the active river channel width in each surveyed reach.

Stream reaches	UTM 32N coordinates	Reach length [m]	Reach width [m]	Reach morphology
Belbo (1)	E: 424991.19 m; N: 4925539.43 m	92	8	C-SS
Ghiandone (2)	E: 373732.28 m; N: 4953061.32 m	105	15	U-M
Ghiandone (3)	E: 375752.25 m; N: 4953863.60 m	57	11	U-S
Orco (4)	E: 401489.62 m; N: 5019384.86 m	580	85	P-PM
Pellice (5)	E: 385031.57 m; N: 4963706.95 m	1500	105	P-PM

Lamprey distribution data were collected by sampling every GU with backpack electrofishing (i.e., two-pass removal method, [92]. To assure the direct association between GUs and collected lampreys, sampled areas were isolated by using nets, and before release within the same sampled GU, each lamprey was measured in terms of total length. The total number of captured lampreys was 78, which were classified into larvae, referred to as ammocoetes (n = 77), and adult (n = 1) life stages by looking at the enlargement and differentiation of the eye and difference in the head shape [125]. Due to a low number of observations of adults but mainly

because the larval phase is prominent in the life cycle of the species, we focused on ammocoetes.

3.2.3 Data analysis

The association of GU characteristics (**Table A-1**) with lamprey presence was explored using probabilistic models to investigate ammocoetes habitat preferences. In particular, the RF [64] classification algorithm was used to identify habitat attributes influencing lamprey distribution.

RF is an ensemble machine learning technique based on the aggregation of a large set of randomized classification trees. In RF, as implemented in R (library randomForest, version 4.6-7, [126]), each tree is trained by selecting a random learning sample (i.e., bootstrap sample) from the original dataset. Selected observations (parent node) are then split into two further subsets (child nodes), depending on the value of a predictor randomly chosen from the variables space. Through a binary recursive partitioning technique, this process is repeated for each child node, which becomes the new parent node, as long as a minimum number of observations is reached in the last terminal nodes. The choice of the predictor for each partitioning (new branch of the trees) is oriented to reduce the Gini impurity, i.e., for maximizing class imbalance in the child nodes. The elements not included in each bootstrap sample are referred to as out-of-bag data (OOB, i.e., cross-validated accuracy estimates) for all trees. For classification RF models, once all trees are fully grown, the majority voting of the OOB elements across all trees determines the responsive class for each observation.

A binary absence/presence model was developed to distinguish between unsuitable and suitable habitats for lamprey ammocoetes. In this way the model was characterized by two boolean responsive classes (stated as 0/1), where 1 denoted a >50% predicted probability of being a suitable GU. As the responsive variable was a binary variable (fish absence/presence), we confined our attention to classification RF models. For classification RF models, the predicted probability is determined through majority voting among all decision trees in the forest (ntree). Among all surveyed GUs, the prevalence (i.e., the frequency of occurrence of the target organism) was in 0.26. Therefore, to address potential bias in the forest generation due to class imbalance, we developed and tested a model for which a random oversampling of the training dataset was priorly performed As a result, the initial dataset of 42 samples (42 GUs) was expanded to 66 samples for model development. In order to optimize the predictive performances of the RF model, minimizing the out-of-bag (OOB) error, a specific framework for variables selection and hyperparameters tuning was implemented. As OOB error increases when the number of predictors is significantly higher than optimal [127], we tried to select a small number (possibly minimal) of variables providing the best possible classification result. To assess the importance of a specific predictor we used a common wrapper for feature selection based on the RF named Boruta [128]. The Boruta algorithm is implemented in R as a package and allows the user to identify

all relevant variables by providing as output a features ranking expressed in terms of importance. From this analysis, the most important predictors were chosen and, to avoid high correlation (Spearman's rho correlation coefficient > 0.7) between selected predictors, were tested by means of the Spearman correlation matrix. The final parsimonious RF model was therefore characterized by 10 variables with high importance for classification results and low correlation. Hyperparameters generally refer to the RF settings which can be tuned by the user (e.g., number of decision trees). For our RF models, hyperparameters tuning involved (i) the number of decision trees for the forest (ntree), and (ii) the number of predictors randomly sampled as candidates at each node (mtry). To establish the suitable ntree value we followed the suggestion of [129], obtaining a number of trees for the final model of 600. The mtry parameter was established equal to the square root of the total number of selected predictors included in each model [130]. For our final parsimonious model mtry was equal to 3. Finally, accuracy, sensitivity, specificity, and true skill statistic (TSS, [131]) were used to assess the predictive performances of the RF model (see **A.3** for further details). The partial dependence plots (or response curve, PDPs), based on the RF results, provided a way to visualize the marginal effect of the selected independent variables on the fish distribution [65] outlining the relationships between individual habitat attributes and the predicted probabilities of fish presence.

3.2.4 Granulometry

In order to better analyze the favored substrate for lamprey ammocoetes, we further collected streambed samples to characterize the sediment preferences of this species. On 16 March 2022, we carried out sampling with an electrofishing device in the Ghiandone stream in Reach 2 and 3 (**Figure 3.1**, **Figure 3.2**a), where the highest density and number of individuals were assessed from the previous field campaigns. While an operator slowly moved the anode on the river bottom, the other two signaled with flags the points from which the lampreys emerged. In total, we considered 26 points in a 70 m-long stream reach. In each of these points we collected three sediment cores with cut-off 100 mL syringes (diameter: 3.6 cm, height: 15 cm – **Figure 3.2**b). Sediment cores were transported to the laboratory, then oven-dried (24 h, 105 °C) to assess dry mass. Samples were processed in a Bertel mechanical sieve shaker for 15 minutes, using four mesh sizes in order to obtain five granulometric ranges: > 2 mm (very fine gravel), 2.0–1.0 mm (very coarse sand), 1.0-0.5 mm (coarse sand), 0.5-0.2 mm (medium sand) and < 0.2 mm (fine sand and smaller) (**Figure 3.2**c,d). For each granulometric fraction we performed a mass evaluation, weighting the fractions to the nearest 0.1 g, and a volumetric evaluation, inserting the fraction into graduated cylinders containing a known water volumes. To estimate the organic fraction in each sediment sample, after oven-drying as reported above, we placed sediments in a muffle furnace

(500°C) for 4 h and reweighed them. The difference between weights indicated the organic fraction of the sediment as ash-free dry mass (AFDM). This value was the employed to assess the percentage organic content of each sediment sample [132].



Figure 3.2. a) Sampling station, Ghiandone river (NW Italy); b) sediment cores; c) Bertel mechanical sieve; d) sample with the five granulometric classes considered.

3.3 Results

3.3.1 Mesohabitat description

In the field campaigns 42 mesohabitats were analyzed within the five selected river reaches. Most of the sampled GUs were riffles (50% of total amount) and glides (26% of total amount). Pools and backwaters corresponded to 17% and 7% of the sample dataset, respectively. As we considered river reaches of different sizes (**Table 3-1**), GU areas varied from a minimum of 6.7 m^2 to a maximum of 950.5 m^2. GU water surface gradients were mostly lower than 2% (69% of total amount), except for Reach 1, where few mesohabitats exhibited gradient values up to 10%. Considering covers, the presence of shallow margins was identified in 20 GUs, whereas boulders and submerged vegetation were identified in 18 and 17 mesohabitats, respectively. Overall, *mesolithal* (33% of the total sampled points) was to be the most frequent substrate category, followed by *microlithal* (26%), *psammal* (14%) and *akal* (10%). Finally, water depth and velocity values varied between 2 and 112 cm and between 0 and 210 cm/s, respectively.

Lamprey ammocoetes were found in 11 GUs: 5 glides, 2 riffles, 2 pools, and 2 backwaters. Such mesohabitats were mostly characterized by shallow water depth

(< 45 cm) and low flow velocities (<45 cm/s), with a prevalent substrate constituted by *psammal* and *akal*. Overall, the highest number of lampreys (29) was assessed in a GU classified as glide in Reach 3 (Ghiandone river). The largest density of individuals (0.48 ind./m^2) was found in a backwater in Reach 2 (Ghiandone river).

3.3.2 Habitat preference analysis

The developed RF models permitted us to identify the most important mesohabitat physical attributes for lamprey ammocoetes presence within GUs, providing the first meso-scale HSC in the literature for the considered species. As the oversampled RF model produced the higher predictive performances in the end this model alone was taken into account (**Figure 3.3**). Cross validation of the final model demonstrated high predictive capability in detecting suitable mesohabitat for lamprey. In particular, model accuracy was assessed as 95.2%, sensitivity (i.e., true positive rate) was 96.8%, specificity (i.e., true negative rate) was 93.6%, and TSS was 90.4%.

Considering predictive variables, the final parsimonious model was characterized by 10 mesohabitat attributes, presented in **Figure 3.3** in the form of PDPs and sorted in terms of variable importance. The most significant attributes were *microlithal*, *akal*, and *psammal* substrates types. From the PDP graphs, *microlithal* substrate type was negatively correlated with the lamprey presence, whilst *psammal* and *akal* were positively correlated. *Mesolithal* showed a similar trend to *microlithal*, pointing out how coarser substrates exerted a negative influence on lamprey presence. The probability of presence of lamprey ammocoetes also increased with (i) the presence of shallow margins in the GUs, (ii) the proportion of low water depths (15-30 cm), and (iii) the proportion of low flow velocities (0-15 cm/s). Symmetrically, the proportion of higher velocities (i.e., 60-75 and 75-90 cm/s) and larger GU gradients had a negative influence on the probability of lamprey presence.

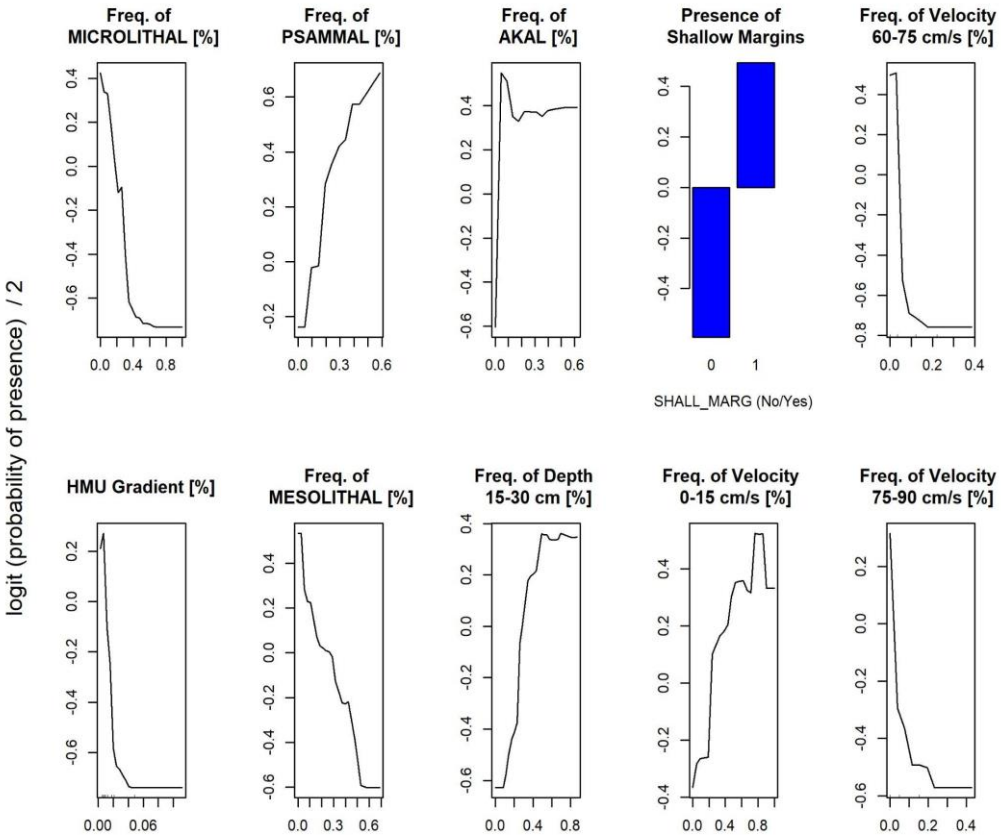


Figure 3.3. *Lampetra zanandreai* ammocoetes RF model. Selected physical attributes (in order of importance) for the oversampled parsimonious model. The relationship between variables and probability of presence is reported using partial dependence plots (PDPs).

3.3.3 Granulometry

We obtained the granulometric profile of the 25 samples collected and we firstly analyzed the relationships between weight and volume. For all granulometric classes we found a significant positive correlation (**Table 3-2**), so we decided to use mass as an indicator of sediment characteristics (following [133]).

Table 3-2. Correlations between volume and mass of the different granulometric size classes.

Size class [mm]	R Spearman (rs)	*p*
< 2.0	rs = 0.947	<.001
2.0 – 1.0	rs = 0859	<.001
1.0 – 0.5	rs = 0.912	<.001
0.5 – 0.2	rs = 0.984	<.001
< 0.2	rs = 0.868	<.001

The average particle size mass profile consists of 34.98% (± 2.86 se) coarse sand, followed by 25.64% (± 2.51 se) very coarse sand, 19.87% (± 1.79 se) medium sand, 13.73% (± 1.86 se) very fine gravel and 5.77% (± 0.72 se) fine sand and smaller particles. In general, most cores are largely composed of intermediate granules (from 2.0 to 0.5 mm). However, a certain tolerance in the particle size range is evident, also highlighted by **Figure 3.4**: the lampreys were found in environments where the coarsest content (> 2 mm) is equal to 33.6% of the total but also in others in which the finest (<0.2 mm) reaches 15.6%. The organic content was meanly 1.14% of sediment samples (mean value), with a minimum of 0.46% and a maximum of 3.42%.

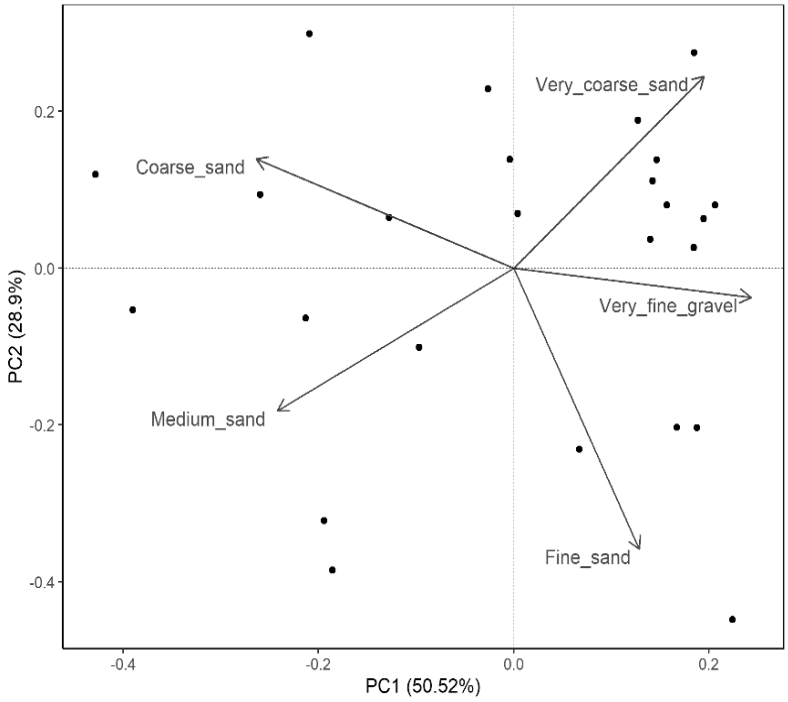


Figure 3.4. Principal Component Analysis ordination plot. Labels indicate granulometric classes, dots represent sample cores.

3.4 Discussion

Studies on Italian cyclostomes have been practically at a standstill for about 50 years - that is, since the phase of the conspicuous research activity stimulated mainly by Giuseppe Zanadrea ended [117]. While numerous aspects of the biology, phylogeny and morphology of this species are well known, virtually nothing is known about its ecological needs. To our knowledge this is the first study focusing on the habitat requirements of Po Brook lamprey.

The application of the MesoHABSIM approach allowed us to demonstrate that ammocoetes of this species can be found in different mesohabitats, such as pools,

glides, riffles and backwaters. However, all the positive samples were characterized mainly by patches of fine sediment (*psammal* and *akal*), shallow water depth (< 45 cm), and low flow velocities (< 45 cm/s). Such results are consistent with [113], who reported that this species inhabits rivers with muddy or sandy bottoms. Furthermore, by comparing our findings with the habitat preferences reported in the literature for ammocetes of other European freshwater lampreys, a certain correspondence may be observed. In particular, [134] used the RF algorithm to understand the relationship between the presence of *L. planeri* and *L. fluviatilis* ammocoetes with respect to different environmental attributes at different scales (regional, catchment and microhabitat) in the Ballinderry river catchment (Northern Ireland). From their analysis it was possible to note that ammocoetes were more abundant in sediment patches characterized by very coarse sand (≥ 1.94 mm). Additionally, measured water depth (range 2-66 cm) and current velocity (range 0-75 cm) values where lamprey ammocoetes were found are in agreement with our data. Indeed, all specimens of Po brook lampreys we captured in the study sites, inhabited GUs characterized by water depth and velocity lower than 76 cm and 70 cm/s, respectively. Similarly, [135], observed that, in the Dordogne river (France), *L. planeri* and *L. fluviatilis* ammocoetes preferred water depth below 50 cm, current velocity up to 50 cm/s and a sediment composition dominated by coarse and median sands (0.2-2 mm).

The use of the RF classification algorithm permitted us to better understand the relationship between *L. zanandreai* ammocoetes distribution and the mesohabitat attributes considered within the MesoHABSIM approach. In particular, the final parsimonious RF model highlighted that lamprey larvae generally preferred mesohabitats characterized by shallow margins with an high proportion of (i) water depths in the range 15-30 cm, (ii) current velocities in the range 0-15 cm/s, and (iii) fine sediment (*psammal* and *akal*).

The high predictive performance (accuracy = 95.2% and TSS = 90.4%) obtained for the developed RF model confirmed the capability of this technique for the definition of HSC in river ecology [65]. In particular, the current approach, which combined the MesoHABSIM methodology with a RF model, is in line with previous studies that pointed out how it can be considered suitable to define available habitat for freshwater fish and macroinvertebrates in rivers [22], [63]. The present study contributes to demonstrate the application potential for this approach. Indeed, this MesoHABSIM application can be seen as an extension of the approach for the definition of meso-scale HSC for Petromyzontidae. In addition, this study can serve as a basis for enhancing the preservation of the endemic Po brook lamprey, through the design of ecological flows and sediment river management, able to maintain specific habitat requirements [54].

Ammocoetes of *L. zanandreai* inhabited depositional zones characterized by fine sediments, generally medium to coarse sand with smaller amounts of finer particles or small gravel. Interestingly, while in lowland running waters these kinds of substrata are often associated with moderate to elevated amounts of organic matter, in the cores positive for the presence of ammocoetes the organic component proved very small (mean value of streambed samples = 1.14%). This finding can

explain the scattered distribution of the specimens. In fact, the occurrence of individuals is typically irregular in the stream reaches we examined, with large apparently suitable areas (judged by the presence of fine sediments) where no ammocetes were found. Probably the distribution of the organisms derives from a trade-off between the texture and composition of the substrate (which allow the larvae to burrow) and the organic substance content. An excessive accumulation of organic matter enhances bacterial biomass growth and therefore reduces oxygen diffusion at the interstitial level.

This study shows that lampreys select mesohabitat not only with precise velocity, depth and grain size ranges, but also with a low organic content. This implies that the chances of finding this species increase in rivers with better quality, in terms of ecological, chemical and hydrological status. Streams and rivers are increasingly threatened by factors acting at global [136] and local [137] scales. In particular, the synergic effects of these factors can be dramatically dangerous, because the reduction of flows can exacerbate the impacts of wastewater discharge, leading to an augmentation of fine organic matter deposition and a consequent diminution of lamprey habitat availability. *Lampetra zanandreai* is an ancient witness of the freshwater faunas of the past, an endemic and highly threatened species that becomes the symbol of an entire large ichthyological district, the Po basin: to protect and conserve Po Brook lamprey, we need a deeper knowledge of its environmental needs.

Chapter 4

4. Mesohabitat spawning preference of the anadromous Twaite shad (*Alosa Fallax*, Lacépède 1803) in the Tagliamento river

4.1 Introduction

Anadromous fish are a particular group of migratory species that exemplify the interlinking of freshwater and marine ecosystems, utilizing both environments to complete their life cycle [138]. These species are born in freshwater rivers or streams, where, after hatching, they spend the early part of their lives. As they grow, they experience physiological changes that allow them to migrate downstream and enter the sea. In the marine environments, they spend a significant portion of their lives, before returning to the rivers for breeding [139]. Anadromous species provides important ecosystem services [140] and are considered essential contributors to the ecological balance of both fluvial and marine ecosystems, transporting marine-derived nutrients back to freshwater environments and providing a significant food source for predators in both environments [141].

However, despite their remarkable adaptability [142], anadromous fish are facing a multitude of challenges and threats that are undermining their existence. Indeed, among the 16 anadromous species that spawn in the European watercourses, one (*Coregonus oxyrinchus*) is considered extinct and 9 are listed as vulnerable or critically endangered in the IUCN (International Union for Conservation of Nature) Red List [105]. Habitat alteration and degradation,

overfishing, and climate change are considered the most significant factors in the severe decline of these species [140]. In particular, river regulation and damming have considerably impacted the streams that serve as breeding and rearing sites for anadromous species. Indeed, river damming determines the fragmentation of the watercourses [143], directly impeding anadromous fish to reach upstream suitable spawning sites. Additionally, dams alter the hydrological regime and impact the supply of sediment and organic material to downstream reaches [3], [4], crucially influencing the generation of physical breeding habitats for these species. In this regard, recent studies (e.g., [140], [144]) have pointed out that most efforts to sustain the conservation of anadromous species and the maintenance of their habitat must focus primarily on improving river continuity and preserving and restoring habitat integrity.

To assess the hydro-morphological impact related to water abstraction and river regulation, Habitat Suitability Models (HSMs) were conceived [32], [84], [145]. HSMs can be used for a variety of purposes, including river management, ecological flows (e-flows) design, river restoration projects, and species conservation plans [17], [28], [34]. These tools allow to predict the suitable habitat patches for a target species (or ecological group) by means of habitat suitability criteria (HSC, or species distribution model) developed on its habitat requirements. Such models usually take into account various environmental parameters such as water depth, flow velocity and substrate composition which are used to analyze their relationships with the species presence [119]. Among the different HSMs, the MesoHABSIM (MesoHABitat SImulation Model, [18]) approach is increasingly used, especially in Italy, where it has been established as a reference method for e-flows design [54]. MesoHABSIM assesses the available habitat for fish or other aquatic organisms by quantifying the suitable mesohabitats. Mesohabitats generally correspond in size and location to geomorphic and hydraulic units (GUs, [60]), such as pools, riffles, glide and rapids. Meso-scale HSMs consider a wide range of habitat attributes, including water depth, flow velocity, substrate composition, presence of shelters and covers for fish, lateral or longitudinal connectivity of the GU with the main river channel and the GU water surface gradient. This wide range of habitat attributes allows a more effective linking between river hydro-morphological features and the distribution of aquatic biota [46], [63]. Furthermore, for large rivers, especially for not wadable conditions, meso-scale HSMs can integrate two-dimensional (2D) hydrodynamic models for simulating water depth and flow velocity distribution within Gus [43], [62].

In the framework of the MesoHABSIM approach, different statistical techniques, such as decision trees (e.g., [48]), logistic regressions (e.g., [21]), and machine learning (e.g., [63]), can be used to develop the HSC. Among the machine learning techniques, Random Forest (RF, [64]) algorithm has been successfully applied for identifying the habitat requirements of endangered fish [63], macroinvertebrates [20], [22] and freshwater lampreys [19]. These applications mainly focused on resident freshwater species [21], while less attention was generally given to species which use the river environments only for a specific part of their life cycle, such as anadromous fish.

Among the anadromous species that can be found in the Italian rivers, we focused our attention on the spawning habitat requirements of the Twaite shad (*Alosa fallax*, Lacépède 1803). *A. fallax* belongs to the family of Clupeidae and its distribution range is quite extensive. It inhabits the northeastern Atlantic Ocean, ranging from Morocco to Iceland and southern Norway, including the Mediterranean, North, and Baltic Seas [146], [147]. In Italy, landlocked population are also present in the biggest lakes of northern part (e.g., Lake Garda, [148]). *A. fallax* is considered vulnerable in the Italian IUCN [149], and it is listed in the Annex II and V of the European Habitats Directive (92/43/EEC), and in the Annex III of the Bern Convention. Recent studies on anadromous populations of *A. fallax* have revealed significant genetic differentiation among individuals inhabiting the European shores [148]. Therefore in this manuscript we generally refer to *A. fallax* as the shad populating the Mediterranean Sea [150]. Several studies investigated the biology of *A. fallax* across European rivers [146], [150]–[152]. The adult freshwater phase of *A. fallax* begins with the spawning migration, which typically occurs from February, in the Southern distribution area, to May, in the Northern distribution range. This migration is more pronounced when water temperatures exceed 10-12°C degrees [146]. Breeding has been documented to occur in both fresh and tidal waters, and mating events typically occurred close to the water surface [152], [153]. In freshwater environments adult shads are able to cover hundreds of kilometers to reach upstream spawning grounds [154], [155]. The spawning period can last 3-4 months, and the mating activity takes place during night at water temperatures around 18-22°C degrees [156].

While the biology of *A. fallax* has been relatively investigated, few researches focused on the spawning habitat requirements of this species [26]. [157] reported that, in different rivers of Wales, *A. fallax* prefers to spawn in the fast-flowing shallower areas (< 0.45 m) of glide, riffle and runs on different type of substrate from gravel to cobbles (0.2-25.6 cm), whereas deeper pools are used for resting during the day. [152], [158] analyzed the spawning habitat used by *A. fallax* in the Ebro river (Spain). By measuring the depth and velocity in some transects they reported that the spawning grounds were characterized by fast flow regions (1-1.5 m/s), ranging from 3 to 4 meters in water depth above gravel substrate. Similar information is reported in [146]. They conducted a review of more dated literature sources and argued that Twaite shad spawns in water depths ranging from 0.15 to 9.5 m above various substrates, ranging from mud to cobbles.

With the aim of developing the first meso-scale HSC in literature for the spawning period of *A. fallax*, we carried out different field campaigns in a hydro-morphologically homogeneous reach of the Tagliamento river (Northeastern Italy). Habitat depiction was achieved following the MesoHABSIM approach. In particular, high resolution spatial information derived from UAS (Uncrewed Aerial Systems), 2D hydrodynamic simulations, and field data were used for the definition and characterization of GUs at the flow conditions available during the spawning period. This information was used to train a classification RF model able to identify

the suitable mesohabitat for *A. fallax* to spawn, by analyzing the local physical habitat attributes of the GUs within the surveyed sub-reach. By recording with an infrared camera the mating activity of the shads along two nights of observation it was further possible to observe and analyze the mating behavior of such species.

4.2 Materials and methods

4.2.1 Study area

The Tagliamento river flows from the Alps to the Adriatic Sea for almost 170 km in the Friuli Venezia Giulia Region (Northeastern Italy), providing a total catchment of about 2850 km^2. The highest peaks of its basin reach 2700 m, while its springs are located near the Mauria Pass at an elevation of about 1200 m. The Tagliamento watershed mainly belongs to the landscape unit of mountainous areas (Alpine and Pre-alpine, 85% of total catchment) from its source to the Pinzano section (**Figure 4.1**a). Downstream the mountainous areas, river banks are not yet confined and the remaining part is occupied by the plains (15% of total watershed). Its fluvial system is characterized by an high coarse sediment supply [159] which bestows a wide braided planform pattern, from Socchieve to Madrisio for almost 90 km of the river course. From this section, the river, having dissipated much of its energy, begins to narrow, evolving into a meandering planform before flowing into the sea. An extensive morphological characterization of the watercourse can be found in [159], [160].

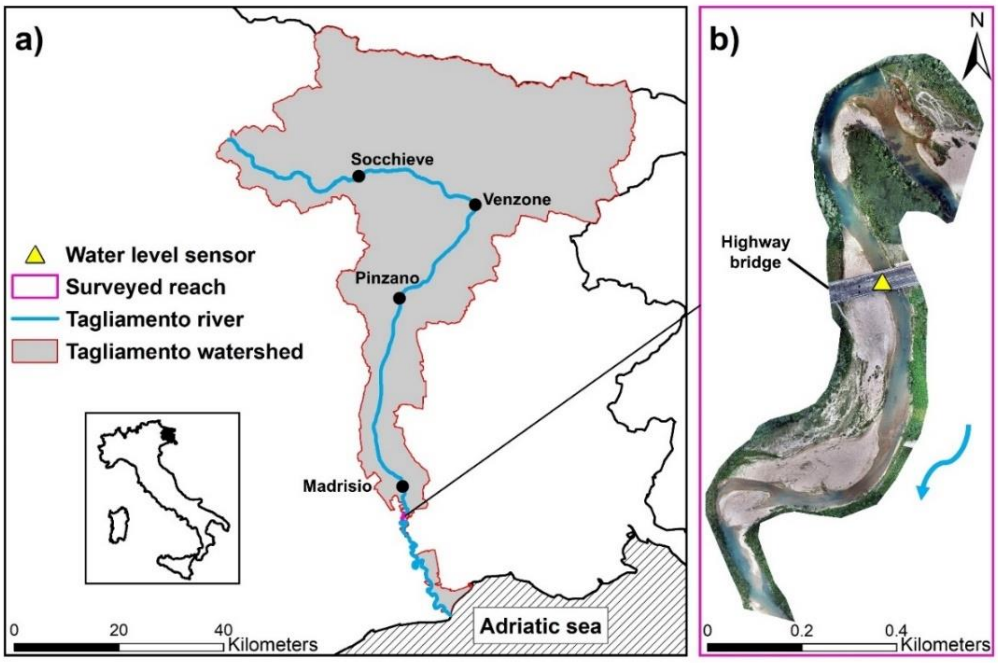


Figure 4.1. The study area: a) the Tagliamento watershed, and b) the surveyed sub-reach, as depicted in the RGB orthomosaic obtained on July 1st 2022. The yellow triangle represent the approximate position of the water level sensor installed in the study site. The primary flow direction is indicated by the blue arrow.

The upper part of Tagliamento basin is characterized by an Alpine climate, whereas in the lower reaches the Mediterranean climate is dominant [161]. Along its course, the river experiences high seasonal variability in flow, with peak discharges occurring during fall (October-November) and spring (May-June). Conversely, extend periods of flow intermittency, which can also determine the complete disappearance of the water table, may occurs in different portion of the braided reach especially during summer. In the downstream part, from Madrisio to the Adriatic Sea, the river returns to be perennial, due to the water supply provided by the groundwater resurgence phenomenon [162]. In the Venzone section, the mean discharge is approximately 90 m^3/s, with estimated 2, 5, and 10-year flood discharges of 1100, 1600, and 2150 m^3/s, respectively [161]. The Tagliamento course is not hindered by any major dam. In the upper part of the basin water withdrawals are mainly related to hydropower production, whereas few weirs for agricultural purposes are located nearby Venzone and Pinzano. In the lower part of its course no river dams or barriers are present and the stream is free to flow to the sea.

The study site is located in the downstream part of the river (**Figure 4.1**), approximately 32 km above the estuary in the Adriatic Sea. In this hydro-morphologically homogeneous reach, the river planform moves into a transitional morphology characterized by a single-thread channels with alternate bars [56]. Surveyed sub-reach provides a total length of almost 1500 m and it is characterized by an average width above 100 m. The mean slope is around 0.001, and sediment is mainly composed by small pebbles (2-6 cm), gravel (0.2-2 cm) and sand (< 0.2 cm). At the surveyed flow conditions, the GUs [60] pattern mainly includes (i) glides and riffles with some woody debris, (ii) deep pools (up to 5 m) with extensive canopy cover, and (iii) few backwaters (**Figure 4.2**). Levees and bank protection structures are present to preserve the surrounding settlements and the highway bridge piles, which have directly affected channel morphological dynamics. During the low flow periods, discharge and water temperature does not varied significantly (**Figure 4.3**) as mainly contribution to flow is provided by groundwaters [162].

4.2.2 Field surveys and data collection

From April 2021 to August 2023, different field campaigns were performed, with the aim of collecting useful data about spawning mesohabitat preferences of *A. fallax* in the surveyed sub-reach. In particular, it was possible to observe, monitor and analyze the habitat used by the *A. fallax* for mating purposes in two consecutive years.

During the middle of May 2022, a reproduction activity of the shad was detected by the authors within the study site. In order to obtain a river habitat depiction at the meso-scale, the wetted area was broken down into GUs [60],

according to the MesoHABSIM approach [54]. Spawning sites were located in particular areas of the surveyed sub-reach characterized mainly by glides and riffles (**Figure 4.2**d). These areas were mapped with a multi-band Real-Time Kinematic Global Navigation Satellite System (RTK GNSS) receiver (Emlid Reach RS2, Emlid, Budapest, Hungary) and registered in a Geographic Information System (GIS) environment. Furthermore, georeferenced information (by means of the RTK-GNSS receiver) about water depth and current velocity were recorded above the spawning sites using the RiverSurveyor M9 Acoustic Doppler Current Profiler (ADCP; Sontek, San Diego, California) installed on a vessel [163] and, in the shallower areas, the OTT MF Pro flow meter (Ott HydroMet, Kempten, Germany). Substrate composition was also assessed following the classification of the MesoHABSIM approach [54]. In particular, individual measuring points were randomly distributed in a stratified manner within the mesohabitats in which spawning was detected. To each measuring point was then assigned the most representative substrate category (**Table A-1**) within the 1 m^2 area. Thanks to the collaboration with the Ente Tutela Patrimonio Ittico (ETPI), during the surveys some female specimens of *A. fallax* with eggs were captured using fishing rods. Fish were captured by Dr. Davide Lesa in the deepest pools where they were resting during the daytime. With the aim of continuously monitoring flow rate and water temperature in the study site, a water level sensor HOBO U20L (Onset Computer Corporation, Bourne, Massachusetts) was installed in a river cross-section next to the highway bridge (**Figure 4.1**). During the survey, river discharge was also measured by means of the RiverSurveyor M9 (Q = 11.80 m^3/s).

Two-dimensional numerical models are extensively employed to simulate depth and velocity in rivers for studying in-stream habitat characteristics (e.g., [42], [43], [164]). In this study, due to the extension of the surveyed reach, UAS were used to obtain high resolution topographical information of the river habitat. Aerial images were collected with a DJI Phantom 4 Pro RTK quadcopter (FC6310R Camera Model), with a focal length of 8.8 mm, 5472x3648 pixel resolution and 2.41x2.41 µm of pixel size. The flight was performed on July 1st 2022 at an average height of 100 m with a ground sample distance of 1.6 cm/pix, when lower water levels were expected to be in the study site. 13 markers were placed within the surveyed area, and their position was measured with a Stonex RTK GNSS receiver to georeferenced the data acquired. The UAS was employed to obtain both the RGB orthomosaic of the study site (**Figure 4.1**b) and the corresponding Digital Elevation Model (DEM, **Figure 4.2**a,b), to be used for developing a 2D hydrodynamic model. Concurrent with the flight, a bathymetric survey was carried out by means of the RiverSurveyor M9. In particular, georeferenced information (by means of the RTK-GNSS receiver) about water depth and current velocity were collected by manually displacing the vessel above the water surface, where local depths were above 0.20 m [165]. Particular attention was given to the deeper areas (e.g., pools) where the riverbed was less visible from aerial pictures and therefore more difficult for the UAS camera to capture. During the survey, the GUs mosaic was outlined at flow conditions of Q = 8.15 m^3/s and complemented with information about local substrate composition and cover presence.

In May 2023, we confirmed the *A. fallax* presence in the study area, which was again used as a spawning site. During this field campaign, spawning activity were observed in the same glides and riffles previously mapped, and some females with eggs were caught again by Dr. Davide Lesa in the same pools. After verifying that no significant morphological changes occurred in the surveyed sub-reach, the data collection operations carried out in May 2022 were substantially repeated. Discharge was measured equal to 11.90 m^3/s, that was very close to the condition assessed during the field campaign of May 2022. During this field campaign, with the aim of recording the mating activity of *A. fallax*, we further utilized a GardePro trail camera A3S (GardePro, Hong Kong) equipped with infrared vision to capture videos over the course of two nights. For a non-intrusive monitoring, we strategically positioned the GardePro trail camera on a river bar, in correspondence of the spawning sites downstream the highway bridge (see **Figure 4.2**d). By framing the water surface, we continuously recorded from 2330 to 0215 hours.

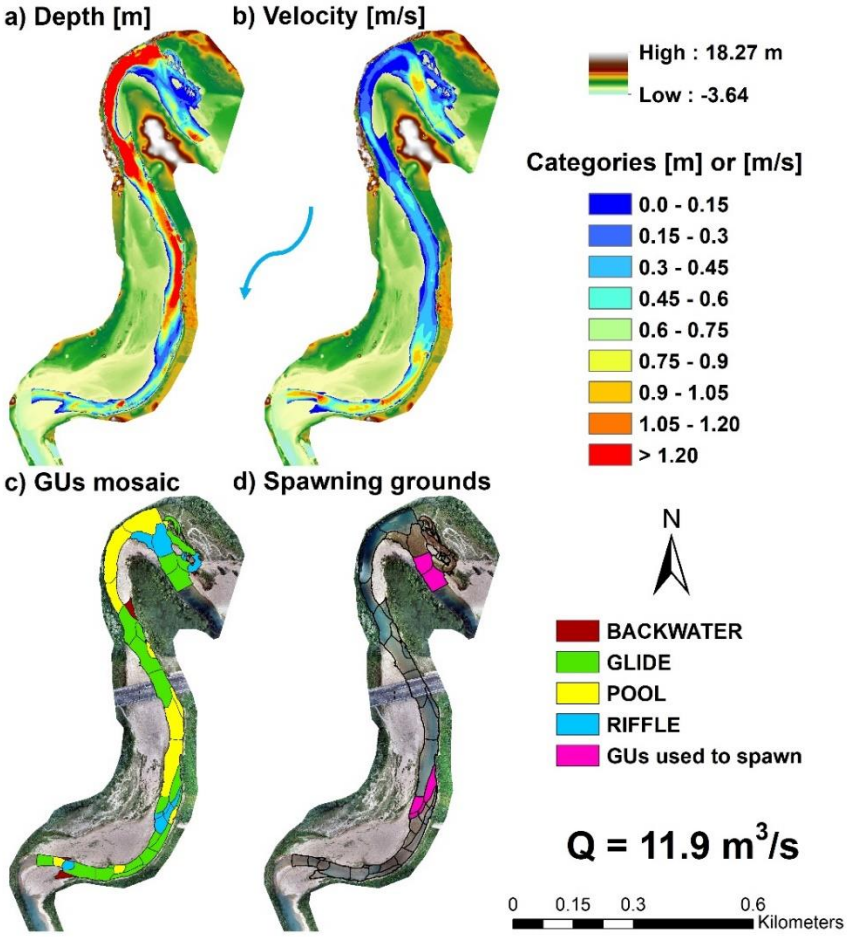


Figure 4.2. The simulation results for a) depth and b) velocity under the flow condition of 11.90 m^3/s, using the bathymetrically corrected DEM as background. Depth and velocity are color-coded according to the corresponding categories of the MesoHABSIM approach (**Table A-1**), ranging from the smallest (in blue) to the highest (in red). c) The geomorphic units (GUs) mosaic at flow rate of 11.90 m^3/s. d) The GUs where the spawning activities of *A. fallax* were observed are highlighted in purple. The primary flow direction is indicated by the blue arrow.

4.2.3 Data analysis and habitat description

The 2D images series captured by the UAS sensors were elaborated using the Metashape software (Agisoft, St. Petersburg, Russia), following a common workflow for river applications (e.g., [166], [167]). In particular, the principles of photogrammetry and the Structure-from-Motion computer vision technique were applied to obtain the RGB orthomosaic (resolution = 1.6 cm) and the 3D model (DEM, resolution = 6 cm) of the surveyed reach. Although the use of remote optical sensors is widely employed in river science applications (e.g., [168], [169]), to date there are no resolutive techniques to achieve an automatic reconstruction of the submerged riverbed topography for shallow streams (e.g., [167]). The primary challenge in obtaining a precise bathymetric profile of the wetted channel using optical photogrammetric techniques lies in compensating for the light refraction as it transitions between air and water, which determines an overall overestimation of riverbed elevations (e.g., [170]). However, for shallow and clear water rivers, the relationship between real depth (i.e., really possessed by the riverbed) and apparent ones (i.e., derived from the photogrammetric procedure) can be considered approximately linear, according to the assumptions of the Snell's Law [171], [172]. Therefore, the georeferenced information collected during the bathymetric survey (i.e., 3386 points) was used to train a linear regression model and estimate the real riverbed elevation. This model aimed at capturing the existing linear relationship between the homologous points collected with the RiverSurveyor M9 system (real depth, y) and derived from the photogrammetric processing (apparent depth, x). The resulting bathymetric model ($y = 1.52*x$, coefficient of determination $R^2 = 0.88$) was then used to reproject the photogrammetric-derived DEM submerged riverbed to the elevations really possessed by the surfaces. For the deeper areas (> 2 m) where the riverbed was not visible from the UAS sensors, a spatial interpolation was performed directly integrating the georeferenced depth collected by the RiverSurveyor M9. This process was mainly performed in a GIS environment, allowing us to obtain a bathymetrically corrected DEM (**Figure 4.2**a,b). To assess the effectiveness of the bathymetric correction applied to the DEM a validation was then performed. Specifically, considering the same data points employed to train the bathymetric model, the elevations of the bathymetrically corrected DEM were compared with river bottom values acquired by the RiverSurveyor M9, during the bathymetric survey. This analysis was conducted using scatter plots, and involved calculating the root mean square errors (RMSE) and the coefficient of determinations (R^2) of the linear regression model of the first quadrant's bisection (i.e., $y = x$, representing a perfect match between homologous points).

To reconstruct the hydrodynamic conditions of water flow during the spawning period of *A. fallax*, a 2D fixed-bottom numerical model was developed with the HEC-RAS (Hydrologic Engineering Center of U.S.A, Davis, California, Version 5.0.7) software. Following the recommendations of [43], the mesh construction was built using the DEM bathymetrically corrected of the study area, with a mean grid-size of 1 m^2. For calibrating the hydrodynamic model, we carefully selected the

Manning's coefficient (n, bed roughness), considered constant for the entire study domain [173], aiming to replicate the local hydraulic conditions measured during the UAS flight. Specifically, we focused on ensuring the best possible agreement between simulated and observed (i.e., derived from the bathymetric survey) depths and velocities, as well as the highest qualitative match between the simulated wetted surface extension and the real one, visible in the RGB orthomosaic. Furthermore, to guarantee model stability and reliability, particular attention was given to the definition of the computational time step, with the aim of maintaining the Courant number below one [174]. Once the model was calibrated, we conducted hydrodynamic simulations using the Saint Venant equations under steady-state conditions at 8.85 and 11.90 m^3/s (**Figure 4.2**). These discharges were chosen as representative of flow conditions commonly encountered by *A. fallax* during their spawning period, as they corresponded to the 25th and 75th percentiles of the flow rate distribution recorded by the water level sensor (**Figure 4.3**). Furthermore, the flow of 8.85 m^3/s closely resembled the hydraulic conditions during the UAS flight, while 11.90 m^3/s substantially overlapped the discharges recorded in both the field campaigns of May 2022 and 2023. This latter simulated discharge allowed a further validation of the hydrodynamic model by comparing the georeferenced water depths and velocity values recorded above the spawning sites using the RiverSurveyor M9 and the OTT MF Pro flow meter (i.e., 1009 points) with the homologous simulated values.

The output of the hydrodynamic simulations was exported in raster format and used synergically with the DEM and the RGB orthomosaic for the identification and definition of the GUs mosaic at the simulated flow conditions, according to what was recorded during the field campaigns. The mesohabitats representation was achieved using a GIS environment, storing the information in polygon shapefiles. As required by the MesoHABSIM approach, each GUs must be described with several habitat attributes (**Table A-1**). Depth and velocity distributions were assessed by extracting them from the output of the hydrodynamic simulations. Substrate composition, GUs longitudinal connectivity, and cover presence was derived from the georeferenced information collected during the field surveys, which were integrated and validated by referring to the RGB orthomosaic. Finally, GUs gradient was defined using the spatial information of both the DEM and the simulated water depths.

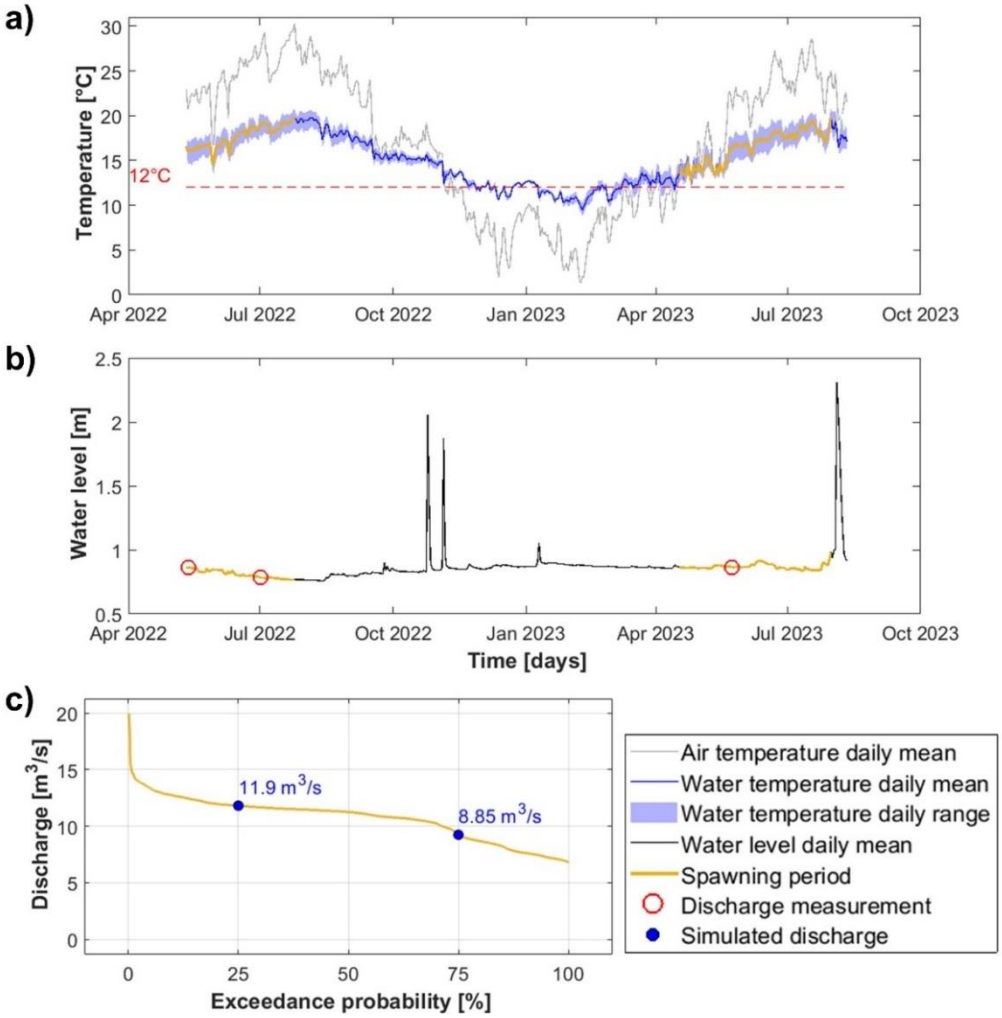


Figure 4.3. a) Daily mean air (in grey) and water temperature (in blue) time series from May 11th 2022 to August 11th 2023 registered by the HOBO U20L in the study site. The minimum threshold corresponding to 12°C, above which spawning activities were assumed to start, is represented by a dotted red line. b) Water level (in black) time series expressed as daily mean values. The date in which the discharge measurements were performed during the field campaigns are displayed using red dots. c) The flow duration curve of the spawning period. The simulated discharges for training the Random Forest model are highlighted in blue. For all images the variable corresponding to the spawning period is represented by a continuous orange line.

The data recorded by the HOBO U20L permitted to obtain a water level and a temperature time series of the study site, spanning from May 2022 to August 2023 (i.e., 15 months, **Figure 4.3**). These locally acquired series were used to infer the spawning period for *A. fallax*. Water temperature is recognized to significantly influence the spawning activity of freshwater fish [175], therefore we mainly focused on this variable for framing the reproduction period. According to [146], we set a minimum daily temperature threshold (12°C) above which spawning activities were assumed to commence (**Figure 4.3**a). Reproduction was considered to persist until the mean water temperature trend continued to increase, i.e., before reaching the annual maximum value. In this way the end of the spawning period approximately coinciding with the end of July for both 2022 and 2023 (lasting 3-4 months, [146]). Over these periods water levels, and consequently discharges, do

not vary significantly (**Figure 4.3**b). The discharge measurements from the field surveys allowed us to establish the correlation between water levels registered by the sensor (**Figure 4.3**) and the evolution of stream flows throughout the entire spawning period. Specifically, we transformed the water level series into a Water Surface Elevation (WSE) series, derived from the hydrodynamic model, assuming a linear relationship between these variables. The linear regression model was trained using both the water levels recorded by the sensor and the simulated WSEs corresponding to all available discharge measurements (i.e., 8.15, 11.80, and 11.90 m^3/s). Consequently, the flow rating curve was determined by interpolating WSE values derived from simulations conducted in the range of 6.00 to 20.00 m^3/s through a third-degree polynomial function, with coefficients determined using the least-squares method (e.g., [176], [177]). The resulting flow duration curve for the spawning period is illustrated in **Figure 4.3**c.

Finally, the videos captured during two nights in May 2023 were analyzed in order to (i) confirm the mesohabitat selection by *A. fallax* for spawning, (ii) better understand the mating behavior of *A. fallax*, and (iii) quantify the occurrence of surface mating episodes from the video records. Considering this latter aspect, particular attention was placed on distinguishing between actual mating events and mere mating attempts. In our video analysis, a successful spawning event was defined as an instance where the fish rapidly circled each other for a minimum of 3 seconds.

4.2.4 Mesohabitat suitability criteria

Probabilistic models were utilized to investigate the spawning habitat preferences of *A. fallax* by examining the association of GUs characteristics with the breeding areas used for mating activity within the surveyed reach (for further details please see **Figure A.1**). To identify the mesohabitat attributes (**Table A-1**) preferred by *A. fallax* for spawning, the Random Forest (RF) classification algorithm, introduced by [64], was employed.

This ensemble machine learning technique has found wide use in ecology due to its numerous advantages in effectively addressing classification problems. RF ability to handle high-dimensional datasets in a time-effective manner, to model intricate interactions among predictor variables, and reduce overfitting makes it particularly well-suited for ecological applications [65]. In particular, RF has been quite leveraged for shaping the HSC of different aquatic organism in the framework of the MesoHABSIM approach [19], [20], [22], [63].

RF, as implemented in R (library randomForest, version 4.6-7, [126]), relies on aggregating a large set of randomized trees, which are trained by selecting a random learning sample, achieved through bootstrap sampling [123], from the original dataset. To construct each branch of the trees a binary recursive partitioning technique is exploited, based on a random selection of a predictor from the variable

space. The value of the predictor which determines each partitioning is established in order to minimize the Gini impurity, thereby maximizing class imbalance in the resulting nodes. This process continues until a specified minimum number of observations in the terminal nodes is reached. The out-of-bag (OOB) data are the elements not included in the bootstrap sample, which, by majority voting, allows for cross-validated accuracy estimates across all trees.

For distinguishing between the unsuitable and suitable mesohabitat for the spawning of the shad, we developed a binary classification model involving two boolean responsive classes (defined as 0/1), where 1 indicated a >50% predicted probability of being a suitable GU for spawning. The predicted probability for classification RF models is determined by aggregating the votes from the majority of decision trees in the forest on OOB data. By considering all GUs described in the surveyed sub-reach at the two simulated flow conditions (8.85 and 11.90 m^3/s), the prevalence (i.e., frequency of mesohabitats in which the breeding activity was observed) was found to be 11.5%. Consequently, with the aim of obtaining a balance database, we implemented and tested a model that involved a prior random oversampling of the training dataset. In particular, we used the Synthetic Minority Over-sampling Technique (SMOTE, [178]), which facilitates the oversampling of the minority class by introducing synthetic instances along the line segments connecting all the k-minority class nearest neighbors. Consequently, the initial dataset of 104 samples (104 GUs) was increased to 184 samples to develop the model.

Our primary focus was on obtaining the final parsimonious model with the highest predictive performance. To achieve this, we conducted rigorous predictors selection and fine-tuned the hyperparameters. In particular, to assess the importance of each predictor, we utilized the Boruta algorithm, a popular wrapper for feature selection in the context of RF modeling [128]. Based on the Boruta analysis, we could select the most important predictors and, to avoid redundancy, we checked for high correlation (Spearman's rho correlation coefficient > 0.8) between them. Among these predictors, a further analysis for selecting the smallest number of variables that provided the best possible classification results was performed, as an excessive number of predictors could lead to increase the OOB error [127]. 12 variables were finally selected for the parsimonious RF model (**Figure 4.4**). Concerning hyperparameters tuning, we directed our attention towards those that are known to have substantial impact on enhancing model accuracy [179]. Specifically, we focused on: (i) the number of decision trees (ntree), and (ii) the number of predictors randomly sampled at each node (mtry). The ntree value was evaluated equal to 1000, following the recommendation of [129]. Whereas the mtry parameter was established equal to 3 and computed as the square root of the total number of selected predictors included in the model, following the approach of [179]. To assess the predictive performance of the RF model, we used accuracy, sensitivity, specificity, and the true skill statistic (TSS), proposed by [131] (see **A.3** for further details). Finally, we employed partial dependence plots (PDPs), which provided valuable insights into the model's interpretability, allowing to visualize

the marginal effect of the selected variables on the spawning habitat preferred by *A. fallax* [65].

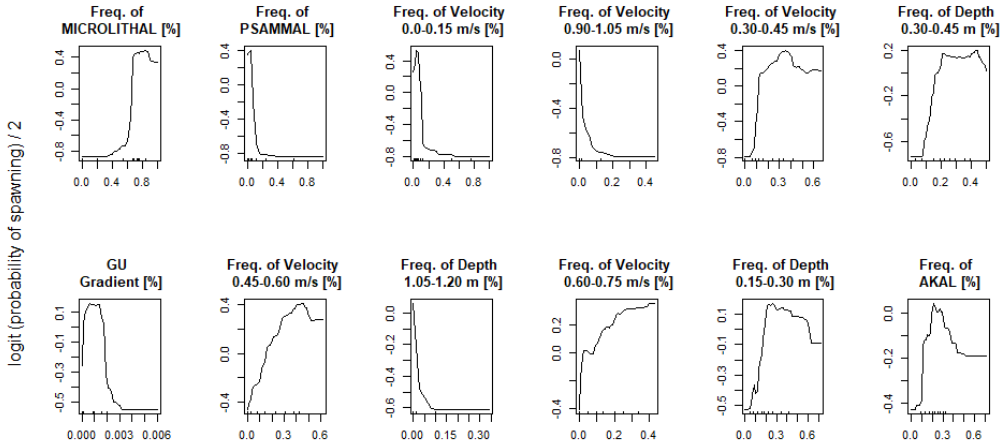


Figure 4.4. The Random Forest model for the spawning period of *A. fallax*. The selected physical attributes (**Table A-1**) for the SMOTE parsimonious model are presented (in order of importance) through Partial dependence plots, which express the relationship between attributes and the probability of presence.

4.3 Results

The validation of the bathymetrically corrected DEM achieved a RMSE of 0.12 m and an R^2 value of 0.92, therefore it was considered suitable to be employed as topographic information for the hydrodynamic model. For calibrating the 2D hydrodynamic model, the highest match between simulated and observed water depths and velocities was obtained for a Manning's coefficient equal to 0.03. In particular, for water depth we achieved a RMSE equal to 0.13 m (R^2 = 0.93), whereas flow velocity showed lower performance (RMSE = 0.14 m/s and R^2 = 0.83). Generally, the highest errors for depth were localized in correspondence of the deepest areas (> 1.50 m), where acquiring river bottom data was more challenging for the UAS sensor. For velocity, we observed that the hydrodynamic model slightly underestimating the highest values (> 0.90 m/s). Considering the hydrodynamic model validation at 11.90 m^3/s, we generally observed a satisfactory match between the observed and simulated depths (RMSE = 0.05 m; Scatter Index = 0.11) and velocities (RMSE = 0.14 m/s; Scatter Index = 0.22).

In the analyzed reach, it was possible to identified 104 GUs, 52 GUs for each simulated flow condition (**Figure 4.2**c). The highest amount of GUs (45.2%) corresponded to glides, followed by pools (21.1%), and riffles (20.2%). The remaining GUs consisted of backwaters, accounting for 13.5% of cases. Water surface area of the identified GUs varied from a minimum of 5.5 m^2, which correspond to a backwater, to a maximum of 4889.6 m^2 which corresponded to a

pool. Mean water depth for the flow rate 8.85 m^3/s was 0.85 m, whereas mean water depth for the flow rate 11.90 m^3/s was 0.88 m. At both flow rates, 78% of submerged channel was characterized by a water depth lower than 1.20 m. However, the deepest pools used by *A. fallax* to rest during the daytime exhibited higher water depths, up to 5.5 m. Mean flow velocities were estimated to 0.33 m/s and 0.38 m/s at the flow rates 8.85 m^3/s and 11.90 m^3/s, respectively. Around 50% of the submerged channel was characterized by flow velocities ranging from 0.30 m/s to 1.20 m/s, whereas, in the deepest pools, they were closed to zero. The riverbed substrate in glides and riffles was mainly constituted by *microlithal* (41.1% of total sampled points) and *akal* (22.9% of total sampled points). *Psammal* and *pelal* were mostly identified as the dominant substrate within pools and backwaters, corresponding to the 26.6% and 4.6% of total sampled points, respectively. Regarding fish covers, woody debris resulted the most common shelter for fish (observed in 68 GUs), followed by shallow margins (observed in 59 GUs). Canopy shading and boulders were observed in 32 and 16 GUs, respectively. Longitudinal and lateral connectivity was observed for all GUs and GUs water surface gradient ranged between 0 and 0.008.

The observed spawning sites used by *A. fallax* were associated with 6 GUs identified under the simulated flow condition of 11.90 m^3/s (**Figure 4.2**d). Such GUs were assumed to be suitable also for the simulated flow condition of 8.85 m^3/s, for which a direct observation in the field was not feasible. This assumption was made after assessing a high degree of consistency in the distribution of depth, velocity, and substrate values between both simulated flow conditions. Indeed, when considering the MesoHABSIM categories (see **Table A-1**), the p-value of the Kolmogorov-Smirnov test was higher than 0.95 for all three variables. Consequently, the total number of GUs deemed suitable for spawning resulted to be 12, with an overall prevalence of 11.5%. Specifically, 8 GUs were identified as glides, and 4 GUs were characterized as riffles. These mesohabitats were mostly defined by medium water depth (between 0.15 and 0.75 m), moderate to high current velocity (between 0.15 and 0.9 m/s), and a substrate composition of *microlithal* and *akal*, with very little sandy patches. Within such GUs, woody debris (100% of suitable GUs) and shallow margins (66.7% of suitable GUs) where the most representative covers.

The water level sensor enabled the assessment of water temperature evolution in the study site over 15 months of monitoring (from May 2022 to August 2023, **Figure 4.3**a). Absolutely, the minimum water temperature (8.6°C) was recorded at the beginning of February 2023, while the maximum temperature (21°C) occurred in late July 2023. For 2022, the spawning period extended from May 11th (the commencement of records) to July 25th, whereas for 2023 it was longer, ranging from April 16th to July 31st. Considering water levels, three significant peaks corresponding to high discharges can be clearly identified in the series (**Figure 4.3**b). The highest value occurred on August 4th, 2023 (2.31 m), with the subsequent two occurring on October 25th (2.06 m) and November 5th (1.87 m), 2022. Minimum water levels were recorded in mid-August 2022, bottoming values of 0.76 m. Focusing on the spawning period, water levels varied between 0.77 m

and 0.98 m (mean value = 0.84 m). Specifically, for 2022, maximum values were recorded at the beginning of the series, reflecting a decreasing trend in the water level series during this season. In contrast, for 2023, water levels were more variable, with periods of higher and lower values, depending on the occurrence of rainy events and the corresponding flow rates. The flow rating curve was computed using 9 data points (i.e., WSEs derived from hydrodynamic simulations), and exhibited a good capability to approximate the data (RMSE = 0.11 m^3/s; $R^2 = 0.99$). During the spawning period the flow rates spanned from 6 to 20 m^3/s (mean value = 10.71 m^3/s), reflecting the same trend described for the water level series (**Figure 4.3**c).

During the analyzed spawning period, mean water temperature was 16.4±1°C, mean air temperature was 21.7±3°C, and the moon was waxing crescent. A total of 72 mating events and 35 mating attempts were video recorded during the two nights of observation (**Figure 4.6**). The majority of the mating events occurred during the first night of observation, accounting for 61% of the total. The peak spawning time for both nights was assessed between 0030 and 0130 hours, encompassing more than 50% of the total recorded events. Mating episodes were generally brief, lasting from 3 up to 11 seconds (mean value = 5.5 s), and involved only a small number of individuals, from 2 to 4 fish were recorded participating simultaneously. Events were often preceded by pre-mating surface activity, consistently occurring upstream in the area used immediately later for spawning. Other features of mating activity recorded with the camera included (i) fast movements for engaging interactions and (ii) tail splashing, which is a common behavior of *A. fallax* during spawning [146], [152].

The implemented RF models allowed the identification of the most important physical habitat attributes for *A. fallax* spawning, leading to the definition of the first HSC in the literature for this species. The SMOTE parsimonious RF model demonstrated superior predictive performance, emerging as the final selected model (**Figure 4.4**). Through cross-validation, this model achieved an overall accuracy of 98.8%, a sensitivity (true positive rate) of 100%, a specificity (true negative rate) of 97.6%, and a TSS of 97.6%. The final RF model incorporated 12 mesohabitat attributes, as depicted in **Figure 4.4** through PDPs and ranked according to their importance. Overall, substrates emerged as the most important predictors. Specifically, *microlithal* (2-6 cm) resulted positively correlated with suitable mesohabitats for spawning, whilst *psammal* (sand) was negatively correlated. Considering velocities, both low (0.0–0.15 m/s) and high (0.90-1.05 m/s) values provided a negative influence on shad mating habitat selection. In contrast, favored categories (0.30-0.45; 0.45-0.60; 0.60-0.75 m/s) corresponded to medium velocities. Similarly, the probability of being a suitable GUs for spawning increased with the presence of medium depths (categories = 0.15-0.30; 0.30-0.45 m), and decreased with the presence of high values (category = 1.05-1.20 m). Finally, low GU gradients (< 0.002) and a presence of *akal* (gravel) from 20% to 40% positively influenced the shad GU selection for spawning.

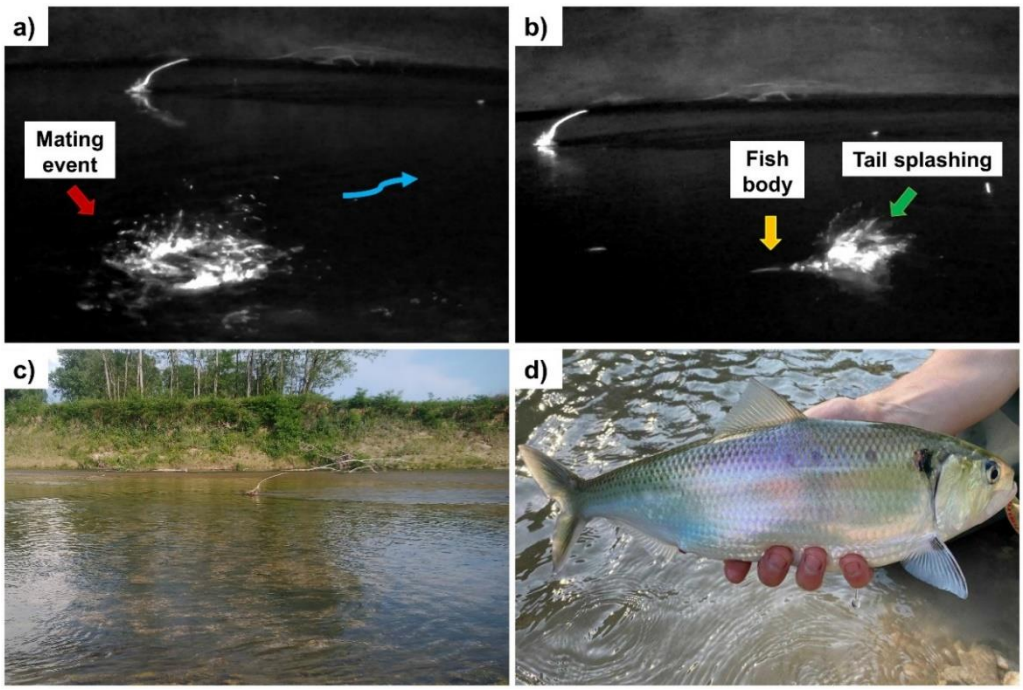


Figure 4.5. Video frames and pictures recorded during the field campaign in May 2023 with infrared and optical cameras. a) Example of successful mating event recorded by the infrared camera. The primary flow direction is indicated by the blue arrow. b) A pre-mating activity (tail splashing). c) A daily vision of the analyzed spawning sites. d) A specimen of *A. fallax* captured by Dr. Davide Lesa within a deep pool closed to the spawning site.

4.4 Discussion

Integrating acoustic devices and optical remote sensing systems for measuring river hydro-morphological dynamics is increasingly used to describe and model river systems [165]. These methods are particularly gaining prominence for depicting physical habitat at the meso-scale in shallow water gravel-bed rivers, especially when conducting in-stream surveys proves challenging [35], [43], [180]. For such applications, one of the main objective is generally the reconstruction of the riverbed topography at an elevated spatial resolution. However, a significant constraint in photogrammetric-derived 3D models consisted in a systematic overestimation of submerged riverbed elevation due to light refraction at the air-water interface. In this study, we used spatially distributed georeferenced depths, collected through a bathymetric survey, for correcting the submerged riverbed derived from the UAS data processing. This correction was achieved through an empirical approach based on the training of a locally calibrated mono-parametric linear regression model. The high data fitting between corrected and measured elevations (RMSE =0.12 m; R^2 = 0.92) aligns with the results obtained by [171]. In particular, they showed that this method generally proves more effective in reprojecting the apparent depths into real values compared to other approaches based exclusively on the Snell's law. Furthermore, if bathymetric data are available,

it is generally easier to be implemented compared to other approaches which performed the correction using trigonometric functions (e.g., [168]) or sophisticated deep learning algorithms (e.g., [181]).

Bathymetric data collected using doppler-based devices, represents a fundamental source of information for calibrating a hydrodynamic model. In this study, to fine-tune model parameters (e.g., bed roughness), we chose a spatially distributed approach (i.e., 3386 points), harnessing the advantages of employing a moving vessel as a data collector. Compared to transect-based procedures, this approach is considered superior in capturing the spatial heterogeneity in hydraulic features, allowing to achieve a higher level of agreement between model predictions and in-stream measurements [163]. The high degree of correspondence between simulated and observed data over the spawning sites can be attributable precisely to the use of this distributed approach. In line with common occurrences in hydrodynamic models (e.g., [163], our model absolutely better predicted depth rather than velocity values. This can be mainly related to the high spatial and temporal variability of velocities recorded through in-stream measurements. Indeed, flow velocity variation are generally influenced by multiple factors such as local channel geometry, bed roughness, potential presence of aquatic vegetation and woody debris.

River habitat evaluation was accomplished using the MesoHABSIM approach, integrating data from various field campaigns and the results of 2D hydrodynamic simulations to describe the GUs. Specifically, georeferenced data obtained from in-stream surveys, along with high spatial resolution information, enabled to obtain a detailed representation of the riverine habitat of the study site. Nonetheless, the flow conditions analyzed for defining the HSC closely resembled those observed during the data collection campaigns, facilitating a more accurate convergence and validation between observed and simulated conditions.

The spawning activities of *A. fallax* were exclusively observed in glides and riffles. These findings align with those reported in [157] for shad populations in Welsh rivers, where the same types of GUs was observed to be used for mating purposes. Another comparable behavior observed in shads corresponds to the utilization of deep pools during the daytime, where fish likely rest and gather before moving to the spawning sites during night [146], [157]. The presence of deep pools in close proximity to suitable spawning sites can provide shelters for *A. fallax* during daytime, and may constitute an important environmental feature.

Reproductive modes among freshwater fish exhibit remarkable diversity, encompassing variations in partner selection, spawning sites and periods, and distinct strategies for parental care [182]. Particularly, defining the spawning period can be challenging due to variations influenced by different environmental factors, which commonly are not monitored (i.e., local water temperature). Given the limitations of performing frequent river surveys, in this study, we attempted to indirectly determine the spawning period of shads using temperature time series locally recorded. This variable is considered to exert a high level of influence on

the spawning period for anadromous fish [175]. Indeed, in a recent study which aimed at predicting the occurrence of spawning in *Alosa alosa*, a species closely related to *A. fallax*, using machine learning algorithms and considering various environmental factors, one of the most significant predictors was found to be precisely temperature [183]. Despite the importance of this information, the monitoring of discharge within the Italian river network is limited to a restricted number of stream gauges, mainly located along major watercourses. Moreover, there is an almost complete absence of gauging stations measuring water temperatures. In the context of climate change, where extreme events (both floods and droughts) are on the rise, and temperatures are increasing, having this source of information can be crucial for the preservation of anadromous species like *A. fallax*. Therefore, mayor attention should be directed toward the installation of monitoring stations for both discharge and temperatures in rivers.

To establish the commencement of the spawning period, we defined 12°C as the minimum water temperature threshold, above which spawning was considered to begin. This value was took as reference after consulting the available literature (e.g., [156]). However, a higher degree of uncertainty surrounded the upper thermal limit we selected, as direct confirmation in the field was not possible to be achieved. In this case, we considered that the spawning period lasted until the day with the maximum annual water temperature is reached. This choice was based on (i) literature, which reports a suitable water temperature range of 18-22°C and a reproduction period lasting 3-4 months [156], (ii) an overall low fluctuation in water levels over the corresponding amount of time, and (iii) information provided by local fishermen on the presence of *A. fallax* in the study site. Compared to the findings reported by [156] and [158] in the literature, the spawning events we documented in May 2023 took place at a marginally lower water temperature, fluctuating between 14.6°C and 17.8°C. This variation could be linked to the particular hydrological characteristics of the study site, where, during periods of low flow, groundwater significantly contributes to the overall flow. Indeed, the maximum water temperature recorded in the dataset (21°C) is comparatively low for rivers at the latitude of the surveyed sub-reach (e.g., [184]). Water level series allowed the definition of the flow evolution during the spawning period of shads. For its definition we calibrated a flow rating curve by means of a consolidated approach successfully employed for large rivers [185]. Due to the scope of the research, the flow duration curve was exclusively defined for the spawning period. During the monitored period the lowest discharges were assessed in summer 2022. This reflects the important drought period which affected Northern Italy along this year [186]. Consequently a slightly general underestimation of the flow range which typically characterized the spawning period of shad in the study site may be occurred.

Monitoring the spawning activity of A. fallax poses significant challenges due to the complexity of obtaining detailed information on mating behavior in the water column and precisely locating spawning grounds at night. Traditional methods, such as electrofishing, are typically unsuitable for assessing the species distribution of nocturnal fish spawners, as they are intrusive and not recommended for nighttime

use. Acoustic records, which rely on direct hearing to locate and count mating events by capturing sounds produced during reproduction (e.g., [152]), have been a common alternative. However, these data collection strategies often struggle to precisely locate mating events and typically require multiple observers distributed along the river reach, making them labor-intensive and prone to human error. In this study, we explored a novel, non-intrusive approach using cost-effective infrared cameras mounted on tripods along the riverbanks near spawning sites. This technique represents a significant advancement in monitoring A. fallax spawning activity, as it allows for continuous and comprehensive visualization of mating events, thereby facilitating a more accurate assessment of both the behavior of individuals involved and the spatial distribution of these events (**Figure 4.5**). The use of infrared cameras enabled the simultaneous monitoring of a substantial river area (10^1-10^3 m^2), comparable to the extent of GUs, providing a feasible solution for assessing the mesohabitats utilized by shads for spawning. This capability offers significant advantages in studies aimed at understanding the habitat requirements of nocturnal fish spawners at the meso-scale. Indeed, as demonstrated in this study, employing such equipment allows for the precise localization of mating events, thereby identifying the GUs used to spawn. Additionally, this approach requires minimal human intervention, reducing the number of operators needed and enabling cost-effective monitoring. The ease of use of commercial infrared cameras further enhances the practicality of this method. To address potential limitations related to spatial resolution, particularly in complex riverine environments, future research could explore the integration of infrared cameras with UAS. Such integration could extend coverage area and improve spatial resolution, making the technique even more effective for applications within the MesoHABSIM framework.

Concerning the mating behavior observed through the analysis of the videos, we noted a close resemblance to descriptions provided by previous researchers studying various shad populations in Europe. This similarity might be linked to the level of genetic differentiations identified in multiple samples of *A. fallax* populations by [148]. These findings indeed suggest a certain level of interactions and potential interchange among populations residing in different regions of the distribution area. In particular, the peak spawning activity took place between 0030 and 0130 hours, a timeframe that aligns with information reported in the literature. [146] mentioned, in their review, a peak in mating activity occurring between 2200 and 0300 hours. More recently, [152] observed a peak time at 0215 hours in the Ebro River, while [187] noted the maximum mating activity between 0100 and 0130 hours for *Alosa alosa* in the Garonne river (France). The duration of mating events we evaluated also corresponded with the findings of previous authors [146], [152]. However, possibly due to the more accurate recording technique we used, we generally observed a slightly longer duration, ranging from 3 to 11 seconds. Interestingly, we observed that the longest mating events typically involved a higher number of individuals. Nocturnal spawning is an adaptive strategy to minimize exposure to predators [188]. Consequently, we speculated that moon

phases might influence the mating activity of *A. fallax*, anticipating a higher activity during the new moon when lower light conditions prevail. Our hypothesis found some support in our observations, as we noted a declining trend in the number of mating events during the two nights of recording under a waxing crescent moon. Interestingly, [187] reported an increasing trend in mating activity for *Alosa alosa* during three nights of observation under a waning crescent moon. However, it is surprising that we could not find additional confirmation of a potential correlation between *A. fallax* mating events and moon phases in the literature. This aspect necessitates further investigations to better understand the environmental factors influencing shad reproduction. Lastly we analyzed the prevalent sense of rotation exhibited by fish during mating events in an attempt to identify any potential preference. We found no significant preferred direction of rotation, as both clockwise and counterclockwise rotations were utilized in nearly equal proportions. However, there was a slight prevalence of clockwise rotation, accounting for 55% of the total visible mating events, compared to counterclockwise rotations. Surprisingly we did not find any existing literature discussing this aspect.

The application of the RF classification algorithm enhanced to comprehend the correlation between the spawning requirements of *A. fallax* and the mesohabitat attributes incorporated in the MesoHABSIM approach. Specifically, the final parsimonious RF model, composed of 12 habitat attributes, revealed that for mating purposes shads typically looked for glides or riffles distinguished by medium depth (0.15-0.45 m), moderate current velocity (0.30-0.75 m/s), and a small-sized substrate (*microlithal* and *akal*). These features closely aligned with the findings reported by [157] and [155] on the spawning sites they identified in Welsh and French rivers, respectively. Focusing on substrates, [157] reported that shads also spawned over coarser substrates (cobble, 6.4-25.6 cm). However, such sediment was almost absent in the study site (less than 1% of the total amount). Conversely, [152] documented mating activities on gravel substrates in the Ebro river (Spain). Nevertheless, they reported the use of higher values of depths and velocities for spawning: 3-4 m for depth and 1-1.5 m/s for velocity. The RF already proved its effectiveness in identifying the habitat requirements for freshwater species in the framework of the MesoHABSIM approach [19], [22], [25], [63]. The high predictive performance (Accuracy = 98.8%; TSS = 97.6%) achieved for current application reaffirms its capabilities. Consequently, this methodology can be considered appropriate for identifying suitable GUs for the spawning of anadromous species.

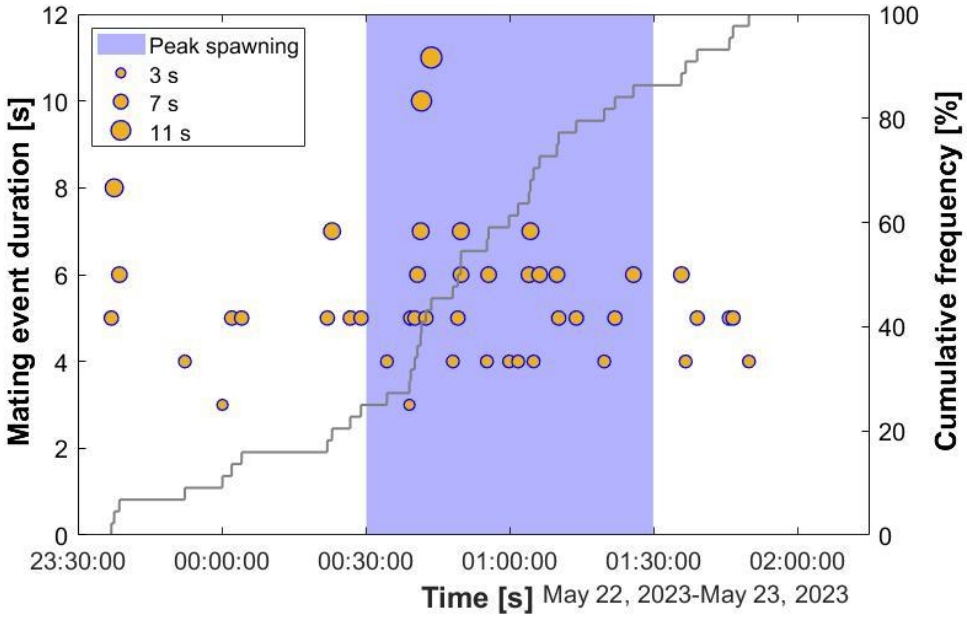


Figure 4.6. Occurrence (orange dot) and duration (dot size) of mating events recorded by the infrared camera during the first night of observation of the field campaign of May 2023. The broken line in grey represents the cumulative frequency of total mating events (44) recorded during the observation period. In blue is highlighted the assessed peak spawning time.

Chapter 5

5. Transferability of Mesohabitat Suitability Criteria in Northern Italy

The work presented in this chapter has been partially derived from [25].

5.1 Introduction

Freshwater ecosystems are globally deemed to be one of the most threatened environment of the world [5]. Among the several pressures on these ecosystems, hydrological and morphological alterations related to hydropower generation and water abstraction are identified as high impact factors determining river ecosystems degradation and biodiversity loss [6].

In order to mitigate such impacts and to enhance water resource management, since 1980s, Habitat Suitability Models (HSMs) were proposed [32] and widely used at the global scale. Despite a high number of different approaches, the most recent meso-scale models, such as the MesoHABitat SImulation Model (MesoHABSIM, [18]), have proved to be adequate for assessing habitat availability for fish in rivers [17]. MesoHABSIM is a methodological approach that utilizes geomorphic and hydraulic units (GUs or mesohabitats, [60]) as spatial unit of analysis (about 10^{-1}-10^{3} m). MesoHABSIM includes a large range of biotic and abiotic habitat attributes (e.g., hydraulic variables, substrate composition, covers and shelters for fish, water surface gradient) which are used to describe habitat availability for fish. For evaluating the amount of available habitat for a certain species or life stages, MesoHABSIM involves the use of binary nested models (absence/presence and presence/abundance), to distinguish between not suitable/suitable habitats and suitable/optimal habitats. Generally, the most reliable

binary models are those developed by using sophisticated machine learning techniques able to analyze the empirical data collected in environmental reference sites [21], [63]. In particular, the use of Random Forest (RF, [64]) classification algorithm has recently increased to identify most important variables that are related to species presence and abundance within mesohabitats [46], [189].

Since HSMs were proposed, freshwater ecologists argued on the possible transferability of micro-scale habitat suitability criteria (HSC), developed in a particular context, to other streams [190]. In this regard, several microhabitat-oriented studies, mostly carried out in Northern America, revealed some critical issues in applying a unique HSC to different hydro-morphological contexts, concluding that site-specific HSC are preferable (e.g., [191]). However, developing site-specific criteria is usually expensive and time-consuming, and, in cases of degraded habitat, may not be feasible. Mayor constraints to successfully allow the transferability of such HSC can be related to the spatial scale of analysis. The microhabitat scale does not consider hydro-morphological variables around each evaluated microhabitat (or point). This approach may have drawbacks on the habitat description. Indeed, environmental conditions around an organism, not only at the point where it is observed, are known to be important factors affecting habitat suitability [192]. For mobile animals, such as fish, a larger spatial extent may be used to describe their habitat preferences in order to increase the validity and reproducibility of a HSC in multiple contexts [59]. The meso-scale HSMs have already proven their effectiveness in supporting HSC transferability between multiple European rivers [59]. In particular, the MesoHABSIM approach coupled with a HSC developed with RF, was recently used to assess the available habitat for the European crayfish (*Austropotamobius pallipes*) in different riverine contexts of Italy [22].

With the aim of testing the transferability of meso-scale fish HSC in Northern Italy, different field data collection campaigns were carried out over the last 10 years in reference sites (i.e., natural conditions of river morphology, flow regime, fish community composition, [63], [91]. RF was used to build meso-scale HSC calibrated with field data collected in Piemonte and Valle d'Aosta Regions. In this study, the calibrated mesohabitat models were applied to 9 river reaches located in other Regions (Emilia-Romagna, ER; Liguria, L; Piemonte, P; Trentino-Alto-Adige, TAD; Valle d'Aosta, VDA) and not included in the model calibration dataset. Together with the application of the MesoHABSIM protocols [54], quantitative fish data collection were carried out within each mesohabitat to describe fish species distribution in terms of presence/absence. Model transferability tests were achieved by comparing the predictions of considered RF models with fish species distribution assessed in the field in terms of accuracy, sensitivity, specificity and TSS (True Skill Statistic, [46], [131]; see **A.3** for further details).

5.2 Materials and methods

5.2.1 Case study

The study sites consisted of nine river reaches, located in Alpine and Apennine catchments, distributed in five regions of Northern Italy (**Figure 5.1**). In particular, four reaches (Belbo, 2; Ghiandone, 3; Orco, 5; and Pellice, 6) were located in the Piemonte Region, two reaches (Argentina, 1; and Malacqua, 4) in the Liguria Region, and one reach (Rabbies, 7; Savara, 8; and Trebbia, 9) respectively in Trentino-Alto Adige, Valle d'Aosta, and Emilia-Romagna Regions. The majority of them (2, 3, 5, 6, 8) were located in Alpine watersheds and belonged to the Po river drainage basin, the longest Italian river. Only reach 9, despite flowing into the Po river, it pertained to the Apennine area, whereas reach 7, positioned in the Alpine area, belonged to the Adige river basin. Furthermore, considering the study sites of Liguria Region, both pertained to Tyrrhenian sea catchments, although reach 1 is located in the Alps, whereas reach 4 in the Apennines.

Despite a quite extensive spatial distribution, considered river reaches are characterized by similar hydro-morphological characteristics [193], resumed in **Table 5-1**. In particular, reaches 1, 4, 7, 8 belong to the landscape unit of mountain areas, whereas 3, 5, 6, 9 are located in the Po river plains, and 2 can be considered as part of the hilly areas. Although 1 and 4 are mountain streams, characterized by a confined straight-sinuous (C-SS, [56]) morphology, they are marked by gentler slopes and by a local fish fauna dominated by cyprinid fishes (e.g., *Barbus plebejus*, *Telestes muticellus*). On the other hand, reach 7 and 8 are typically Alpine high gradient streams [91], where exclusively brown and marble trout can be found. The remaining reaches (2, 3, 5, 6, 9) are mostly characterized by unconfined or partly confined valley edges and by a prevalent cyprinid fish community. Only in reach 5, due to the proximity to the mountainous area of its watershed, trout populations are present.

5.2.2 MesoHABSIM approach

MesoHABSIM is a methodological approach that models fluvial habitats based on a specific hierarchical structure of morphological classification [56]. It allows the evaluation of available habitat for freshwater species using geomorphic and hydraulic units (GUs or mesohabitats, [60]) as a primary metric. GUs are evaluated in terms of habitat suitability (suitable/not suitable) by the application of a HSC and accordingly to their local biophysical attributes. These riverine features (**Table A-1**) involve both abiotic (flow velocity, depth and substrate composition) and biotic (biotic substrate, presence of aquatic or overhanging vegetation) factors, which mainly influence the patterns of habitat use by freshwater fishes [18].

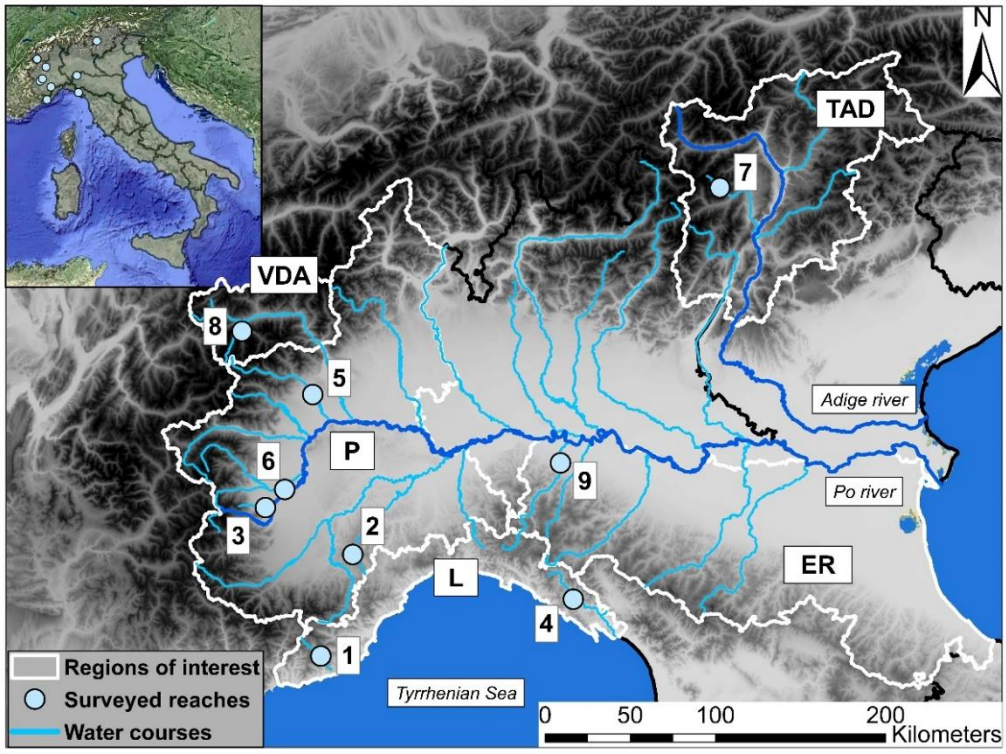


Figure 5.1. Location of the surveyed reaches considered in the study. Regions of interest: ER = Emilia-Romagna; L = Liguria; P = Piemonte; TAD = Trentino-Alto-Adige; VDA = Valle d'Aosta. Surveyed river reaches: 1 = Argentina; 2 = Belbo; 3 = Ghiandone; 4 = Malacqua; 5 = Orco; 6 = Pellice; 7 = Rabbies; 8 = Savara; 9 = Trebbia.

5.2.3 Field data collection

GUs depiction and fish data collection were carried out following the MesoHABSIM protocols and standards [54]. In particular, by using a hierarchical structure of morphological classification [56], [60] it was possible to identify a morphologically homogeneous reach in each considered river with (i) limited hydrological and morphological alterations, and (ii) quite natural conditions of fish community composition. The study sites (**Table 5-1**, sub-reaches) were then selected and the GUs description was based on a mobile mapping technique defined in [54], [91]. This mapping technique allowed the user to record the so called 'GUs mosaic', outlying the wetted perimeter of sampled mesohabitats and gathering all their abiotic and biotic factors (**Table A-1**). It is based on the use of a rangefinder (LTI, Trupulse 360R), a rugged field computer (e.g., Panasonic Toughpad FZM1, with GPS positioning) and a Geographic Information System (GIS) software. In particular, by means of the rangefinder, the GU areas were delineated and stored in the GIS environment, and the mesohabitat-scale features (GU type, GU longitudinal connectivity, GU gradient, cover, shores characteristics) were recorded. Depth and velocity values were measured using a flow meter (e.g., Marsh McBirney Flo-Mate 2000) and substrate compositions were assessed from each of the mapped mesohabitats [54]. Moreover, at each river survey, flow discharge was measured at

the beginning and the end of each study site. Finally, the recorded information was organized and processed with GIS software to produce detailed maps of the aquatic habitat in the study area. Fish data were collected by sampling each GUs within the study site with backpack electrofishing (i.e., two-pass removal method, [92]) before the GUs depiction. To ensure the direct association between sampled GUs and the captured fish species, each mesohabitat was kept separated by using nets [63]. Collected fish were identified at species level and measured in terms of total length (TL) before being released within the same sampled mesohabitat. This latter measurement was then used to classify each specimen as adult or juvenile according to the length/age relationships reported in [21].

Table 5-1. Name, location, morphological classification, and characteristics of surveyed reaches. River morphology codes (according to [56]: C = confined; P = partly confined; U = unconfined; SS = straight-sinuous; M = meandering; PM = pseudo-meandering; B = braided. Reach width represents the mean value of the active river channel width in each surveyed reach.

River/Creek	Reach name	Region	UTM 32N coordinates	Basin area [km^2]	Reach morphology	Reach length [m]	Reach width [m]
Argentina	1	Liguria	E: 406244.02 m; N: 4865984.92 m	209	C-SS	306	18
Belbo	2	Piemonte	E: 424991.19 m; N: 4925539.43 m	470	C-SS	92	8
Ghiandone	3	Piemonte	E: 373716.49 m; N: 4953060.71 m	100	U-M	160	15
Malacqua	4	Liguria	E: 554450.8 m; N: 4899310.76 m	30	C-SS	211	16
Orco	5	Piemonte	E: 401489.62 m; N: 5019384.86 m	913	P-PM	580	85
Pellice	6	Piemonte	E: 385031.57 m; N: 4963706.95 m	371	P-M	1500	105
Rabbies	7	Trentino-Alto Adige	E: 640563.96 m; N: 5140724.51 m	150	C-SS	132	9
Savara	8	Valle d'Aosta	E: 359939.34 m; N: 5056504.41 m	146	C-SS	235	20
Trebbia	9	Emilia-Romagna	E: 546950.03 m; N: 4979274.44 m	1070	U-B	760	400

5.2.4 Mesohabitat suitability criteria

Based on the available information about fish communities, as well as the data collected during the field campaigns, meso-scale HSC for 5 freshwater fish species were selected to test their transferability capabilities. These models were previously developed using the Random Forests (RF) classification algorithm to distinguish between presence and absence of the fish, using field data collected at the meso-scale in several years of sampling in reference sites of the Italian Alps [63], [91].

For juvenile brown and marble trout a global model was considered since it's challenging to clearly identify the juvenile specimens from simple field recognition [194]. **Table 5-2** reports the species and the life stages for which the corresponding RF models were tested in terms of transferability among surveyed reaches.

Table 5-2. Random Forests models of freshwater fish species and life stages considered in the study. For each model the reaches name in which it was applied with the corresponding total amount of sampled GUs are reported.

Species (Eng.)	Species (Lat.)	Life stage	Reach name	Sampled GUs
Brown trout	*Salmo trutta*	A	5, 8	72
Marble trout	*Salmo marmoratus*	A	5, 7	27
Juvenile trout	*Salmo trutta/marmoratus*	J	5, 7, 8	87
Bullhead	*Cottus gobio*	A	3, 6	16
Italian barbel	*Barbus plebejus*	A	1, 2, 3, 4, 5, 6, 9	105
Italian vairone	*Telestes muticellus*	A	1, 2, 3, 4, 5, 6, 9	105
		J	1, 2, 3, 4, 5, 6, 9	105

Models predictions in terms of GUs suitability were achieved by using SimStream-Web software [54], a specific web service developed to implement the MesoHABSIM approach in Italy. This software makes all the RF models used in this study available to any user, facilitating their application in hydro-morphological impact assessments of regulated rivers (see **153** for further details). The physical attributes of each GUs were taken into account in order to assess the rank of suitability (not suitable/suitable) of each sampled mesohabitats according to the application of a specific RF model. Models predictions were then compared with the observations collected during the field campaigns. Finally, to test model transferability, the predictive performances of considered RF models were assessed using four performance metrics, i.e., accuracy, sensitivity, specificity, and true skill statistic (TSS, [46], [131]).

5.3 Results

Field data consisted of 180 sampled mesohabitats distributed within the 9 study sites. In particular, most of the analyzed GUs were found to be as riffles (30% of total amount), followed by glides (21%), rapids (17%), and pools (14%). Whereas backwaters and cascades were respectively sampled only in the 6% and 5% of total GUs amount. In total, more than 5000 fish were captured within surveyed mesohabitats. Overall, the most common fish species was found to be the Italian vairone (*Telestes muticellus*), which represented 52% of total specimens. By way of example, in **Figure 5.2** are represented (i) the GUs mosaic, and (ii) the observed and (iii) predicted distributions for adult brown trout (Salmo trutta) assessed in reach 8.

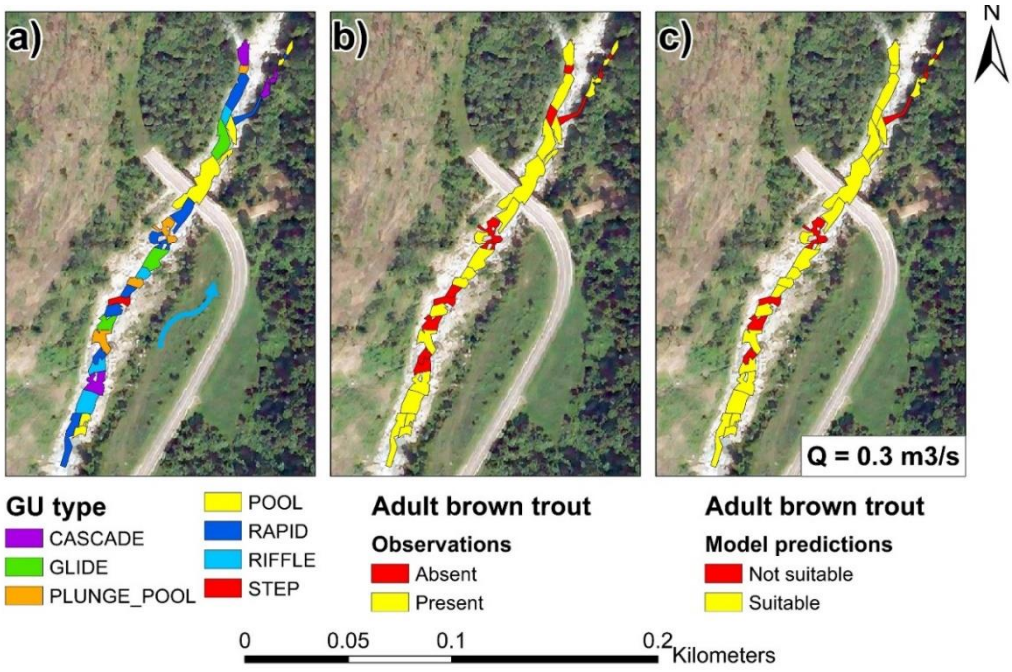


Figure 5.2. GUs, observed distribution, and habitat suitability map for reach 8. a) GUs mosaic and b) observed distribution for adult brown trout (Salmo trutta) assessed during the field campaign at 0.3 m3/s of discharge. c) predicted distribution for adult brown trout by the application of corresponding RF model.

The considered RF models showed quite high predictive performances for assessing the presence or absence of individuals within surveyed mesohabitats, with slight differences depending on the specific HSC (**Table 5-3**). Overall, models accuracy varied from 0.75 to 0.82 and TSS from 0.52 to 0.75, whereas sensitivity and specificity exhibited scores in range 0.75-1 and 0.72-1, respectively. Considering accuracy, the juvenile trout model showed the highest value (0.82), followed by the adult marble trout and bullhead models (0.81 each). These two latter models, furthermore, exhibited the highest TSS scores (0.75 for bullhead and 0.72 for marble trout). The Italian barbel model, on the contrary, resulted to be globally the least accurate (accuracy = 0.75 and TSS = 0.52). Finally, models sensitivity was generally assessed to be greater than specificity, except for bullhead, which exhibited the highest prevalence (0.75, ratio between fish presence and total observations).

Table 5-3. Predictive performances obtained for the considered RF models.

Species (Eng.)	Life stage	Prevalence	Accuracy	Sensitivity	Specificity	TSS
Brown trout	A	0.60	0.77	0.78	0.74	0.53
Marble trout	A	0.33	0.81	1.00	0.72	0.72
Juvenile trout	J	0.62	0.82	0.87	0.73	0.60
Bullhead	A	0.75	0.81	0.75	1.00	0.75
Italian barbel	A	0.40	0.75	0.80	0.72	0.52
Italian vairone	A	0.64	0.80	0.83	0.74	0.57
	J	0.68	0.78	0.80	0.72	0.53

5.4 Discussion

Results of the present application demonstrated that the considered meso-scale HSC based on RF can be considered transferable among streams of Northern Italy. In particular, we assessed quite high predictive performances for all analyzed models (Accuracy ≥ 0.75 and TSS ≥ 0.52), no matter the considered life stage, the number of GUs used as validation dataset, and the spatial location of the surveyed river reaches. Such results, in our opinion, can be related to the structure of the MesoHABSIM approach, which (i) enables river habitat description using an ecologically relevant spatial scale, (ii) is based on a robust and adequate hydro-morphological characterization of the analyzed GUs, (iii) may include in the analysis a large range of biotic and abiotic environmental descriptors, not only at the point where the organism is observed.

However, we observed some variation in the performance of the HSC models across different species, with predictive capabilities for the Italian vairone and Italian barbel being marginally lower compared to other species. This discrepancy may be attributed to the broader range of river habitats utilized by these rheophilic cyprinid species, as opposed to the more specialized habitats used by the salmonids and cottids studied. Indeed, these cyprinid species were found across a larger number of monitored reaches (7 out of 9), suggesting that their mesohabitat usage is more variable. This variability might result in a slightly reduced ability of the RF models to accurately predict the presence or absence of these species within the GUs.

Applying the MesoHABSIM approach to the entire Northern Italian territory should be of primary importance for ecological flow assessment and the design of habitat restoration measures. The use of validated meso-scale HSC can generate a robust habitat assessment for water abstraction licensing. Starting from 2017, MesoHABSIM has been increasingly used in Italy, as it was established as a reference method for ecological flows design and impact assessment of water abstractions [54]. In this regard, the present study can provide important insights for a wider application of this approach to the entire Italian context. Accordingly, further river sites, belonging for instance to the Center or Southern Italy, can be selected in order to increase the validation dataset and to verify models

transferability in other regions. Furthermore, due to a general lack of knowledge on the habitat requirements for endemic Italian freshwater species [26], additional fish data collection and meso-scale HSC for different fish species should be developed and validated.

PART II: non-perennial rivers

Chapter 6

6. Exploiting Sentinel-2 dataset to assess flow intermittency in non-perennial rivers

The work presented in this chapter has been partially derived from [29], with my primary contribution being the conceptualization and development of the Random Forest models used to establish daily-scale hydrological conditions in analyzed river reaches.

6.1 Introduction

Non-perennial rivers (NPRs) are ubiquitous watercourses which are characterized by the occurrence of non-flowing periods, with dry stream beds or chains of isolated ponds of water. A recent study [74] assessed that water ceases to flow for at least one day per year along more than half of the world's river network. In addition, the extension of NPRs network is expected to increase in the near future because of anthropogenic pressures such as water withdrawals, land use change and climate change. These causes can turn perennial rivers into non-perennial ones or increase the non-flowing periods in streams which are already non-perennial [77].

Due to the combination and succession of both terrestrial and aquatic ecosystems, the time-averaged biodiversity of non-perennial rivers is extremely high. These watercourses may support important ecosystem processes and provide valuable goods and services, such as the provision of materials (water and timber), freshwater and riparian biodiversity, regulation of biogeochemical cycles, and an ecological corridor for both wild and herded animals [79]. These highly dynamic environments require specific management framework to protect their ecological

and socio-economic values [72]. In Europe, it is necessary to develop reliable methods and indicators for the assessment of "ecological status" for these types of water bodies, as required by the European Water Framework Directive (WFD, [195]). However, non-perennial rivers are still not fully recognized in the WFD, in which they are a classified type of water bodies only in Mediterranean regions [196].

One of the main obstacles for the implementation of correct management policies is the lack of information on the ecological functioning of non-perennial rivers. In particular, there is no adequate data about the duration and frequency of non-flowing periods that are the primary determinants of ecosystem processes. River flow intermittence influence directly or indirectly biological communities, depending on the characteristics of low flow and non-flowing periods. The knowledge of flow intermittence patterns (frequency and duration of water presence at the reach scale) is essential for many applications such as the setting of ecological flow requirements, the evaluation of hydrological alteration, the estimation of the river capacity to assimilate potential contaminants and the optimized programming of monitoring plans [197]. The application of WFD requires the classification of ecological status based on comparison with a reference condition (i.e., a similar but undisturbed river). Consequently, it is necessary to know the degree of intermittence (undisturbed and possibly altered) in order to correctly apply the directive [198], [199].

Hydrological indicators used to measure flow intermittence patterns are estimated through sufficiently long time series of measured or simulated streamflow on a daily or monthly scale. For streams characterized by rapid flow regime changes, such as the small streams of Mediterranean-climate, daily data recorded over at least 20 years are often necessary [200]. However, streamflow gauges are rarely present in NPRs [74] and have some criticisms in representing the spatial variability of areas submerged by water, especially during the low flow period and during the ponding condition, i.e., when the water in river channels is confined in isolated ponds [201]. Given the scarcity of direct discharge measures, hydrological models were proposed to simulate discharge time series and the regime over a long period of time [200]. However, the use of hydrological models may require a large amount of data to quantify the parameters governing the rainfall-runoff processes [202]. Another significant limitation is the lack of traditional gauging stations for calibrating the models [203]. In addition, many models have been developed with reference to perennial rivers and may be unsuitable for simulating the hydrologic regime of NPRs [204]. To simplify the problem, some authors have developed models to predict the intermittence class alone rather than the continuous series of flow rates over time. [197] used random forest models to relate intermittence classes to climate, catchment area, shape and slope. They attributed the model's poor performance to the fact that intermittency is also governed by other factors such as water table fluctuations and seepage through river bed. These processes, which are strongly heterogeneous, result in a low spatial correlation of intermittence patterns. [74] developed a statistical random forest (RF) model to estimate the distribution of intermittent rivers and ephemeral

streams across the globe. Observed streamflow data were linked to 113 potential predictors related to climate, physiography, land cover, soil, geology and groundwater.

It is important to state that knowledge of the flow rate (measured or simulated) in a specific section of a river is not sufficient to describe the space-pattern of presence/absence of water along entire river segments [205]. In the presence of strong spatial variability in the flow occurrence and surface water presence, the extrapolation of point measurements, recorded in one river cross-section, to ungauged ones may generate high uncertainty, even one has to predict presence/absence of surface water. Moreover, NPRs may be characterized by long non-flowing periods with presence of isolated pools and ponds. The spatial extension and duration of this ponding condition cannot be easily extrapolated from traditional ganging station and an overall view of the river reach is necessary to identify frequency and duration of such hydrological condition (namely ponding condition). This is possible with an airborne or ground photographic survey. However, due to the high costs, the spatial coverage and temporal resolution of these surveys are limited and therefore they lack in capturing the high spatio-temporal variability of NPRs' hydrological conditions.

In this context, the use of satellite data constitutes a unique and crucial resource. Satellite data has the potential to cost-effectively monitor large areas (global coverage) with high temporal resolutions (in some cases daily or weekly acquisitions are available). Their use for monitoring the hydrological conditions of NPRs has so far been limited by two factors: the spatial resolution of the satellite images and the availability of images at affordable costs. High resolutions are needed for monitoring small rivers, a characteristic often associated with the transient hydrological regime. Very high-resolution images (space resolution of the order of 0.5 m) are available for commercial use but their use for continuous monitoring in long time intervals is limited by the high costs of the products. Among freely distributed multispectral images with systematic global coverage, the Sentinel-2 mission provides the highest spatial resolution (10 or 20 m, depending on the band) and revisiting frequency (10 days, with one satellite in orbit since 2015 and 5 days with two satellite since 2017).

Satellite monitoring of river wet channels has received much attention in the recent scientific literature. [206] used Landsat TM (Thematic Mapper) and ETM (Enhanced Thematic Mapper Plus) images, with 30 m spatial resolution, for wet channel mapping of narrow (less than three pixels wide) and large rivers. [207] used Landsat 4-5 and 8 to identify morphological changes in the Po river over a time period of approximately 30 years. [208] used Sentinel-2 images to delimit water, vegetation, and dry-sediment on various Italian rivers from 30 to 300 m wide. [209] detected changes in the size of water pools in non-perennial rivers with average width of 40–100 m in the Western Cape, South Africa, using a combination of Landsat 8 and Sentinel-2 datasets. [210] employed the archive of Landsat-5 and Landsat-7 to estimate a parameter that describes the shape of the relationship

between wet channel width and its frequency of occurrence, for more than one million river reaches in Australia. This parameter was used to classify the degree of intermittency as a function of the frequency with which the river width is close to its maximum or minimum value.

In this study we developed a procedure to estimate the duration of three different hydrological conditions (flowing, ponding and dry conditions) in NPRs. To do this we processed Sentinel-2 data to generate false color images (FCIs) in which the water pixels stand out from the background. Field data and very high-resolution images acquired in various conditions of water flow were used to evaluate the reliability and operational limits of satellite observations. Three different hydrological condition were identified for all suitable and available archive images (seven years of observation). This information was used to calibrate Random Forest (RF, [64]) models able to predict the daily occurrence of each hydrological condition at the river reach scale, using precipitation and air temperature data as input variables. In particular, two types of binary RF models were developed, the first was implemented to differentiate between flowing and non-flowing (ponding and dry) conditions and the second further detailed the non-flowing condition by discriminating between ponding and dry conditions. The analysis was developed for five morphologically homogeneous river reaches belonging to three small streams in the Campania Region (Southern Italy): Sciarapotamo, Mingardo and Lambro.

6.2 Materials and methods

6.2.1 Case study

The study cases are five reaches of the river network of the “Cilento, Vallo di Diano and Alburni” National Park, located in the province of Salerno, in the Campania Region (Southern Italy). The National Park covers an area of 1810 km^2, stretching from the Tyrrhenian coast to the foot of the Apennines (see **Figure 6.1**), with an altitude range from sea level to the top of the Cervati Mountain, at 1898 m a.s.l. Established in 1991 to preserve its great flora and fauna biodiversity, it is one of the widest Italian National Park. It includes 29 Sites of Community Interest (SIC) and 8 Special Protection Areas (SPA), set in application of the European Habitat (92/43 / EEC) and Birds (79/409 / EEC) Directives. Fauna species of considerable community importance are present, such as the otter (*Lutra lutra*), that is the icon symbol of the park , many amphibians (e.g., *Bombina pachipus* and *Salamandrina terdigitata*), odonates (*Oxygastra curtisii* and *Coenagrion mercuriale*) and fish (*Lampetra planeri* and *Rutilus rubilio*). From a geological point of view the Park is mainly composed of carbonate and terrigenous mountain massifs, marly-clayey hills as well as alluvial and coastal plains [211]. A system of carbonate aquifers produces a complex underground circulation and the presence of several springs. The climate is characterized by a wet season from September to May, the rainiest month is November with an average of around 90 mm, the driest month is July with

an average of around 10 mm. The total annual average is around 2553 mm [212]. While, considering only the period of observation (2015-2021) it was on average 1300 mm. The warm season June-September has a maximum daily temperature above 27°C, and the cool season November-March has a maximum daily temperature below 17°C. Five morphologically homogeneous river reaches were investigated: three reaches (M1, M2, M3) belong to the Mingardo, one (L1) to the Lambro and one (S1) to the Sciarapotamo streams (see **Figure 6.1**).

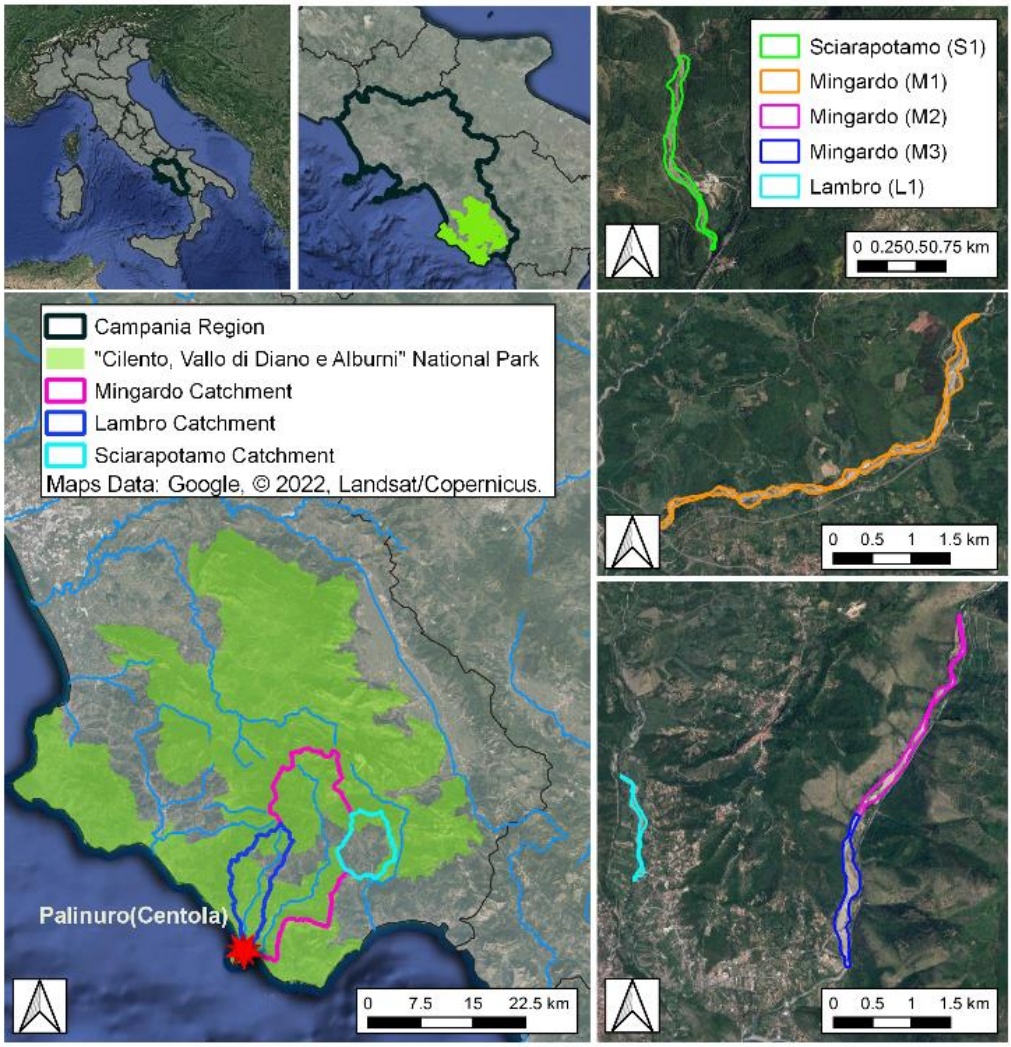


Figure 6.1. Geographical framework of the study area.

In **Table 6-1** some significant characteristics of the studied reaches are reported. The drained catchments were calculated by placing the closure section at the downstream end of each reach, the average width was calculated from the ratio of the area of the active channel to the length of the center line. River reach morphology was evaluated following the approach proposed by [56].

Table 6-1. Characteristics of the studied reaches. Reach morphology codes: C = confined; PC = partially confined; U = unconfined; W = wandering; S = sinuous.

Catchment	Reach	Drained catchment [km^2]	Average width [m]	Reach morphology
Sciarapotamo	S1	54	107	PC-W
Mingardo	M1	180	77	PC-W
Mingardo	M2	221	62	C-S
Mingardo	M3	225	117	PC-W
Lambro	M4	74	38	U-W

The Sciarapotamo river is a right tributary of the Bussento river, it has a catchment area of about 54 km^2 and a length of about 11 km. The study reach (S1) ends at about 500 m upstream of the confluence with the Bussento river, (**Figure 6.1**), it has a narrow channel with a wandering planform (braiding index = 1.21, and sinuosity index = 1.09, [56]). The River Basin Management Plan (RBMP), developed by the Southern Apennines Basin Authority (Autorità di Bacino Distrettuale dell'Appennino Merdionale), classified the Sciarapotamo as intermittent. It has only one withdrawal from groundwater and with reference to the WFD, it is deemed to have high ecological status and good chemical status.

The Mingardo river is characterized by the largest drainage area (about 232 km^2). It originates in the Gelbison mountain and flows in the Tirreno sea close to the village of Palinuro with a total length of 38 km. Three reaches are investigated, the upstream wandering channel (M1) and two other consecutive reaches closer to the outlet, the upstream of these two is a single-thread sinuous reach (M2) and the subsequent one is a wandering reach (M3). The main outlet of the floodplain aquifer is into the river, around 600 m downstream the end of reach M3. According to the RBMP all the studied reaches of the Mingardo are perennial, there are withdrawals from groundwater and springs, and the ecological and chemical status are good for all the reaches [195].

Finally, the Lambro river, with a total length of 22 km and a drained catchment of about 78 km^2, originates in the Gelbison mountain and flows into the Tirreno sea about 500 meters north of the mouth of the Mingardo river. The studied reach (L1) is wandering. According to the RBMP the Lambro is perennial, there are withdrawals from springs for both domestic use and irrigation. The ecological status is sufficient and so is the chemical status ([195].

6.2.2 Remote sensing datasets and filed surveys

The choice of the most suitable sensor to observe a specific physical process depends on many factors [213]. One of the most important aspects is the definition

of the needed spatial resolution of satellite data that depends on the dimension of the target. Following [206] the minimum width of the river that can be monitored is equal to three image pixels. When the objective is to monitor the hydrological conditions of non-perennial rivers, the width of the wet channel is also particularly relevant. Another critical issue is represented by the temporal resolution, which depends on the speed of evolution of the observed process [214]. A weekly revisit frequency may be not sufficient in many cases, because the flooding or drying process of the river can be much quicker. Moreover, to fully describe frequency and duration of NPR hydrological conditions, a multi-year archive of data must be available. Given the large number of required images, the cost of imagery acquisition can become a limiting factor. Among the multispectral images freely distributed with systematic global coverage, the Sentinel-2 mission provides the highest spatial resolution and revisit frequency. Sentinel-2 is a mission of the European Space Agency (ESA) under the Copernicus program. It comprises a constellation of two identical satellites, Sentinel-2A and Sentinel-2B launched on 23 June 2015 and 17 March 2017, respectively. With both satellites in orbit, in the studied area the revisit frequency is 5 days. Both satellites carry on board the Multispectral Instrument (MSI), which provides 13 spectral bands in the visible, near infrared (NIR) and short wave infrared (SWIR) wavelengths, with four bands at 10 m (B2, B3, B4, B8), six bands at 20 m (B5, B6, B7, B8a, B11, B12), and three bands at 60 m (B1, B9, B10). In **Table 6-2**, the spectral characteristics of Sentinel-2 data are shown.

Each Sentinel-2 image is a tile of 100 km x 100 km. Given the limited spatial extension of the selected river basins, all the analyzed river reaches were included within the same image. For the present study, we downloaded 141 images covering the years from 2015 to present from the Copernicus Open Access Hub (https://scihub.copernicus.eu/dhus/#/, last accessed on 8 December 2021). Level-2A Bottom-of-Atmosphere (BOA) images are available for most of the dataset, with the exception of images acquired in the early years of mission operation; for which an atmospheric correction with the Sen2cor tool of Sentinel Application Platform (SNAP) was performed. The lower resolution bands were all resampled to a resolution of 10 meters using the bilinear interpolation provided by SNAP tool.

A very high-resolution satellite image (VHR), an orthophoto and field observations were then used as ground truths. The VHR image used is the one provided free of charge by Google Earth Pro, dating on June 14th 2019. The orthophoto was produced through a survey with a UAS (Uncrewed Aerial Systems) performed on December 13th 2021. The UAS mounted a Hasselblad L1D-20c camera with exclusive Hasselblad Natural Colour Solution (HNCS) technology. The restitution and ortho-rectification of the acquired images were performed in Agisoft Metashape environment. Geo-located ground pictures and measurements of the width and depth of water ponds were taken during field surveys performed on June 26th 2020, July 26th 2020, September 19th 2020 and February 6th 2021.

Table 6-2. Characteristics of Sentinel-2 Multispectral Instrument (MSI).

Wave length range [nm]	Spatial resolution [m]			Spectral region
	10	20	60	
423-463			B1	Coastal aerosol
458-523	B2			Blue
543-578	B3			Green
650-680	B4			Red
698-713		B5		Red Edge
733-748		B6		Red Edge
773-793		B7		Red Edge
785-899	B8			NIR
855-875		B8a		NIR narrow
925-965			B9	Water - Vapour
1350-1410			B10	SWIR - Cirrus
1565-1655		B11		SWIR
2100-2280		B12		SWIR

6.2.3 Meteo-hydrological data

The meteo-hydrological data were extracted from the "Centro Funzionale Multirischi della Protezione Civile Regione Campania" website (http://centrofunzionale.regione.campania.it/) covering the period 2015-2021. We used daily time series of rainfall, air temperature (maximum, mean, minimum) and water levels. The available measuring stations within or adjacent to the Sciarapotamo, Lambro and Mingardo catchments were respectively 6, 3 and 8 for rainfall and 3, 5 and 3 for temperature. Rainfall and temperature data were spatially interpolated on catchments area using Thiessen polygons method. Daily water levels were available at two gauging stations, located 500 m downstream L1 and M3 reaches respectively.

6.2.4 Method for the identification of the hydrological condition

To distinguish as best as possible wet channel, sand and vegetated bars, the difference between spectral signatures of water, sediment and vegetation can be

exploited [215]. Different spectral signatures are due to the fact that the reflected and emitted quantity of electromagnetic energy differs as the wavelength and the land usage conditions vary. Consequently, starting from the VHR image provided by Google Earth Pro, the geo-located pictures and the orthophoto derived by the UAS survey, we extracted several polygons with known land covers (water, bare sediments, grass and bushes). We plotted the spectral signatures across the Sentinel-2 bands, for the different soil cover classes, using the pixels contained within their respective polygons. All the Sentinel-2 bands were used except the atmospheric bands B1, B9 and B10. To account for the difference between seasonal variations of the hydrological condition, the spectral signatures were extracted in winter (February 2021), late spring (June 2019) and late autumn (December 2021). In the cases where the Google Earth Pro image (June 2019) and field observations (February 2021) were used as ground truth we considered four cover classes: water, bare sediments, grass and bushes. Whereas, in the case in which the more resolute, UAS acquired, orthophoto was available (December 2021), it was possible to further differentiate the areas with deeper water from those with shallower water.

A set of three bands was identified in which the three land covers water, sediment, and vegetation are most distinguishable. The three bands were overlaid to create false-color images (FCIs). The FCIs were then used to identify the hydrological condition on the day of the satellite acquisition. Specifically three hydrological conditions were distinguished: 1. the longitudinal flow of water is continuous, this condition was named “flowing” (F); 2. there is no continuous flow, but a pattern of disconnected water ponds is present, this condition was named “ponding” (P), and 3. the riverbed is completely dry, or the water ponds are too small to be detected, this condition was named “dry” (D). The identification of the three hydrological conditions was performed by visual interpretation of the FCIs. We inspected the FCIs at a fixed mapping scale of 1:20000 to obtain a standardized result. Possible interpretation ambiguities were minimized by using three simple and well recognizable categories (flowing, ponding and drying) and by having the same interpreter perform the visual inspection on all of the imagery for consistency.

The hydrological condition identification is easily reproducible by anyone using the free Sentinel-2 dataset and the FCI_maker code that we developed and made available (https://code.earthengine.google.com/220275e2e31d308773432fdecadc8a2f). The FCI_maker code allows to visualize the FCIs images, it works in the Google Earth Engine (GEE) that is a freely available cloud computing portal, containing data collection of satellite imagery with global cover [216].

6.2.5 Random Forest Classification

The Random Forest [64] classification algorithm, as implemented in R [126], was used to explore the relationship between the meteo-hydrological data (rainfall

and air temperature) and the hydrological condition (F/P/D) of non-perennial rivers. The classification algorithm was trained using as predicted feature the classified hydrological conditions, while the predictor features were represented by the rainfall and temperature data spatially interpolated at the catchment scale by Thiessen polygons. For this analysis, the water level time series were not taken into account as they were available only nearby reach M3 and L1. As the hydrological regime of non-perennial rivers can be disassembled into one flowing condition (F) and two non-flowing conditions (P and D conditions, [30]), we developed binary classification RF models able to distinguish between flowing/non-flowing (F/NF) conditions and the ponding/dry (P/D) conditions. In this way for permanent ponding reaches (river stretches that never achieve a totally dry condition and wetted areas persist over time among subsequent flowing conditions) exclusively one F/NF model was calibrated, whereas for drying reaches (river stretches that can experience the total disappearance of water table during non-flowing period) both F/NF and P/D models were applied. RF models were developed both at the local (individual reach models) and regional scale (all reaches together, Global Model - GM) and all model performances were evaluated. To address potential bias in the RF models due to class imbalance, we developed classification models using a random oversampling of the training dataset, by randomly sampling with replacement the observations from the minority class in both F/NF and P/D dataset (see e.g., [74]). As for reaches M1 and M2 a total dry condition was never assessed from the image analysis therefore exclusively the F/NF models were calibrated. In total 10 RF classification models were developed and tested.

As primary predictor variables of NPRs hydrological conditions, we considered (i) the daily time series of rainfall (R) and (ii) maximum, mean and minimum air temperature (T_MAX, T_MEAN, T_MIN) from 2015 to 2021. To explore the effect of rainfall and temperature at different temporal scales, we aggregated the daily records into cumulative rainfall (R) variables and average temperature variables (T_MAX, T_MEAN, T_MIN) before the satellite image acquisition. For cumulative and average variables we considered 6 different time intervals, i.e., 3-5-7-10-30-90 days. A total of 28 predictor variables were therefore included in the RF analysis, using the following codes: R3, R5, R7, R10, R30 and R90 for rainfall variables, and T3_, T5_, T7_, T10_, T30_, T90_MAX, MEAN, MIN for air temperature variables.

To optimize the predictive performances of each RF model, we minimized the out-of-bag (OOB) error carrying out variables selection and hyperparameters tuning. To reduce the number of predictors in RF models, we tried to select the smallest number of variables providing the best possible classification result (parsimonious model). Variables selection was performed by (i) using a common algorithm for features selection named Boruta [128] and (ii) avoiding high correlation (Spearman's rho correlation coefficient > 0.7) between selected variables [46]. The Boruta algorithm is implemented in R as a package and allows the user to identify the most important predictors for classification purposes. It relied on the random forest classification algorithm and, through an iterative procedure, the most significative predictors are identified by comparing the

relevance of these features with a randomized version of them. Three hyperparameters were tuned [46], [129], [130]: (i) the number of decision trees (ntree) defined as two times the replicates required to stabilize the OOB error, (ii) the number of variables randomly sampled in each node (mtry) computed as the square root of the total number of predictor features considered in each model (with a minimum of 2), and (iii) the amount of observations used to train each tree (sampsize) to maximize models performance. Predictive performances of developed RF models were assessed using four common performance metrics, i.e., accuracy, sensitivity, specificity, and true skill statistic (TSS, [46], [131]; see **A.3** for further details). Finally, individuals RF models were used to predict the daily occurrence of the hydrological condition in all considered reaches when the Sentinel-2 images were not available or exploitable during the period 2015-2021.

6.3 Results

6.3.1 Spectral signature analysis and false color images

The spectral signatures of the various analyzed land covers are shown in **Figure 6.2**a,b,c. It can be seen that the reflectance values in the infrared bands are higher for shallow water than for deep water. This may be due to the fact that when the water depth is shallow the reflectance is affected by the response of the underlying sediment bed. The sediment curve of **Figure 6.2**c is lower than the ones in **Figure 6.2**a,b. This could be linked to the variation in water content, in fact at higher water content, the reflectance of sediment is known to be smaller in all wavelengths [217]. This explanation seems confirmed by the observation that the number of dry days before the acquisitions of June (**Figure 6.2**a), February (**Figure 6.2**b) and December (**Figure 6.2**c) was 10, 4 and 1 respectively.

We can observe that the classes water, grass and bushes are little distinguishable in RGB images, because the red (B4), green (B3) and blue (B2) have very similar reflectance values. However, these bands allow to easily distinguish the mentioned classes from the sediments. In NIR bands, the reflectance is more variable between different land covers. For example, in B8 water and grass reflectance values are very different while sediment and bushes are still indistinguishable from each other.

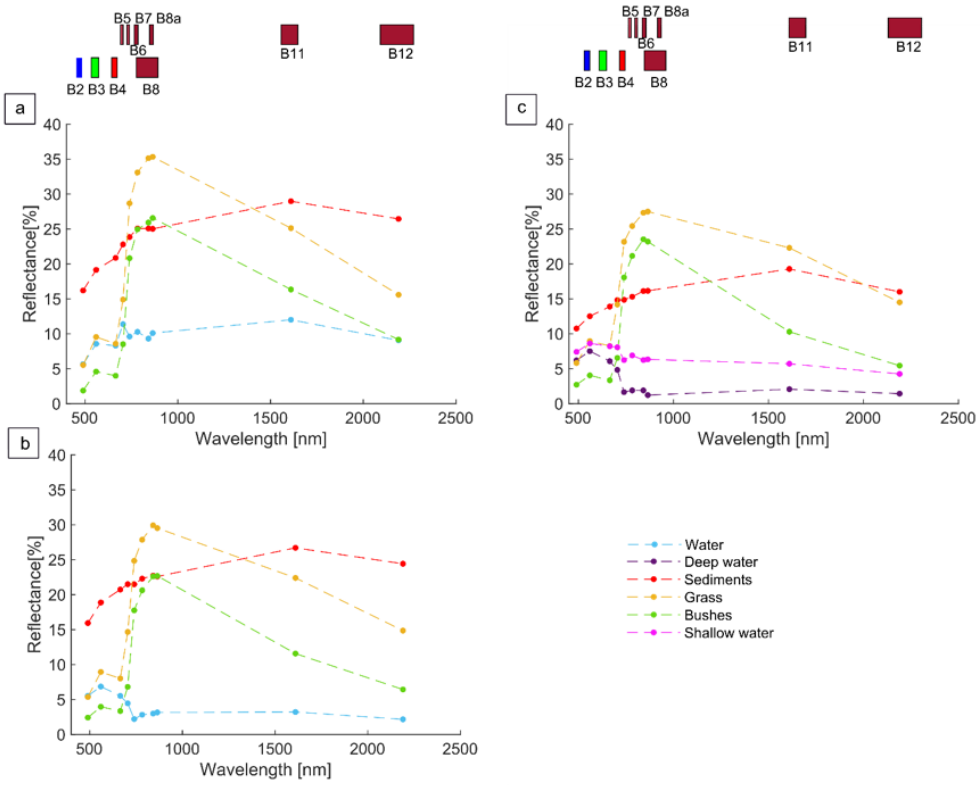


Figure 6.2. a) Spectral signature of late spring season, Google Earth of June 2019, b) spectral signature of winter, field pictures of February 2021, c) spectral signature of late autumn season, ortophoto of December 2021.

In the SWIR, both B11 and B12 allow to distinguish fairly well all the classes. Unfortunately, these two bands have a coarser spatial resolution (20 m) than visible and B8 bands which are provided at 10 m. Since RGB images do not allow to differentiate adequately the land cover classes (see **Figure 6.3**b), it is more convenient to create FCIs through the composition of 3 bands to allow better distinction between classes. An optimal composition was obtained with the bands B11 of the SWIR, the B8 of the NIR and the B4 of the visible. Despite the good capabilities of the SWIR bands for class separation, we used only one of the two, due to their coarser resolution. The B11 was finally chosen because it has higher capability of distinguishing between grass and water in summer season. Examples of FCIs obtained by the composition of bands 11, 8 and 4 and RGB are reported in **Figure 6.3**c and **Figure 6.3**b. In the FCIs composition, the color red was associated with B11, green with B8, and blue with B4. Consequently, the water has a black or dark blue color, while the vegetation has a green color with decreasing intensity, in some cases almost tending to yellow, as it passes from thick vegetation to sparse vegetation. The light pink color, on the other hand, is associated with sediments or soil without vegetation cover. In some situations (e.g., dry or large sediments), the sediments can also take on a white color (see **Figure 6.4**c). It can be seen that in the FCIs the presence of water can be distinguished much better than in the RGB image (see **Figure 6.3**b,c).

6.3.2 Comparison of false color images with ground truth

To assess the actual possibility of observing the hydrological condition from the FCIs analysis, several comparisons were made with the ground truths introduced in paragraph "Method for the identification of the hydrological condition". The test case's comparisons are summarized in **Table 6-3**. It is worth noting that the field surveys and the orthophoto are contemporary with the Sentinel-2 acquisitions while the Google Earth Pro image was acquired two days after the coupled Sentinel-2 image. In the two-day interval between the two acquisitions, there was no precipitation, so the only possible changes were due to evaporation and consequent possible reduction in water surface area. However, since this was a very short period it is reasonable to assume that there was no significant change in the extension of the wet channel. The set of ground truths used provided a fairly good description of the various seasonal hydrological condition.

Table 6-3. Pairs of Sentinel-2 and ground truth images.

Test case	Ground truth source	Ground truth date	Sentinel-2 date	Study Reach
1	Google Earth Pro	14 June 2019	12 June 2019	M1, M2, M3, L1
2	Field survey	6 June 2020	26 June 2020	S1
3	Field survey	26 July 2020	26 July 2020	S1
4	Field survey	19 September 2020	19 September 2020	S1, M3
5	Field survey	6 February 2021	6 February 2021	M1, M3, S1
6	Drone	13 December 2021	13 December 2021	M3, S1

For the sake of brevity, only a selection of the performed comparisons is shown below. **Figure 6.3** shows the test case n°1 for the M1 reach. It can be noticed that the wet channel clearly stands out from the other component of the river corridor in the FCIs images (**Figure 6.3**c). On the contrary the wet channel is not easily distinguishable in the RGB (**Figure 6.3**b) obtained by the same Sentinel-2 acquisition.

Despite the much coarser resolution of the FCI (**Figure 6.3**c) compared to the VHR (**Figure 6.3**a), the wet channel is about equally visible and the continuous flow condition (F) can be clearly identified.

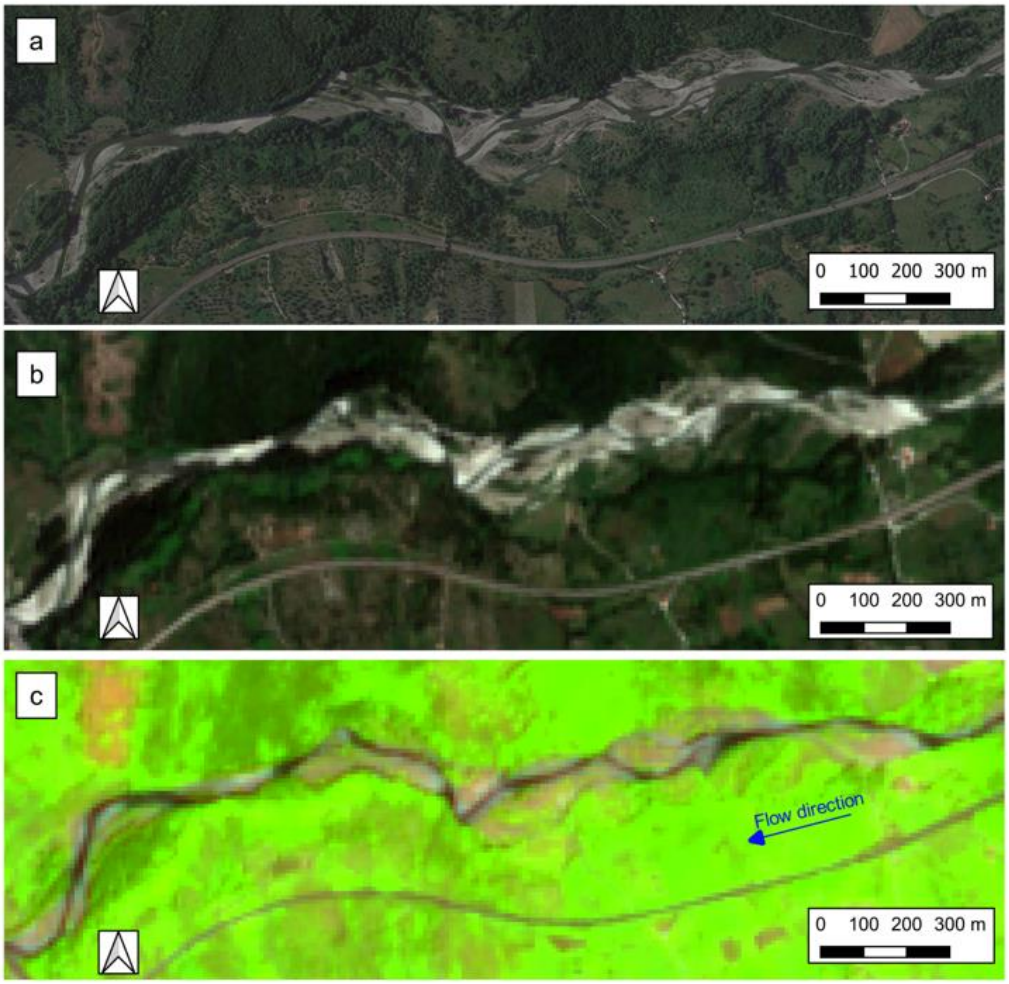


Figure 6.3. Test case n°1, M1 reach, (a) Maps Data: Google, © June 14th 2019, (b) RGB extracted by Sentinel-2 acquisition of June 12th 2019 and (c) FCI extracted by Sentinel-2 acquisition of June 12th 2019.

Figure 6.4 shows the test case n° 4 for M3 reach and for a section downstream of it. In this date the upstream section is completely dry as confirmed by the geo-localized photo c1. In the downstream part, in correspondence of the photo c2, it is possible to notice, both in the FCI and in the ground photo, an elongated pond in correspondence of the left bank of the riverbed. Immediately downstream, in the section framed by photo c3, a wet channel can be seen in the FCI which is confirmed in the ground photo. It can be seen that the FCI allows for a clear distinction between the different hydrological conditions that occur along the riverbed.

A possible source of misclassification is the presence of the bridge, which in this case takes on a color similar to water. However, the location of infrastructure can be usually established from other sources.

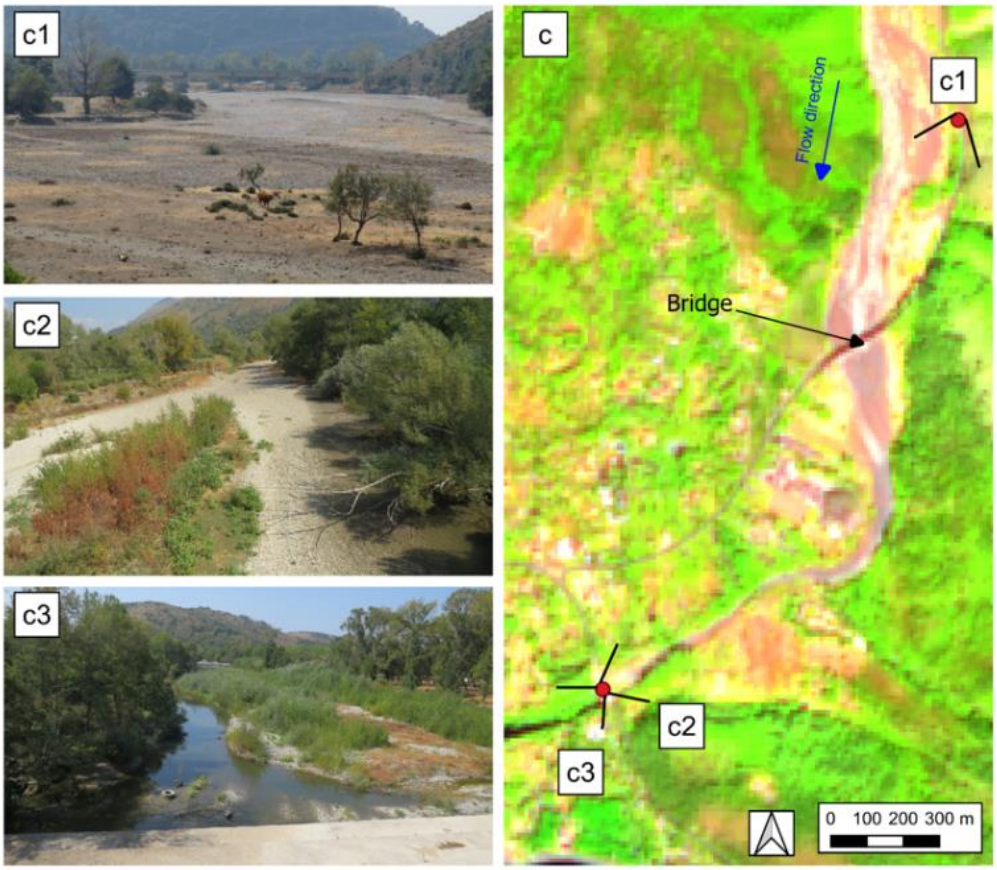


Figure 6.4. Test case n°4, M3 reach, (c) FCI extracted by Sentinel-2 image of September 19th 2020 with the geolocation points of the photos, (c1),(c2) and (c3) geo-located photos take on September 19th 2019.

Figure 6.5 shows the test cases n°2 (June 2020), n°4 (September 2020) and n°5 (February 2021) for S1 reach. The FCIs of **Figure 6.5**a,b,c and the corresponding ground photos of **Figure 6.5**d,e,f show the temporal evolution of the water presence. On June 2020 the FCI shows a P condition which is confirmed by the ground photo. In particular, the pond visible from the photo (**Figure 6.5**d) is recognizable in the FCI (**Figure 6.5**a) despite the very small size. In September 2020 at the end of the summer dry season, the bed is completely dry (**Figure 6.5**b,e). In the FCI of February 2021 (**Figure 6.5**c) a continuous flow line (F condition) is visible, as confirmed by the contemporaneous surveys (**Figure 6.5**f). **Figure 6.5**d,e,f were taken from a point on the adjacent street to the S1 reach.

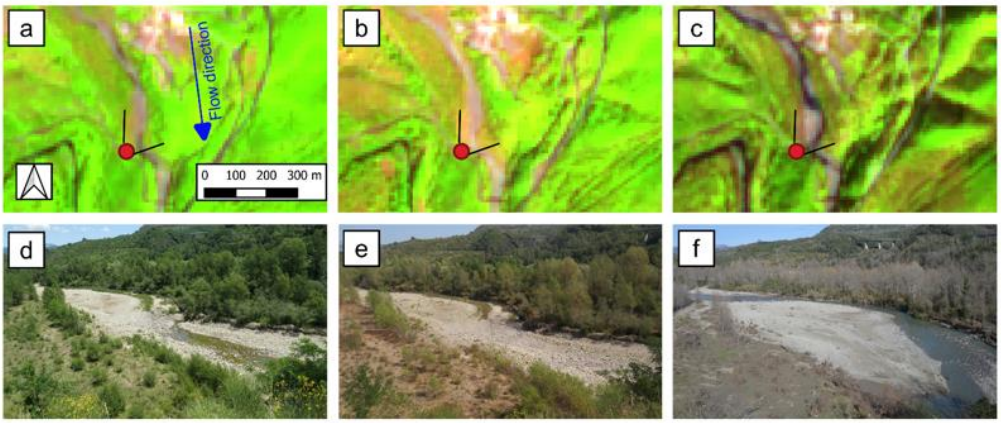


Figure 6.5. Test cases n°2,4,5, S1 reach, (a) FCI of June 26th 2020, (b) FCI of September 19th 2020, (c) FCI of February 6th 2021, (red point) photo shooting location, (d) photo taken on June 26th 2020, (e) photo taken on September 19th 2020, and (f) photo taken on February 6th 2021.

Figure 6.6 shows the test cases n°2 (June 2020), n°3 (July 2020) and n°5 (February 2021) for S1 reach. **Figure 6.6**a1 shows the photo taken in correspondence of a pond with a length greater than 50 m and a width less than 5 m, the reduced size in width means that the pond is not clearly recognizable in the FCI of 26 June 2020 (**Figure 6.6**a). The ponds wider than 10 m, shown in **Figure 6.6**a2,a4, are clearly visible in the FCI of 26 June 2020 (**Figure 6.6**a). **Figure 6.6**b2,b4 show the photos acquired on 26 July 2020, taken in correspondence of the same points represented in **Figure 6.6**a2,a4, in the month of July (see **Figure 6.6**b2,b4) the ponds were almost dry and are not visible in the FCI. Probably the reduction of the ponds is due to the low monthly rainfall (44.2 mm) and average monthly temperature (24°C) occurred during the month. **Figure 6.6**b3,c3 show images taken from the same point, where **Figure 6.6**b3 shows a D condition correctly identified in **Figure 6.6**b,c3 shows a well recognizable F condition in FCI. Finally, **Figure 6.6**c5 shows a photo taken in correspondence of the wet channel with a width of 20 m, while in **Figure 6.6**c6 is showed the photo taken in correspondence of the wet channel with a width of about 9 m. From **Figure 6.6**c, where the channel has a width of 20 m (**Figure 6.6**c5), it is possible to identify the presence of water in FCI (**Figure 6.6**c), while, when the width of the wet channel is reduced (**Figure 6.6**c6), and is equal to 9.4 m, it is not possible to clearly distinguish the presence of water in FCI (**Figure 6.6**c). The analysis described in this paragraph showed that the minimum width of ponds identifiable by FCI is highly variable. In some cases, it is even possible to identify ponds with widths between 6 m and 10 m. In other conditions, however, ponds or wet channels larger than 10 m and less than 15 m are not clearly identifiable. This depends on the relative position of the object with respect to the pixels. In fact, pixel-size water surface contained in only one pixel is identified, whereas if it covers, only partially, two or more pixels the identification is more complicated.

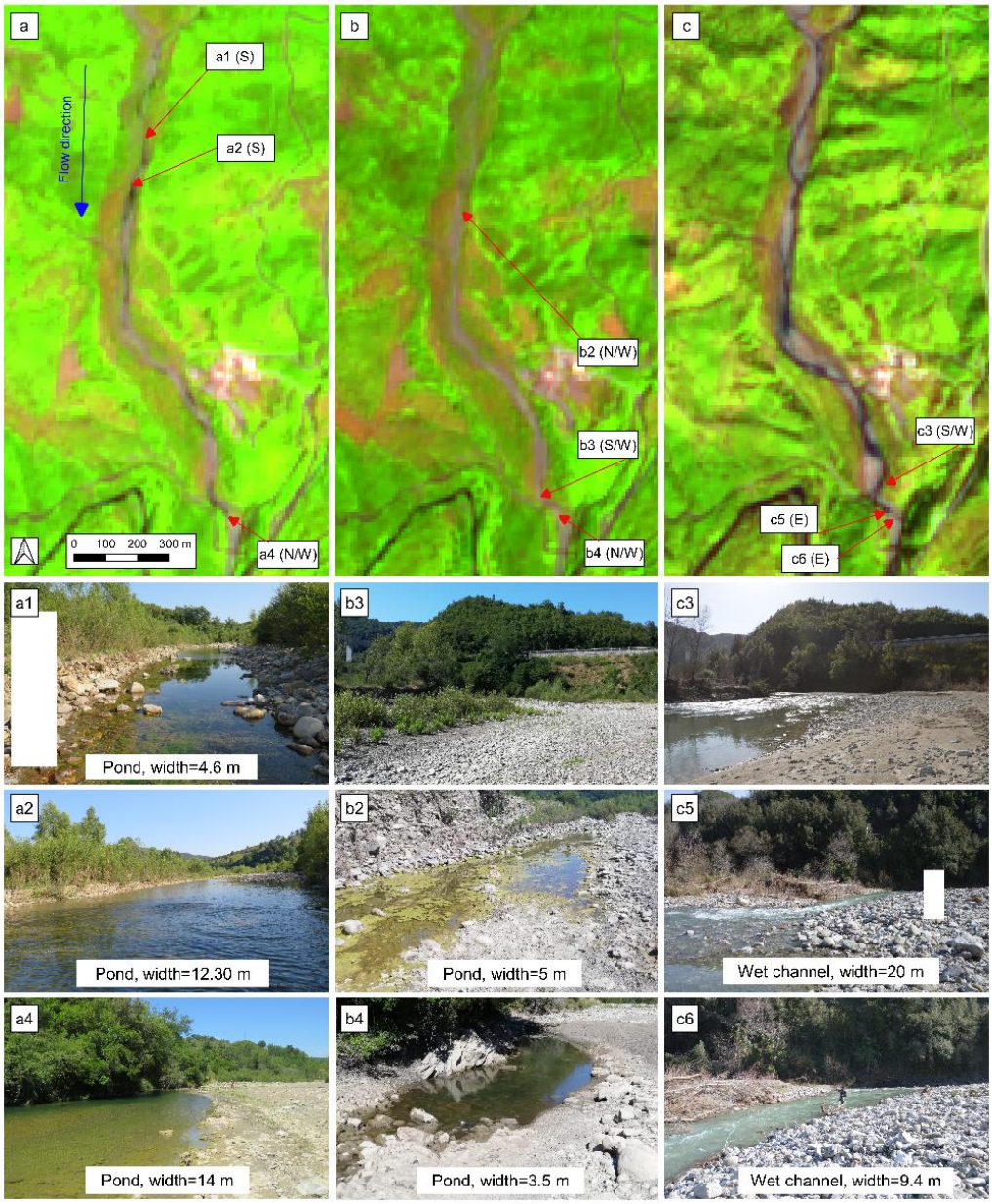


Figure 6.6. Test cases n°2,3,5, S1 reach, (a) FCI of June 26th 2020, (b) FCI of July 26th 2020, (c) FCI of February 6th 2021, (a1,a2 and a4) photos taken on June 26th 2020, (b3,b2 and b4) photos taken on September 19th 2020, and (c3,c5 and c6) photos taken on February 6th 2021. Photo-taking orientation are reported in brackets in the labels of a, b and c panels. Note: White boxes are used to cover people incidentally taken from the photos.

6.3.3 Relation between hydrological condition extracted by FCIs and hydrological data

In this paragraph is shown a comparison between the classification of hydrological condition obtained only from the FCIs analysis and the water level measurements available for M3 and L1 reaches. The daily water levels were recorded by two gauging stations, both located about 500 m downstream of reach

M3 and L1 respectively. **Figure 6.7**a,b show the distribution of water levels for considered hydrological conditions (Flowing, Ponding and Dry) for M3 and L1 reaches.

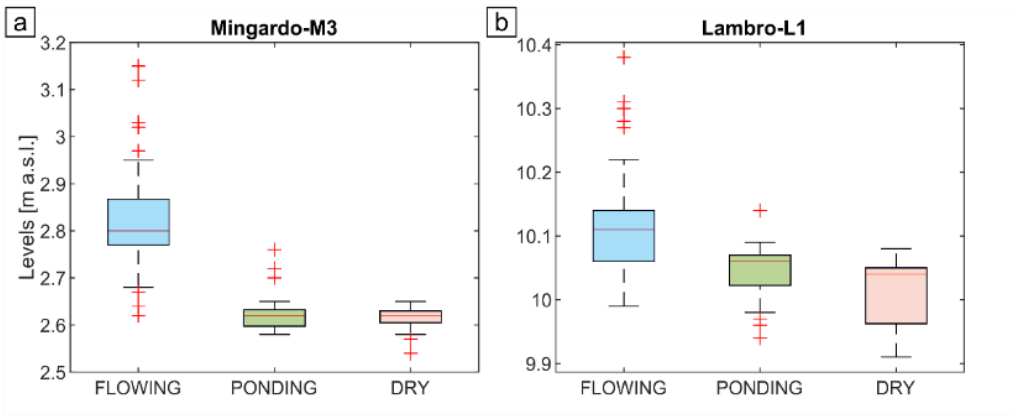


Figure 6.7. Distribution of water levels for considered hydrological conditions: Flowing, Ponding and Dry. (a) M3 reach, (b) L1 reach.

For the M3 reach of the Mingardo river (**Figure 6.7**a) it is observed that, despite small regions of superposition, the water level measurements could be used to distinguish the F condition from the NF one (P and D conditions). The ANOVA test, conducted between the "Dry" and "Ponding" groups of the M3 reach, provided a p-value equal to 0.16. For L1 reach (**Figure 6.7**b), the regions of superposition are present for all three hydrological conditions, and in this case the water levels are less indicative of which status occurs along L1 reach.

6.3.4 Random Forest results of oversampled models

Cross validation (i.e., out-of-bag estimate) of oversampled RF models showed very high predictive capabilities, slightly different depending on the binary classification model (F/NF or P/D). Overall, the F/NF models performed better compared to the P/D ones, with accuracy ranging from 0.94 to 0.98 (mean = 0.955) and TSS from 0.88 to 0.95 (mean = 0.91). For P/D models, accuracy and TSS exhibited slightly lower scores ranging from 0.82 to 0.92 (mean = 0.865) and from 0.64 to 0.84 (mean = 0.73) respectively. On the one hand, for F/NF models, specificity (range 0.94-1.0, mean = 0.983) generally resulted greater than sensitivity (range 0.89-0.96, mean = 0.927), except for S1 reach. On the other hand, specificity (ranging from 0.77 to 0.92, mean = 0.843) was assessed to be lower than sensitivity (ranging from 0.86 to 0.92 , mean = 0.888) for the P/D models. Furthermore, global models (GMs) generally were found to be slightly less accurate in predicting the correct hydrological condition compared to the locally calibrated models (i.e., individual reach models). In particular, for F/NF models the GM exhibited the lowest scores in terms of accuracy (0.94) and TSS (0.88). Whereas the GM for P/D models performed better exclusively compared to the M3 model which, due to a

reduced number of observations in the training dataset (44), resulted to be globally the least accurate (accuracy = 0.82 and TSS = 0.64).

Our analysis demonstrated that the developed RF models are able to predict a specific hydrological condition (flowing/ponding/dry) occurring at the daily scale in every river reach. This quite robust prediction was achieved only using spatially interpolated rainfall and air temperature data. As the oversampled RF models demonstrated higher performances, exclusively these models were finally considered for further use and presented in **Table 6-4**.

Concerning selected variables, the cumulative 90-days rainfall (R90) resulted relevant in 90% of all models, and turned to be the most important predictor in 70% of them. Whereas R10 and R30 were found to be important predictors to distinguish between F/NF and P/D conditions in 100% of models respectively. R30 was furthermore assessed as significant predictor for the F/NF model of S1 reach. T90_MAX exhibited high importance especially considering F/NF models in which is present in 5 of 6 cases (83% of F/NF models). On the other hand, T90_MEAN was established as predictive variable for both binary models of S1 reach, and T30_MAX resulted an important predictor for P/D models in GM and M3 reach.

Table 6-4. Predictive variables and performances obtained for the oversampled RF models. Models variables are listed in terms of descending importance for classification result (from left to right). Binary models code: F/NF = non-flowing/flowing, P/D = dry/ponding. Predictive variables code: R90 = cumulative 90-days rainfall, R30 = cumulative 30-days rainfall, R10 = cumulative 10-days rainfall, T90_MAX = average of previous 90-days maximum air temperature, T30_MAX = average of previous 30-days maximum air temperature, T90_MEAN = average of previous 90-days mean air temperature.

Binary model	Model name	Predictive variables	Accuracy	Sensitivity	Specificity	TSS
F/NF	GM	R90, T90_MAX, R10	0.94	0.90	0.98	0.88
	S1	T90_MEAN, R30, R10	0.95	0.96	0.94	0.90
	M1	R90, R10, T90_MAX	0.95	0.91	1.00	0.91
	M2	R90, T90_MAX, R10	0.95	0.89	1.00	0.89
	M3	R90, T90_MAX, R10	0.98	0.96	0.99	0.95
	L1	T90_MAX, R90, R10	0.96	0.94	0.99	0.93
P/D	GM	R90, R30, T30_MAX	0.84	0.87	0.81	0.67
	S1	T90_MEAN, R90, R30	0.92	0.92	0.92	0.84
	M3	R90, T30_MAX, R30	0.82	0.86	0.77	0.64
	L1	R90, R30, T90_MAX	0.88	0.90	0.87	0.77

6.3.5 Duration of hydrological condition

As the individual RF models demonstrated higher predictive capabilities, these models were than used to predict the duration daily frequency of each hydrological condition (F/P/D) in all considered reaches. In this way it was furthermore possible to determine the duration of F, P and D conditions for each reach during the period 2015-2020 (**Figure 6.8**).

Figure 6.8 shows that all the studied reaches are characterized by non-continuous water flow periods. In particular, for S1, L1 and M3 reaches, there is a period characterized by a completely dry river bed (D). Whereas for M1 and M2 reaches the dry condition never occurred, and, at non-flowing condition, isolated ponds of water are always present along these reaches (permanent ponding reaches).

For S1 and L1 reach, the average duration of NF was assessed to be about 4 months, and the dry bed period varied from a minimum of 27 days to a maximum of 149 days. For the other reaches, the yearly duration of the NF period has strong annual variations. For sections M1 and M2 the NF period varied between 5 and 113 days. For reach M3 the NF period was higher and with more pronounced variations (between 32 and 192 days). The duration of D period for M3 reach ranged between a minimum of 7 days to a maximum of 191 days. It is important to note that the obtained estimations of the yearly duration of the hydrological condition are affected by some uncertainty related to RF models performances. Particularly, uncertainty in the case of the drying reaches (S1, L1, M1) was higher, as misclassifications were produced by both F/NF and P/D models accuracy.

Overall, the longest duration of the ponding or dry-bed periods was observed in the year 2016/2017 for all the reaches studied. This longer duration is also reflected by the drought analysis conducted in Campania by [212], which showed that a severe drought period occurred in 2017. The year with the shortest NF duration is the year 2017/2018 for S1, M1, M2, M3, while for L1 reach the years 2017/2018 and 2018/2019 have a similar duration of NF period, with the latter slightly shorter.

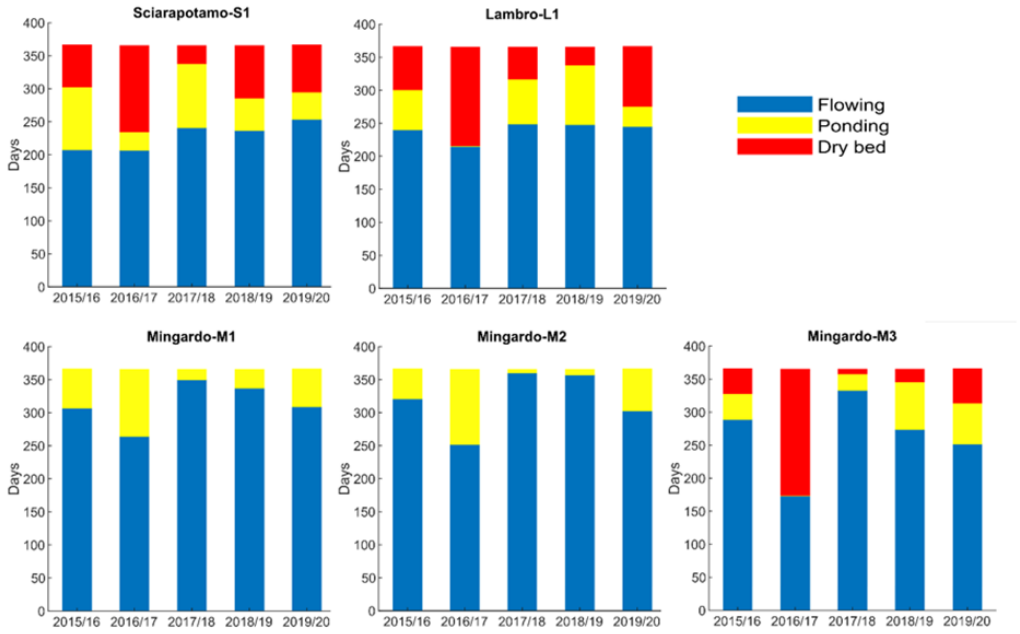


Figure 6.8. Daily occurrences of flowing (blue), ponding (yellow) and dry (red) conditions predicted by the individual RF models for each reach during the study period from 2015 to 2020.

6.4 Discussion

In this work, the Sentinel-2 dataset was exploited to monitor the hydrological condition of non-perennial rivers. Since the launch of the first of the two Sentinel-2 satellites (2015), 7 years of observations are available with a total dataset of 342 images for the observed area. Among these, 141 were actually exploitable, i.e., without cloud cover, with an effective revisit time of 15 days on average. The effective revisit time is reduced to 10 days on average in the dry season, from June to October, which is the most relevant period to observe the occurrence of ponding and dry conditions.

The analysis of the spectral signatures of the land cover present in the non-perennial stream corridors revealed significant seasonal variations. Variation in water content of sediment bars and variation in water depth of the wet channel or ponds result in different reflectance values. This behavior makes it complicated to define an algorithm capable of distinguishing classes of sediment and water in a stable manner over time. However, spectral responses were sufficiently differentiated to distinguish the macro classes water, soil, and vegetation in a false-color image based on the B11, B8, and B4 bands.

This color combination makes it possible to identify the presence of water and distinguish the three hydrological conditions. We have verified that this operates on several rivers from different geographical areas (e.g., Taro, Trebbia, Parma in northern Italy; Palancia river and Rambla de la Viuda in Spain). It follows that it is

possible to apply the proposed method even when high-resolution images are not available and thus without repeating the analysis of spectral signatures. A classification with more classes, distinguishing for example, deeper pools from shallower pools or wet-sediment from dry-sediment may be possible. However, to further increase land cover classes, the spectral signatures should be derived from a much larger number of acquisitions and ground truths than the ones used in this study. In any case, the relationship between the spatial extent of the surfaces belonging to the different classes and the resolution of the satellite image is an important limiting factor. Our analyses demonstrated that the minimum width of a pond or wet channel that can be observed is variable depending on how the object is contained within the pixel. The comparisons with field measurements showed that it is possible to identify objects with a minimum width between 6 m and 15 m. Consequently, more refined classifications with a larger number of classes are meaningful only for very wide riverbeds in which the different classes have sufficiently large sizes.

The FCIs are much clearer than images in true color (see **Figure 6.4**) and allow to distinguish the condition of continuous water flow (F) from the one characterized by the presence of isolated ponds of water (P) and the dry bed condition (D). This information can be used to define whether a river is non-perennial and, if so, to what degree, as proposed in many literature studies. For example, the four classes considered in the MIRAGE toolbox [218]: permanent, intermittent with pools in the non-flowing period, intermittent with dry channel in the non-flowing period, and episodic-ephemeral could be identified.

In the ponding condition it would be useful to identify the presence of pools, i.e., geomorphic units characterized by higher than average water depth. Combining the FCIs with an up-to-date DTM would provide such a distinction. Unfortunately, this approach is limited by the availability of DTMs with a frequency comparable to the rate of bedform change. An alternative possibility would be to observe on the FCIs the duration of water presence and identify pools as those where water presence persists longer.

The comparison between the punctual water level measurements, carried out with the traditional gauging systems and the satellite observations showed that the punctual measurements do not allow the distinction between the D and the P conditions in both examined reaches (see **Figure 6.7**). Moreover, for L1 reach it is not even possible to distinguish the F condition from the NF condition. Quite clearly, the water level at one point in a cross-section, is influenced by the local landscape, for example the presence of a pool or sediment deposit, and therefore cannot give information on the flow condition of the adjacent reach. This is particularly relevant during low flow conditions. The considerations made show that even a greater, though desirable, spread of gauging stations would not allow appropriate identification of hydrological condition in non-perennial rivers and that satellite data are a crucial resource for this purpose.

Manual assignment of hydrological condition becomes time-consuming when the number of fluvial reaches to be observed is considerable. The results obtained can be used as baseline information to develop and calibrate an automatic algorithm

for hydrological conditions classification. The availability of such an algorithm will allow larger portions of the river network to be monitored.

The discontinuous observations of hydrological condition derived from Sentinel-2 images can be effectively exploited to calibrate models capable of making predictions on a daily basis. In this regard, the use of machine learning techniques (e.g., RF) which employ as predictor variables widely available hydrological data (such as rainfall or air temperature) resulted to be quite effective to this purpose. In particular, our approach, due to the very high predictive performances obtained for the developed RF models, can provide a valuable solution for assessing the flowing/ponding/dry duration in ungauged NPRs of Mediterranean region. In order to properly explore the relationship between the hydrological condition and the available data, the RF models were developed both at the local (individual reach, S1, M1, M2, M3 and L1) and global scale (all the reaches together, GM). Furthermore, we oriented our analysis developing binary classification RF models able to distinguish between both F/NF and the P/D conditions. This two-step approach performed well, especially for distinguishing between the dry and the ponding condition, and was furthermore motivated in order to reduce class imbalance in the training dataset. Moreover it allows to proper consider the peculiarities of both permanent ponding and drying non-perennial river reaches. Indeed, a classification model with three classes (F/P/D) can be applied only in NPRs with the occurrence of all the three hydrological conditions and may have lower performances compared to the presented approach (i.e., the 3-classes model accuracy were 0.84, 0.84 and 0.85, for L1, M3 and S1 reaches respectively, together with very low sensitivity values in the range 0.31-0.61 for the ponding class).

Among the predictive variables, it was observed that precipitation variables with higher temporal scales resulted to be of primary importance to correctly predict the hydrological condition in considered reaches. Indeed, the cumulative 90-days rainfall (R90) resulted relevant in 90% of all models. Only for F/NF model of S1 the most important precipitation predictor was assessed to be the cumulative 30-days rainfall (R30). Such result can be related to the specific characteristics of the considered reach, which mainly distinguishes itself due to the lowest drainage catchment extension (54 km^2), and consequently to a lower time of concentration. R10 resulted as an important predictor for all F/NF models. In our opinion, this variable can embody the amount of cumulative rainfall required to generate a new flow condition after a period of non-flowing in the considered reaches. On the other hand, the cumulative 30-days rainfall (R30) was found to be important for distinguishing between the occurrence of the ponding and dry condition. In this case, the R30 variables can be seen as a proxy of the groundwater level, therefore the grater the R30 value the higher the probability of being a day of ponding condition.

The implemented models take into account only precipitation and air temperature predictors and neglects many others that are significant in governing

intermittency, such as catchment area, shape, orientation, slope, water table fluctuations and water seepage through riverbed. This is probably the reason why locally calibrated models are more accurate. However, in the study cases, also the global model showed high performances, but this may be due to the fact that considered rivers have similar hydro-climatic and geo-morphological characteristics. The availability of satellite observations makes it possible to obtain data for model calibration at the river reach scale. This allows to overcome the limitation of global models that can hardly describe the strong heterogeneity of the processes that determine a low spatial correlation of intermittence patterns as also observed by [197].

Once the Random Forest model has been calibrated in the period in which satellite images are available, it is possible to extend in the past the analysis of the hydrological regime to the entire time series of precipitation and temperature. However, it is important to consider that the model is calibrated against the actual presence of water in recent years so it cannot be applied to simulate the regime in previous periods if the basin conditions or water withdrawals have changed.

Recently, RF models were used by [74] to simulate the natural regime of rivers across the globe. This approach does not allow to reproduce the actual regimes, i.e., those impacted by withdrawals and reservoirs, and consequently may underestimate the total number of non-perennial rivers. Likewise, hydrologic models calibrated against long historical data fail to model the actual river regime when changes related to climate, land use, reservoirs regulation and withdrawals occurred. In contrast, the approach developed in this paper, being based on observations of the regime in recent years may allow to make a more robust classification of F/NF conditions at the reach scale and can used to estimate the effect of anthropogenic pressures due to water withdrawals. The regimes observed in different reaches of the same region allow to understand the peculiar reaction of each reach to the same atmospheric forcing such as dry periods. For example, the extreme drought experienced in the year 2016/17 resulted in a longer "dry" period in many reaches while in others the bed did not dry completely.

Chapter 7

7. Meso-scale habitat modeling in non-perennial rivers

7.1 Introduction

Non-perennial rivers (NPRs) are generally defined as streams that, in some points along their course, experience the lack of surface flow during some portion of the year [83]. According to the occurrence and duration of the zero-flow condition they can be distinguished into intermittent rivers or episodic/ephemeral streams [219]. The first rarely achieve a waterless status, the latter frequently experience the disappearance of the water table [220].

Laid on the borderline between aquatic and terrestrial ecosystems, non-perennial rivers continuously shift their status according to the fluctuation of their hydrological condition. These watercourses are characterized by a high seasonal variation of the flow regime that modifies the nature of their ecosystem from lotic (flowing condition) to lentic (ponding condition) until a terrestrial one (dry condition, [30]).

NPRs are widely distributed all around the world, representing more than half of global stream network [74], [221]. They commonly occur in arid and semi-arid zones [222], particularly, they result predominant in the Mediterranean watersheds, where the marked dry/wet climate patterns favorite their occurrence [83], [223]. NPRs of the Mediterranean region are extremely precious ecosystems, providing suitable habitat for thousands of unique and endemic freshwater species, most of which are currently threatened or endangered [223]. Nevertheless, these ecosystems are historically neglected both at regulatory and scientific level [81], [222], mainly because they were largely considered to be of low ecological and economic value. In Europe, the Water Frame Directive (WFD, [195]), which is proposed to protect all kind of water bodies, concretely exclude from biomonitoring a high number of NPRs, due to their general limited catchment extension (<10 km^2). Proper

environmental management and monitoring is also precluded by the lack of a standardized approaches developed to evaluate and model habitat dynamics of these ecosystems. In this regard, classic habitat suitability models (e.g., [32], [38]) result poorly adapted to the non-perennial rivers-case, due to their inability of assessing habitat evolution when discharge is close to zero or when remaining aquatic habitat are represented by isolated, disconnected pools [30]. After flow interruption, indeed, water surface moves into a framing of isolated wetted areas that still potentially provide a suitable environment for freshwater species [83]. The habitat-pattern during this condition (ponding condition) is clearly dependent to the local hydro-geo-morphological features of the river (e.g., shape and planforms of the channel, groundwater table level, water temperature), and it is also related to the amount of time since discharge ceased.

This study proposed a new approach to model and assess fish habitat availability in non-perennial rivers, taking into account flowing and non-flowing periods. As an example of application, analyses were conducted in a hydro-morphologically homogeneous reach of the Sangone river (Northwestern Italy), aiming to model the spatio-temporal variation of physical habitat. The MesoHABitat SImulation Model (MesoHABSIM, [18]) was applied using a specific module for NPRs (i.e., NPRS-module), which has been integrated in the available SimStream-Web service (https://mesohabsim.isprambiente.it/app/home/). High-resolution aerial images derived from UAS (Uncrewed Aerial Systems), Sentinel-2 satellite images, two-dimensional (2D) hydrodynamic simulations and field data were used for fish habitat description to define and characterize the mesohabitats under considered flow conditions.

7.2 Materials and methods

7.2.1 Study area

To apply meso-scale habitat modeling to NPRs, the Sangone river was used as a case study. Sangone is a small stream that entirely flows within the Piemonte Region of Northwestern Italy (**Figure 7.1**). Originating from the Alps at an elevation of 2000 meters above sea level, it stretches for nearly 50 kilometers until it joins the Po river near the metropolitan city of Torino, situated at 220 meters above sea level. The river's average slope is 2.7%, and its catchment area covers 268 km^2, occupied almost equally by plains (53%) and mountainous areas (47%).

The Sangone watershed can be divided into two main parts, delineated by a noticeable narrowing of its basin near the village of Trana, where a gauging station monitors mean daily discharge (**Figure 7.1**). Operating for over 20 years, from July 2002 to December 2022, this station provides valuable insights into local hydrology. The mean discharge was estimated at 3.05 m^3/s, with maximum and minimum values reaching 121.7 m^3/s and 0.27 m^3/s, respectively. No zero-flow values have been ever recorded. Peak discharges typically occur during spring

(April-June) and fall (October-November), while low-flow periods are common in summer (July-September). Within the Sangone catchment, a rain gauge also operates, covering the same temporal interval as the flow records (**Figure 7.1**). Mean cumulative annual rainfall corresponds to 1314 mm. In the upper part of the Sangone, characterized by a perennial hydrologic regime, primary pressure arises from water abstraction for hydropower generation. However, these withdrawals return the water to the river before the Trana section, ensuring that the gauging station measurements represent the natural flow regime. In the downstream part, below the village of Trana, hydro-morphological impacts escalate significantly due to the presence of agricultural water diversions (**Figure 7.1**). Along this lower segment, before its junction with the Po river, prolonged flow intermittency may occur, especially during summer, when water table level is depressed for intense agricultural water withdrawals.

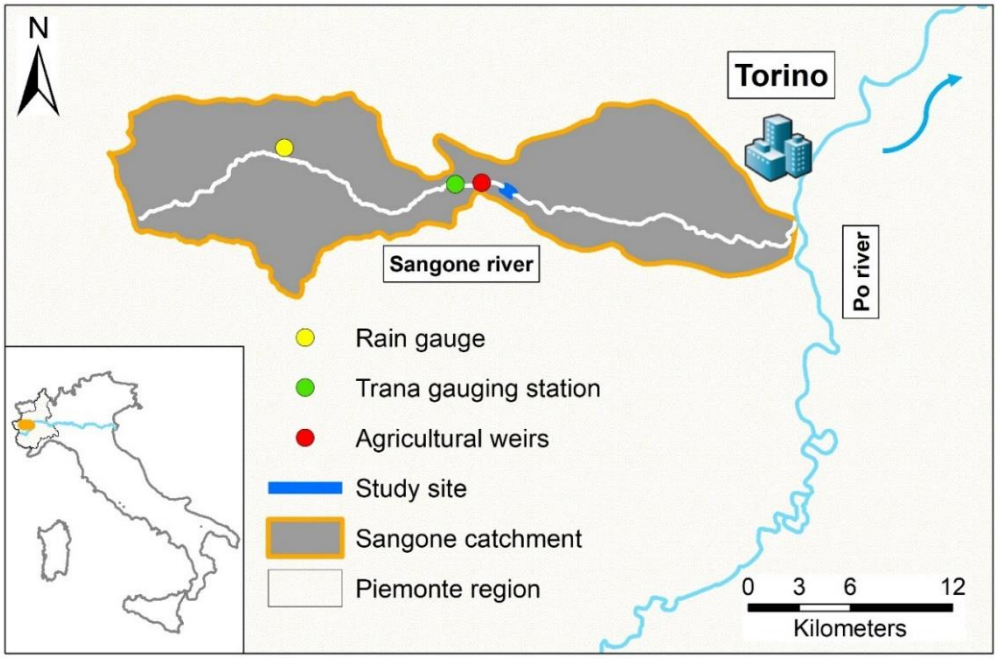


Figure 7.1. The study area. The Sangone river and its catchment near the metropolitan city of Torino. The study site (in blue) located below the Trana gauging station (represented by a green dot) and the main agricultural weirs (represented by a red dot), which hindered the lower part of the watercourse. The location of the rain gauge belonging to the upper part of Sangone catchment is represented by a yellow dot. The main flow direction is indicated by the blue arrow.

The study site is located in the middle part of the Sangone catchment, just downstream of the main agricultural weirs located in the correspondence of the village of Trana (**Figure 7.1**). In this reach, river banks are not yet confined and the river planform moves into a sinuous with alternate bars morphology characterized by some multi-thread sections [56]. For the MesoHABSIM application, a surveyed sub-reach of 430 m length was selected, spanning from 10 to 20 times the average river width [54]. The mean slope is approximately 1%, and the geomorphic units composition is predominantly represented by riffles, glides, backwaters and rapids.

Riverbed sediments consist mainly of pebbles (diameter: 6-20 cm) and cobbles (diameter: 20-40 cm), whereas fish shelters are mainly constituted by boulders, emerging vegetation, shallow margins, and canopy shading (**Figure 7.2**).

7.2.2 The MesoHABSIM module for NPRs

The meso-scale habitat model, MesoHABSIM, is a methodological approach that models aquatic habitats using geomorphic and hydraulic units (GUs, such as pools, glides and riffles) as spatial unit of analysis. GUs correspond in size and location to mesohabitats and are evaluated in terms of habitat suitability due to their local hydro-morphological conditions [28]. MesoHABSIM is characterized by a specific data collection strategy and analytical techniques that allow to compute the habitat availability for target species under variable discharge conditions [18]. It provides habitat time-series, that represent habitat variation over time to predict the magnitude and duration of stressful events for the aquatic fauna [28], [48].

MesoHABSIM enables the characterization of the fluvial habitat through the evaluation of specific physical attributes collected in the field or simulated through hydrodynamic models [54], [62]. These physical attributes include both abiotic (water depth, flow velocity and sediment composition) and biotic (biotic substrate, cover and shelter availability) factors (see **Table A-1**, for details), which mainly influence mesohabitat use by fish [18].

To quantify the amount of available habitat for target species, habitat suitability criteria (HSC, e.g., [19], [20]) are applied to each GU. For Italian freshwater fish, these criteria are typically defined by analyzing empirical data on species distribution at the mesohabitat scale using machine learning techniques (e.g., [63]). GU physical attributes falling within specified ranges of variables determined the mesohabitat classification as suitable (if the fish is predicted as present) or optimal (if the fish is predicted as abundant) according to the HSC [54]. The total amount of available habitat (H_A) is then computed for each surveyed flow condition using the following equation:

$$H_A = H_s * 0.25 + H_o * 0.75 \qquad (1)$$

where H_s and H_o represent the amount of mesohabitats extent classified as suitable and optimal, respectively. H, H_s and H_o can be expressed in m^2 or in terms of percentage of the maximum wetted area for the selected case study.

In NPRs aquatic habitat varies with flow rate during flowing conditions and with time during non-flowing conditions [30]. The interplay between flow, time and habitat availability is therefore elaborated by means of the construction of a specific rating curve able to consider simultaneously the intermittent behavior of aquatic habitat availability. This curve directly derives from the traditional habitat-flow rating curve of common habitat models, by adding a second quadrant to the graph. This second quadrant depicts the recession of wetted area and habitat availability after flow cessation. The resulting curve is then called habitat-flow-time rating curve (**Figure 7.5**a).

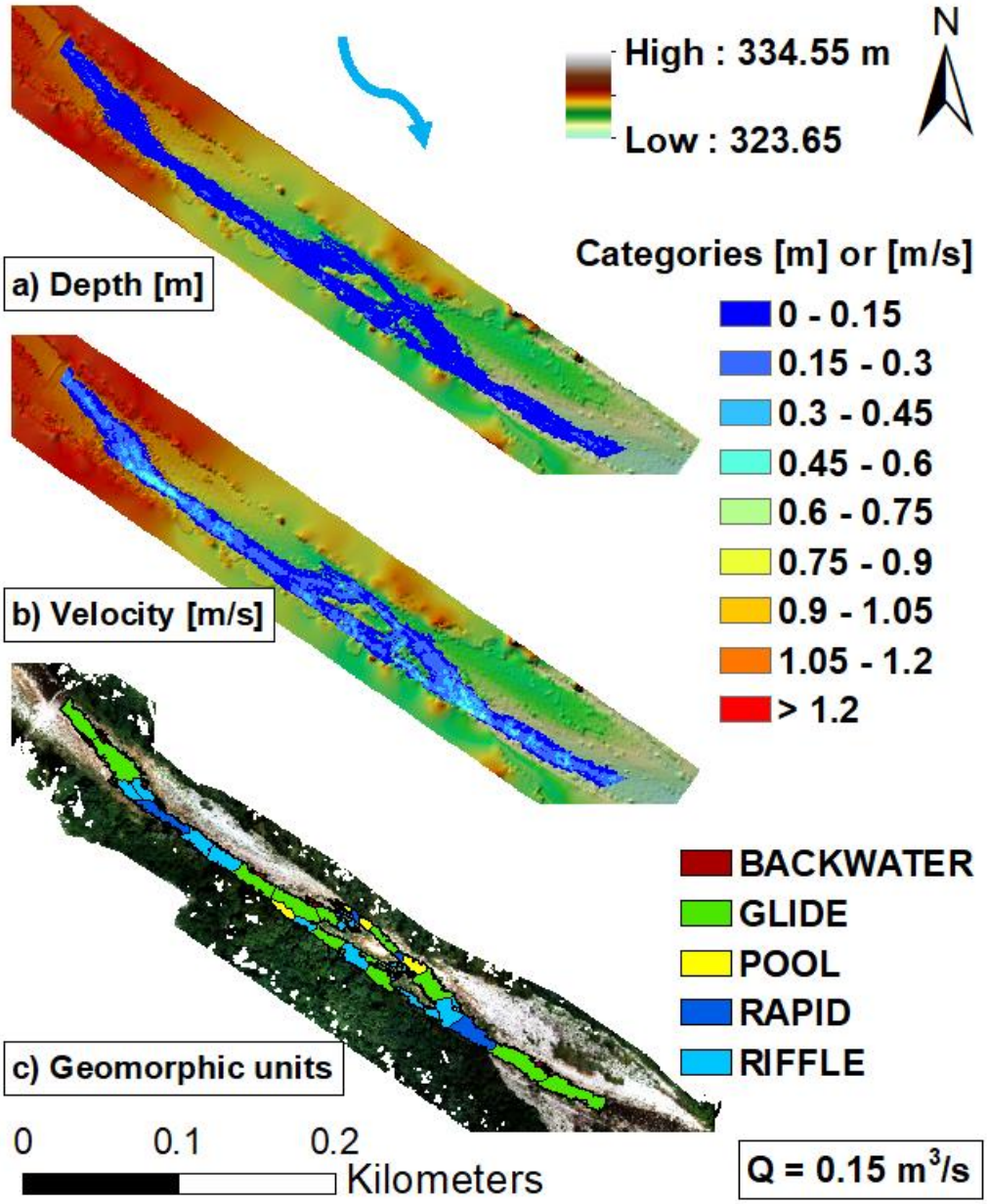


Figure 7.2. Simulation results for a) water depth and b) velocity under the flow condition present during the UAS flight (Q = 0.15 m^3/s), utilizing the bathymetrically-corrected DEM as background. Depth and velocity are color-coded according to the corresponding categories of the MesoHABSIM approach (**Table A-1**), ranging from the smallest (in blue) to the highest (in red). c) Corresponding GUs mosaic overlaid on the RGB orthomosaic. The main flow direction is indicated by the blue arrow.

The definition of the habitat-flow-time rating curve leads to the generation of the habitat time-series for NPRs that enable analyzing the spatio-temporal variation of aquatic habitat availability during both flowing and non-flowing periods (**Figure 7.5**c,d). Specifically, the flow time series are converted into habitat time series by means of the following system of equations:

$$\begin{cases} H_A(t) = H\big(Q(t)\big), Q > 0 \\ H_A(t) = H(t), \quad Q \leq 0 \end{cases} \qquad (2)$$

where H is the habitat-vs.-flow/time functions for a given species or life stage, Q(t) is the streamflow at time t, and $H_A(t)$ is the available habitat area for time t in the time series.

To facilitate habitat modeling for NPRs, the new MesoHABSIM NPRs-module has been developed and it is freely available to all users through the SimStream-Web service (https://mesohabsim.isprambiente.it/app/home/), at the web page of the Italian National Institute for Environmental Protection and Research (ISPRA). The SimStream-Web service can be therefore considered the leading software for implementing the MesoHABSIM approach, for both perennial and non-perennial rivers.

7.2.3 Hydro-morphological data collection and analysis

In this study, due to the extension of the surveyed sub-reach, UAS (Uncrewed Aerial Systems) were utilized to acquire high-resolution topographical data of the river habitat. Aerial images were captured using a DJI Phantom 4 Pro RTK quadcopter (FC6310R Camera Model). The flight was conducted on July 12th 2021, at an average height of 80 meters, during low water levels. The UAS allowed to capture both the RGB orthomosaic and the corresponding Digital Elevation Model (DEM) of the study site (**Figure 7.2**). These data were obtained using photogrammetric and Structure-from-Motion (SfM) techniques with Metashape software (Agisoft, St. Petersburg, Russia), following a standard workflow for river applications (i.e., [166]). The DEM acquisition was finalized to develop a 2D hydrodynamic model.

Given challenges in accurately determining submerged riverbed elevations from photogrammetric data due to light refraction at the air-water interface, a bathymetric correction was performed on the DEM using GIS tools. The submerged surface was reprojected to correct for overestimations of elevation using a linear model based on Snell's law. Given generally shallow water depths at the surveyed flow conditions (maximum measured depth = 0.38 m), a linear model with an intercept of 1.33 was assumed for the bathymetric correction [171]. This resulted in a bathymetrically-corrected DEM suitable for developing the 2D hydrodynamic model.

During the UAS flight, a river survey according to the MesoHABSIM approach was further performed [54]. In this way, the mosaic of GUs was outlined at flow conditions of Q = 0.15 m^3/s and supplemented with details on local substrate composition and cover presence.

For calibrating the hydrodynamic model, georeferenced information on water depth and current velocity was also collected above 60 points within the study site using an OTT MF Pro flow meter (Ott HydroMet, Kempten, Germany), and a multi-band Real-Time Kinematic Global Navigation Satellite System (RTK GNSS) receiver.

Hydrodynamic flow conditions were simulated using a 2D fixed-bottom numerical model developed with HEC-RAS (Hydrologic Engineering Center of

U.S.A, Davis, California, Version 5.0.7) software. Four discharges (i.e.,0.15, 1, 2, 3 m^3/s), representing flow percentiles between the 97th to the 30th of the flow time series recorded in Trana, were simulated under steady-state conditions to accurately describe aquatic habitat in the surveyed sub-reach. The lowest discharge, corresponding to the measured flow during the river survey, was used for model calibration (**Figure 7.2**). This calibration involved selecting the Manning's coefficient to achieve optimal agreement between simulated and measured depth and velocity values, as well as qualitative overlap between simulated wetted areas and those observed in the RGB orthomosaic.

For non-flowing conditions, the wetted areas extension, at the first day after flow cessation (ponding phase), was obtained using the corrected DEM, artificially fulfilling with water the more depressed areas. Multispectral Sentinel-2 images corresponding to the ponding condition were then used to qualitatively validate the estimated wetted area represented by a framing of isolated pools and ponds.

As required by the MesoHABSIM approach, GU mosaics for the five simulated conditions (four discharges and one ponding phase) were outlined and described with all their local habitat attributes (**Table A-1**) by synergistically integrating in a GIS environment the field-collected information (e.g., substrate and cover distribution) with high-resolution data represented by the RGB orthomosaic, the bathymetrically-corrected DEM, and the simulated water depths and velocities.

To gather information on the fish community in the surveyed sub-reach of the Sangone river, an electro-fishing campaign was conducted concurrently with the UAS flight. A total length of 150 m was sampled using backpack electrofishing, and mobile mapping techniques were employed to record the wetted perimeter and physical habitat attributes of sampled GUs (see, **Table A-1**, for details). A two-pass removal method for fish sampling was applied to ensure high capture rates (e.g., [92]). The observed fish species were Italian vairone (*Telestes muticellus*), Padanian goby (*Padogobius bonelli*), Italian chub (*Squalius squalus*), Italian barbel (*Barbus plebejus*), Italian minnow (*Phoxinus lumaireul*), and Italian brook barbel (*Barbus caninus*). Captured fish were classified in terms of adult and juvenile life stages and then released back into the same mesohabitat. In this study, adult and juvenile *T. muticellus* and adult *P. bonelli* were selected as target species to assess aquatic habitat availability for both rheophilic (*T. muticellus*) and benthic (*P. bonelli*) fish species [117]. These species are endemic in Northern Italy and represent important ecological target for the study site. The HSC for *T. muticellus* and *P. bonelli* are currently available in the SimStream-Web service (see **153** for further details) and were developed using fish data collected in reference sites of the Alpine regions of Italy (e.g., [63]).

The obtained habitat availability (1) during both flowing and non-flowing conditions were interpolated using a mathematical spline function to generate the habitat-flow-time rating curves for the selected fish species (**Figure 7.5**a). Finally, the flow time series was transformed to habitat time series (2), to estimate habitat variation during both flowing and non-flowing periods (**Figure 7.5**).

7.2.4 Hydrological characterization

To describe aquatic habitat variation in NPRs, it is essential to comprehensively understand the local hydrological regime and the frequency and duration of flow intermittence. In this study, we integrated Sentinel-2 multispectral images with locally measured discharge and rainfall data to estimate the duration of the ponding condition in the surveyed sub-reach. Specifically, our aim was to identify the shortest duration of the ponding condition, representing the minimum number of days required for the surveyed sub-reaches to become completely dry after flow cessation. This information was utilized to define the amount of time in which aquatic habitat availability gradually reduces to zero, necessary to build the habitat-flow-time rating curves via the SimStream-Web service (**Figure 7.5**a).

For the satellite image analysis, we employed the methodology proposed by [29]. A detailed overview of this approach is presented in previous Chapter **6** of this thesis. This approach effectively allows to detect the presence of surface water within a river corridor through a supervised analysis of false-color images created with a specific combination of Sentinel-2 bands (i.e., bands 11-8-4). For this analysis, we utilized the geemap package [224] to access the Google Earth Engine collection of Sentinel-2 data and classify the images based on the observed hydrological condition (flowing, ponding, or dry; see **Figure 7.3**). To evaluate the effectiveness of this methodology to the study site, we priory conducted a qualitative assessment by comparing the RGB orthomosaic with a few images captured by Sentinel-2 sensors before and after to the date of the UAS flight.

By analyzing the discharge and rainfall time series, we identified periods of prolonged drought in the study site staring from June 2015, date from which Sentinel-2 acquisitions became available. These periods were determined by identifying the minimum values of moving averages for the available discharge and precipitation data series across various time intervals (i.e., 15, 30-, 45-, 60-, 90-days). We focused on these periods due to their likely association with shorter duration of the ponding condition. By concentrating our efforts on these specific timeframes, we minimized the workload needed for the supervised classification of false-color images to determine the hydrological conditions for the entire satellite image series [29].

Due to the presence of agricultural weirs upstream of the surveyed sub-reach (**Figure 7.1**), the flow time series measured in Trana (i.e., the natural flow series) does not accurately reflect the actual hydrological regime of the study site. Particularly during summer, when water abstractions for irrigation intensify, the discharge in the surveyed sub-reach are much lower, leading to periods of zero-flow. To address this discrepancy, an additional analysis was conducted to approximately define the altered flow conditions downstream of the agricultural weirs. By overlapping discharge data with the hydrological conditions derived from the satellite image analysis, a threshold flow value (Q*) was established below which a non-flowing condition (ponding or dry condition) starts. This analysis focused specifically on the most severe drought period previously identified in the time series. Due to the very low variability, the discharge threshold was assumed

constant for all the period, and was used to define the altered discharge series by subtracting such value from the flow series registered in Trana. Finally, the discharge time series (**Figure 7.5**b) were converted into habitat terms (2) using the habitat-flow-time rating curves (**Figure 7.5**a) to evaluate the spatio-temporal evolution of aquatic habitat during the monitored period (**Figure 7.5**c,d).

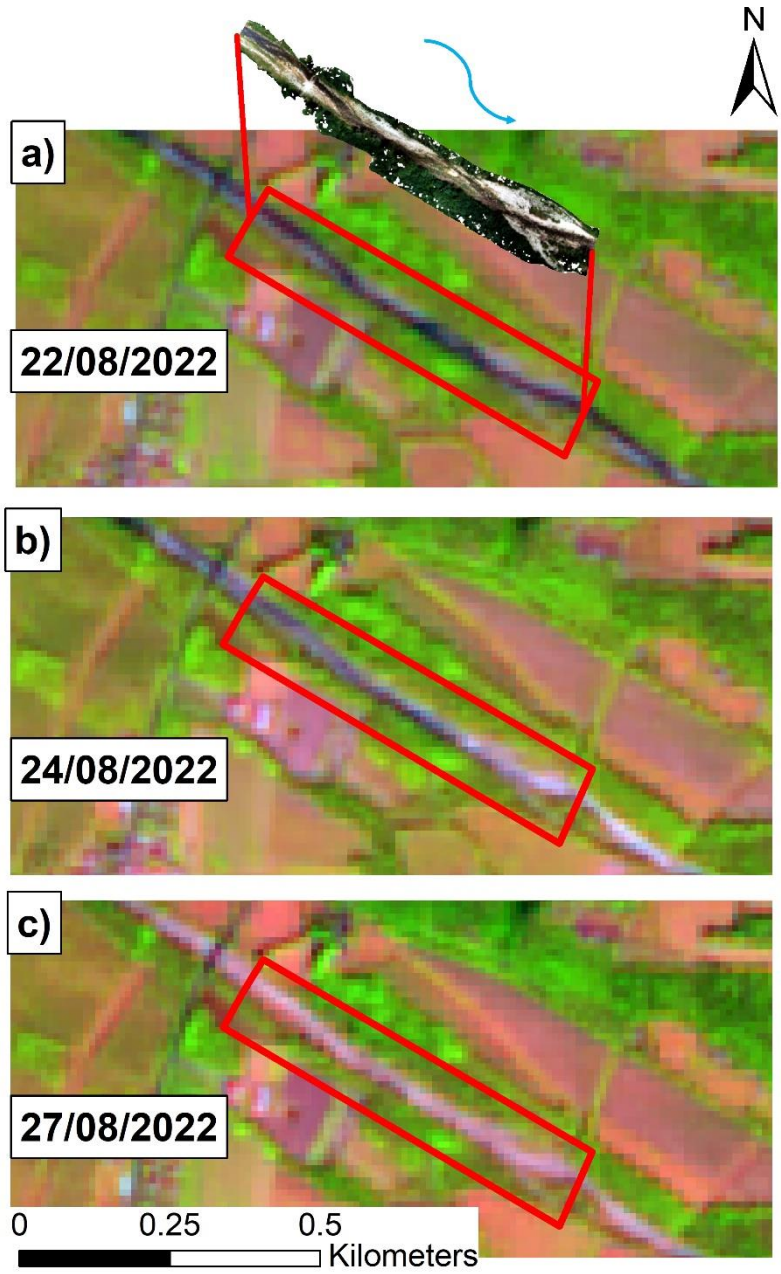


Figure 7.3. Sentinel-2 false-color images (bands 11-8-4) corresponding to a) flowing (August 22nd 2022), b) ponding (August 24th 2022), and c) dry (August 27th 2022) conditions during the most drought event of summer 2022. The RGB orthomosaic representing the surveyed reach (in red) is depicted on the top of the image. The main flow direction is indicated by the blue arrow. The recession in the extent of the wetted area, transitioning from a flowing phase to completely dry within five days, is clearly evident.

7.3 Results

To calibrate the 2D hydrodynamic model, the highest match between simulated and measured water depths and velocities was achieved with a Manning's coefficient of 0.042. Specifically, for water depth, we obtained a Root Mean Square Error (RMSE) of 0.07 m and a coefficient of determination (R^2) of 0.87, indicating a high level of accuracy. However, flow velocity exhibited slightly lower performance with an RMSE of 0.1 m/s and an R^2 of 0.74. Both the bathymetric correction applied to the DEM as well as the 2D hydrodynamic model setting were considered suitable for the following ecological analyses.

In total, 172 GUs were delineated and described across the five simulated conditions, among these 14 mesohabitats (8% of the total GUs) were identified as isolated ponds, representing the remaining wetted areas during the non-flowing condition at the first day after flow cessation (ponding phase). Overall, glides comprised the majority (35% of the total GUs) closely followed by riffles (33% of the total GUs). Backwaters, rapids, and pools corresponded to 10%, 9%, and 4% of cases, respectively. The water surface area of identified GUs varied significantly, ranging from a minimum of 1.8 m^2 (attributed to a backwater) to a maximum of 675.0 m^2 (attributed to a glide). Water depths across all considered discharges were generally shallow (**Figure 7.2**), with a maximum value of 0.59 m. At the lowest flow conditions (Q = 0.15 m^3/s), the vast majority of depths were below 0.3 m (mean value = 0.21 m), while at the highest flow conditions (Q = 3 m^3/s), they remained below 0.6 m (mean value = 0.23 m). Conversely, flow velocities tended to increase with flow rates. At 0.15 m^3/s, the mean water velocity was 0.21 m/s, whereas at 3 m^3/s, it rose to 0.66 m/s. The riverbed substrate primarily consisted of *mesolithal* (49.6%), *macrolithal* (33.8%), and *microlithal* (14.9%), with *psammal* and *pelal* being considerably less present, each accounting for less than 1% of the total. In terms of fish cover and shelters, boulders were the most common one, observed in nearly all GUs (98% of total), followed by emerging vegetation (present in 87 GUs), shallow margins (present in 69 GUs), and canopy shading (present in 63 GUs). Among all mesohabitats, water surface gradients ranged from 0.0 to 0.068.

Considering the resulting habitat-flow-time rating curves (**Figure 7.5**a), for adult *T. muticellus*, available habitat exhibited a monotonically increasing trend from 0.15 to 2 m^3/s, reaching 16.6% of the channel area, after which it remained relatively constant until reaching 3 m^3/s. At low flows (e.g., 0.15 m^3/s) and during the ponding condition (as depicted in the second quadrant of corresponding rating curve), the extent of suitable habitat was minimal, approaching 0.0 m^2 (below 1% of the channel area). Conversely, juvenile *T. muticellus* showed the maximum available habitat extent at 0.15 m^3/s, covering 14.9% of the channel area. However, as flow rates increased, habitat availability decreased, representing 2.3% of the channel area at 3 m^3/s. During the ponding condition, the remaining isolated ponds still provided potential residual habitat for juvenile vairone, corresponding to 8.5% of the channel area at the first day after flow cessation. This residual habitat persisted until a completely dry condition was reached after 5 days. Adult *P. bonelli*

displayed a similar trend in habitat availability to juvenile *T. muticellus*, especially during the ponding condition, though habitat values were generally higher. Specifically, the rating curve for this species exhibited a local maximum value at 1 m^3/s, covering 60.2% of the channel area, after which available habitat monotonically decreased at higher flow rates, reaching 30.0% of the channel area at 3 m^3/s.

The comparison between the RGB orthomosaic and the Sentinel-2 image closest to the date of the UAV flight clearly allowed to distinguish between submerged and emerged areas, revealing a satisfactory agreement in the spatial extension of aquatic habitat. Thus, the methodology proposed by [29] was considered applicable to the surveyed sub-reach (see **Figure 7.3**). The analysis of discharge and rainfall time series allowed to identify three main drought periods in the available time series: September-October 2017, July-August 2018, and June-September 2022. Consequently, 72 Sentinel-2 images (actual revisit time = 3.4 days) from these periods with reduced cloud cover were considered and classified according to the current hydrological conditions (flowing, ponding or dry). Overall, the dry condition was predominantly observed (45.8% of total images), followed by the flowing condition (37.5% of total images). The ponding condition was less frequently observed (16.7% of total images). Among these periods, the most severe drought was noted in summer 2022, with the most prolonged continuous dry condition lasting over 40 consecutive days between July and August. In total, for this period, 34 available satellite images were classified for assessing the daily hydrological condition characterizing the study site (**Figure 7.4**). From this analysis, the shortest ponding condition duration was estimated to be 5 days (see **Figure 7.3**), occurring in two separate events during late August and early September 2022 (**Figure 7.4**). This information was assumed to define the time required by the study site to reach a totally dry condition, in the second quadrant of the habitat-flow-time rating curves (**Figure 7.5**a). The threshold flow value (Q*) for the Trana time series, below which continuous flow is expected to cease in the surveyed reach, was estimated to be 0.92 m^3/s (**Figure 7.4**). Below this discharge value, from June to September 2022, almost 97% of classified satellite images corresponded to ponding or dry condition.

The estimated altered flow time series of the surveyed sub-reach, below the agricultural weirs, during summer 2022 is presented in **Figure 7.5**b. In **Figure 7.5**c and **Figure 7.5**d, the corresponding habitat time series for the adult stage of *T. muticellus* and *P. bonelli* are also depicted, respectively. From June to September, three flowing impulses supplied the surveyed sub-reach. Each discharge peak produced a corresponding spike in the habitat series. After each flowing phase, ponding conditions established before transitioning to a completely dry condition. The shortest ponding condition durations, corresponding to 5 days, occurred in late August and early September. According to the corresponding habitat-flow-time rating curves, once continuous flow ceased, habitat availability for adult *T. muticellus* rapidly drops to zero, while the decrease for adult *P. bonelli* is more

gradual. The extensive drought period in July and August 2022 is clearly represented in the habitat time series (**Figure 7.5**c).

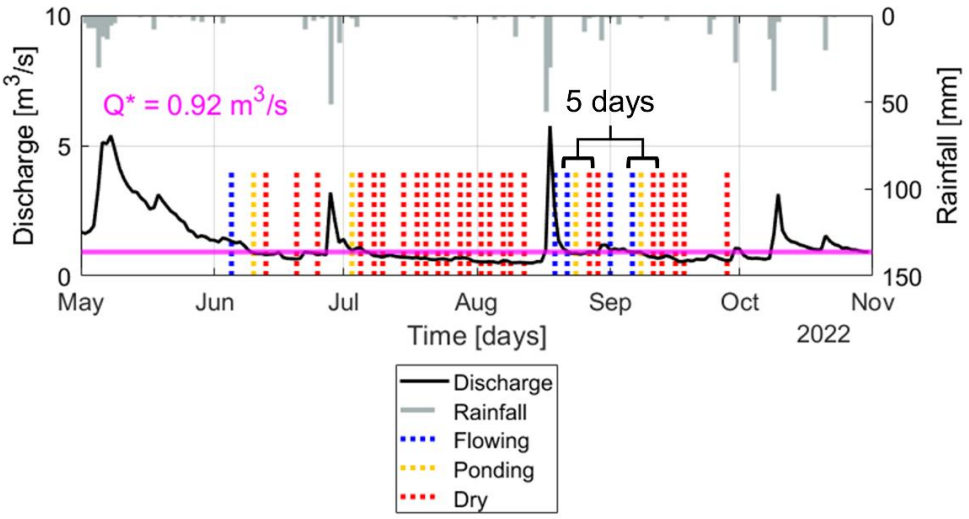


Figure 7.4. Time series of discharge (in black) and rainfall (in gray) during the most severe drought period affecting the study site, which corresponded to summer 2022 (June-September). The hydrological conditions classified from the Sentinel-2 images analysis during the same period are presented by dotted segments in blue (flowing condition), yellow (ponding condition), and red (dry condition). The threshold flow value (Q*) below which in the surveyed sub-reach are observed discharge interruptions is represented in magenta. The shortest ponding condition durations corresponding to 5 days assessed in two events in late August and early September are highlighted.

7.4 Discussion

The calibration of the 2D hydrodynamic model was a crucial step to achieve a representative depiction of the aquatic physical habitat. The model was effectively calibrated, as evidenced by the low RMSE for water depths (0.07 m) and the high R^2 (0.87). This indicates a strong correlation between simulated and measured values, suggesting that the model accurately captures the hydrodynamic behavior of the surveyed sub-reach. However, it is important to note that the performance for flow velocity simulation showed slightly lower accuracy, with a higher RMSE (0.1 m/s) and a lower R^2 (0.74). This lower performance can be related to the complexity of flow dynamics in GUs characterized by steep water surface gradient (i.e., riffles and rapids) and the presence of coarse substrates (i.e., *mesolithal* and *macrolithal*), [163].

For each considered flow condition, an average of 40 submerged GUs belonging to five different types were identified. This means that every 100 m of river length contains an average of 10 mesohabitats, suggesting that the study site exhibits a good density and diverse range of mesohabitats [60]. In the analyzed GUs, water depths remained mainly shallow, while flow velocities slightly increased with higher simulated discharges. Additionally, we observed a steep

increase in the wetted area as flow increased (**Figure 7.5**a). This behavior is related to the morphology of the surveyed sub-reach, which is characterized by a low level of confinement and a relatively wide channel, which facilitate the lateral inundation of the river corridor while maintaining shallow water levels. The substrate composition mainly included coarse grain sizes (e.g., *mesolithal* and *macrolithal*), resulting in a high distribution of boulders as cover attributes. The massive presence of boulders is related to the intense sediment transport of Sangone river during floods. These findings regarding the substrate distribution assessment seem to confirm the choice of a relatively high Manning's coefficient (i.e., 0.042) for calibrating the hydrodynamic model [225]. The presence of canopy shading was mainly due to the presence of riparian vegetation along the river banks, whereas woody debris and log jams were rarely observed in the study site.

The electro-fish sampling highlighted a significant presence and variety of fish species within the surveyed sub-reach, underscoring the ecological importance of the study site as a suitable environment for this species. These findings align with recent literature on the biodiversity of NPRs, which considers such systems as important spots of freshwater species richness (e.g., [30], [223]). These results lay the groundwork for further ecological assessments and conservation efforts aimed at protecting and enhancing habitat quality to preserve fish biodiversity in the surveyed sub-reach.

Meso-scale habitat simulation models (e.g., MesoHABSIM) have been widely used in the context of water resources planning and management in perennial rivers [17], [28]. They have been successfully applied in different Mediterranean watersheds. [22] used the MesoHABSIM approach to develop a habitat suitability model for European crayfish (*Austropotamobius pallipes*) in seven small perennial and non-perennial streams in northern and central Italy. [48] implemented this methodology to assess adequate e-flows for a highly regulated river in Greece based on habitat requirements for autochthonous fish species. [30] highlighted the potential of meso-scale habitat suitability models for describing the available aquatic habitat in non-perennial rivers using fish species as ecological targets. The results from the current study in the Sangone river seems equally promising, especially regarding the effectiveness and flexibility of the innovative MesoHABSIM module for evaluating the aquatic habitat in NPRs. This model adapted well to describe aquatic habitat availability for fish in the surveyed sub-reach, showing interesting potential for future applications.

The habitat availability for *T. muticellus*, assessed through the HSC included in SimStream-Web, indicated that adults prefer moderate flow conditions. The available habitat reaches its maximum at 2 m^3/s and does not increase further with higher discharges. In contrast, juvenile vairone exhibited a different pattern. Habitat availability for juveniles was highest at the lowest flow conditions (0.15 m^3/s) and decreased as the flow increased. This indicates that juvenile vairone, in the study site, thrive in lower flow conditions, possibly due to their smaller size, which makes them more suited to slower-moving water. These results align with the findings from electro-fishing, which identified juvenile *T. muticellus* as the most common

fish across all sampled GUs at 0.15 m³/s. For adult *P. bonelli*, the assessed available habitat was generally significantly higher than for *T. muticellus* among all simulated discharges. This is related to the corresponding HSC, which generally evaluated the GUs as optimal, especially at lower flow conditions (i.e., 0.15 and 1 m³/s). These results are consistent with the electro-fishing observations, which identified a structured population of goby within the study site. Furthermore, the habitat features of the surveyed sub-reach generally correspond to the autecological requirements of *P. bonelli*, which, being a benthic species, prefers coarse substrates such as large cobbles and boulders [26], [226]. During ponding conditions, the remaining isolated ponds still provided residual habitats for juvenile vairone and adult goby until the reach transitioned to a completely dry phase. These findings align with previous research, which indicates that flow cessation and the subsequent formation of isolated ponds serve as refuges for fish, allowing several species to coexist and survive until flow resumes [227]. Nonetheless, to preserve these species, it is crucial to maintain adequate surface flow regimes to minimize the duration of non-flowing periods (fewer than five days), thus avoiding completely dry conditions.

Further field surveys were planned at the study site during the summers of 2021 and 2022 to assess habitat availability during zero-flow periods, prior to reaching a completely dry condition. However, these attempts did not capture the ponding phase. Specifically, in late summer 2021, the surveyed reach had already transitioned into a permanent flowing condition, and in 2022, further attempts were limited to June and July, where the reach was in a totally dry condition. The 2022 observations, presented in **Figure 7.4**, highlight the rarity and brief duration of the ponding phase, with only four instances detected over a four-month period. This reinforces the difficulty of observing ponding in the field. Additionally, the study site is downstream of agricultural weirs, which introduce variability in the transition from flowing to dry conditions due to unpredictable water abstraction practices. These practices can cause rapid shifts between hydrological phases, further complicating efforts to predict and observe the ponding phase. Given these limitations, an alternative method was used to estimate residual aquatic habitat during the non-flowing period. This involved artificially filling the bathymetrically corrected DEM with water in a GIS environment, assuming that isolated ponds would form in the most depressed areas of the site. While this approach is not fully precise, it was qualitatively validated through false-color satellite image analysis, following the methodology outlined in [29]. The combination of accurate DEM data and satellite imagery provides a useful tool for quickly estimating aquatic habitat at the meso-scale in NPRs during the ponding phase.

To conservatively safeguard the river ecosystem, we focused on habitat-flow-time rating curves representing the worst-case scenario, where the site would reach a completely dry condition in the shortest possible time after flow cessation. To establish this, we identified the most severe drought periods affecting the Sangone river using local hydrological data. Satellite image analysis determined that the river could transition from flowing to dry conditions in as little as 5 days, observed twice in late August and early September 2022. Although some uncertainties

remain, satellite image analysis provides a reliable minimum estimate for the transition time between flowing and dry phases, based on the shortest interval between two consecutive images classified as flowing and dry. Conversely, locally recorded hydrological data in traditional gauging stations proved unsuitability for realistically assessing the frequency and duration of different hydrological conditions within the surveyed reach. However, uncertainties arise in estimating the ponding phase duration, particularly due to the spatial resolution of the Sentinel-2 sensor (10 m), which may struggle to detect ponds smaller than this threshold (see Chapter **7** for further details). Furthermore, it's important to highlight that the Sentinel-2 satellite, used in this study, has a revisit time of 2-5 days depending on the geographic location, which limits the usage of such sensors in NPRs with ponding phases shorter than this threshold. In the study, with a mean revisiting time of 3.4 days, we were able to asses 5 days as minimum ponding time duration.

Local hydro-geo-morphological features play a critical role in determining the occurrence and duration of the ponding phase, which can vary significantly both across different sections of the same river and within the same reach over time. Reducing uncertainties around the ponding phase duration is essential for accurately assessing the hydro-morphological impacts of water abstraction and for defining e-flows in regulated NPRs. Achieving this requires increasing the temporal resolution of satellite imagery potentially through hydrological modeling (e.g., [29]) or additional groundwater level monitoring or by deploying strategically placed cameras to capture multiple daily images of the study site.

Information on ponding duration was essential for defining the habitat-flow-time rating curves for the surveyed reach, enabling an evaluation of aquatic habitat changes during the worst-case scenario for ponding phase duration as estimated from Sentinel-2 imagery. However, SimStream-Web allows for the consideration of various scenarios based on the specific hydro-morphological context of the river reach. For example, different ponding phase durations (such as the mean duration over a period of interest) can be explored, allowing for the computation of alternative habitat-flow-time rating curves and corresponding habitat time series.

The integration of satellite imagery with discharge and rainfall data allowed us to estimate the hydrologic regime characterizing the lower part of the Sangone course, affected by flow intermittency due to water abstractions. This approach not only identified drought periods causing discharge interruptions but also provided insights into the duration and frequency of different hydrological conditions. From this analysis, the summer of 2022 emerged as the most severe period. Specifically, considering the available discharge and rainfall data, the mean discharge in 2022 was assessed at 1.09 m^3/s (-64.3% from the mean value) and cumulative rainfall at 720 mm (-45.2% from the mean value). These results align with the analysis of [186], which identified 2022 as a period characterized by a prolonged dry spell which affected the entire Northern Italy.

The threshold flow value (Q*) for the Trana time series, estimated at 0.92 m^3/s, provided a critical benchmark for identifying periods when continuous flow ceased in the surveyed sub-reach. This threshold was used to define the altered discharge

series below the agricultural weirs. Although it was a quite rough estimate, the comparison between discharge, rainfall, and satellite data confirmed that the occurrence of hydrological conditions was correctly assessed, providing valuable insight for the definition of the hydrologic regime in NPR reaches. Furthermore, at a local scale, these findings can lead to a better water resource management within the Sangone catchment. Indeed, the continuously available discharge information registered in Trana can be used by local authorities as a proxy for anticipating zero-flow occurrences in the downstream reaches due to over-exploitation for agricultural purposes, helping to prevent extended drought periods.

Due to increasing anthropogenic pressures and climate change patterns, intermittency in watercourses is globally increasing [83]. Rivers that normally presented a perennial behavior are changing their nature, assuming intermittent features along their course [77]. This situation is particularly evident in the Sangone river, where current water abstraction licensing poses a significant threat to the survival of the aquatic ecosystem in its downstream reaches. An overall increase in the duration and frequency of zero-flow periods in different reaches below the village of Trana is observable in recent years, particularly during the summer months (July-September). To mitigate this situation, ecological flows (e-flows) must be defined and implemented, taking into account the frequency and duration of the ponding and the dry conditions. In this context, the innovative MesoHABSIM NPRs-module emerges as a valuable tool for enhancing the water resource management of the Sangone river. By quantifying the habitat for aquatic organisms over flows and time after flow cessation, this module allows to analyze the deviation between natural and altered habitat time series. Consequently, different e-flows scenarios can be tested and evaluated to minimize the environmental impacts during low flow and drought periods, enhancing freshwater ecosystems and conserving local biodiversity.

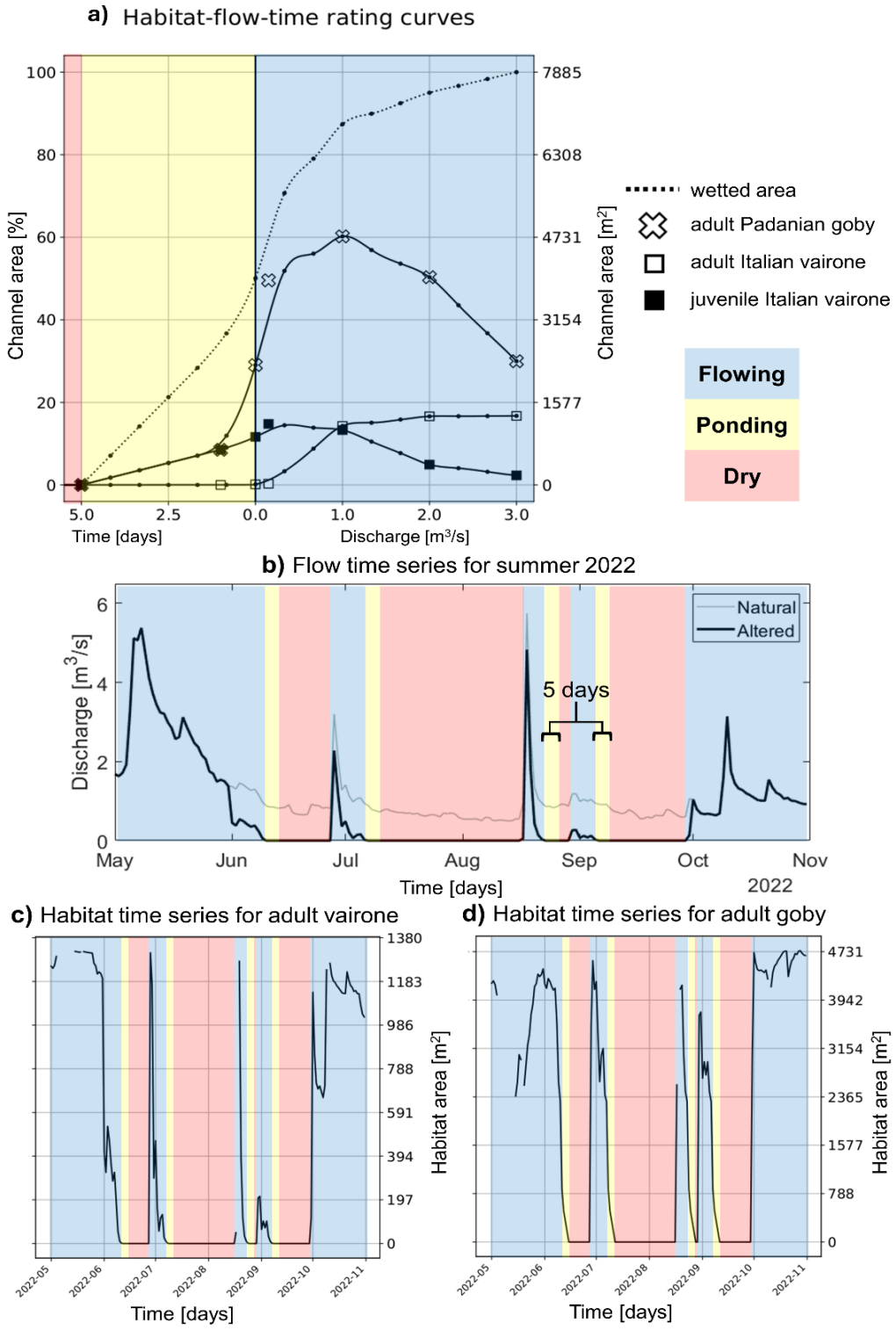


Figure 7.5. a) The habitat-flow-time rating curves for the surveyed sub-reach computed using SimStream-Web. The evolution of total wetted area (%) and available habitat (%) for adult (black filled square dot) and juvenile (black empty square dot) *T. muticellus*, and adult *P. bonelli* (black empty ex dot) per discharge and time. The flowing condition is highlighted in blue, the ponding condition, estimated to stand for 5 days, in yellow, and the dry condition in red. b) The altered flow time series estimated in the surveyed sub-reach during summer 2022. The corresponding habitat time series for c) adult *T. muticellus* and d) adult *P. bonelli* obtained via SimStream-Web. The sequence of periods corresponding to each assessed hydrological condition is highlighted. For discharges higher than 3 m³/s, conversion into habitat terms was not possible, and these values were replaced with not-a-number (NaN) values.

Chapter 8

8. Conclusions

This thesis focuses on advancing meso-scale habitat modeling for both perennial and non-perennial rivers, enhancing the applicability of the MesoHABSIM approach, particularly in Italy. The MesoHABSIM is increasingly recognized as a important tool for assessing the impact of water abstraction and designing e-flows in regulated rivers, promoting sustainable water resource management while preserving river ecosystems and associated services. However, its broader implementation is limited by gaps in knowledge regarding freshwater species' habitat preferences and, consequently, in the availability of habitat suitability criteria. Additionally, when such HSC are available, they require validation to demonstrate their transferability within the different river contexts.

Part I of this thesis try to address these limitations by (i) highlighting the current gaps in understanding the habitat preferences of Italian autochthonous freshwater species, (ii) developing novel HSC for two endemic and threatened species (i.e., *Lampetra zanandreai* and *Alosa Fallax*), and (iii) assessing the transferability of meso-scale HSC across rivers in Northern Italy.

River habitat modeling has traditionally focused on perennial rivers, and very few applications are currently available in non-perennial ones. Major constraints are related to a general lack of information about the spatio-temporal distribution of flow intermittency and NPRs hydrological regimes, as well as challenges in effectively modeling aquatic habitat availability when discharge is close to or equals zero.

Part II of this thesis try to overcome these constrains by proposing new theoretical approaches and analytical tools to (i) characterize flow intermittency and the hydrological regime of NPRs, and (ii) describe the aquatic habitat evolution during flowing and non-flowing periods.

Part I. Given the significant field efforts and data analysis involved in developing empirical HSC for freshwater species, it is essential to have a clear understanding of which species require prioritized investigations. For this reason, a

literature review on the current knowledge on the habitat preferences of Italian freshwater fish was performed. The systematic review revealed significant knowledge gaps and limited data availability for many species. Specifically, more than 30% of Italian fish species lacked sufficient information. It emerged that species with higher economic value or wider distribution areas tend to have more information, while purely endemic species are generally underrepresented. This highlights the need for increasing researches and investments in studying the aquatic habitats requirements of purely endemic Italian species, with the aim of better designing and organizing habitat restoration efforts and conservation plans for threatened ones. A crucial issue identified within the review process is the lack of information on spawning habitat requirements. Despite the critical role of reproduction in fish life cycle, there is a general scarcity of studies on this aspect, particularly for Italian endemic species. This gap in knowledge underscores the importance of conducting further research on spawning habitat requirements to preserve freshwater fish biodiversity. Meso-scale HSC developed using literature information have shown effectiveness in predicting fish distribution in certain contexts, such as the Argentina Creek. However, the limited data availability on habitat requirements for several species or life stages poses significant challenges for a widespread definition of literature-based HSC, thus constraining the application of MesoHABSIM throughout Italy. Nevertheless, the systematic literature review marks a step forward in addressing this challenge by offering valuable insights to assist ecologists in the development of novel HSC.

With the aim of improving the number of available meso-scale HSC for Italian freshwater species, an investigation on the habitat preferences of Po brook lamprey (*Lampetra zanandreai*) ammocoetes was conducted in four rivers of Piemonte Region (Northwestern Italy). This species was chosen based on identified gaps in the available literature, which revealed a notable lack of knowledge regarding lamprey habitat requirements. The development of HSC involved integrating the MesoHABSIM methodology with machine learning techniques, utilizing the Random Forest classification algorithm. This approach enabled to explore the relationship between habitat attributes and lamprey distribution within GUs, revealing a preference for mesohabitats characterized by shallow depth, low flow velocity, and fine sediment patches. The high predictive performance of the developed HSC suggested the potential to extend the applicability of the MesoHABSIM approach to include the Petromyzontidae family. Furthermore, this study laid the groundwork for implementing habitat preservation measures aimed at conserving the endemic and threatened Po Brook lamprey through effective management strategies involving e-flows design and sediment control. Another important aspect explored in this study is the role of organic matter levels in substrate composition on lamprey distribution within mesohabitats. Specifically, lampreys exhibit a preference for sand and gravel with low organic content. Consequently, it becomes evident that lampreys demonstrate specific requirements not only for habitat patches characterized by particular velocity, depth, and grain size ranges, but also for those with minimal organic content. This implies that the possibility of encountering this species is higher in rivers featured by better

ecological, chemical, and hydro-morphological conditions. Therefore, lampreys can play a pivotal role as indicators of freshwater ecosystem quality in rivers belonging to the Po river basin. Hence, further researches aimed at gaining a deeper understanding of the environmental requirements of lamprey ammocoetes are required.

From the findings of the literature review, attention was focused in development of HSC for the spawning period of the anadromous Twite shad (*Alosa fallax*), by investigating the habitat requirements of this species during the reproduction period in the Tagliamento river (Northeast Italy). Habitat depiction was achieved in the framework of the MesoHABSIM approach. Riverine habitat attributes were characterized using high-resolution spatial data derived from UAS and acoustic-based devices, a locally calibrated 2D hydrodynamic model, and field data collected during the spawning period. The incorporation of UAS and a 2D hydrodynamic model played a crucial role in refining the depiction of flow conditions within the mesohabitats throughout the monitored period. Equally, the georeferenced data acquired from various in-stream surveys facilitated to complement the habitat depiction, offering an exhaustive characterization of the riverine areas utilized for spawning. The synergy of these different data sources facilitated a nuanced and accurate representation of the fluvial habitat during the spawning period of the *A.fallax*. For the HSC definition, a classification RF model was employed to discern the specific GU and associated habitat attributes that the shad prefers for spawning. The model pointed out that glides and riffles characterized by shallow water depth, moderate current velocity, and small size sediment (diameter 0.2-6 cm) are the preferred areas for the fish to spawn. The study significantly enhanced the comprehension of the specific habitat elements that contribute to successful shad reproduction. This information is highly valuable for conservation and management efforts, as it offers a detailed blueprint of the environmental conditions necessary for the species' mating activities. The study provides actionable insights that can inform targeted conservation strategies aimed at preserving and enhancing the spawning habitats of the shad population. The successful application of an infrared camera for monitoring the mating activity and behaviour of *A fallax* at night opens up new possibilities for non-intrusive and effective observation. This technology can be incorporated into future monitoring and conservation programs to assess the ongoing status of *A. fallax* populations as well as for evaluating the impact of habitat management strategies. Finally, the congruence in mating behaviour, and temporal patterns with previous studies collectively contribute to a richer understanding of shad reproductive ecology. These insights are crucial for fisheries management, conservation practices, and a broader comprehension of Mediterranean population of *A. fallax*.

Empirical HSC developed within the MesoHABSIM approach typically rely on independent datasets collected in natural reference sites. Ideally, these data should encompass diverse hydro-morphological contexts where the species are naturally present. This diversity enhances the models' robustness, ensuring broader validity and applicability. However, validation using independent data not included in the

calibration dataset is essential to confirm model applicability in different river systems. Recent field campaigns in Northern Italy allowed to assess the transferability across different rivers of five meso-scale HSC previously developed with the Random Forest classification algorithm and made available in the SimStream-Web service for applications of the MesoHABSIM approach in Italy. All these HSC exhibited high transferability, regardless of life stage, validation dataset size, or spatial location of surveyed reaches. Such findings can be attributed to the use of an ecologically relevant spatial scale (i.e., mesohabitat), a robust hydro-morphological characterization, and the inclusion of diverse environmental descriptors within the MesoHABSIM approach. These findings support promoting MesoHABSIM's application across Italian rivers for e-flows design and habitat restoration plans.

Overall, these studies significantly enhance the applicability of the MesoHABSIM approach by generating new ecological data and meso-scale HSC for endemic and endangered Italian freshwater species. They demonstrated the effectiveness of the MesoHABSIM approach in accurately quantify the aquatic habitat availability for diverse freshwater organisms even during critical phases of their life cycle (i.e., spawning). The developed meso-scale HSC can be integrated into the SimStream-Web service, facilitating the mitigation of hydro-morphological impacts in regulated rivers through the design of e-flows and habitat restoration initiatives aimed at conserving these species. However, given the pivotal role of HSC in species conservation and the substantial gaps in knowledge regarding the habitat preferences of Italian freshwater species, further investigations are urgently required. In this context, these studies serve as a valuable resource to prioritize species in need of research attention. Moreover, they offer an analytical procedure that can be utilized for defining new HSC for other threatened freshwater species.

Part II. River habitat modeling for non-perennial rivers is in its nascent stage, with initial applications emerging only recently. However, to effectively apply such models, a thorough understanding of the hydrological regime of the monitored reach is essential, information often lacking in existing data. In the second part of this thesis a methodology to identify NPRs and to assess their degree of temporariness was proposed. The data used are Sentinel-2 multispectral satellite images, distributed free of charge by the European Space Agency. Analysis of the spectral signatures of the water, sediment, and vegetation classes allowed the identification of bands in which the spectral differences between the three classes are greatest. The related false colour images composed of the B11, B8 and B4 bands resulted to bring out the differences between the three classes particularly well. In particular, with this band combination it was possible to identify three main hydrologic conditions: flowing, ponding, and dry. Comparison with very high-resolution images and field observations showed very good agreement between estimated and actual hydrologic conditions. The analyses indicated that wet channels or ponds are distinguishable if they are larger than 6 or 15 meters in size, making this approach suitable for a wide range of river reaches (i.e., those with mean widths exceeding three image pixels). The set of hydrologic conditions

derived from the image analysis was used to calibrate Random Forest models capable of predicting the occurrence and duration of each condition on a daily basis. Two types of binary models were implemented, the first was used to distinguish between flowing and non-flowing conditions and the second further detailed the non-flowing condition by separating between ponding and dry conditions. Several rainfall and temperature variables were tested as model predictors. Among these, the cumulative rainfall and temperature with higher temporal scales resulted in the most relevant predictors for considered models. Our analysis revealed that locally calibrated RF dels generally performed better for assessing the duration of hydrologic conditions in NPRs, nevertheless global models can be developed for multiple rivers reaches characterized by kindred hydro-climatic contexts. The daily series of hydrologic conditions allow the estimation of the degree of temporariness of rivers through, for example, the duration of the dry and the non-flowing periods. The methodology developed in this study can make a crucial contribution for evaluating the spatio-temporal distribution of flow intermittency and estimating the hydrological regime of NPRs. The free and global coverage of the source data, Sentinel-2 satellite mission imagery, and the easy-to-use method, may allow a cost-effective application in different river reaches worldwide.

Once the hydrological regime of a non-perennial river reach is characterized, the new NPRs-module can be applied to assess aquatic habitat availability during both flowing and non-flowing periods, providing a comprehensive tool for managing and preserving these ecosystems. This NPRs-module was presented in the final chapter of this thesis, by focusing the analysis on a reach of the Sangone river (Northwestern Italy) characterized by flow intermittency and totally dry conditions. The hydrological characterization was achieved by integrating satellite data with locally measured discharge and rainfall information to identify the occurrence and duration of non-flowing periods. The satellite images analysis was based on the methodology proposed in previous Chapter **6**. The study employed the innovative NPRs-module to describe habitat evolution during both flowing and non-flowing periods. The Italian vairone (*Telestes muticellus*) and the Padanian goby (*Padogobius bonelli*), two endemic fish inhabiting the Sangone river, were chosen as appropriate ecological target. Mesohabitat depiction was achieved by integrating high-resolution spatial data derived from UAS, a locally calibrated 2D hydrodynamic model, and field data. The methodology for assessing the presence of water using false-colour Sentinel-2 images resulted suitable for the Sangone river, demonstrating its effectiveness and reliability. This approach allowed to successfully identify the occurrence and duration of the non-flowing conditions, detecting the most sever drought period affecting the study site. The application of the NPRs-module proved effective in assessing habitat availability for the target species in the surveyed reach. The SimStream-Web service emerged as a valuable tool for supporting the analysis of the spatio-temporal variation of aquatic habitat in NPRs. The integration of remote sensing and habitat modeling techniques offered a comprehensive tool for sustainable water resource management in NPRs.

The increasing intermittency of watercourses due to anthropogenic pressures and climate change poses unprecedented challenges for the survival of river ecosystems and their biodiversity. This situation necessitates effective solutions and innovative tools to rapidly and extensively assess the spatio-temporal distribution of flow intermittency in river networks, offering practical solutions for characterizing the hydrological regime of NPRs reaches and describing the aquatic habitat evolution during non-flowing periods. In this context, the satellite image analysis proposed in this thesis can make a crucial contribution by identifying and mapping water presence in NPRs and estimating in a cost-effective manner the frequency and duration of the different hydrologic conditions (flowing, ponding, dry). Furthermore, the new NPRs-module, unlike traditional HSMs, provides a suitable solution for analyzing the spatio-temporal aquatic habitat evolution even when surface flow drops to zero. This NPRs-module consequently allows the design of e-flow release scenarios to mitigate the impacts of extended dry periods related to water abstraction, aiming to preserve aquatic ecosystems and maintain biodiversity in NPR environments.

Chapter 9

9. Limitations and perspectives

Finally, several ideas for future research have emerged from both the limitations and potential of this thesis. These are briefly outlined below:

Expanding MesoHABSIM applicability. Rivers are highly complex ecosystems, supporting a vast array of species at various life stages. Traditionally, river habitat modeling has focused primarily on fish due to their more comprehensive habitat requirements and their relevance from a management perspective. This thesis has also mainly focused on freshwater fish species, particularly in Italy. However, aquatic habitats are equally critical for many other organisms, such as macroinvertebrates or amphibians, which are frequently more numerous than fish. Moreover, river habitat availability assessment traditionally focused on aquatic species, determining a general underestimation of total river habitat, which is composed also by the terrestrial part. For instance, certain bird species utilize exposed gravel bars for nesting. Given its reference spatial unit (i.e., the geomorphic unit scale [60]), generally recognized as intrinsically connected to the life cycle of different communities, the MesoHABSIM approach offers a valuable opportunity to address this gap. Its flexibility allows the integration of additional habitat attributes for other species, making it possible to extend this approach beyond fish or even aquatic habitat. This expansion could lead to more comprehensive river management strategies that protect entire river ecosystems from hydro-morphological impacts. In this regard pioneering approaches have recently been explored (e.g., [20]) providing successful findings.

Application of MesoHABSIM in large rivers. While the field data collection protocol of the MesoHABSIM approach is well-established for small rivers using mobile mapping techniques, applying it to larger rivers (with widths exceeding 40-50 m) presents challenges. Advanced tools, such as UAS and 2D hydrodynamic modeling, show great potential for improving habitat modeling in large rivers. These technologies have been explored in meso-scale river habitat modeling over

the past 15 years, and their potential, as well as their limitations, are now well understood, allowing researchers to define an operational framework. The maturity of this research therefore allows for the standardization of protocols for both data collection and processing using such technologies, enabling the transfer of knowledge from academia to public and private sectors. However, further efforts are still needed to develop robust and effective algorithms for mapping morphological and hydraulic units under different simulated discharge conditions. While significative progress has been made in this area (e.g., [62]), additional work is necessary to make these algorithms more widely applicable.

Improving meso-scale HSC robustness and applicability. In Italy, biomonitoring of river species (e.g., fish, macroinvertebrates) is typically conducted following species-specific protocols, which provide valuable insights into population health and habitat quality. However, these protocols often do not align with the requirements for developing species distribution models, especially at the meso-scale. Harmonizing biomonitoring protocols with the MesoHABSIM approach could be a productive way forward. By developing a common field protocol, it would be possible to simultaneously collect both quantitative biological data and physical habitat descriptions. This integration, using the information collected in reference sites, could greatly expand the datasets for developing new meso-scale HSCs or validating existing ones, thereby increasing the accuracy and robustness of these models. Harmonizing these efforts would also enhance the effectiveness of conservation initiatives and improve the efficient use of resources by public authorities responsible for protecting river ecosystems.

Developing metrics for assessing river connectivity. As part of the EU Biodiversity Strategy for 2030, there is a goal to remove river barriers to restore 25000 km of free-flowing rivers. However, identifying which barriers to remove while balancing human needs with ecosystem restoration is complex. There are currently few metrics capable of assessing the ecological benefits of barrier removal in a clear and robust way. Anadromous species, such as the Twaite shad, offer valuable insights in this area, as they rely on river longitudinal connectivity for reproduction. Focusing research on the ecological needs and spatial distribution of such species during their reproductive cycles could inform the development of new metrics for assessing river connectivity. Additionally, innovative non-intrusive biomonitoring techniques (e.g., infrared cameras) for these species could provide important information improving the assessments of barrier removal effectiveness in river networks.

Advancing hydrological characterization of NPRs. While this thesis has demonstrated the potential of Sentinel-2 imagery to characterize the degree of intermittency in non-perennial rivers, challenges remain. Currently, interpreting hydrological conditions is a fully supervised process, which can lead to misclassification due to human error and essentially slow down large-scale implementation. Our research group is currently exploring different approaches to automate the classification of Sentinel-2 images. Continued work in this area could lead to the development of an algorithm capable of reliably identifying hydrological

conditions across diverse river systems. This would enhance the applicability of the proposed procedure and allow for more efficient monitoring of NPR reaches, which are globally increasing.

Improving habitat modeling in NPRs. As presented in this thesis, the MesoHABSIM methodology has been adapted for non-perennial rivers, but challenges remain in modeling habitat availability during zero-flow phases. Quantifying habitat recession and the duration of the ponding phase is particularly challenging, as it can vary both within and between years. Additionally, habitat parameters (e.g., distance between isolated ponds, water temperature) may need to be incorporated into species distribution models to assess habitat suitability over time during the ponding phase. Further research is necessary to address these open questions. Currently, our research group is evaluating the potential of new satellite constellations, such as Cubesat, which offer daily temporal resolution but are not freely available to all users. We are also exploring the Sentinel-1 sensor, which uses SAR (Synthetic Aperture Radar) technology, providing reduced revisit times (1-3 days) and overcoming limitations posed by cloud cover. For smaller non-perennial rivers that cannot be observed remotely, strategically positioned cameras can offer an alternative by capturing daily images and providing consistent, localized data for habitat modeling. Identifying the critical physical attributes that distinguish suitable from unsuitable ponds during non-flowing conditions presents another layer of complexity due to the potential interaction of multiple adverse factors. The combined effects of these factors can accelerate the decline in habitat suitability, requiring a more in-depth and comprehensive understanding of the process. However, as practical applications of the new NPRs module is expected to expand across different river contexts, it is likely that these applications may suggest future improvements to better describe habitat availability evolution during non-flowing periods.

References

[1] J. A. Yeakley *et al.*, "Ecosystem Services of Streams and Rivers," in *River Science: Research and Management for the 21st Century*, John Wiley & Sons, Ltd, 2016, pp. 335–352.

[2] M. Bussettini and P. Vezza, "Guidance on Environmental Flows - Integrating E-flow Science with Fluvial Geomorphology to Maintain Ecosystem Services," 2020.

[3] N. L. Poff *et al.*, "The natural flow regime: A paradigm for river conservation and restoration," *Bioscience*, vol. 47, no. 11, pp. 769–784, 1997, doi: 10.2307/1313099.

[4] E. Wohl *et al.*, "The natural sediment regime in rivers: Broadening the foundation for ecosystem management," *Bioscience*, vol. 65, no. 4, pp. 358–371, 2015, doi: 10.1093/biosci/biv002.

[5] D. Dudgeon *et al.*, "Freshwater biodiversity: Importance, threats, status and conservation challenges," *Biol. Rev. Camb. Philos. Soc.*, vol. 81, no. 2, pp. 163–182, 2006, doi: 10.1017/S1464793105006950.

[6] B. M. Renöfält, R. Jansson, and C. Nilsson, "Effects of hydropower generation and opportunities for environmental flow management in Swedish riverine ecosystems," *Freshw. Biol.*, vol. 55, no. 1, pp. 49–67, 2010, doi: 10.1111/j.1365-2427.2009.02241.x.

[7] A. J. Reid *et al.*, "Emerging threats and persistent conservation challenges for freshwater biodiversity," *Biol. Rev.*, vol. 94, no. 3, pp. 849–873, Jun. 2019, doi: 10.1111/brv.12480.

[8] G. Grill *et al.*, "Mapping the world's free-flowing rivers," *Nature*, vol. 569, no. 7755, pp. 215–221, May 2019, doi: 10.1038/s41586-019-1111-9.

[9] N. Alexandratos and J. Bruinsma, "World agriculture towards 2030/2050: the 2012 revision," Jun. 2012, doi: 10.22004/AG.ECON.288998.

[10] C. Zarfl, A. E. Lumsdon, J. Berlekamp, L. Tydecks, and K. Tockner, "A global boom in hydropower dam construction," *Aquat. Sci.*, vol. 77, no. 1, pp. 161–170, 2015, doi: 10.1007/s00027-014-0377-0.

[11] M. Carolli *et al.*, "Impacts of existing and planned hydropower dams on river fragmentation in the Balkan Region," *Sci. Total Environ.*, vol. 871, p. 161940, May 2023, doi: 10.1016/j.scitotenv.2023.161940.

[12] C. Schneider, C. L. R. Laizé, M. C. Acreman, and M. Flörke, "How will climate change modify river flow regimes in Europe?," *Hydrol. Earth Syst. Sci.*, vol. 17, no. 1, pp. 325–339, 2013, doi: 10.5194/HESS-17-325-2013.

[13] I. Maddock, A. Harby, P. Kemp, and P. Wood, "Ecohydraulics: An Integrated Approach," *Ecohydraulics An Integr. Approach*, pp. 1–446, Jan. 2013, doi: 10.1002/9781118526576.

[14] S. P. Rice, S. Little, P. J. Wood, H. J. Moir, and D. Vericat, "The relative contributions of ecology and hydraulics to ecohydraulics," *River Res. Appl.*, vol. 26, no. 4, pp. 363–366, May 2010, doi: 10.1002/rra.1369.

[15] European Commission, "Ecological flows in the implementation of the Water Framework Directive: guidance document n°31." p. 108, 2015, doi: 10.2779/775712.

[16] C. Comoglio, P. Vezza, P. Parasiewicz, K. Suska, J. Petela, and O. Calles, “Habitat suitability models as tools for implementing the" ecohydraulic trinity",” 2016.
[17] Y. Yi, X. Cheng, Z. Yang, S. Wieprecht, S. Zhang, and Y. Wu, “Evaluating the ecological influence of hydraulic projects: A review of aquatic habitat suitability models,” *Renew. Sustain. Energy Rev.*, vol. 68, pp. 748–762, 2017, doi: 10.1016/j.rser.2016.09.138.
[18] P. Parasiewicz, “The Mesohabsim model revisited,” *River Res. Appl.*, vol. 23, no. 8, pp. 893–903, Oct. 2007, doi: 10.1002/rra.1045.
[19] G. Negro *et al.*, “Ecological notes on an endemic freshwater lamprey, Lampetra zanandreai (Vladykov, 1955),” *Eur. Zool. J.*, vol. 90, no. 2, pp. 556–567, 2023, doi: 10.1080/24750263.2023.2226680.
[20] B. Pinna, A. Laini, G. Negro, G. Burgazzi, P. Viaroli, and P. Vezza, “Physical habitat modeling for river macroinvertebrate communities,” *J. Environ. Manage.*, vol. 358, p. 120919, 2024, doi: 10.1016/j.jenvman.2024.120919.
[21] P. Vezza, P. Parasiewicz, M. Rosso, and C. Comoglio, “Defining minimum environmental flows at regional scale: Application of mesoscale habitat models and catchments classification,” *River Res. Appl.*, vol. 28, no. 6, pp. 717–730, Jul. 2012, doi: 10.1002/rra.1571.
[22] P. Vezza, D. Ghia, and G. Fea, “Quantitative habitat models for the conservation of the endangered European crayfish Austropotamobius pallipes complex (Astacoidea: Astacidae),” in *A Global Overview of the Conservation of Freshwater Decapod Crustaceans*, Springer International Publishing, 2016, pp. 339–358.
[23] J. M. Nestler, R. T. Milhous, T. R. Payne, and D. L. Smith, “History and review of the habitat suitability criteria curve in applied aquatic ecology,” in *River Research and Applications*, Oct. 2019, vol. 35, no. 8, pp. 1155–1180, doi: 10.1002/rra.3509.
[24] E. Wohl *et al.*, *Synthesizing the scientific foundation for ordinary high water mark delineation in fluvial systems*. US Army Engineer Research and Development Center, Cold Regions Research and Engineering Laboratory., 2016.
[25] G. Negro *et al.*, “Transferability of Mesohabitat Suitability Criteria in Northern Italy,” in *Proceedings of the IAHR World Congress*, 2022, pp. 1416–1423, doi: 10.3850/IAHR-39WC2521716X20221044.
[26] G. Negro, S. Fenoglio, E. Quaranta, C. Comoglio, I. Garzia, and P. Vezza, “Habitat Preferences of Italian Freshwater Fish: A Systematic Review of Data Availability for Applications of the MesoHABSIM Model,” *Frontiers in Environmental Science*, vol. 9. Frontiers, p. 305, Jul. 27, 2021, doi: 10.3389/fenvs.2021.634737.
[27] N. Smialek, J. Pander, M. Mueller, R. van Treeck, C. Wolter, and J. Geist, “Do we know enough to save European riverine fish?-A systematic review on autecological requirements during critical life stages of 10 rheophilic species at risk,” *Sustain.*, vol. 11, no. 18, p. 5011, Sep. 2019, doi: 10.3390/su11185011.
[28] P. Parasiewicz *et al.*, “Applications of the MesoHABSIM Simulation Model,” in *Ecohydraulics: An Integrated Approach*, Chichester, UK: John Wiley & Sons, Ltd, 2013, pp. 109–124.
[29] C. Cavallo, M. N. Papa, G. Negro, M. Gargiulo, G. Ruello, and P. Vezza, “Exploiting Sentinel-2 dataset to assess flow intermittency in non-perennial

rivers," *Sci. Rep.*, vol. 12, no. 1, pp. 1–16, Dec. 2022, doi: 10.1038/s41598-022-26034-z.

[30] V. Acuña *et al.*, "Accounting for flow intermittency in environmental flows design," *Journal of Applied Ecology*, vol. 57, no. 4. pp. 742–753, 2020, doi: 10.1111/1365-2664.13590.

[31] A. H. Hirzel and G. Le Lay, "Habitat suitability modelling and niche theory," *J. Appl. Ecol.*, vol. 45, no. 5, pp. 1372–1381, Oct. 2008, doi: 10.1111/j.1365-2664.2008.01524.x.

[32] K. D. Bovee, "A guide to stream habitat analysis using the instream incremental flow methodology," Fort Collins, Colorado (USA), 1982.

[33] G. E. Petts, "Instream Flow Science For Sustainable River Management1," *JAWRA J. Am. Water Resour. Assoc.*, vol. 45, no. 5, pp. 1071–1086, Oct. 2009, doi: 10.1111/J.1752-1688.2009.00360.X.

[34] M. Acreman and M. J. Dunbar, "Defining environmental river flow requirements - A review," *Hydrol. Earth Syst. Sci.*, vol. 8, no. 5, pp. 861–876, 2004, doi: 10.5194/hess-8-861-2004.

[35] P. Parasiewicz, K. Ryan, P. Vezza, C. Comoglio, T. Ballestero, and J. N. Rogers, "Use of quantitative habitat models for establishing performance metrics in river restoration planning," *Ecohydrology*, vol. 6, no. 4, pp. 668–678, 2013, doi: 10.1002/eco.1350.

[36] W. R. T. Darwall and J. C. Vié, "Identifying important sites for conservation of freshwater biodiversity: extending the species-based approach," *Fish. Manag. Ecol.*, vol. 12, no. 5, pp. 287–293, Oct. 2005, doi: 10.1111/J.1365-2400.2005.00449.X.

[37] C. J. Gippel and M. J. Stewardson, "Use of wetted perimeter in defining minimum environmental flows," *River Res. Appl.*, vol. 14, no. 1, pp. 53–67, 1998, doi: 10.1002/(sici)1099-1646(199801/02)14:1<53::aid-rrr476>3.0.co;2-z.

[38] K. Jorde, *Ökologisch begründete, dynamische Mindestwasserregelungen bei Ausleitungskraftwerken*. Eigenverl. des Inst. für Wasserbau, Univ. Stuttgart, 1997.

[39] C. Hauer, G. Mandlburger, and H. Habersack, "Hydraulically related hydro-morphological units: description based on a new conceptual mesohabitat evaluation model (MEM) using LiDAR data as geometric input," *River Res. Appl.*, vol. 25, no. 1, pp. 29–47, Jan. 2009, doi: 10.1002/RRA.1083.

[40] N. L. Poff and J. K. H. Zimmerman, "Ecological responses to altered flow regimes: a literature review to inform the science and management of environmental flows," *Freshw. Biol.*, vol. 55, no. 1, pp. 194–205, Jan. 2010, doi: 10.1111/J.1365-2427.2009.02272.X.

[41] P. Parasiewicz, E. Castelli, J. N. Rogers, P. Vezza, and A. Kaupsta, "Implementation of the Natural Flow Paradigm to Protect Dwarf Wedgemussel (Alasmidonta heterodon) in the Upper Delaware River," in *River Research and Applications*, Feb. 2017, vol. 33, no. 2, pp. 277–291, doi: 10.1002/rra.3112.

[42] I. G. Jowett and M. J. Duncan, "Effectiveness of 1D and 2D hydraulic models for instream habitat analysis in a braided river," *Ecol. Eng.*, vol. 48, pp. 92–100, 2012, doi: 10.1016/j.ecoleng.2011.06.036.

[43] D. Farò, K. Baumgartner, P. Vezza, and G. Zolezzi, "Sensitivity of fish habitat suitability to multi-resolution hydraulic modeling and field-based description of meso-scale river habitats," *J. Hydrol. X*, vol. 21, p. 100160,

2023, doi: 10.1016/j.hydroa.2023.100160.
[44] G. R. Pisaturo, M. Righetti, M. Dumbser, M. Noack, M. Schneider, and V. Cavedon, “The role of 3D-hydraulics in habitat modelling of hydropeaking events,” *Sci. Total Environ.*, vol. 575, pp. 219–230, Jan. 2017, doi: 10.1016/J.SCITOTENV.2016.10.046.
[45] J. Rosenfeld, “Assessing the habitat requirements of stream fishes: an overview and evaluation of different approaches,” *Trans. Am. Fish. Soc.*, vol. 132, pp. 953–968, Sep. 2003, doi: 10.1577/T01-126.
[46] P. Vezza, R. Muñoz-Mas, F. Martinez-Capel, and A. M. Mouton, “Random forests to evaluate biotic interactions in fish distribution models,” *Environ. Model. Softw.*, vol. 67, pp. 173–183, May 2015, doi: 10.1016/j.envsoft.2015.01.005.
[47] S. H. Hamilton, C. A. Pollino, and A. J. Jakeman, “Habitat suitability modelling of rare species using Bayesian networks: Model evaluation under limited data,” *Ecol. Modell.*, vol. 299, no. 1, pp. 64–78, Mar. 2015, doi: 10.1016/J.ECOLMODEL.2014.12.004.
[48] E. T. Koutrakis *et al.*, “Evaluation of ecological flows in highly regulated rivers using the mesohabitat approach: A case study on the Nestos River, N. Greece,” *Ecohydrol. Hydrobiol.*, vol. 19, no. 4, pp. 598–609, 2019, doi: 10.1016/j.ecohyd.2018.01.002.
[49] A. M. Mouton *et al.*, “Optimisation of a fuzzy physical habitat model for spawning European grayling (Thymallus thymallus L.) in the Aare river (Thun, Switzerland),” *Ecol. Modell.*, vol. 215, no. 1–3, pp. 122–132, Jul. 2008, doi: 10.1016/j.ecolmodel.2008.02.028.
[50] J. D. Alcaraz-Hernández, R. Muñoz-Mas, F. Martínez-Capel, V. Garófano-Gómez, and P. Vezza, “Generalized additive models to predict adult and young brown trout (Salmo trutta Linnaeus, 1758) densities in Mediterranean rivers,” *J. Appl. Ichthyol.*, vol. 32, no. 1, pp. 217–228, Feb. 2016, doi: 10.1111/jai.13025.
[51] I. G. Jowett, “RHYHABSIM: River hydraulic and habitat simulation,” *New Zeal. Freshw. Fish. Misc. Rep. (New Zealand)*, vol. 49, 1989.
[52] P. Steffler and J. Blackburn, “Two-dimensional depth averaged model of river hydrodynamics and fish habitat,” *River2D user’s manual, Univ. Alberta, Canada*, 2002.
[53] P. Parasiewicz and M. J. Dunbar, “Physical habitat modelling for fish–,” *Arch. Hydrobiol. Suppl*, vol. 1352, no. 4, pp. 239–268, 2001.
[54] P. Vezza, A. Zanin, and P. Parasiewicz, “Manuale tecnico-operativo per la modellazione e la valutazione dell’integrità dell’habitat fluviale,” Roma (IT), 2017.
[55] C. Wolter, A. D. Buijse, and P. Parasiewicz, “Temporal and Spatial Patterns of Fish Response to Hydromorphological Processes,” *River Res. Appl.*, vol. 32, no. 2, pp. 190–201, Feb. 2016, doi: 10.1002/rra.2980.
[56] M. Gurnell *et al.*, “REstoring rivers FOR effective catchment Management (REFORM). Deliverable D2.1 Part I. A hierarchical multi-scale framework and indicators of hydromorphological processes and forms,” 2014.
[57] J. L. Kemp, D. M. Harper, and G. A. Crosa, “Use of ‘functional habitats’ to link ecology with morphology and hydrology in river rehabilitation,” *Aquat. Conserv. Mar. Freshw. Ecosyst.*, vol. 9, no. 1, pp. 159–178, Jan. 1999, doi: 10.1002/(SICI)1099-0755(199901/02)9:1<159::AID-AQC319>3.0.CO;2-M.
[58] A. Eisner, C. Young, M. Schneider, and I. Kopecki, “MesoCASiMiR: New

mapping method and comparison with other current approaches," in *Proceedings of final COST 626 meeting in Silkeborg*, 2005, pp. 65–95.

[59] P. Borsányi, K. Alfredsen, A. Harby, O. Ugedal, and C. Kraxner, "A Meso-scale Habitat Classification Method for Production Modelling of Atlantic Salmon in Norway," *Hydroécologie Appliquée*, vol. 14, pp. 119–138, 2004, doi: 10.1051/hydro:2004008.

[60] B. Belletti *et al.*, "Characterising physical habitats and fluvial hydromorphology: A new system for the survey and classification of river geomorphic units," *Geomorphology*, vol. 283, pp. 143–157, Apr. 2017, doi: 10.1016/j.geomorph.2017.01.032.

[61] M. Rinaldi, N. Surian, F. Comiti, and M. Bussettini, "IDRAIM – Sistema di valutazione idromorfologica, analisi e monitoraggio dei corsi d'acqua," 2016.

[62] D. Farò, K. Baumgartner, P. Vezza, and G. Zolezzi, "A novel unsupervised method for assessing mesoscale river habitat structure and suitability from 2D hydraulic models in gravel-bed rivers," *Ecohydrology*, vol. 15, no. 7, pp. 1–18, 2022, doi: 10.1002/eco.2452.

[63] P. Vezza, P. Parasiewicz, O. Calles, M. Spairani, and C. Comoglio, "Modelling habitat requirements of bullhead (Cottus gobio) in Alpine streams," *Aquat. Sci.*, vol. 76, no. 1, pp. 1–15, 2014, doi: 10.1007/s00027-013-0306-7.

[64] L. Breiman, "Random forests," *Mach. Learn.*, vol. 45, no. 1, pp. 5–32, Oct. 2001, doi: 10.1023/A:1010933404324.

[65] D. R. Cutler *et al.*, "Random Forests for classification in ecology," *Ecology*, vol. 88, no. 11, pp. 2783–2792, Nov. 2007, doi: 10.1890/07-0539.1.

[66] M. Adamczyk, P. Parasiewicz, P. Vezza, P. Prus, and G. De Cesare, "Empirical validation of MesoHABSIM models developed with different habitat suitability criteria for bullhead Cottus gobio L. as an indicator species," *Water (Switzerland)*, vol. 11, no. 4, p. 726, 2019, doi: 10.3390/w11040726.

[67] R. T. Milhous, *Reference manual for generation and analysis of habitat time series: Version II*, vol. 90. US Department of the Interior, Fish and Wildlife Service, 1990.

[68] P. Vezza *et al.*, "Habitat indices for rivers: Quantifying the impact of hydro-morphological alterations on the fish community," in *Engineering Geology for Society and Territory - Volume 3: River Basins, Reservoir Sedimentation and Water Resources*, 2015, pp. 357–360.

[69] A. H. Arthington and J. M. Zalucki, "Comparative evaluation of environmental flow assessment techniques: Review of methods," *LWRRDC Occas. Pap. Ser. 27/98*, p. 141, 1998.

[70] E. Vassoney, A. Mammoliti Mochet, E. Desiderio, G. Negro, M. G. Pilloni, and C. Comoglio, "Comparing Multi-Criteria Decision-Making Methods for the Assessment of Flow Release Scenarios From Small Hydropower Plants in the Alpine Area," *Front. Environ. Sci.*, vol. 9, p. 635100, Apr. 2021, doi: 10.3389/fenvs.2021.635100.

[71] V. Akstinas *et al.*, "The combined impact of hydropower plants and climate change on river runoff and fish habitats in lowland watersheds," *Water (Switzerland)*, vol. 13, no. 24, p. 3508, Dec. 2021, doi: 10.3390/w13243508.

[72] C. Magand, M. Helena Alves, E. Calleja, T. Datry, G. Dörflinger, and J. England, "Intermittent rivers and ephemeral streams: what water managers

need to know," 2020, doi: 10.5281/zenodo.3888474.
[73] F. Gallart *et al.*, "TREHS: An open-access software tool for investigating and evaluating temporary river regimes as a first step for their ecological status assessment," *Sci. Total Environ.*, vol. 607–608, pp. 519–540, Dec. 2017, doi: 10.1016/J.SCITOTENV.2017.06.209.
[74] M. L. Messager *et al.*, "Global prevalence of non-perennial rivers and streams," *Nature*, vol. 594, no. 7863, pp. 391–397, Jun. 2021, doi: 10.1038/s41586-021-03565-5.
[75] P. Döll and H. M. Schmied, "How is the impact of climate change on river flow regimes related to the impact on mean annual runoff? A global-scale analysis," *Environ. Res. Lett.*, vol. 7, no. 1, p. 014037, Mar. 2012, doi: 10.1088/1748-9326/7/1/014037.
[76] D. Pumo, D. Caracciolo, F. Viola, and L. V. Noto, "Climate change effects on the hydrological regime of small non-perennial river basins," *Sci. Total Environ.*, vol. 542, pp. 76–92, Jan. 2016, doi: 10.1016/J.SCITOTENV.2015.10.109.
[77] T. Datry, S. T. Larned, and K. Tockner, "Intermittent Rivers: A Challenge for Freshwater Ecology," *Bioscience*, vol. 64, no. 3, pp. 229–235, Mar. 2014, doi: 10.1093/BIOSCI/BIT027.
[78] L. Gruppuso *et al.*, "Flow Intermittency Affects Leaf Decomposition and Benthic Consumer Communities of Alpine Streams: A Case Study along the Po River," *Water (Switzerland)*, vol. 14, no. 2, p. 258, Jan. 2022, doi: 10.3390/W14020258/S1.
[79] D. C. Allen *et al.*, "River ecosystem conceptual models and non-perennial rivers: A critical review," *Wiley Interdiscip. Rev. Water*, vol. 7, no. 5, p. e1473, Sep. 2020, doi: 10.1002/wat2.1473.
[80] O. Llanos-Paez and V. Acuña, "Analysis of the socio-ecological drivers of the recreational use of temporary streams and rivers," *Sci. Total Environ.*, vol. 807, p. 150805, Feb. 2022, doi: 10.1016/j.scitotenv.2021.150805.
[81] M. Leone, F. Gentile, A. Lo Porto, G. F. Ricci, and A. M. De Girolamo, "Ecological flow in southern Europe: Status and trends in non-perennial rivers," *Journal of Environmental Management*, vol. 342. Academic Press, p. 118097, Sep. 15, 2023, doi: 10.1016/j.jenvman.2023.118097.
[82] Z. Wang and E. R. Vivoni, "Detecting Streamflow in Dryland Rivers Using CubeSats," *Geophys. Res. Lett.*, vol. 49, no. 15, pp. 1–10, 2022, doi: 10.1029/2022GL098729.
[83] O. T. McDonough, J. D. Hosen, and M. A. Palmer, "Temporary streams: the hydrology, geography, and ecology of non-perennially flowing waters," *River Ecosyst. Dyn. Manag. Conserv.*, pp. 259–290, 2011.
[84] P. Parasiewicz, "MesoHABSIM: A concept for application of instream flow models in river restoration planning," *Fisheries*, vol. 26, no. 9, pp. 6–13, Sep. 2001, doi: 10.1577/1548-8446(2001)026<0006:m>2.0.co;2.
[85] R. Muñoz-Mas, S. Fukuda, P. Vezza, and F. Martínez-Capel, "Comparing four methods for decision-tree induction: A case study on the invasive Iberian gudgeon (Gobio lozanoi; Doadrio and Madeira, 2004)," *Ecol. Inform.*, vol. 34, pp. 22–34, Jul. 2016, doi: 10.1016/j.ecoinf.2016.04.011.
[86] P. G. Bianco, "Mediterranean endemic freshwater fishes of Italy," *Biol. Conserv.*, vol. 72, no. 2, pp. 159–170, Jan. 1995, doi: 10.1016/0006-3207(94)00078-5.
[87] P. Gaudin, "Habitat shifts in juvenile riverine fishes," *River Syst.*, vol. 12, no. 2–4, pp. 393–408, Feb. 2001, doi: 10.1127/lr/12/2001/393.

[88] M. Kottelat and J. Freyhof, *Handbook of European freshwater fishes*. Cornol (CH): Publications Kottelat, 2007.

[89] L. Bernatchez, "The evolutionary history of brown trout (Salmo trutta L.) inferred from phylogeographic, nested clade, and mismatch analyses of mitochondrial DNA variation," *Evolution (N. Y).*, vol. 55, no. 2, pp. 351–379, 2001, doi: 10.1111/j.0014-3820.2001.tb01300.x.

[90] C. Hauer, M. Liedermann, and H. Habersack, "The application of hydrodynamic models as integrative tool between flood protection and ecological demands using a morphologically based evaluation method," 2006.

[91] P. Vezza, P. Parasiewicz, M. Spairani, and C. Comoglio, "Habitat modeling in high-gradient streams: The mesoscale approach and application," *Ecol. Appl.*, vol. 24, no. 4, pp. 844–861, 2014, doi: 10.1890/11-2066.1.

[92] M. R. Meador, J. P. McIntyre, and K. H. Pollock, "Assessing the Efficacy of Single-Pass Backpack Electrofishing to Characterize Fish Community Structure," *Trans. Am. Fish. Soc.*, vol. 132, no. 1, pp. 39–46, Jan. 2003, doi: 10.1577/1548-8659(2003)132<0039:ateosp>2.0.co;2.

[93] G. H. Copp, "Microhabitat use of fish larvae and 0+ juveniles in a highly regulated section of the River Great Ouse," *Regul. Rivers Res. Manag.*, vol. 13, no. 3, pp. 267–276, May 1997, doi: 10.1002/(SICI)1099-1646(199705)13:3<267::AID-RRR454>3.0.CO;2-B.

[94] N. Lamouroux, H. Capra, M. Pouilly, and Y. Souchon, "Fish habitat preferences in large streams of southern France," *Freshw. Biol.*, vol. 42, no. 4, pp. 673–687, Dec. 1999, doi: 10.1046/j.1365-2427.1999.00521.x.

[95] M. W. Hardisty, "The Life History and Growth of the Brook Lamprey (Lampetra planeri)," *J. Anim. Ecol.*, vol. 13, no. 2, p. 110, 1944, doi: 10.2307/1444.

[96] F. T. Vriese, S. Semmekrot, and A. J. P. Raat, "Assessment of spawning and nursery areas in the River Meuse," *Water Sci. Technol.*, vol. 29, no. 3, pp. 297–299, Feb. 1994, doi: 10.2166/wst.1994.0124.

[97] R. H. K. Mann, "Environmental requirements of European non-salmonid fish in rivers," *Hydrobiologia*, vol. 323, no. 3, pp. 223–235, 1996, doi: 10.1007/BF00007848.

[98] European Commission, "Biodiversity Strategy for 2030 - Bringing nature back into our lives," Brussels (BE), 2020.

[99] M. Klaar, G. H. Copp, and R. Horsfield, "Autumnal habitat use of non-native pumpkinseed Lepomis gibbosus and associations with native fish species in small English streams," *Folia Zool.*, vol. 53, no. 2, pp. 189–202, 2004.

[100] D. Giannetto, A. Carosi, L. Ghetti, G. Pedicillo, L. Pompei, and M. Lorenzoni, "Ecological traits of Squalius lucumoni s (Actinopterygii, Cyprinidae) and main differences with those of Squalius squalus in the Tiber River Basin (Italy)," *Knowl. Manag. Aquat. Ecosyst.*, vol. 409, p. 4, 2013, doi: 10.1051/kmae/2013049.

[101] P. Tutman, J. Dulčić, and B. Glamuzina, "First record of Po brook lamprey, Lethenteron zanandreai (Cephalaapidomorphi: Petromyzontiformes: Petromyzontidae), in the Hutovo Blato wetland, Bosnia and Herzegovina," *Acta Ichthyol. Piscat.*, vol. 39, no. 1, pp. 55–58, 2009.

[102] P. Tutman, J. Freyhof, J. Dulčić, B. Glamuzina, M. G.- Zootaxa, and U. 2017, "Lampetra soljani, a new brook lamprey from the southern Adriatic Sea basin (Petromyzontiformes: Petromyzontidae)," *Zootaxa*, vol. 4273, no.

4, pp. 531–548, 2017, doi: 10.11646/zootaxa.4273.4.4.
[103] J. Holcik and M. Mrakovčić, “First record of Lethenteron zanandreai (Cyclostoma, Petromyzontidae) in the Adriatic basin of the Balkan peninsula and its zoogeographic consequences,” *Folia Zool.*, vol. 46, no. 3, pp. 263–271, 1997.
[104] P. G. Bianco, “Lethenteron zanandreai (Vladikov,1955).,” in *The freshwater fishes of Europe, 1*, 1986, pp. 237–246.
[105] IUCN, “IUCN Red List of Threatened Species,” 2022. https://www.iucnredlist.org/ (accessed May 31, 2024).
[106] V. Caputo, M. Giovannotti, P. Nisi Cerioni, A. Splendiani, M. Marconi, and J. Tagliavini, “Mitochondrial DNA variation of an isolated population of the Adriatic brook lamprey Lampetra zanandreai (Agnatha: Petromyzontidae): phylogeographic and phylogenetic inferences,” *J. Fish Biol.*, vol. 75, no. 9, pp. 2344–2351, Dec. 2009, doi: 10.1111/J.1095-8649.2009.02413.X.
[107] G. Zanandrea, “Ulteriori rilievi biometrici su Lampetra zanandreai Vladykov,” *Ital. J. Zool.*, vol. 28, no. 2, pp. 703–715, Jan. 1961, doi: 10.1080/11250006109436447.
[108] G. Zanandrea, “Studies on European Lampreys,” *Evolution (N. Y).*, vol. 15, no. 4, p. 523, Dec. 1961, doi: 10.2307/2406320.
[109] G. Zanandrea, “Isolamento geografico della Lampreda di ruscello nella pianura padana,” *Ital. J. Zool.*, vol. 22, no. 2, pp. 191–196, Jan. 1955, doi: 10.1080/11250005509439198.
[110] G. Zanandrea, “Rapporti tra l’alto e il medio versante adriatico d’italis nella biogeografia delle lamprede,” *Ital. J. Zool.*, vol. 29, no. 2, pp. 727–734, 1962, doi: 10.1080/11250006209440656.
[111] G. Zanandrea, “Posizione sistematica e distribuzione geografica di Lampetra zanandreai Vladykov,” *Mem. del Mus. Civ. di Stor. Nat. di Verona*, vol. 6, pp. 207–237, 1958.
[112] G. Zanandrea, “Neotenia in Lampetra planeri zanandreai (Vladykov) e l’endocrinologia sperimentale dei Ciclostomi,” *Ital. J. Zool.*, vol. 23, no. 2, pp. 413–427, Jan. 1956, doi: 10.1080/11250005609439253.
[113] G. Zanandrea, “Le lamprede della pianura padana e del rimanente versante adriatico d’Italia,” *Ist. Poligr. dell o Stato*, 1965.
[114] B. Bertolini, “The structure of the liver cells during the life cycle of a brook-lamprey (Lampetra zanandreai),” *Zeitschrift für Zellforsch. und Mikroskopische Anat.*, vol. 67, no. 3, pp. 297–318, May 1965, doi: 10.1007/BF00339377/METRICS.
[115] V. Caputo, M. Giovannotti, P. N. Cerioni, A. Splendiani, J. Tagliavini, and E. Olmo, “Chromosomal study of a lamprey (Lampetra zanandreai Vladykov, 1955) (Petromyzonida: Petromyzontiformes): Conventional and FISH analysis,” *Chromosom. Res.*, vol. 19, no. 4, pp. 481–491, May 2011, doi: 10.1007/S10577-011-9197-4/FIGURES/3.
[116] J. Tagliavini, R. Tizzi, F. Conterio, P. Mariottini, and G. Gandolfi, “Mitochondrial DNA sequences in three genera of Italian lampreys,” *Ital. J. Zool.*, vol. 61, no. 4, pp. 331–333, 1994, doi: 10.1080/11250009409355903.
[117] S. Zerunian, *Pesci delle acque interne d’Italia*, vol. 20. Roma (IT): Ministero dell’ambiente e della tutela del territorio. Direzione conservazione della natura, 2004.
[118] C. Renaud, “Lampreys of the World: an Annotated and Illustrated Catalogue of Lamprey Species Known To Date,” *FAO Species Cat. Fish. Purp.*, vol. 5, no. 5, p. 118, 2011.

[119] B. Ahmadi-Nedushan, A. St-Hilaire, M. Bérubé, É. Robichaud, N. Thiémonge, and B. Bobée, "A review of statistical methods for the evaluation of aquatic habitat suitability for instream flow assessment," *River Res. Appl.*, vol. 22, no. 5, pp. 503–523, 2006, doi: 10.1002/rra.918.

[120] A. M. Mouton, J. D. Alcaraz-Hernández, B. De Baets, P. L. M. Goethals, and F. Martínez-Capel, "Data-driven fuzzy habitat suitability models for brown trout in Spanish Mediterranean rivers," *Environ. Model. Softw.*, vol. 26, no. 5, pp. 615–622, May 2011, doi: 10.1016/j.envsoft.2010.12.001.

[121] J. S. Evans, M. A. Murphy, Z. A. Holden, and S. A. Cushman, "Modeling species distribution and change using random forest," *Predict. Species Habitat Model. Landsc. Ecol. Concepts Appl.*, pp. 139–159, 2011, doi: 10.1007/978-1-4419-7390-0_8.

[122] L. Breiman, J. H. Friedman, R. A. Olshen, and C. J. Stone, *Classification and regression trees*. Routledge, 1984.

[123] L. Breiman, "Bagging predictors," *Mach. Learn.*, vol. 24, no. 2, pp. 123–140, 1996, doi: 10.1007/BF00058655/METRICS.

[124] T. Virbickas, P. Vezza, J. Kriaučiūnienė, V. Akstinas, D. Šarauskienė, and A. Steponėnas, "Impacts of low-head hydropower plants on cyprinid-dominated fish assemblages in Lithuanian rivers," *Sci. Rep.*, vol. 10, no. 1, pp. 1–14, Dec. 2020, doi: 10.1038/s41598-020-78701-8.

[125] V. D. Vladykov, "Lampetra zanandreai, a New Species of Lamprey from Northern Italy," *Copeia*, vol. 3, pp. 215–223, Aug. 1955, doi: 10.2307/1440464.

[126] A. Liaw and M. Wiener, "Classification and regression by randomForest," *R news*, vol. 2, no. 3, pp. 18–22, 2002, Accessed: May 30, 2024. [Online]. Available: https://journal.r-project.org/articles/RN-2002-022/RN-2002-022.pdf.

[127] R. Kohavi and G. H. John, "Wrappers for feature subset selection," *Artif. Intell.*, vol. 97, no. 1–2, pp. 273–324, Dec. 1997, doi: 10.1016/S0004-3702(97)00043-X.

[128] M. B. Kursa and W. R. Rudnicki, "Feature selection with the boruta package," *J. Stat. Softw.*, vol. 36, no. 11, pp. 1–13, Sep. 2010, doi: 10.18637/jss.v036.i11.

[129] J. S. Evans and S. A. Cushman, "Gradient modeling of conifer species using random forests," *Landsc. Ecol.*, vol. 24, no. 5, pp. 673–683, May 2009, doi: 10.1007/s10980-009-9341-0.

[130] P. Probst, M. N. Wright, and A. L. Boulesteix, "Hyperparameters and tuning strategies for random forest," *Wiley Interdiscip. Rev. Data Min. Knowl. Discov.*, vol. 9, no. 3, pp. 1–15, 2019, doi: 10.1002/widm.1301.

[131] O. Allouche, A. Tsoar, and R. Kadmon, "Assessing the accuracy of species distribution models: Prevalence, kappa and the true skill statistic (TSS)," *J. Appl. Ecol.*, vol. 43, no. 6, pp. 1223–1232, Dec. 2006, doi: 10.1111/j.1365-2664.2006.01214.x.

[132] J. B. Logue, C. T. Robinson, C. Meier, and J. R. Van Der Meer, "Relationship between sediment organic matter, bacteria composition, and the ecosystem metabolism of alpine streams," *Limnol. Oceanogr.*, vol. 49, no. 6, pp. 2001–2010, Nov. 2004, doi: 10.4319/LO.2004.49.6.2001.

[133] G. J. Holland, S. P. R. Greenstreet, I. M. Gibb, H. M. Fraser, and M. R. Robertson, "Identifying sandeel Ammodytes marinus sediment habitat preferences in the marine environment," *Mar. Ecol. Prog. Ser.*, vol. 303, pp.

269–282, Nov. 2005, doi: 10.3354/MEPS303269.
[134] C. E. Goodwin, J. T. A. Dick, D. L. Rogowski, and R. W. Elwood, “Lamprey (Lampetra fluviatilis and Lampetra planeri) ammocoete habitat associations at regional, catchment and microhabitat scales in Northern Ireland,” *Ecol. Freshw. Fish*, vol. 17, no. 4, pp. 542–553, Dec. 2008, doi: 10.1111/J.1600-0633.2008.00305.X.
[135] C. Taverny, G. Lassalle, I. Ortusi, C. Roqueplo, M. Lepage, and P. Lambert, “From shallow to deep waters: habitats used by larval lampreys (genus Petromyzon and Lampetra) over a western European basin,” *Ecol. Freshw. Fish*, vol. 21, no. 1, pp. 87–99, Jan. 2012, doi: 10.1111/J.1600-0633.2011.00526.X.
[136] E. Piano, A. Doretto, S. Mammola, E. Falasco, S. Fenoglio, and F. Bona, “Taxonomic and functional homogenisation of macroinvertebrate communities in recently intermittent Alpine watercourses,” *Freshw. Biol.*, vol. 65, no. 12, pp. 2096–2107, Dec. 2020, doi: 10.1111/FWB.13605.
[137] S. Guareschi, A. Laini, E. Racchetti, T. Bo, S. Fenoglio, and M. Bartoli, “How do hydromorphological constraints and regulated flows govern macroinvertebrate communities along an entire lowland river?,” *Ecohydrology*, vol. 7, no. 2, pp. 366–377, Apr. 2014, doi: 10.1002/ECO.1354.
[138] M. F. Willson, S. M. Gende, and B. H. Marston, “Fishes and the Forest: Expanding perspectives on fish-wildlife interactions,” *Bioscience*, vol. 48, no. 6, pp. 455–462, 1998.
[139] R. M. McDowall, “Why are so many boreal freshwater fishes anadromous? Confronting ‘conventional wisdom,’” *Fish Fish.*, vol. 9, no. 2, pp. 208–213, 2008, doi: 10.1111/j.1467-2979.2008.00271.x.
[140] P. R. Almeida *et al.*, “The decline of the ecosystem services generated by anadromous fish in the Iberian Peninsula,” *Hydrobiologia*, vol. 850, no. 12–13, pp. 2927–2961, 2023, doi: 10.1007/s10750-023-05179-6.
[141] M. F. Willson and K. C. Halupka, “Anadromous Fish as Keystone Species in Vertebrate Communities,” *Conserv. Biol.*, vol. 9, no. 3, pp. 489–497, 1995, doi: 10.1046/j.1523-1739.1995.09030489.x.
[142] M. H. Schiewe, “Salmon,” *Encycl. Biodivers. Second Ed.*, vol. 6, pp. 522–531, 2013, doi: 10.1016/B978-0-12-384719-5.00293-8.
[143] C. Seliger and B. Zeiringer, “River Connectivity, Habitat Fragmentation and Related Restoration Measures,” in *Riverine Ecosystem Management*, Springer International Publishing, 2018, pp. 171–186.
[144] P. J. T. M. van Puijenbroek, A. D. Buijse, M. H. S. Kraak, and P. F. M. Verdonschot, “Species and river specific effects of river fragmentation on European anadromous fish species,” *River Res. Appl.*, vol. 35, no. 1, pp. 68–77, 2019, doi: 10.1002/rra.3386.
[145] I. G. Jowett, “Instream flow methods: A comparison of approaches,” *Regul. Rivers Res. Manag.*, vol. 13, no. 2, pp. 115–127, 1997, doi: 10.1002/(SICI)1099-1646(199703)13:2<115::AID-RRR440>3.0.CO;2-6.
[146] M. W. Aprahamian, C. D. Aprahamian, J. L. Bagliniere, R. Sabatie, and P. Alexandrino, “Alosa alosa and Alosa fallax spp. Literature Review and Bibliography,” Bristol (UK), 2003.
[147] E. I. Kukuev and A. M. Orlov, “New Subspecies of Twaite Shad Alosa fallax balticus (Clupeidae),” *Inl. Water Biol.*, vol. 11, no. 4, pp. 407–416, 2018, doi: 10.1134/S1995082918040119.
[148] S. J. Sabatino, R. Faria, and P. B. Alexandrino, “Genetic structure, diversity,

and connectivity in anadromous and freshwater Alosa alosa and A. fallax," *Mar. Biol.*, vol. 169, no. 1, pp. 1–14, 2022, doi: 10.1007/s00227-021-03970-4.

[149] C. Rondinini, A. Battistoni, and C. Teofili, "Lista Rossa IUCN dei vertebrati italiani 2022," *Com. Ital. IUCN e Minist. dell'Ambiente e della Sicur. Energ. Roma, Italy*, 2022.

[150] P. G. Bianco, "The status of the twaite shad, Alosa agone, in Italy and the Western Balkans," *Mar. Ecol.*, vol. 23, no. SUPPL. 1, pp. 51–64, 2002, doi: 10.1111/j.1439-0485.2002.tb00007.x.

[151] D. Doherty, N. O'Maoiléidigh, and T. K. McCarthy, "The biology, ecology and future conservation of twaite shad (Alosa fallax lacépède), allis shad (Alosa alosa L.) and Killarney shad (Alosa fallax killarnensis tate regan) in Ireland," *Biol. Environ. Proc. R. Irish Acad.*, vol. 104, no. 3, pp. 93–102, 2004, doi: 10.3318/BIOE.2004.104.3.93.

[152] M. A. López *et al.*, "First characterization of the spawning habitat and mating behaviour of Twaite shad in the Ebro River (Western Mediterranean)," *J. Appl. Ichthyol.*, vol. 27, no. SUPPL. 3, pp. 53–55, 2011, doi: 10.1111/j.1439-0426.2011.01852.x.

[153] V. Magath and R. Thiel, "Stock recovery, spawning period and spawning area expansion of the twaite shad Alosa fallax in the Elbe estuary, southern North Sea," *Endanger. Species Res.*, vol. 20, no. 2, pp. 109–119, 2013, doi: 10.3354/esr00490.

[154] Y. L. Manyukas, "Biology of the Atlantic shad, Alosa fallax fallax," *J. Ichthyol.*, vol. 29, pp. 125–128, 1989.

[155] J. P. Quignard and C. L. Douchement, "Alosa fallax fallax (Lacépède, 1803)," in *The freshwater fishes of Europe, 2*, 1991, pp. 225–253.

[156] M. W. Aprahamian, J. L. Baglinière, M. R. Sabatié, P. Alexandrino, R. Thiel, and C. D. Aprahamian, "Biology, status, and conservation of the anadromous Atlantic twaite shad Alosa fallax fallax," *Am. Fish. Soc. Symp.*, vol. 2003, no. 35, pp. 103–124, 2003.

[157] P. A. Caswell and M. W. Aprahamian, "Use of river habitat survey to determine the spawning habitat characteristics of twaite shad (alosa fallax fallax)," *BFPP - Bull. Fr. la Pech. la Prot. des Milieux Aquat.*, no. 362–363, pp. 919–929, 2001, doi: 10.1051/kmae:2001027.

[158] M. A. López, N. Gázquez, J. M. Olmo-Vidal, M. W. Aprahamian, and E. Gisbert, "The presence of anadromous twaite shad (Alosa fallax) in the Ebro River (western Mediterranean, Spain): An indicator of the population's recovery?," *J. Appl. Ichthyol.*, vol. 23, no. 2, pp. 163–166, Apr. 2007, doi: 10.1111/j.1439-0426.2006.00797.x.

[159] L. Ziliani and N. Surian, "Evolutionary trajectory of channel morphology and controlling factors in a large gravel-bed river," *Geomorphology*, vol. 173–174, pp. 104–117, 2012, doi: 10.1016/j.geomorph.2012.06.001.

[160] L. Ziliani and N. Surian, "Reconstructing temporal changes and prediction of channel evolution in a large Alpine river: the Tagliamento river, Italy," *Aquat. Sci.*, vol. 78, no. 1, pp. 83–94, 2016, doi: 10.1007/s00027-015-0431-6.

[161] W. Bertoldi *et al.*, "Understanding reference processes: linkages between river flows, sediment dynamics and vegetated landforms along the Tagliamento River, Italy," *River Res. Appl.*, vol. 25, no. 5, pp. 501–516, 2009.

[162] D. Rapti-Caputo and C. Vaccaro, “Deep alluvial aquifer system: An example from the Tagliamento River hydrogeological basin (NE Italy),” *Boll. di Geofis. Teor. ed Appl.*, vol. 50, no. 1, pp. 39–50, 2009.
[163] R. D. Williams, J. Brasington, M. Hicks, R. Measures, C. D. Rennie, and D. Vericat, “Hydraulic validation of two-dimensional simulations of braided river flow with spatially continuous aDcp data,” *Water Resour. Res.*, vol. 49, no. 9, pp. 5183–5205, 2013, doi: 10.1002/wrcr.20391.
[164] G. B. Pasternack, C. L. Wang, and J. E. Merz, “Application of a 2D hydrodynamic model to design of reach-scale spawning gravel replenishment on the Mokelumne River, California,” *River Res. Appl.*, vol. 20, no. 2, pp. 205–225, 2004, doi: 10.1002/rra.748.
[165] M. Muste, D. Kim, and V. Merwade, “Modern Digital Instruments and Techniques for Hydrodynamic and Morphologic Characterization of River Channels,” *Gravel-Bed Rivers Process. Tools, Environ.*, pp. 315–341, Feb. 2012, doi: 10.1002/9781119952497.CH24.
[166] A. S. Woodget, P. E. Carbonneau, F. Visser, and I. P. Maddock, “Quantifying submerged fluvial topography using hyperspatial resolution UAS imagery and structure from motion photogrammetry,” *Earth Surf. Process. Landforms*, vol. 40, no. 1, pp. 47–64, 2015, doi: 10.1002/esp.3613.
[167] C. A. Puig-Mengual, A. S. Woodget, R. Muñoz-Mas, and F. Martínez-Capel, “Spatial validation of submerged fluvial topographic models by mesohabitat units,” *Int. J. Remote Sens.*, vol. 42, no. 7, pp. 2391–2416, 2021, doi: 10.1080/01431161.2020.1862433.
[168] J. T. Dietrich, “Bathymetric Structure-from-Motion: extracting shallow stream bathymetry from multi-view stereo photogrammetry,” *Earth Surf. Process. Landforms*, vol. 42, no. 2, pp. 355–364, 2017, doi: 10.1002/esp.4060.
[169] A. M. Lingua, P. Maschio, A. Spadaro, P. Vezza, and G. Negro, “Iterative refraction-correction method on MVS-SfM for shallow stream bathymetry,” *Int. Arch. Photogramm. Remote Sens. Spat. Inf. Sci.*, vol. 48, no. 1/W1-2023, pp. 249–255, May 2023, doi: 10.5194/ISPRS-ARCHIVES-XLVIII-1-W1-2023-249-2023.
[170] G. Tewinkel, “Water depths from aerial photographs.,” *Photogramm. Eng.*, vol. 29, no. 6, pp. 1421–1428, 1963.
[171] I. G. Yudha Partama, A. Kanno, Y. Akamatsu, R. Inui, and M. Goto, M, Sekine, “A Simple and Empirical Refraction Correction Method for UAV-Based Shallow-Water Photogrammetry,” *Int. J. Sch. Sci. Res. Innov.*, vol. 11, no. 4, pp. 254–261, 2017.
[172] P. Vezza, L. Astegiano, S. Fukuda, A. Lingua, C. Comoglio, and G. Palau-Salvador, “Using structure from motion techniques to describe and evaluate instream physical habitat,” 2016.
[173] A. P. Nicholas, “Investigation of spatially distributed braided river flows using a two-dimensional hydraulic model,” *Earth Surf. Process. Landforms*, vol. 28, no. 6, pp. 655–674, 2003, doi: 10.1002/esp.491.
[174] S. Chang and X. Wang, “Courant Number Insensitive CE/SE Euler Scheme,” *38th AIAA/ASME/SAE/ASEE Jt. Propuls. Conf. & Exhib.*, Jul. 2002, doi: 10.2514/6.2002-3890.
[175] N. W. Pankhurst and P. L. Munday, “Effects of climate change on fish reproduction and early life history stages,” *Mar. Freshw. Res.*, vol. 62, no. 9, pp. 1015–1026, 2011, doi: 10.1071/MF10269.
[176] R. W. Herschy, “Streamflow measurement: Third edition,” *Streamflow*

Meas. Third Ed., pp. 1–507, Jan. 2008.
[177] J. D. Fenton, "On the generation of stream rating curves," *J. Hydrol.*, vol. 564, pp. 748–757, 2018, doi: 10.1016/j.jhydrol.2018.07.025.
[178] N. V. Chawla, K. W. Bowyer, L. O. Hall, and W. P. Kegelmeyer, "SMOTE: Synthetic Minority Over-sampling Technique," *J. Artif. Intell. Res.*, vol. 16, pp. 321–357, Jun. 2002, doi: 10.1613/JAIR.953.
[179] P. Probst, M. N. Wright, and A. L. Boulesteix, "To tune or not to tune the number of trees in random forest," *J. Mach. Learn. Res.*, vol. 18, pp. 1–8, 2018.
[180] G. B. Pasternack, *2D modeling and ecohydraulic analysis*. University of California at Davis, 2011.
[181] P. Agrafiotis, D. Skarlatos, A. Georgopoulos, and K. Karantzalos, "DepthLearn: Learning to correct the refraction on point clouds derived from aerial imagery for accurate dense shallow water bathymetry based on SVMs-fusion with LiDAR point clouds," *Remote Sens.*, vol. 11, no. 19, 2019, doi: 10.3390/rs11192225.
[182] R. J. Wootton and C. Smith, *Reproductive Biology of Teleost Fishes*. Wiley Blackwell, 2014.
[183] A. Paumier, H. Drouineau, S. Boutry, N. Sillero, and P. Lambert, "Assessing the relative importance of temperature, discharge, and day length on the reproduction of an anadromous fish (Alosa alosa)," *Freshw. Biol.*, vol. 65, no. 2, pp. 253–263, 2020, doi: 10.1111/fwb.13418.
[184] O. Vigiak, A. Pistocchi, A. Aloe, and R. Ludwig, "Empirical modelling of river water temperature in water scarce European basins," *Proc. - 22nd Int. Congr. Model. Simulation, MODSIM 2017*, no. December, pp. 880–886, 2017, doi: 10.36334/modsim.2017.g4.vigiak.
[185] M. M. Qader Mirza, "The choice of stage-discharge relationship for the ganges and Brahmaputra rivers in Bangladesh," *Nord. Hydrol.*, vol. 34, no. 4, pp. 321–342, 2003, doi: 10.2166/nh.2003.0010.
[186] D. Bonaldo *et al.*, "The summer 2022 drought: a taste of future climate for the Po valley (Italy)?," *Reg. Environ. Chang.*, vol. 23, no. 1, pp. 1–6, 2023, doi: 10.1007/s10113-022-02004-z.
[187] M. C. Langkau, D. Clavé, M. B. Schmidt, and J. Borcherding, "Spawning behaviour of Allis shad Alosa alosa: New insights based on imaging sonar data," *J. Fish Biol.*, vol. 88, no. 6, pp. 2263–2274, 2016, doi: 10.1111/jfb.12978.
[188] M. Šmejkal *et al.*, "Nocturnal spawning as a way to avoid egg exposure to diurnal predators," *Sci. Rep.*, vol. 8, no. 1, pp. 1–7, 2018, doi: 10.1038/s41598-018-33615-4.
[189] R. Muñoz-Mas, P. Vezza, J. D. Alcaraz-Hernández, and F. Martínez-Capel, "Risk of invasion predicted with support vector machines: A case study on northern pike (Esox Lucius, L.) and bleak (Alburnus alburnus, L.)," *Ecol. Modell.*, vol. 342, pp. 123–134, Dec. 2016, doi: 10.1016/j.ecolmodel.2016.10.006.
[190] J. G. Williams, T. P. Speed, and W. F. Forrest, "Comment: Transferability of Habitat Suitability Criteria," *North Am. J. Fish. Manag.*, vol. 19, no. 2, pp. 623–625, 1999, doi: 10.1577/1548-8675(1999)019<0623:ctohsc>2.0.co;2.
[191] M. A. Bozek and F. J. Rahel, "Generality of microhabitat suitability models for young Colorado River cutthroat trout (Oncorhynchus clarki pleuriticus)

across sites and among years in Wyoming streams," *Can. J. Fish. Aquat. Sci.*, vol. 49, no. 3, pp. 552–564, 1992, doi: 10.1139/f92-065.
[192] S. Allouche, "Nature and functions of cover for riverine fish," *BFPP - Bull. Fr. la Pech. la Prot. des Milieux Aquat.*, vol. 366, no. 365–366, pp. 297–324, 2002, doi: 10.1051/kmae:2002037.
[193] B. Gumiero, B. Maiolini, F. Comiti, and F. Moroni, "The Italian rivers," in *Rivers of Europe*, Elsevier, 2022, pp. 655–683.
[194] P. Berrebi, M. Povz, D. Jesensek, G. Cattaneo-Berrebi, and A. J. Crivelli, "The genetic diversity of native, stocked and hybrid populations of marble trout in the Soca river, Slovenia," *Heredity (Edinb).*, vol. 85, no. 3, pp. 277–287, Sep. 2000, doi: 10.1046/j.1365-2540.2000.00753.x.
[195] European Union, "Directive 2000/60/EC of the European Parliament and of the Council of 23 October 2000 establishing a framework for Community action in the field of water policy," vol. 327. pp. 1–73, 2000.
[196] W. van de Bund, "Water Framework Directive intercalibration technical report. Part I: Rivers," 2009.
[197] T. H. Snelder *et al.*, "Regionalization of patterns of flow intermittence from gauging station records," *Hydrol. Earth Syst. Sci.*, vol. 17, no. 7, pp. 2685–2699, 2013, doi: 10.5194/HESS-17-2685-2013.
[198] A. Munné and N. Prat, "Defining river types in a Mediterranean area: a methodology for the implementation of the EU Water Framework Directive," *Environ. Manage.*, vol. 34, no. 5, pp. 711–729, Nov. 2004, doi: 10.1007/S00267-003-0098-Y.
[199] O. Oueslati, A. M. De Girolamo, A. Abouabdillah, T. R. Kjeldsen, and A. Lo Porto, "Classifying the flow regimes of Mediterranean streams using multivariate analysis," *Hydrol. Process.*, vol. 29, no. 22, pp. 4666–4682, Oct. 2015, doi: 10.1002/hyp.10530.
[200] A. M. De Girolamo, E. Barca, G. Pappagallo, and A. Lo Porto, "Simulating ecologically relevant hydrological indicators in a temporary river system," *Agric. Water Manag.*, vol. 180, pp. 194–204, 2017.
[201] C. A. Krabbenhoft *et al.*, "Assessing placement bias of the global river gauge network," *Nat. Sustain.*, vol. 5, no. 7, pp. 586–592, 2022.
[202] A. M. De Girolamo and A. Lo Porto, "Land use scenario development as a tool for watershed management within the Rio Mannu Basin," *Land use policy*, vol. 29, no. 3, pp. 691–701, 2012.
[203] M. Sivapalan, "Prediction in ungauged basins: a grand challenge for theoretical hydrology.," *Hydrol. Process.*, vol. 17, pp. 3163–3170, 2003, doi: https://doi.org/10.1002/hyp.5155.
[204] M. J. Kirkby *et al.*, "Classifying low flow hydrological regimes at a regional scale," *Hydrol. Earth Syst. Sci.*, vol. 15, no. 12, pp. 3741–3750, 2011.
[205] M. A. Zimmer *et al.*, "Zero or not? Causes and consequences of zero-flow stream gage readings," *Wiley Interdiscip. Rev. Water*, vol. 7, no. 3, p. e1436, 2020.
[206] H. Jiang, M. Feng, Y. Zhu, N. Lu, J. Huang, and T. Xiao, "An automated method for extracting rivers and lakes from Landsat imagery," *Remote Sens.*, vol. 6, no. 6, pp. 5067–5089, 2014.
[207] C. Cavallo, M. Nones, M. N. Papa, M. Gargiulo, and G. Ruello, "Monitoring the morphological evolution of a reach of the Italian Po River using multispectral satellite imagery and stage data," *Geocarto Int.*, vol. 37, no. 25, pp. 8579–8601, 2022.
[208] P. E. Carbonneau *et al.*, "UAV-based training for fully fuzzy classification

of Sentinel-2 fluvial scenes," *Earth Surf. Process. landforms*, vol. 45, no. 13, pp. 3120–3140, 2020.

[209] D. Seaton, T. Dube, and D. Mazvimavi, "Use of multi-temporal satellite data for monitoring pool surface areas occurring in non-perennial rivers in semi-arid environments of the Western Cape, South Africa," *ISPRS J. Photogramm. Remote Sens.*, vol. 167, pp. 375–384, 2020.

[210] J. Hou, A. I. J. M. Van Dijk, L. J. Renzullo, R. A. Vertessy, and N. Mueller, "Hydromorphological attributes for all Australian river reaches derived from Landsat dynamic inundation remote sensing," *Earth Syst. Sci. Data*, vol. 11, no. 3, pp. 1003–1015, 2019.

[211] N. Santangelo, A. Santo, D. Guida, R. Lanzara, and V. Siervo, "The geosites of the Cilento-Vallo di Diano national park (Campania region, southern Italy)," *Quat*, vol. 18, pp. 101–112, 2005.

[212] A. Longobardi, O. Boulariah, and P. Villani, "Assessment of centennial (1918–2019) drought features in the Campania region by historical in situ measurements (southern Italy)," *Nat. Hazards Earth Syst. Sci.*, vol. 21, no. 7, pp. 2181–2196, 2021.

[213] D. Gilvear and R. Bryant, "Analysis of remotely sensed data for fluvial geomorphology and river science," *Tools Fluv. Geomorphol.*, pp. 103–132, 2016.

[214] R. J. Boothroyd, R. D. Williams, T. B. Hoey, B. Barrett, and O. A. Prasojo, "Applications of Google Earth Engine in fluvial geomorphology for detecting river channel change," *Wiley Interdiscip. Rev. Water*, vol. 8, no. 1, p. e21496, 2021.

[215] C. Cavallo, M. N. Papa, M. Gargiulo, G. Palau-Salvador, P. Vezza, and G. Ruello, "Continuous monitoring of the flooding dynamics in the Albufera Wetland (Spain) by Landsat-8 and Sentinel-2 datasets," *Remote Sens.*, vol. 13, no. 17, p. 3525, 2021.

[216] N. Gorelick, M. Hancher, M. Dixon, S. Ilyushchenko, D. Thau, and R. Moore, "Google Earth Engine: Planetary-scale geospatial analysis for everyone," *Remote Sens. Environ.*, vol. 202, pp. 18–27, 2017.

[217] W. L. Balsam, B. C. Deaton, and J. E. Damuth, "The effects of water content on diffuse reflectance spectrophotometry studies of deep-sea sediment cores," *Mar. Geol.*, vol. 149, no. 1–4, pp. 177–189, 1998.

[218] N. Prat *et al.*, "The mirage toolbox: an integrated assessment tool for temporary streams," *River Res. Appl.*, vol. 30, no. 10, pp. 1318–1334, 2014.

[219] A. H. Arthington, J. M. Bernardo, and M. Ilhéu, "Temporary rivers: Linking ecohydrology, ecological quality and reconciliation ecology," *River Res. Appl.*, vol. 30, no. 10, pp. 1209–1215, Dec. 2014, doi: 10.1002/rra.2831.

[220] A. Anna, C. Yorgos, P. Konstantinos, and L. Maria, "Do intermittent and ephemeral mediterranean rivers belong to the same river type?," *Aquat. Ecol.*, vol. 43, no. 2, pp. 465–476, 2009, doi: 10.1007/s10452-008-9176-9.

[221] T. Datry *et al.*, "Science and Management of Intermittent Rivers and Ephemeral Streams (SMIRES)," *Res. Ideas Outcomes*, vol. 3, p. e21774, 2017, doi: 10.3897/rio.3.e21774.

[222] S. T. Larned, T. Datry, D. B. Arscott, and K. Tockner, "Emerging concepts in temporary-river ecology," *Freshw. Biol.*, vol. 55, no. 4, pp. 717–738, 2010, doi: 10.1111/j.1365-2427.2009.02322.x.

[223] N. T. Skoulikidis *et al.*, "Non-perennial Mediterranean rivers in Europe: Status, pressures, and challenges for research and management," *Sci. Total*

Environ., vol. 577, pp. 1–18, 2017, doi: 10.1016/j.scitotenv.2016.10.147.
[224] Q. Wu, "geemap: A Python package for interactive mapping with Google Earth Engine," *J. Open Source Softw.*, vol. 5, no. 51, p. 2305, 2020.
[225] V. te Chow, "Open-Channel Hydraulics, Classical Textbook Reissue." MC Graw Hill Seattle, WA, 1988.
[226] M. Lugli, L. Bobbio, P. Torricelli, and G. Gandolfi, "Breeding ecology and male spawning success in two hill-stream populations of the freshwater goby, Padogobius martensi," *Environ. Biol. Fishes*, vol. 35, no. 1, pp. 37–48, Sep. 1992, doi: 10.1007/BF00001156.
[227] A. Kerezsy, K. Gido, M. F. Magalhães, and P. H. Skelton, *The Biota of Intermittent Rivers and Ephemeral Streams: Fishes*. Elsevier Inc., 2017.

Appendix A

Appendix A. General Appendix

A.1 Physical habitat attributes of the MesoHABSIM model

Table A-1. The physical habitat attributes of the MesoHABSIM model used for the geomorphic units (GUs) description in Chapter 2, 3, 4, 5, and 7. In cyan are highlighted the 44 predictors taken into account in Chapter 3 and 4 for the development of Habitat Suitability Criteria (HSC) using the classification Random Forest (RF) algorithm. The same habitat attributes are considered to establish the rank of suitability (not suitable/suitable/optimal) of each GUs for quantifying the available habitat for target species in Chapter 2, 5, and 7.

Habitat attribute	Units	Number of Categories	Categories /Description
Geomorphic units (GUs)	yes/no	17	pothole, cascade, rapid, riffle, step, pool, glide, dune, aquatic vegetation, secondary channel, flood lake, wetland, artificial element, waterfall, plunge pool, backwater, rock glide
GU gradient	%	1	water surface mean gradient of the GU
GU longitudinal connectivity	yes/no	1	habitat binary attribute describing mesohabitats longitudinal river connectivity
Depth	percentage of random samples	9	0-0.15, 0.15-0.30, 0.30-0.45, 0.45-0.60, 0.60-0.75, 0.75-0.90, 0.90-1.05, 1.05-1.20, > 1.20 cm
Velocity	percentage of random samples	9	0-0.15, 0.15-0.30, 0.30-0.45, 0.45-0.60, 0.60-0.75, 0.75-0.90, 0.90-1.05, 1.05-1.20, > 1.20 cm/s
Substrate	percentage of random samples	12	*gigalithal* (GI), *megalithal* (ME), *macrolithal* (MA), *mesolithal* (MS), *microlithal* (MI), *akal* (AK), *psammal* (PS), *pelal* (PE), *detritus* (DE), *xylal* (XY), *sapropel* (SA), *phytal* (PH)
Cover	yes/no	11	boulder (BD), canopy shading (CS), overhanging vegetation (OV), roots (RO), submerged vegetation (SV), floating vegetation (FV), emerging vegetation (EV), undercut bank (UB), woody debris (WD), riprap (RI), shallow margins (SM)

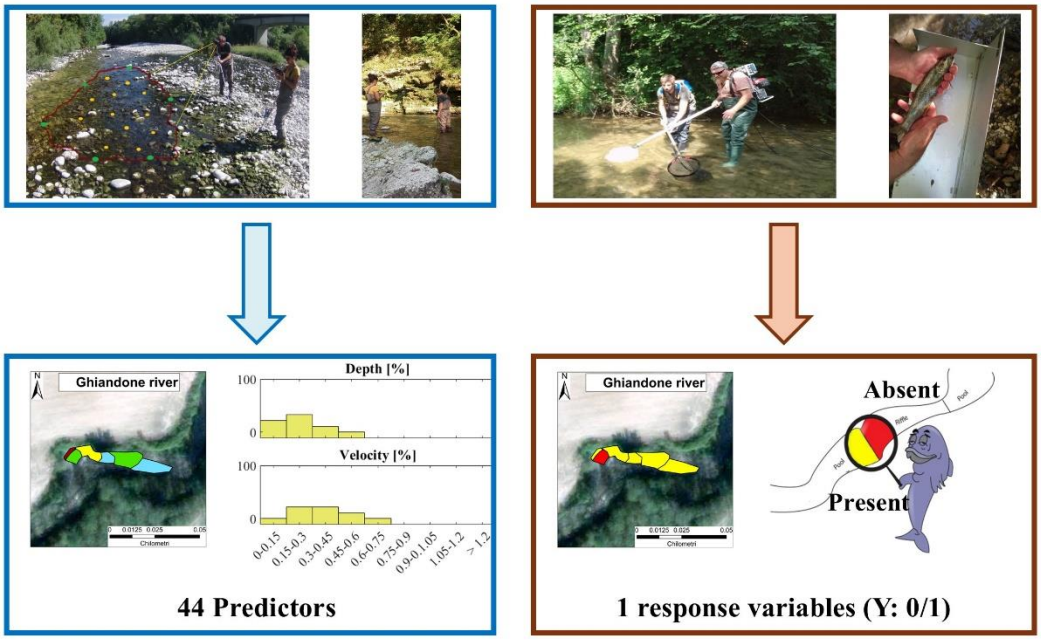
Froude number	(velocity)/ $(9.81*depth)^{0.5}$		average over the GU area
Flow velocity standard deviation	cm/s	1	SD over GU area

A.2 Workflow for the development of Habitat suitability Criteria with the Random Forest classification algorithm:

Figure A.1. The workflow followed in Chapter **3** and **4** for the development of Habitat Suitability Criteria (HSC) using the classification Random Forest (RF) algorithm. a) Hydro-morphological characterization of the riverine habitat. Each Geomorphic Unit (GU) serves as a sample for training the trees of the forest. The habitat attributes (see **Table A-1** for details) collected for each GU, organized into 44 categories, are used as predictors to define the models. b) Species distribution is assessed for each GU and represent the observations (Y). c) RF model predictions yield a probability of presence based on majority voting among the decision trees in the forest; if this probability exceeds 50%, the GU is classified as suitable (1) for the species. If not, the GU is classified as not suitable (0). Model performances are than evaluated using the statistical metrics reported in **A.3**. d) A representation of the input table, characterized by 44 predictors and 1 response variable (fish: absent, 0/present, 1), used for the RF models definition. The codes used for the habitat attributes are listed in **Table A-1**.

a) Hydro- morphological characterization

b) Species distribution assessment



c) Classification Random Forest model

Model performances		Y = 1	Y = 0
RF	1	TP	FP
	0	FN	TN

d) Random Forest model input table

Samples	HMU NUM	HMU TYPE	GU gradient	GU connectivity	DEPTH [%]	VELOCITY [%]	SUBSTRATE [%]	COVERS [0/1]	FROUDE NUM	VELOCITY SD	Y [0/1]
	1	GLIDE	…	…	…	…	…	…	…	…	0
	2	POOL	…	…	…	…	…	…	…	…	1
	3	RAPID	…	…	…	…	…	…	…	…	0
	4	BACKWATER	…	…	…	…	…	…	…	…	0
	…	…	…	…	…	…	…	…	…	…	…
	n	RIFFLE	…	…	…	…	…	…	…	…	1

0-0.15	0.15-0.3	0.3-0.45	0.45-0.6	0.6-0.75	0.75-0.9	0.9-1.05	1.05-1.2	>1.2

0-0.15	0.15-0.3	0.3-0.45	0.45-0.6	0.6-0.75	0.75-0.9	0.9-1.05	1.05-1.2	>1.2

GI	ME	MA	MS	MI	AK	PS	PE	DE	XY	SA	PH

BD	CS	OV	RO	SV	FV	EV	UB	WD	RI	SM

A.3 Metrics for assessing Habitat Suitability Criteria performances:

- **Accuracy:**

$$Accuracy = \frac{TP+TN}{N} \qquad (3)$$

- **Sensitivity:**

$$Sensitivity = \frac{TP}{TP+TN} \qquad (4)$$

- **Specificity:**

$$Specificity = \frac{TN}{TN+FN} \qquad (5)$$

- **True Skill Statistic (TSS):**

$$TSS = Sensitivity + Specificity - 1 \qquad (6)$$

Where *TP* represents the true positives; *FP* the false positives; *FN* the false negatives; *TN* the true negatives; and *N* the total sample size (sum of *TP*, *FP*, *FN*, and *TN*).

A.4 The Random Forest models considered in Chapter 5 and 7.

In Chapter 5 and 7 the following Random Forest models, presented in terms of partial dependence plots, were considered. These HSC were previously developed using field data collected over several years in reference sites within the Italian Alps (see references [21] and [63]), and are available to users of the SimStream-Web service for the application of the MesoHABSIM approach in Italy.

For Chapter 5, in which the transferability of 5 models was tested, exclusively the absence/presence HSC were considered. For Chapter 7, both absence/presence and presence/abundance HSC were applied to quantify habitat availability in the Sangone river.

- **Adult Brow trout (*Salmo trutta*) – Chapter 5:**

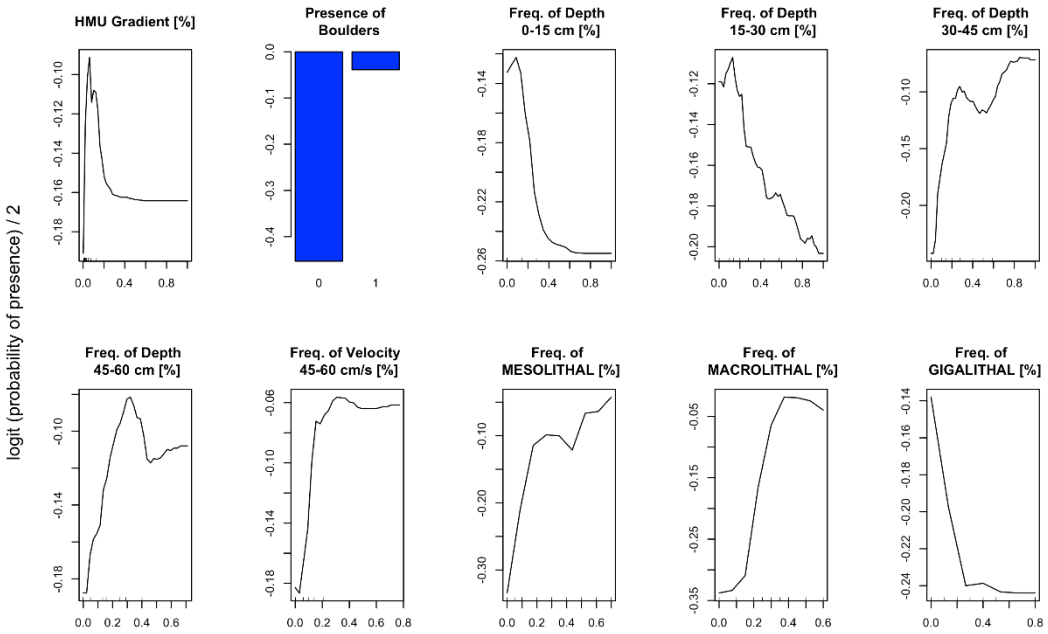


Figure A.2. The absence/presence Random Forest model of adult Brown trout (*Salmo trutta*) available in SimStream-Web (https://mesohabsim.isprambiente.it/app/home/).

- **Adult Marble trout (*Salmo marmoratus*) – Chapter 5:**

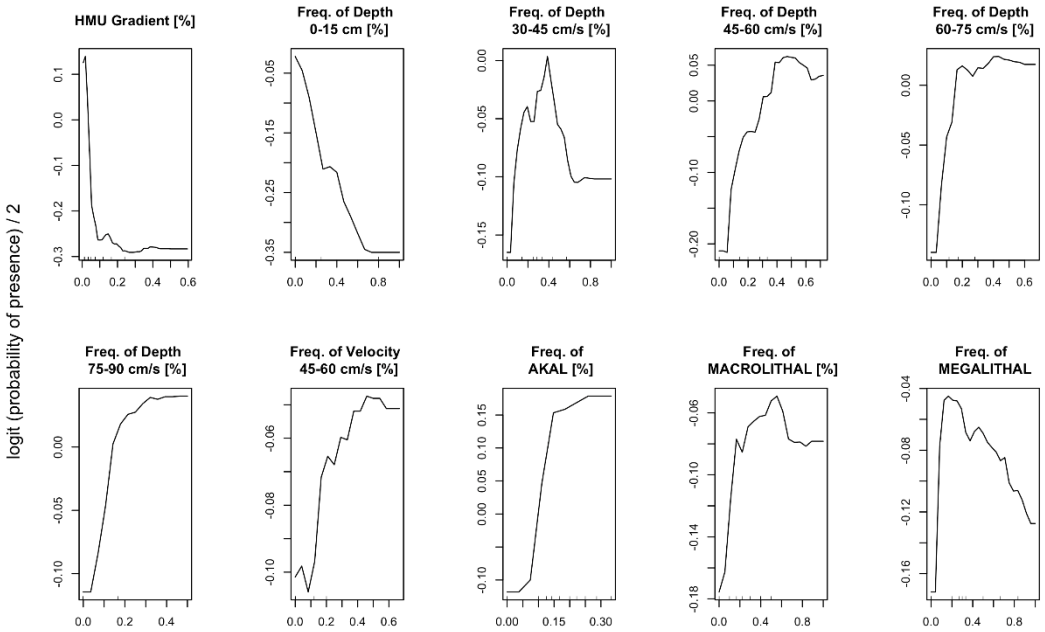


Figure A.3. The absence/presence Random Forest model of adult Marble trout (*Salmo marmoratus*) available in SimStream-Web (https://mesohabsim.isprambiente.it/app/home/).

- **Juvenile trout (*Salmo trutta/marmoratus*) – Chapter 5:**

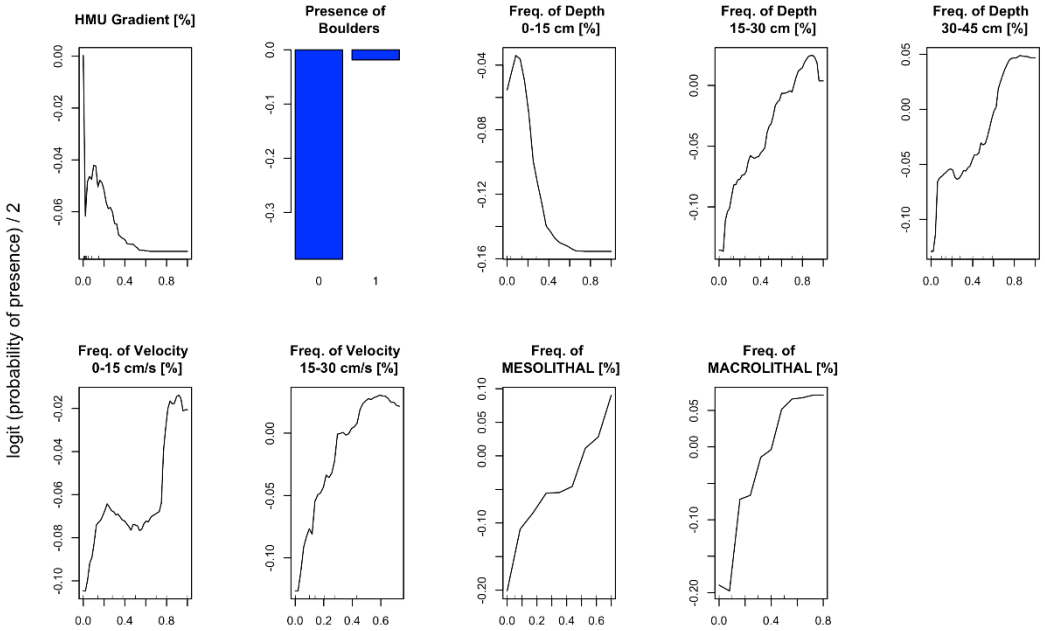


Figure A.4. The absence/presence Random Forest model of juvenile trout (*Salmo trutta/marmoratus*) available in SimStream-Web (https://mesohabsim.isprambiente.it/app/home/).

- **Adult Bullhead (*Cottus gobio*) – Chapter 5:**

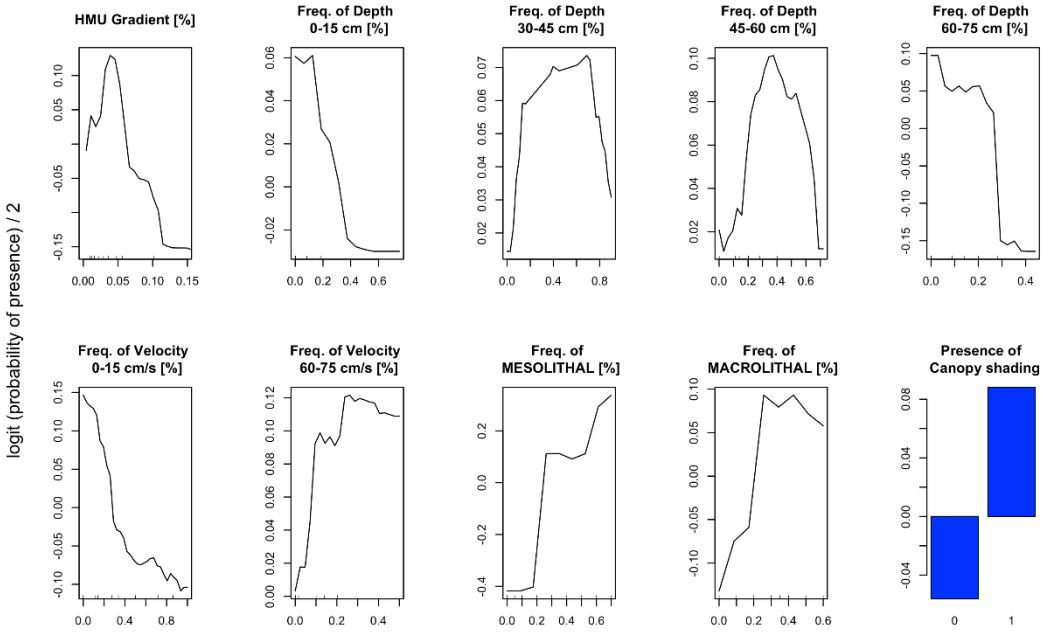


Figure A.5. The absence/presence Random Forest model of adult Bullhead (*Cottus gobio*) available in SimStream-Web (https://mesohabsim.isprambiente.it/app/home/).

- **Adult Italian barbel (*Barbus plebejus*) – Chapter 5:**

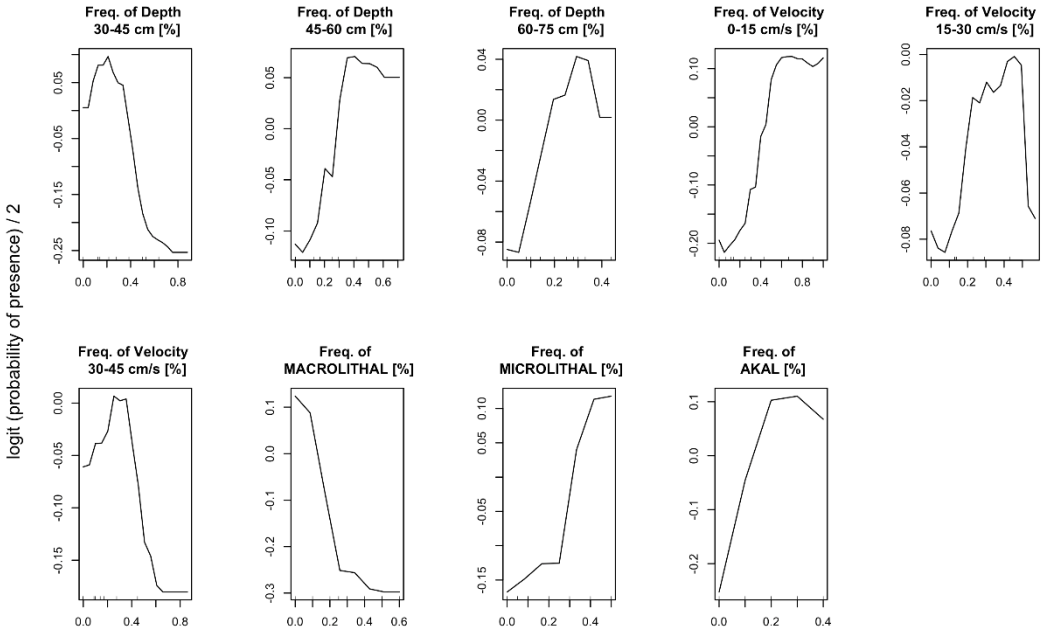


Figure A.6. The absence/presence Random Forest model of adult Italian barbel (*Barbus plebejus*) available in SimStream-Web (https://mesohabsim.isprambiente.it/app/home/).

- **Adult Italian vairone (*Telestes muticellus*) – Chapter 5 and 7:**

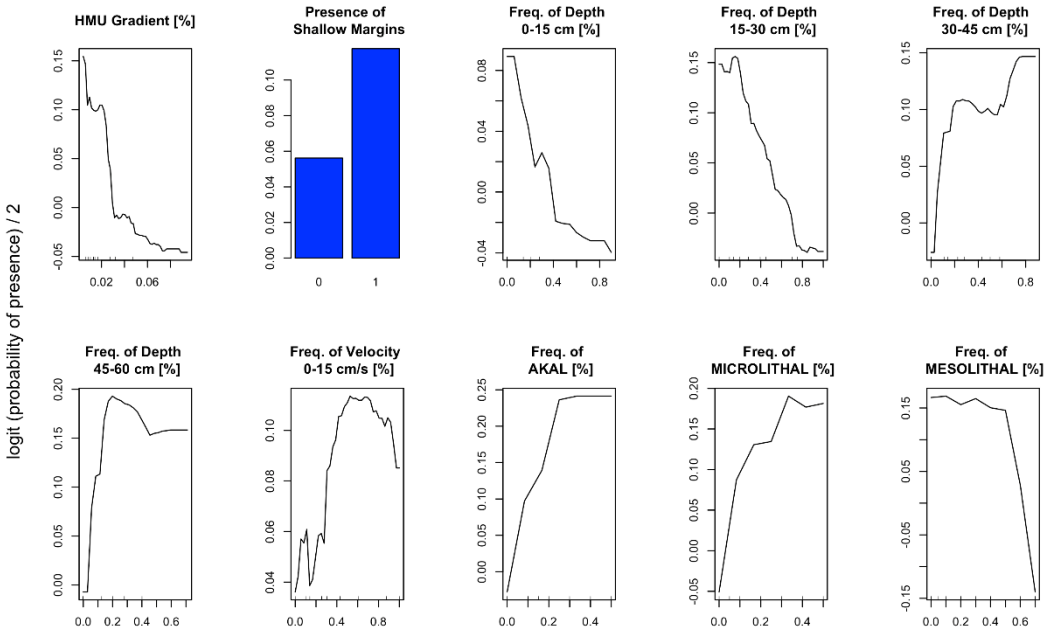


Figure A.7. The absence/presence Random Forest model of adult Italian vairone (*Telestes muticellus*) available in SimStream-Web (https://mesohabsim.isprambiente.it/app/home/).

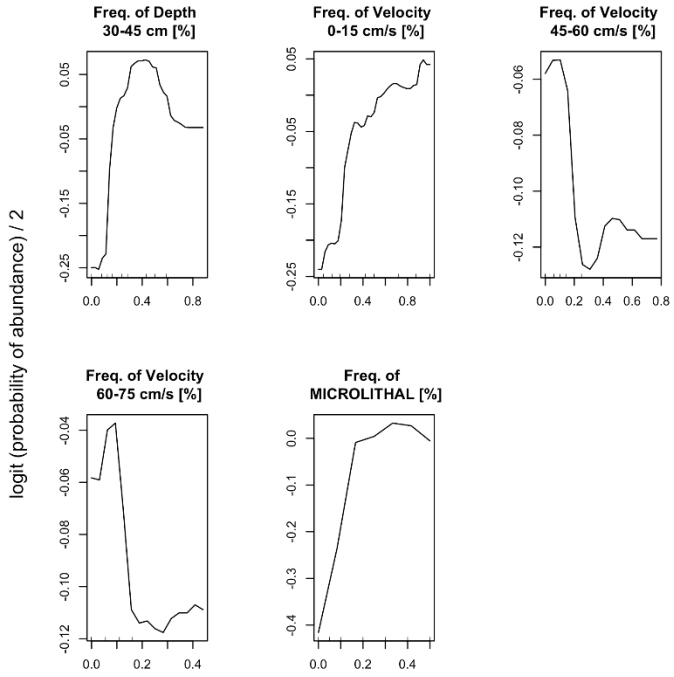


Figure A.8. The presence/abundance Random Forest model of adult Italian vairone (*Telestes muticellus*) available in SimStream-Web (https://mesohabsim.isprambiente.it/app/home/).

- **Juvenile Italian vairone (*Telestes muticellus*) – Chapter 5 and 7:**

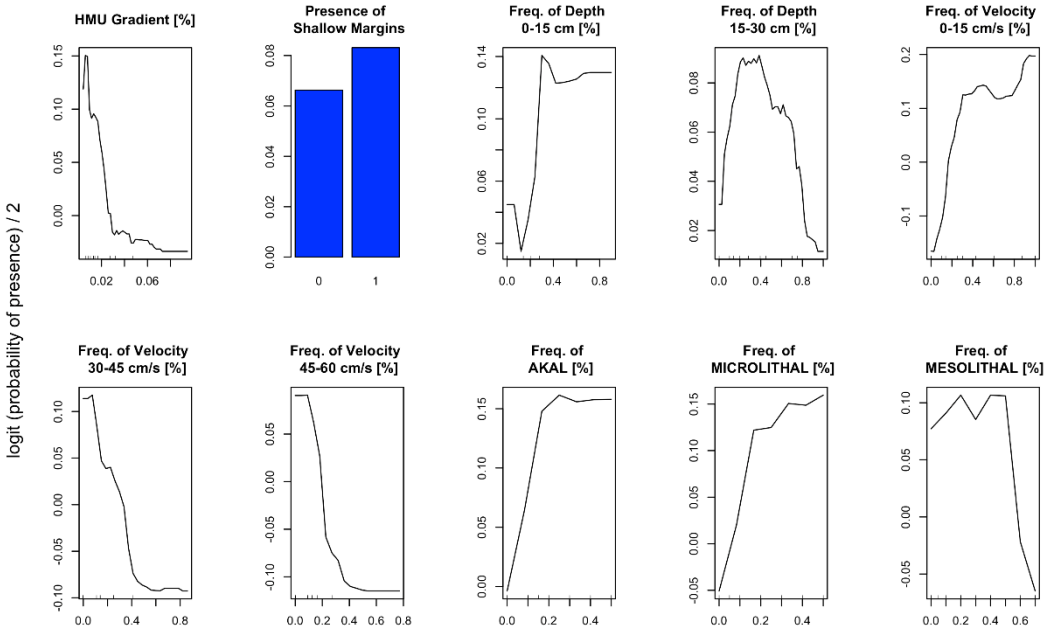


Figure A.9. The absence/presence Random Forest model of juvenile Italian vairone (*Telestes muticellus*) available in SimStream-Web (https://mesohabsim.isprambiente.it/app/home/).

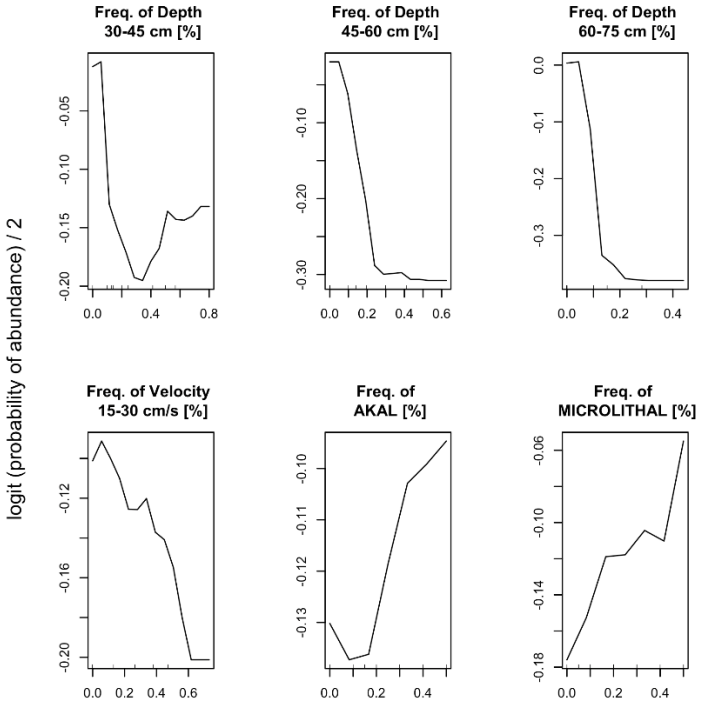


Figure A.10. The presence/abundance Random Forest model of juvenile Italian vairone (*Telestes muticellus*) available in SimStream-Web (https://mesohabsim.isprambiente.it/app/home/).

- **Adult Padanian goby (*Padogobius bonelli*)– Chapter 7:**

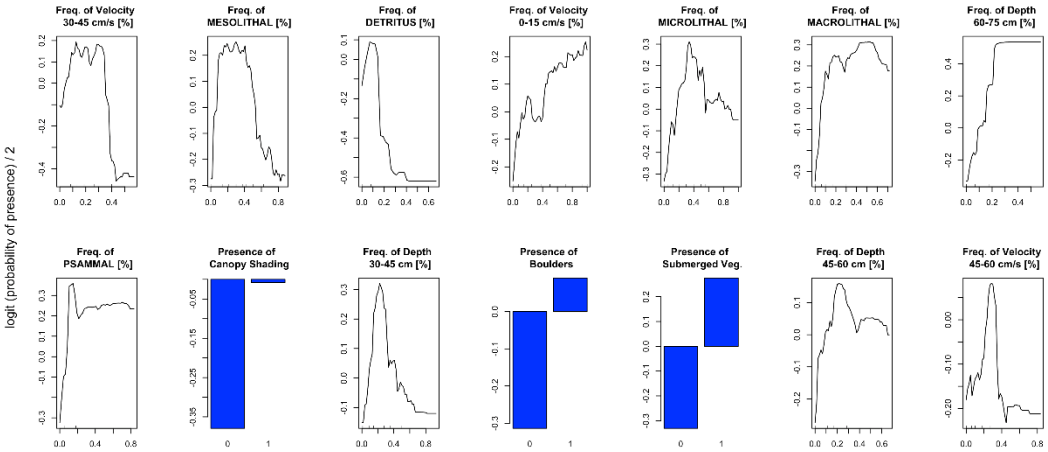


Figure A.11. The absence/presence Random Forest model of adult Padanian goby (*Padogobius bonelli*) available in SimStream-Web (https://mesohabsim.isprambiente.it/app/home/).

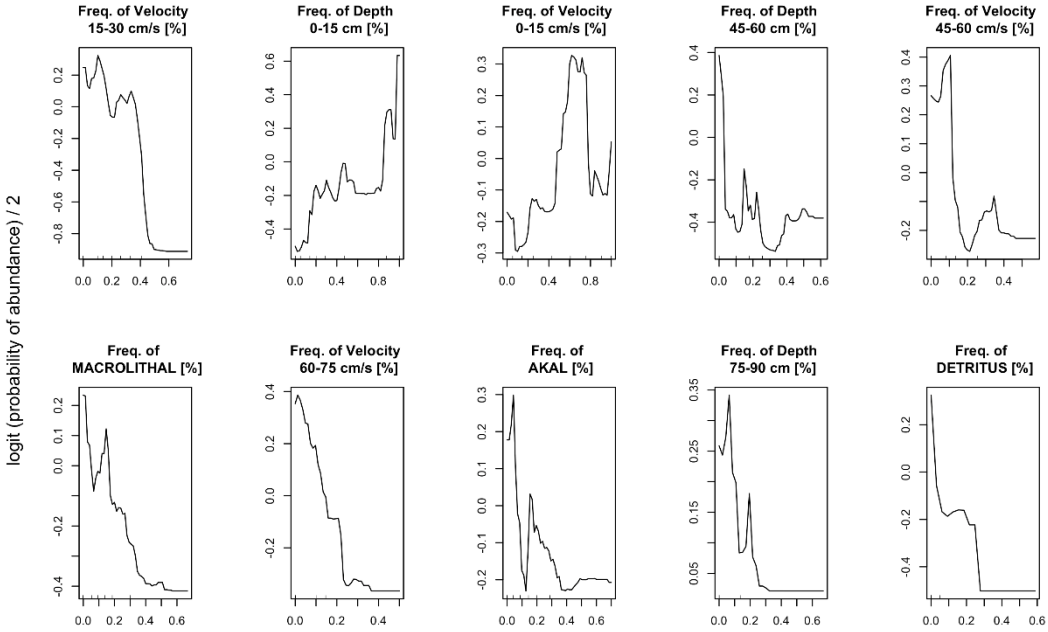


Figure A.12. The presence/abundance Random Forest model of adult Padanian goby (*Padogobius bonelli*) available in SimStream-Web (https://mesohabsim.isprambiente.it/app/home/).

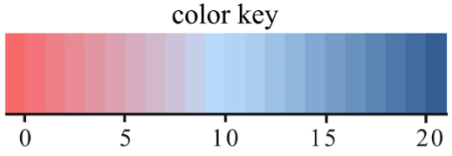
Appendix B

Appendix B. Appendix for Chapter 2

B.1 Number of bibliography sources per species

Table B-1. Number of bibliography sources (Num.) reporting the preferred categories (Cat.) of habitat attributes derived from the review analysis for each species, life stage (A=adult, J=juvenile) and bioperiod (S=spawning). Species are sorted with respect to the total amount of corresponding number of bibliography sources found (Pub.). The color-gradient is picturing high (21, blue) to low (0, red) number of bibliography sources reporting the preferred habitat categories . Water depth (D) and current velocity (V) are represented by 9 categories of 15 cm (from 0 up to > 120 cm) and 15 cm/s (from 0 up to > 120 cm/s) respectively. The codes used for substrate and cover/shelter categories are reported in **Table A-1**. The Table shows, in numerical terms, the results depicted in **Figure 2.1**.

Species	Pub.	Depth (D)						Velocity (V)						Substrate						Cover					
		A		J		S		A		J		S		A		J		S		A		J		S	
		Num.	Cat.	Num.	Cat.	Num.	Cat.	Num.	Cat.	Num.	Cat.	Num.	Cat.	Num.	Cat.	Num.	Cat.	Num.	Cat.	Num.	Cat.	Num.	Cat.	Num.	Cat.
S.cephalus/S. squalus	37	8	45-60	15	30-45	5	0-15	8	0-15	16	0-15	6	15-30	5	AK	9	AK	3	MI	5	WD	6	EV	1	SV
G. gobio/G. benacensis	36	8	30-45	16	30-45	3	0-15	10	0-15	16	0-15	4	0-15	11	PS	13	PS	5	MI	2	WD	3	SV	2	SV
Thymallus thymallus	35	10	75-90	11	45-60	14	30-45	8	45-60	10	45-60	13	45-60	8	MS	8	MS	16	MI	5	BD	2	BD	1	BD
Cottus gobio	33	16	15-30	17	15-30	1	15-30	9	30-45	11	0-15	1	15-30	20	MS	21	MS	4	MS	3	WD	3	WD	0	
Barbatula barbatula	31	13	0-15	16	0-15	2	15-30	7	0-15	10	0-15	2	15-30	12	MI	15	MI	2	AK	5	SV	7	SV	2	SV
Phoxinus phoxinus	30	14	15-30	16	15-30	1	15-30	11	0-15	14	0-15	2	15-30	11	MI	13	MI	3	MI	5	SV	8	SV	0	
Lampetra planeri	25	3	30-45	6	15-30	7	15-30	2	30-45	7	0-15	4	15-30	4	PS	12	PS	8	MI	1	OV	4	SV	3	OV
Lampetra fluviatilis	23	3	45-60	5	45-60	5	45-60	3	30-45	4	0-15	4	60-75	1	MS	7	PS	9	MI	1	OV	3	SV	1	BD
A. alburnus/A. alborella	21	5	105-120	5	45-60	2	0-15	5	0-15	9	0-15	3	15-30	5	PS	5	PS	3	PH	5	SV	5	EV	2	SV
Anguilla anguilla	21			13	45-60					10	15-30					9	MI					6	SV		
Perca fluviatilis	16	4	105-120	4	45-60	2	45-60	6	0-15	8	0-15	2	0-15	4	PE	5	PE	1	MI	2	SV	4	SV	1	SV
Salaria fluviatilis	16	4	30-45	4	30-45	5	15-30	4	15-30	4	15-30	2	0-15	12	MS	12	MS	7	MS	2	SV	2	SV	2	BD
Tinta tinca	16	4	> 120	6	> 120	2	15-30	3	0-15	4	0-15	4	0-15	5	PE	7	PE	6	PH	5	SV	8	SV	6	SV
Cobitis taenia	14	5	30-45	6	15-30	1	0-15	3	0-15	3	0-15	1	0-15	12	PS	11	PS	3	PH	4	SV	4	SV	3	EV
E. lucius/E. cisalpinus	14	3	105-120	2	60-75	4	30-45	3	0-15	4	0-15	5	0-15	4	PE	4	PE	6	PH	2	SV	2	SV	6	SV
Padogobius bonelli	14	4	15-30	3	15-30	1	15-30	1	45-60	1	30-45	0		9	MS	9	MS	6	MA	0		0		2	SV
Scardinius erythrophthalmus	14	1	60-75	1	45-60	3	0-15	0		2	0-15	3	0-15	3	PE	4	PE	5	PH	4	SV	5	SV	5	SV
Telestes muticellus	14	5	30-45	3	30-45	1	15-30	3	15-30	4	15-30	3	15-30	5	AK	5	AK	6	MI	2	WD	3	WD	0	
Alosa fallax	13					7	15-30					0						9	MI					1	OV
Salmo marmoratus	12	4	90-105	3	60-75	4	75-90	3	30-45	3	30-45	3	30-45	6	MA	7	MS	3	MI	1	BD	1	BD	0	
Salmo trutta (Adriatic lin.)	12	4	45-60	4	30-45	2	15-30	5	15-30	4	30-45	2	30-45	6	MA	5	MA	4	MI	4	BD	3	BD	0	
Cyprinus carpio	11	2	45-60	3	45-60	1	30-45	1	0-15	2	0-15	3	0-15	3	PE	4	PE	6	PH	1	SV	1	SV	5	SV
Padogobius nigricans	10	3	30-45	3	30-45	0		1	30-45	1	30-45	0		7	MS	6	MS	3	MA	0		0		1	SV
Protochondrostoma genei	8	2	15-30	2	15-30	0		1	15-30	1	15-30	0		5	MI	5	MI	4	AK	0		0		0	
Lampetra zanandreai	6	1	0-15	0		0		0		0		0		3	PE	3	PE	5	MI	0		0		0	
Barbus plebejus	4	1	45-60	0		0		1	30-45	1	30-45	0		2	MI	1	MI	2	MI	0		0		0	
Chondrostoma soetta	4	0		0		2	45-60	0		0		1	60-75	2	MI	2	MI	3	MI	0		0		0	
Sabanejewia larvata	4	0		0		0		0		0		0		4	PE	4	PE	0		3	SV	3	SV	0	
Squalius lucumonis	4	2	30-45	2	30-45	1	0-15	2	15-30	2	15-30	0		1	MI	1	MI	1	MI	0		0		0	
Barbus caninus	3	0		0		0		0		0		0		3	MI	3	MI	2	MI	1	BD	1	BD	0	
Rutilus pigus	3	0		0		1	45-60	0		0		1	45-60	1	AK	1	AK	2	MS	1	EV	1	EV	0	
Salmo cettii	3	1	60-75	1	60-75	0		0		0		0		2	MI	2	MI	2	MI	2	SV	2	SV	0	
Sarmarutilus rubilio	3	0		0		0		0		0		0		3	AK	3	AK	2	MI	1	SV	1	SV	2	SV
Alburnus albidus	2	0		0		0		0		0		0		1	AK	1	AK	1	AK	0		0		0	



Appendix C

Appendix C. Further personal contributions in published articles on applications of the MesoHABSIM approach

C.1 Comparing Multi-Criteria Decision-Making Methods for the Assessment of Flow Release Scenarios From Small Hydropower Plants in the Alpine Area

Authors. Erica Vassoney, Andrea Mammoliti Mochet, Erika Desiderio, **Giovanni Negro**, Maria Gabriella Pilloni, Claudio Comoglio.

Year. 2021

Abstract. Growing energy demand and targets for reducing greenhouse gas emissions are driving a significant hydropower (HP) generation expansion in the Alpine area. However, despite its advantages, HP implementation causes several impacts on the ecological status of river systems and the preservation of characteristic landscapes. The use of decision-making tools, like multi-criteria decision-making (MCDM) methods, can provide helpful support to achieve more sustainable solutions for complex water management problems. In Aosta Valley (NW Italy), an MCDM experimental approach is being applied to define the optimal environmental flow scenario to be released by HP plants, in an attempt to balance energy production needs, economic profitability and environmental safeguard. Four criteria are considered (energy, environment and fishing, landscape, economy) and key stakeholders are involved in the entire decision-making process. However, there is a need to test also other MCDM methodologies in order to understand if an alternative approach could be more suitable for future, more complex, HP management decisions. Therefore, in this paper, seven different MCDM methods are applied to an existing small run-of-the-river HP plant for the selection of the optimal flow release scenario, i.e., SAW, WPM, AHP, TOPSIS, VIKOR, ELECTRE III, and the initially adopted method, SHARE MCA. The results

obtained with the application of the different MCDM methods are investigated and statistically compared. The strengths and weaknesses of the different methodological approaches are also discussed. Based on the comparative results and the consequent evaluations, SHARE MCA, WPM, and VIKOR appear to have the most interesting characteristics in terms of overall feasibility.

C.2 The combined impact of hydropower plants and climate change on river runoff and fish habitats in lowland watersheds

Authors. Vytautas Akstinas, Tomas Virbickas, Jūratė Kriaučiūnienė, Diana Šarauskienė, Darius Jakimavičius, Vytautas Rakauskas, **Giovanni Negro**, Paolo Vezza.

Year. 2021

Abstract. Aquatic ecosystems are particularly vulnerable to anthropogenic activity and climate change. The changes in flow regimes in Lithuanian lowland rivers due to the operation of hydropower plants (HPPs) and the impact of altered flow on some fish species have already been studied. The impact of climate change on future natural river runoff and the structure of fish assemblages was also investigated. However, it is still unknown how the combined effect of climate change and flow regulation related to hydropower generation may affect fish assemblages in the downstream river reaches below the Lithuanian HPPs. In this study, the physical habitat modeling system MesoHABSIM was used to simulate spatial and temporal changes in aquatic habitats availability for different fish species under the influence of HPP at different climate change scenarios. Changes in the available habitat were assessed for common fish species in four HPP-affected rivers representing different hydrological regions of Lithuania. The modeling results showed that the operation of HPP under climate change conditions in most rivers could be beneficial for small benthic fish species such as gudgeon (*Gobio gobio*) and stone loach (*Barbatula barbatula*). Meanwhile, for larger fish species (e.g., chub *Squalius cephalus* and vimba *Vimba vimba*) the alteration in the temporal availability of suitable habitat was relatively higher.